



**Introduction of Novel Bicyclic Germylenes
Exhibiting Unexpected Reactivity**

Von der Fakultät für Mathematik und Naturwissenschaften
der Carl von Ossietzky Universität Oldenburg
zur Erlangung des Grades und Titels einer

Doktorin der Naturwissenschaften (Dr. rer. nat.)

angenommene Dissertation
von

M.Sc. Marie Sophie Würdemann
geboren am 24. Dezember 1995 in Oldenburg

The herein presented work was performed in the Institute of Chemistry at the Carl von Ossietzky Universität Oldenburg under supervision of Prof. Dr. Thomas Müller from August 2020 until December 2023.

This work was supported by the Deutsche Forschungsgemeinschaft (DFG: MU-1440, 13-1) and by the Carl von Ossietzky Universität Oldenburg (CvO).

Referee: Prof. Dr. Thomas Müller

Second Referee: Prof. Dr. Kim Baines

Day of Disputation: 15.02.2024

Acknowledgements

First and foremost, I would like to thank my supervisor Prof. Thomas Müller for the opportunity to prepare this thesis in his group and for the interesting topic. Thank you for all the fruitful discussions and your critical advice, which really helped develop my knowledge and this research. I thank Prof. Kim Baines for being the second referee as well as for hosting my research internship at Western University during my masters.

I would like to thank Lena Albers for the scientific support and input as well as Uwe Vehlow, Maria Ahrnsen and Celine True for their technical support in the laboratories. Furthermore, I would like to thank Petra Rösner for handling the bureaucraties. A special thanks to Steffen Kühn for the initial studies and to Prof. Andreas Orthaber from Uppsala University for sending some samples to Oldenburg.

Many thanks to the analytical department: Andrea Tschirne and Angela Sündermann for measuring the NMR spectra and making the many special requests and appointments possible; Marc Schmidtmann and Alex Weiz for the X-ray analyses; Francesco Fabbretti for recording the high resolution mass spectra.

My sincere thanks to the past and present members of the Müller group: Thank you Saskia Rathjen, Sandra Künzler, Anastasia Merk, Wiebke Wohltmann, Jelte Nimoth and Gül Özpınar as well as Nadeschda Geibel, Corinna Girschik, Chenghuan Liu, Amrit Chandi and Elias Drösemeier (who also contributed to this work) for the pleasant and friendly work environment. My special thanks to Lukas Bührmann for the scientific discussions and for your friendship. I enjoyed working with all of you! I would also like to thank the other students who contributed to this work: Tobias Bötzel, Tobias Zimmermann and Meemke Scholz. Your work and effort is appreciated. Additionally, I want to thank the Beckhaus group, especially Simon De Graaff and Kerstin Fitschen, for the kind mutual support.

Nicht zuletzt möchte ich mich herzlich bei meinen Eltern, meinen Großeltern, meinem Bruder und meinen Freunden für ihren Rückhalt und ihr Verständnis während der Promotion, aber auch während des gesamten Studiums bedanken. Ich kann nicht in Worte fassen, wie dankbar ich bin, euch zu haben!

Conference Contributions

Under the title *Phospha-BCH-Germynes – Synthesis and Reactivity*, three talks were given at national and international conferences:

51st Silicon Symposium

San Diego, March 2022

International Conference on Phosphorus, Boron and Silicon

Berlin, March 2023

Awarded best oral presentation of a young scientist.

Norddeutsches Doktorandenkolloquium

Berlin, October 2023

Awarded best oral presentation of a young scientist.

Abstract

Carefully designed low-coordinated main group compounds can mimic transition metal complexes with regards to small molecule activation. This is due to their frontier molecular orbitals, which feature donor and acceptor orbitals that are close in energy. The design of new low-coordinated main group compounds, fulfilling these criteria, is a desirable target as they offer a more sustainable alternative for the commonly used transition metal complexes. Within the present work, a novel family of germynes, low-coordinated germanium compounds in the oxidation state +II, were synthesised and characterised: aminophospha-bicyclohexene-germylenes. They consist of a phosphorus-containing bicyclic backbone and are stabilised by homoconjugation. The homoconjugation effects lowering of the LUMO, which features large contributions from the germanium p-orbital. This indicates reduced electrophilicity and increased nucleophilicity of the germylene. With the phosphorus atom, a second σ -donor was introduced into the molecule. Therefore, the reactivity of the herein introduced compounds was tested regarding the amphiphilic character of the germylene but also regarding the cooperating or competing reactivity of those two donor sites. In general, it was shown that the herein synthesised aminophospha-bicyclohexene-germylenes exhibit unexpected reactivity. The self-induced, bimolecular elimination of the germanium atom is a striking reaction, which indicates the amphiphilic character of the germylene. However, upon modification of the backbone, this reaction could be prevented, and reactivity studies were conducted. Reacting aminophospha-bicyclohexene-germylenes with hard electrophiles like protons and methylium ions led to the formation of phosphonium salts. The formation of the respective germylium ions was not observed. However, evidence was found that the germylene reacts with chalcogens and transition metal complexes, though this finally led to the loss of germanium from the starting material. The experimental analyses of the structure and properties of aminophospha-bicyclohexene-germylenes as well as the examination of possible reaction products were furthermore supported using DFT calculations.

Kurzzusammenfassung

Geschickt gestaltete niedrigkoordinierte Hauptgruppenelementverbindungen sind in der Lage, Übergangsmetallkomplexe im Hinblick auf die Aktivierung kleiner Moleküle zu imitieren. Diese Eigenschaft geht auf deren Frontorbitale zurück, welche energetisch wenig separierte Donor- und Akzeptororbitale aufweisen. Die Synthese neuer niedrigkoordinierter Hauptgruppenelementverbindungen, die diese Kriterien erfüllen, ist ein erstrebenswertes Ziel, da diese eine nachhaltigere Alternative zu den üblicherweise verwendeten Übergangsmetallkomplexen bieten. Im Zuge der vorliegenden Arbeit wurde eine neue Familie von Germylenen, niedrigkoordinierte Germaniumverbindungen in der Oxidationsstufe +II, synthetisiert und charakterisiert: Aminophospha-Bicyclohexen-Germylene. Diese bestehen aus einem phosphorbasierten bicyclischen Grundgerüst und sind durch Homokonjugation stabilisiert. Die Homokonjugation senkt das LUMO, welches große Beiträge des p-Orbitals des Germaniums aufweist, energetisch ab, wodurch eine verringerte Elektrophilie und eine gesteigerte Nucleophilie des Germylens zu erwarten sind. Mit dem Phosphoratom wurde ein zweiter σ -Donor in das Grundgerüst eingebaut. Die Reaktivität der vorgestellten Verbindungen wurde daher im Hinblick auf die amphiphile Reaktivität des Germylens, aber auch vor dem Hintergrund der Kooperativität oder Konkurrenz der beiden Donorzentren untersucht. Generell konnte gezeigt werden, dass die hier synthetisierten Aminophospha-Bicyclohexen-Germylene eine unerwartete Reaktivität aufweisen. Eine Besonderheit stellt dabei die selbstinduzierte, bimolekulare Eliminierung des Germaniumatoms dar, welche auf den amphiphilen Charakter des Germylens hinweist. Durch gezielte Modifikation des Grundgerüsts konnte die Reaktion jedoch unterdrückt und Reaktivitätsstudien durchgeführt werden. Gegenüber harten Elektrophilen wie Protonen oder Methylkationen reagierten Aminophospha-Bicyclohexen-Germylene unter Bildung der Phosphoniumsalze. Die Bildung der entsprechenden Germyliumionen wurde nicht beobachtet. Hinweise auf die Reaktion des Germylens konnten jedoch in Reaktivitätsstudien gegenüber Chalkogenen wie auch Übergangsmetallkomplexen beobachtet werden, wenngleich diese auch die Eliminierung von Germanium oder entsprechenden Germaniumverbindungen bedeuteten. Der Aufbau, die Eigenschaften sowie auch mögliche Reaktionsprodukte der Aminophospha-Bicyclohexen-Germylene wurden neben den experimentellen Untersuchungen durch DFT-Rechnungen unterstützt.

Table of Contents

1	Introduction.....	1
1.1	Low-Coordinated Main Group Compounds.....	1
1.1.1	Tetrylenes.....	2
1.1.2	Frustrated Lewis Pairs.....	5
1.1.3	Heavier Alkene and Alkyne Analogues.....	7
1.1.4	Accessing Main Group Heterofulvenes.....	11
2	Motivation and Objective.....	16
3	Results and Discussion.....	18
3.1	Synthesis of the Precursors.....	18
3.1.1	1,1-Dichloro-2,5-Bis(trialkylsilyl)tetroles and Their Tetrolediide Salts.....	18
3.1.2	Aminodichlorophosphanes.....	20
3.1.3	Aryldichlorophosphanes.....	22
3.1.4	Dichloroarsines.....	24
3.1.5	Dichlorostibanes.....	24
3.2	Aminophospha-BCH-Germylenes.....	26
3.2.1	Synthesis.....	26
3.2.2	Structural Features of Aminophospha-BCH-Germylenes.....	31
3.2.3	Structural Features of Aminophospholes.....	36
3.2.4	NMR Spectroscopic Analysis of Mixtures.....	37
3.2.5	Comparative Analysis of the NMR Spectroscopic Data.....	41
3.2.6	Replication of the ³¹ P NMR Spectroscopic Data.....	46
3.2.7	Germanium Elimination from Phospha-BCH-Germylenes.....	49
3.3	Attempting to Expand the Scope: Pnicta-BCH-Germylenes.....	60
3.3.1	Arylphospha-BCH-Germylenes.....	60
3.3.2	Pnicta-BCH-Silylenes.....	63
3.3.3	Arsa- and Stiba-BCH-Germylenes.....	65
3.3.4	Digression to Group 16: Germaselenone.....	66
3.4	Reactivity Studies on Aminophospha-BCH-Germylenes.....	68
3.4.1	Oxidation Reactions.....	69
3.4.2	Reactivity Towards Small Electrophiles.....	80
3.4.3	Reactivity Towards Lewis Acids.....	91
3.4.4	Reactivity Towards Transition Metal Complexes.....	97
3.5	Phosphanylgermolides and Diphosphanylgermoles.....	110

3.5.1	Synthesis of Diaminochlorophosphanes	110
3.5.2	Reactions with Chloro(<i>bis</i> (diisopropylamino))phosphane	112
3.5.3	Reactions with ClP(N ⁱ Pr ₂)(Pip) and ClP(Pip) ₂	119
3.5.4	Short Summary: Chapter 3.5	125
4	Summary & Outlook	126
5	Experimental Part	132
5.1	Operational Methods and Tools	132
5.2	Experimental Procedures	134
5.2.1	Germoles	134
5.2.2	Aminodichlorophosphanes	137
5.2.3	Diaminochlorophosphanes	139
5.2.4	Aryldichlorophosphanes	140
5.2.5	Stibanes	142
5.2.6	Selenium Dichloride	144
5.2.7	Phospha-BCH-Germylenes & Phospholes	144
5.2.8	Group 16 Substituted Phospholes	155
5.2.9	Phosponium & Phospholium Salts	157
5.2.10	Transition Metal Complexes	165
5.2.11	Phosphagermapentafulvene Dimer	166
5.2.12	Diaminophosphanylgermolide Salts	166
5.2.13	Bis(diaminophosphanyl)germoles	168
6	References	171
7	Appendix	176
7.1	Abbreviations and Symbols	176
7.2	Computational Details	177
7.3	Other Programs and Methods	181
7.4	Crystallographic Data	182

1 Introduction

The activation of small, thermodynamically stable molecules like carbon monoxide, carbon dioxide, methane and dihydrogen is challenging as it requires harsh conditions or catalytic activation. Traditionally, transition metal complexes are used in the latter respect as they offer flexible features such as the ability to coordinate substrates, variable oxidation states, and electron donating and accepting properties at the same time.^[1-2]

The use of transition metal complexes on the other hand, is not ideal as they often are expensive and toxic and the metals themselves are rather rare. Since parallels have been drawn between the frontier molecular orbitals of certain low-coordinated main group compounds and those of transition metal complexes^[3], the research in this field has expanded. As main group elements are more earth abundant and cheaper than transition metals, the replacement of transition metal complexes by low-coordinated main group compounds, in the field of small molecule activation and bond activation in general, is desirable and also more sustainable.^[1, 4]

Carefully designed heteroalkenes and heavier carbene analogues as well as frustrated Lewis pairs (FLPs) exhibit accessible donor and acceptor orbitals that are separated only moderately in energy, thus being capable of mimicking transition metal complexes in activating small molecules or individual bonds in more complex molecules.^[1, 3-5] However, today, one of the greatest challenges lies in the liberation of the substrate upon activation and binding to the catalyst. This was and is the impulse to synthesise new stable heteroalkenes, heavier carbene analogues and FLPs that fulfill these requirements and can therefore be applied in bond activation reactions and further processing of the activated species.

1.1 Low-Coordinated Main Group Compounds

The field of research on low-coordinated main group compounds is relatively young but widely projecting. Thus, in the following, the focus will mostly be on selected examples, containing Group 14 and 15 elements; and more precisely on germynes, digermenes, digermynes and germaphosphenes (Figure 1).

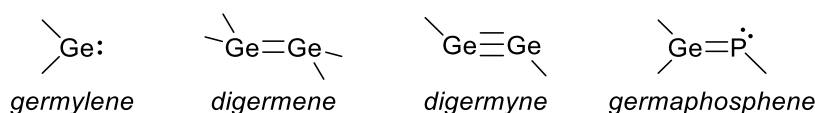


Figure 1 – Selection of germanium containing low-coordinated main group compounds.

1.1.1 Tetrylenes

Tetrylenes are divalent Group 14 compounds in the oxidation state +II. Unlike their lightest homologue, methylene (CH_2), heavier tetrylenes (EH_2) exhibit a singlet ground state. Due to the larger HOMO-LUMO energy gap in the latter, causing the lower ability to form hybrid orbitals, the energy gained upon triplet formation is not enough to compensate for that energy gap.^[6] Therefore, heavier tetrylenes ($\text{E} = \text{Si}, \text{Ge}, \text{Sn}, \text{Pb}$) feature a lone pair of electrons in an orbital with high s-character and an orthogonal vacant p-orbital, making them amphiphilic reagents (Figure 2). The trend as well as the stability of tetrylenes increase down the group.^[7]

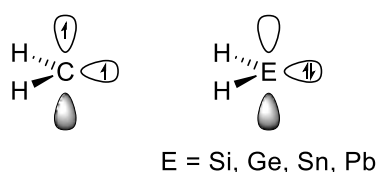


Figure 2 – Carbenes (triplet ground state) and heavier tetrylenes (singlet ground state).

The main reason for the late isolation of low-coordinated main group compounds was the lack of knowledge on how to stabilise them. It is now known that there are several strategies to achieve sufficient stabilisation, mainly relying on the principles of kinetic or thermodynamic stabilisation or a mix of both. Tetrylenes tend to dimerise, oligomerise or polymerise unless they are sufficiently stabilised. However, the form of stabilisation also impacts their reactivity, e.g. their ability to activate small molecules and other σ -bonds. The σ -donating and π -accepting properties of tetrylenes can be tuned by the choice and design of their substituents, which impact not only their stability but also the HOMO-LUMO energy gap. The latter is a determining factor when it comes to bond activation reactions: a larger energy gap correlates with a more sluggish reactivity.^[7-9]

Especially silylenes and germylenes require sophisticated design to be isolated in the monomeric form. The most common strategies are: kinetic stabilisation by using very bulky substituents; thermodynamic stabilisation by introduction of neighbouring π -donating atoms and the use of inter- or intramolecular Lewis basic donors (Figure 3).^[1, 4, 7] Since the main subject of this work are germylenes, they were chosen as a proxy for the following illustrations.

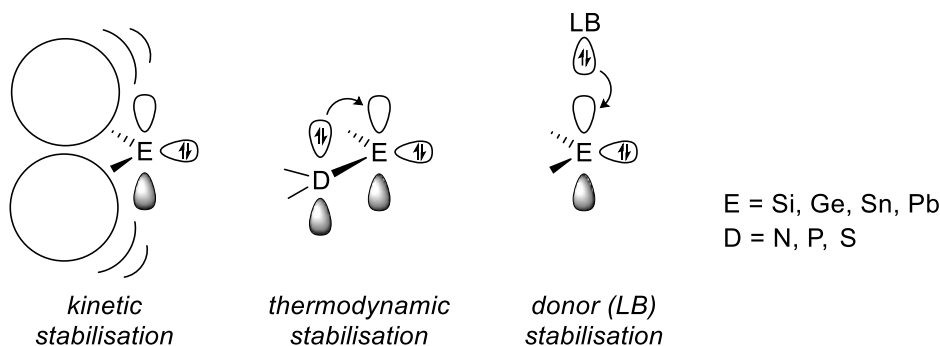


Figure 3 – Stabilisation strategies for tetrylenes.

The first example of a stable, monomeric dialkylgermylene **1** was introduced by Lappert and coworkers in 1976^[10] and the first monomeric diarylgermylene **2** was isolated by Okazaki and Tokitoh in 1994^[11]. Both germylenes are kinetically stabilised by their bulky substituents (Figure 4, left). The diarylgermylene **1**, however, was found to be dimeric in the solid state; which is also the first digermene ever reported.^[10] Exchange of the bis(trimethylsilyl)methyl groups for even more sterically demanding groups enabled Jutzi and coworkers to conduct the first structural characterisation of a monomeric dialkylgermylene.^[12] The sensitivity towards steric protection was also shown for the diarylgermylene **2**: Exchanging only one of the large aryl substituents for a less sterically demanding mesityl substituent resulted in the formation of an in-solution equilibrium of the germylene and the corresponding digermene. The pull-effect of the aryl groups increases the germylene reactivity, which is why the diarylgermylene **2** is capable of undergoing insertion reactions into typical σ -bonds (e.g. MeI, MeOH and Et₃SiH) as well as [4+1] and [3+1] cycloaddition reactions.^[7] In the following years and decades, other kinetically stabilised diarylgermylenes were developed and their participation in bond activation reactions was shown. The diarylgermylene **3**, introduced by Power and coworkers, for example, is capable of activation of dihydrogen and ammonia (Figure 4, right).^[13]

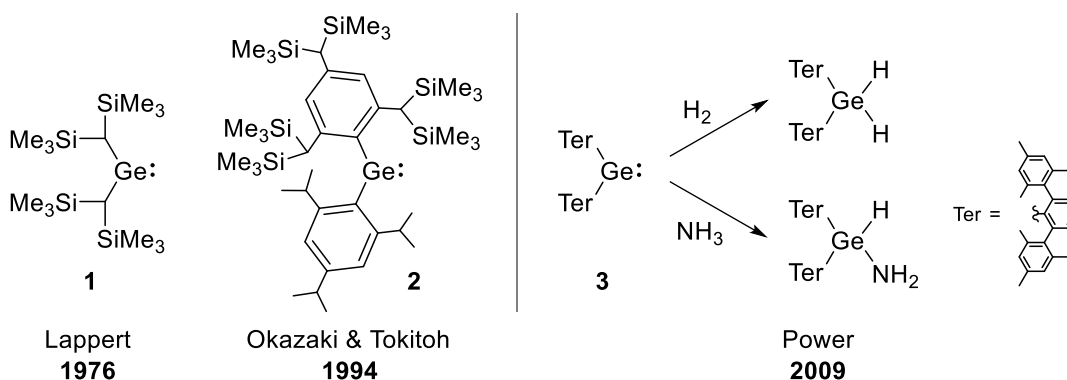


Figure 4 – First stable dialkyl- **1** and diarylgermylene **2** (left)^[10-11], and first reported activation of dihydrogen and ammonia by germylene **3** (right).^[13]

The introduction of π -stabilising neighbouring atoms effects thermodynamic stabilisation of the germylene. Typical substituents are nitrogen, phosphorus and sulfur but also silicon, due to the β -silyl effect. The electropositive silicon substituent furthermore enhances the germylene reactivity by lowering the HOMO-LUMO energy gap, as for example shown by Aldridge and coworkers, who reported on a silyl-substituted germylene **4**, which activates dihydrogen and ammonia at ambient temperature (Figure 5).^[14] One of the probably most prominent examples of π -stabilised germylenes are N-heterocyclic germylenes **5** (NHGe's), first introduced by Meller and coworkers in 1985.^[1, 7, 15] Analogously to their lighter homologues, N-heterocyclic carbenes, the donation of electrons into the vacant p-orbital makes NHGe's particularly stable. However, the frontier molecular orbitals are lower in energy than those of NHC's, making NHGe's weaker σ -donors and better π -acceptors. Still, NHGe's can be used as ligands for transition metal complexes^[16] but are not suitable for the activation of small inert molecules like dihydrogen, carbon monoxide or carbon dioxide.^[7]

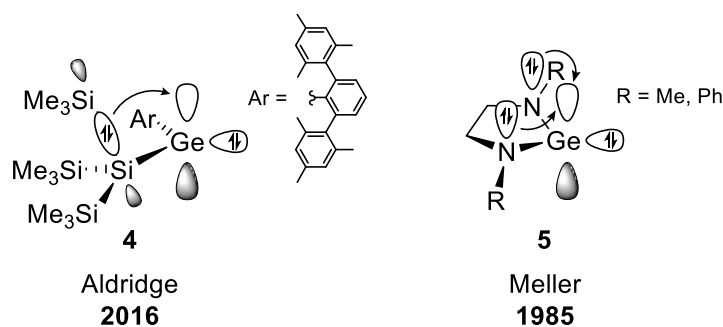


Figure 5 – Stabilisation by electron donating substituents: a silyl-substituted germylene (left) and first reported NHGe's (right).^[14-15]

The stabilisation of germylenes by Lewis basic donors relies on the donation of electrons into the vacant p-orbital of the germylene. The coordination of a Lewis basic donor formally makes the germylene tri- or, in case of two donors, tetracoordinated. The donor can either be external, e.g. solvent molecules or other weak Lewis bases, or internal. Intramolecularly stabilised germylenes typically feature a Lewis basic heteroatom, mostly nitrogen, oxygen or phosphorus, incorporated in a flexible side-arm of the germylene. The coordination of a Lewis basic donor (inter- and intramolecular) provides both, thermodynamic and kinetic stabilisation. In most cases this does not lower the reactivity of the germylene, as the donors are easily exchanged or can “turn away” from the germylene. A prominent and widely applied example of intramolecularly stabilised germylenes are amidinatochlorogermylenes **6**, first introduced by Jones and coworkers in 2008 (Figure 6).^[7, 17]

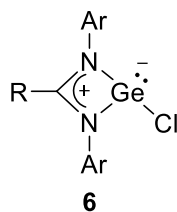
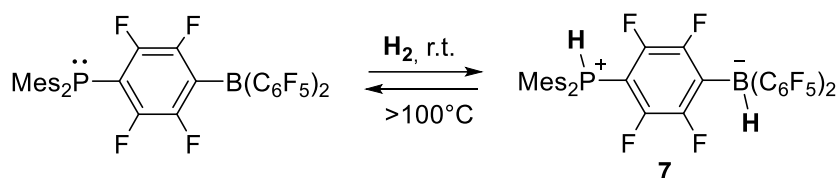


Figure 6 – Amidinatochlorogermylene **6** as a representative for intramolecularly stabilised germynes.^[17]

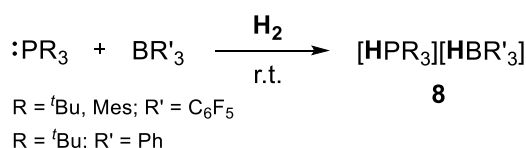
1.1.2 Frustrated Lewis Pairs

To date, one of the biggest problems concerning the substitution of transition metal complexes with low-coordinated main group compounds in bond activation reactions is the reversibility. Most compounds found to activate and bind e.g. dihydrogen, are not able to liberate it again. This, however, is a key property for processing of the activated substrate. In 2006, Stephan and coworkers, reported on the first metal-free binding and liberation of dihydrogen. The phosphoniumborate **7** liberated dihydrogen upon heating (>100°C). It was postulated that the liberation proceeds upon proton or hydride migration. At ambient temperature, dihydrogen was added again (Scheme 1).^[18]



Scheme 1 – First reported metal-free reversible activation and binding of H₂.

One year later, the authors introduced the concept of frustrated Lewis pairs (FLPs). Using stoichiometric mixtures of sterically demanding phosphanes and boranes that, eponymous for these acid-base pairs, are not able to form classical Lewis acid-base adducts, dihydrogen activation was achieved at ambient temperature. Liberation of dihydrogen from the obtained phosphonium borate **8** was not achieved, even upon heating to 150°C (Scheme 2).^[19]



Scheme 2 – Ambient-temperature H₂ activation by a readily available FLP.

It is necessary to note that today, two different activation mechanisms are suggested. The first one, including the above shown example, is the heterolytic bond cleavage, proceeding upon formation of an encounter complex, which polarises the substrate (Figure 7, top). The second mechanism proceeds upon single electron transfer (SET) from the Lewis base to the Lewis acid. The resulting radical ion pair (RIP) then reacts with the substrate (Figure 7, bottom). The latter process was only first reported in 2017^[20] and is usually indicated by intense colour change.^[21]

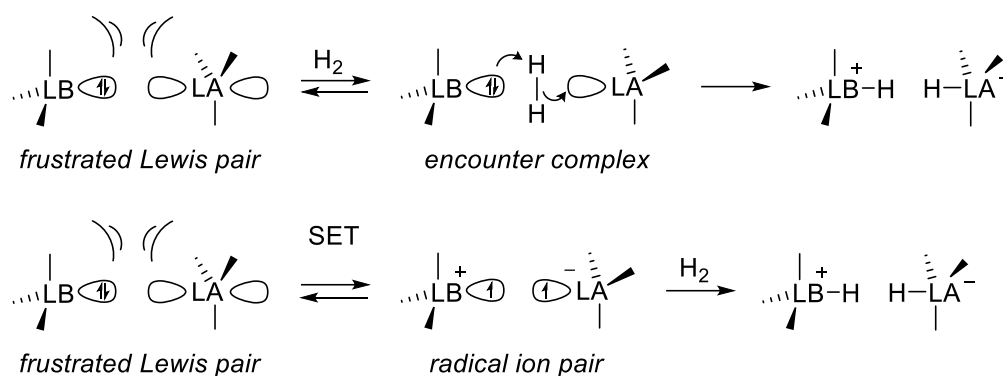
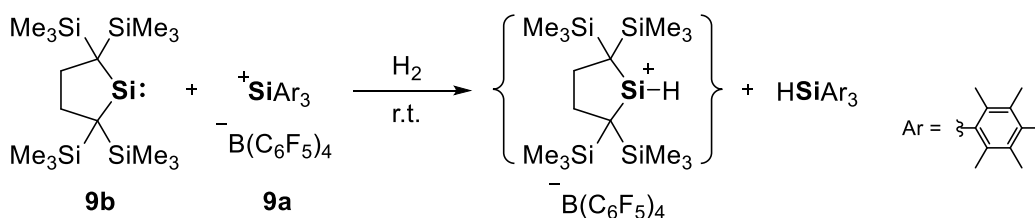


Figure 7 – Heterolytic and homolytic bond cleavage reactions.

FLP chemistry was developed extensively in recent years. Though phosphane/borane pairs, as shown above, are still amongst the most popular FLPs, this field of chemistry is not restricted to Group 13 and Group 15 based Lewis acids and bases. In 2008, the groups of Tamm and Stephan reported on the use of NHCs as Lewis bases and thereby extended FLP chemistry to Group 14.^[22-23] In 2011, Müller and coworkers first reported on the use of silylium ions **9a** as Lewis acidic part and later extended their studies and were furthermore able to show, that also silylium/phosphane pairs are able to undergo the SET process.^[24-26] Then in 2014, the authors combined these two Group 14 approaches and reported on a Group 14/Group 14 FLP, namely the silylium/silylene pair **9**, which successfully activated dihydrogen (Scheme 3).^[27]



Scheme 3 – Reported dihydrogen activation using a silylium/silylene FLP **9**.

The amphiphilic character of the silylene **9b** (introduced by Kira and coworkers^[28]) was illustrated also in FLP chemistry context. In 2017, Dong *et al.* showed, that the silylene **9b** can

not only act as the Lewis basic part of an FLP, but also as the Lewis acidic part when combined with a Lewis base.^[29]

Today, numerous FLPs, are known and their reactivity range includes the activation of small molecules and other inert bonds, as well as the reversible dihydrogen and carbon dioxide binding^[30-31] and the usage of activated dihydrogen in hydrogenation catalysis.^[32-33]

1.1.3 Heavier Alkene and Alkyne Analogues

Different to alkenes and alkynes ($E = C$), multiply bonded heavier tetrylenes possess a trans-bent structure. This is for the same reason that causes tetrylenes to exhibit a singlet ground state: the lower ability to form hybrid orbitals. The element-element double bonds are therefore best described as double donor-acceptor bonds rather than σ - and π -bonds, as for the carbon analogues (Figure 8).^[1, 4, 10] The strategies for stabilising multiply bonded low-coordinated main group compounds are basically the same as for tetrylenes (described above).

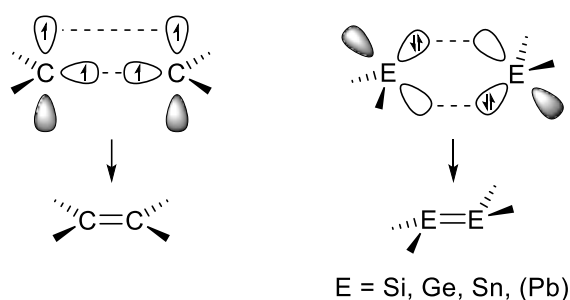


Figure 8 – Binding situation and structure of ditetrylenes.

1.1.3.1 Tetrel-Tetrel Multiple Bonds

The first multiply bonded main group compound showing activity in bond activation reactions, which also lead to the comparison of low valent main group compounds with transition metal complexes, was a digermynes, reported in 2005 by Power and coworkers.^[3] The diarylgermyne activated dihydrogen at ambient temperature. However, heavier homologues of alkynes do not possess a typical triple bond. Going down Group 14, the degree of non-bonded electrons increases. For digermynes, for example, adding up to a double donor-acceptor bond and two non-bonded electrons. Those can either be located at one germanium atom or one at each germanium atom, causing the presence of a donor and an acceptor site. This marks the distinct difference to the carbon analogues (Figure 8).^[4] Bond activation reactions proceed upon

synergistic interaction of the frontier molecular orbitals with those of the substrate; depicted in Figure 9.^[1, 4]

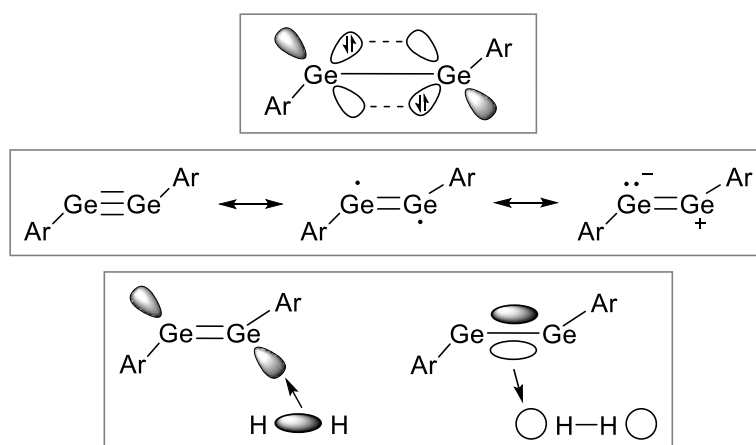


Figure 9 – Binding situation in digermynes and exemplary bond activation reaction.

Examples of compounds containing (heavier) Group 14-Group 14 multiple bonds have been known years before the first main group compound-bond activation reaction was reported. In 1973, Lappert and coworkers reported on the isolation of the distannylene **10**, and later, in 1976, of the digermene **11**.^[10, 34] The corresponding disilene **12** was synthesised by West and coworkers in 1981.^[35] Another striking example was reported the same year by Brook and coworkers, synthesising the first silene **13** (Si=C).^[36] In 1991, Baines and coworkers reported on the preparation of germasilene **14**, a heavier mixed tetrel-tetrel doubly bonded species (Figure 10). Though not isolated, the authors were able to trap the germasilene by insertion reaction into the methanol O-H bond at low temperature.^[37-38]

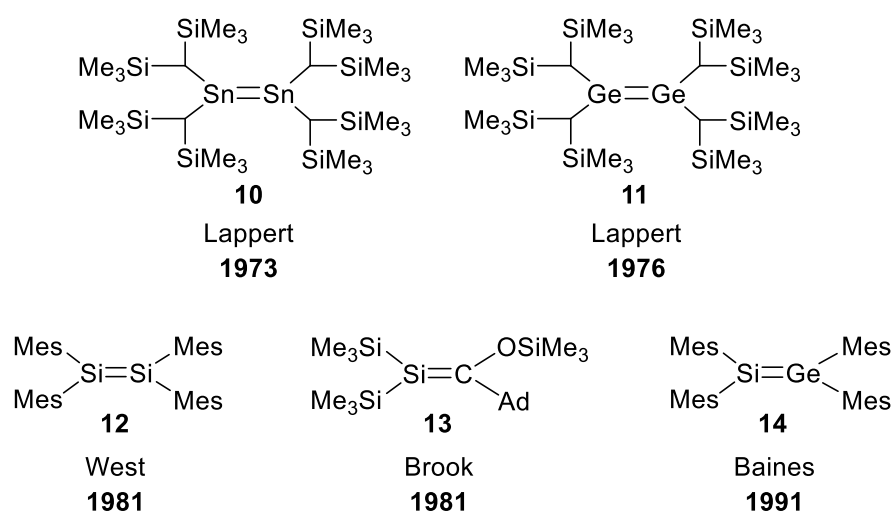


Figure 10 – The first distannene **10**, digermene **11**, disilene **12**, silene **13** and germasilene **14** reported in the literature.^[10, 34-37]

In recent years, a lot of progress was made synthesising new compounds containing heavier Group 14-Group 15 multiple bonds and studying their reactivity as well as the corresponding mechanisms. In 2017, for example, the groups of Inoue and Rieger reported on the first ambient-temperature activation of dihydrogen by a disilene. The diiminodisilylsilene features a long Si=Si double bond and a highly twisted molecular structure; rather uncommon for disilenes with silicon as the second lightest tetrylene. Due to its structural features, the disilene was found to selectively undergo trans-addition of dihydrogen, which is different to the typical syn-addition onto alkenes.^[39]

1.1.3.2 Tetrel-Pnictogen Multiple Bonds

The isolation of compounds featuring mixed heavier main group element multiple bonds is even more challenging than the isolation of homonuclear heavier main group multiple bonds. This is due to the polarisation of the bond, which makes those compounds more reactive; and therefore, even more destined to undergo bond activation reactions.

The first compound, containing a heavier Group 14-Group 15 triple bond was isolated in 1981 by Becker and coworkers. The phosphalkyne **15**, with the phosphorus atom in the coordination number 1 ($\lambda^3 \sigma^1$) was synthesised from a phosphalkene by elimination of hexamethyldisiloxane.^[40] Compounds containing phosphorus atoms with the coordination number II ($\lambda^3 \sigma^2$), e.g. phosphalkenes, are more widely studied today.^[41] However, alkene and alkyne analogues, containing two heavier Group 14-Group 15 elements multiple bonds are rare, with silaphosphenes as the most researched class (Figure 11).^[42-43]

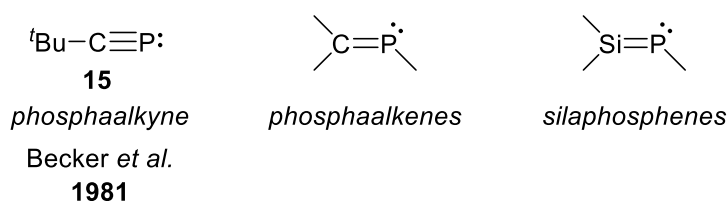
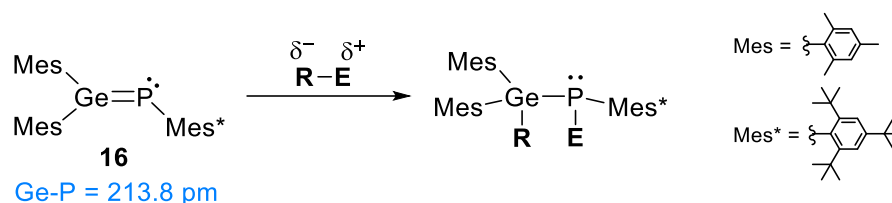


Figure 11 – Selected examples of Group 14-Group 15 multiple bonds.

The first isolation of a germaphosphene, as will be attempted to synthesise within this work, was reported in 1985 by Escudie, Couret, Satge and coworkers.^[44] The aryl-substituted germaphosphene **16** was synthesised via dehydrofluorination reaction of fluorogermaphosphane. It was the first structurally characterised compound to contain a $\text{E}^{14}=\text{E}^{15}$ double bond, involving two heavier elements ($\text{Ge}=\text{P} = 213.8 \text{ pm}$; vs.

Ge-P = 233-235 pm).^[45] The germaphosphene **16** was shown to be highly reactive towards electrophiles and nucleophiles. For example, aligning with the polarisation of the double bond, it regioselectively reacts with electrophiles (substrates containing acidic hydrogen atoms), as well as with nucleophiles (organometallic compounds) by addition of the partially negative charged atom (**R** = nucleophilic part; **E** = H, Li, MgX) to the germanium atom (Scheme 4). Furthermore, addition of halogens was observed, presumably proceeding through a radical pathway.^[46]



Scheme 4 – First stable germaphosphene **16** and its reactivity towards polarised bonds.

More examples of stable compounds containing Ge=P double bonds, or Ge–P bonds of double bond character, were reported several years later, however, to date there are still only few examples present.^[47-53] Most of these examples, shown in Figure 12, exhibit Ge–P bonds that are shorter than typical Ge–P single bonds (Ge–P = 223-229 pm vs. 233-235 pm^[45]), but also longer than the double bond reported by Escudie *et al.* (Ge–P = 213.8 pm).^[45] In 2009, Lee *et al.* reported on the synthesis of a closely related germaphosphene **17**, exhibiting silyl groups instead of aryl groups at the germanium atom. The Ge=P bond length is comparable to that reported for the all-aryl substituted germaphosphene **16** (Ge=P (**17**) = 217.48 pm; $\Delta(\text{Ge=P}) = 3.7$ pm). The most striking difference is the recorded ³¹P NMR chemical shift which is shifted to extreme low field ($\delta^{31\text{P}} = 416.3$ (**17**); $\Delta(\delta^{31\text{P}}) = 240.9$ ^[44]), due to the impact of the silyl groups.^[53] The cyclic compound (**18**) synthesised in 2016 by Del Rio *et al.* features frontier molecular orbitals that support the idea of a Ge=P double bond, however, it was shown that its reactivity is that of a phosphinylidene stabilised germylene, very similar to that of N-heterocyclic germylenes, and that the strong Ge–P interaction arises from the strongly π -stabilising phosphanylidene moiety.^[50] On the contrary, Nesterov *et al.* showed, that their *germylene phosphinidene NHC complex* **19** undergoes reversible [2+2] cycloaddition reaction with diphenylketene, though the frontier molecular orbitals do not suggest the presence of π -bonding interaction between germanium and phosphorus.^[51] Most recently, Raiser *et al.* reported on the synthesis of a cationic compound (**20**) containing a Ge=P double bond. The bond length is in close proximity to those reported by Escudie *et al.* and Lee *et al.* (Ge=P = 216.3 pm).^[45, 52-53] Still, to the best of our

knowledge, small molecule activation, using germaphosphenes or other heavier multiply bonded Group14-Group 15 element compounds, was not achieved and reported to date.

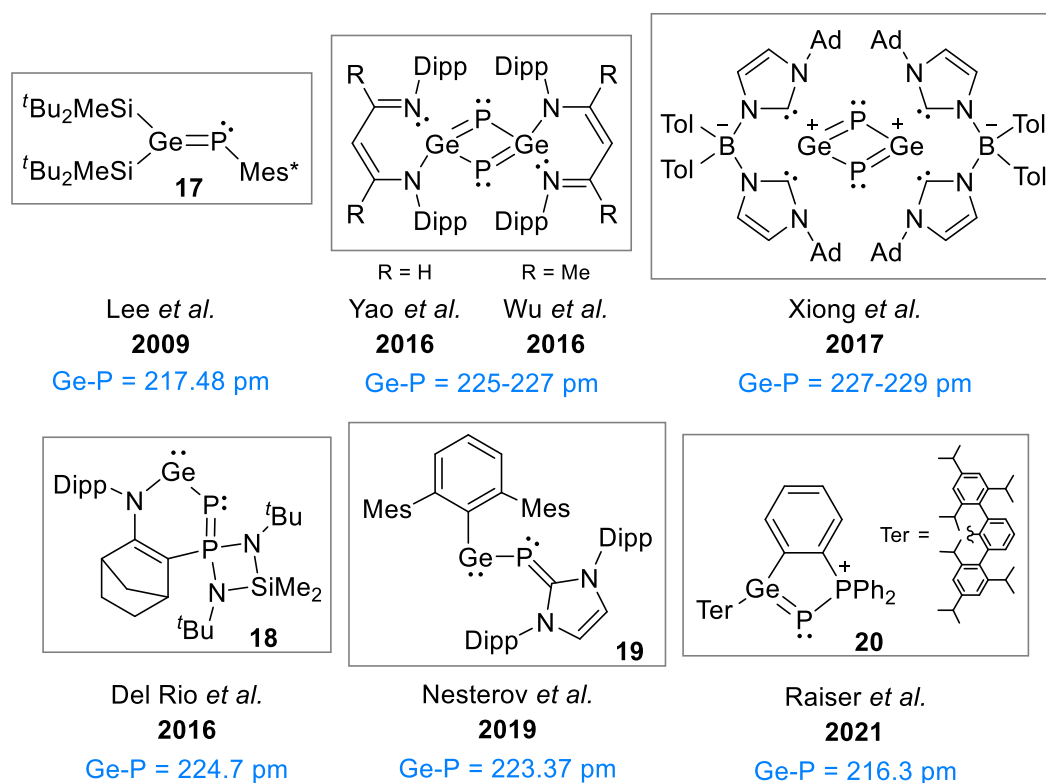


Figure 12 – Reported compounds exhibiting Ge=P double bonds or double bond character (Ad = adamantyl).

1.1.4 Accessing Main Group Heterofulvenes

A new type of an intramolecularly stabilised germynes was introduced by the group of Müller in 2016. Their hafnocena-bicyclohexene-germylene (hafnocena-BCH-germylene) **21** is stabilised by delocalisation of electrons from the remote double bond into the vacant p-orbital of the germanium atom through homoconjugation (Figure 13).^[54] This type of stabilisation had previously only been described for borane complexes and Group 14 element cations. In the following years, the authors introduced more, related compounds, including a hafnocena-BCH-silylene^[55] and a sila-BCH-silylene^[56]. The denotation as bicyclic tetrylenes was justified based on structural and NMR spectroscopic parameters. Saito and coworkers, however, reported on the related tin-based compound as a tin(0) butadiene complex.^[57]

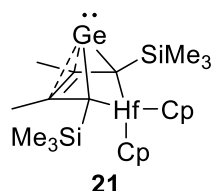
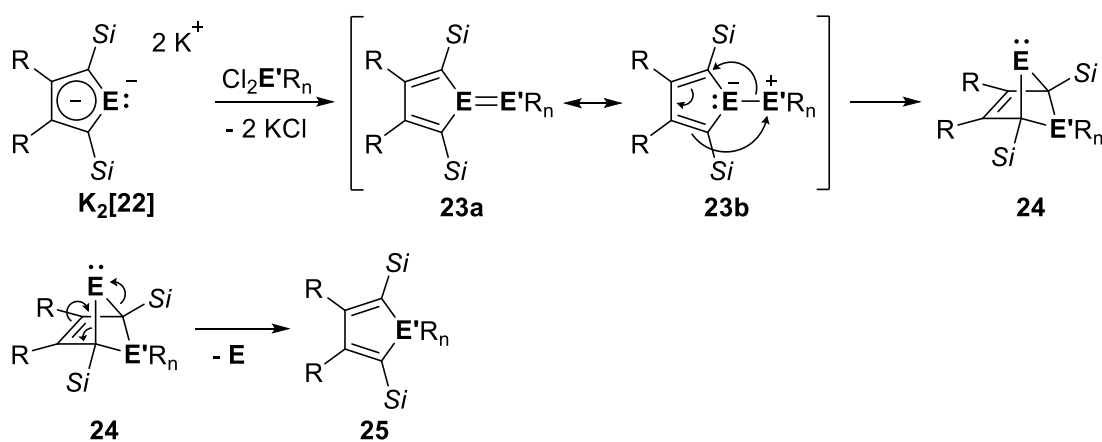


Figure 13 – The first example of a germylene, stabilised by homoconjugation.^[54]

The initial target within those studies was the synthesis of heavier fulvenes, derived from tetrolediide salts **K₂[22]**. Via double salt metathesis reaction upon combination with the respective element dihalogenide compounds (X_2ER_n), the heterofulvenes **23** were supposed to be obtained. However, they underwent rearrangement reactions and their isomers, BCH-tetrylenes **24**, were isolated. This particular mechanism was not only supported by DFT calculations, but moreover did the authors find evidence for the presence of a heterofulvene intermediate **23**, the isomer of a sila-BCH-silylene, by recording low-temperature NMR spectra.^[58] These heterofulvenes **23a** exhibit strongly polarised element-element bonds and are therefore best described in the corresponding ylidic resonance form **23b**. This also pictures their anticipated suitability for bond activation reactions (Scheme 5).

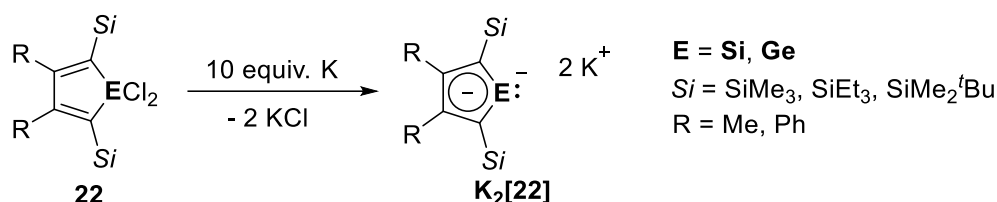


Scheme 5 – Mechanistic representation of the formation of BCH-tetrylenes **24** and elimination of the tetrel.^[58]

Moreover, in some cases the BCH-tetrylenes **24** are not stable. For a sila-BCH-germylene **24** ($E = \text{Ge}$, $E'R_n = \text{Si}(\text{SiMe}_3)_2$), the authors described the elimination of elemental germanium from the intermediate formed BCH-germylene, to give the corresponding silole **25** ($E = \text{Si}$) (Scheme 5).^[58]

The precursors (Scheme 6), dipotassium tetrolediides **K₂[22]**, occupy frontier molecular orbitals of the same symmetry and similar energy difference than tetrylenes. It was shown that the

relatively small HOMO-LUMO energy gap, compared to alkyl-substituted tetrolediide salts, is caused by the triarylsilyl groups in the 2,5-position. This makes these tetrolediides **[22]** particularly reactive.^[59] Nevertheless, the salt metathesis reaction seems to be the driving force regarding the reaction towards elementdichloride compounds.



Scheme 6 – Reduction of 1,1-dichlorotetroles **22** by potassium metal, to give the dipotassium tetrolediides **K₂[22]**.^[60]

Despite the above named reactions towards Group 4 and Group 14 element compounds, giving BCH-tetrylenes **24**, reactions of these 2,5-bis(trialkylsilyl) substituted tetrolediide salts **K₂[22]** towards lighter Group 4 element compounds, Group 3 and Group 13 based compounds as well as towards Lanthanide complexes are reported in the literature. Except the reaction towards boron-based reagents, where borole complexes of germanium **26** were formed, the respective element germole complexes **27a-e** were obtained (Figure 14).^[61-65]

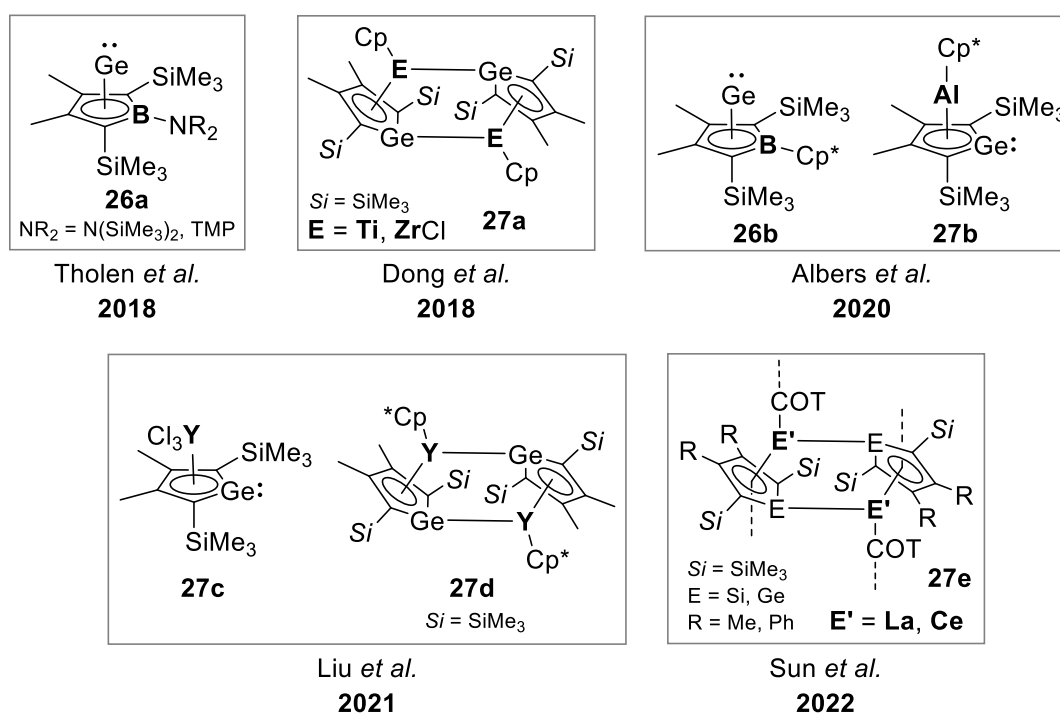
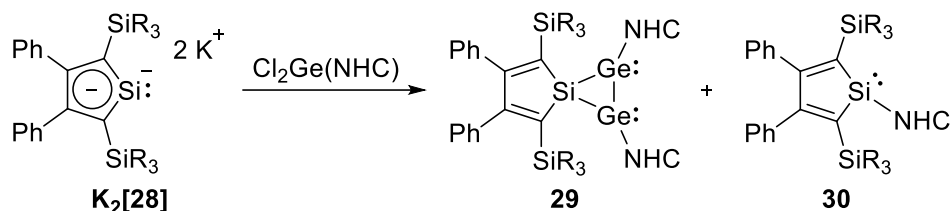


Figure 14 – Reported heterole complexes obtained from reactions of silole- and germole-diide salts **K₂[22]**.^[61-65]

Additionally, the reactivity of donor stabilised tetrylenes towards tetroldiide salts has previously been studied, using dipotassium siloleidiide **K₂[28]** (R = Me, Et) and NHC-stabilised germanium dichloride as precursors.^[66] There, instead of the targeted sila-germavinylidene, a NHC-stabilised three-membered digermylene **29** alongside the NHC-stabilised cyclic silylene **30** was obtained (Scheme 7).



Scheme 7 – Observed digermylene formation upon reaction of the siloleidiide salt **K₂[28]** with NHC stabilised germanium dichloride.

Up to that point, the studies were restricted to element dihalide precursors from the Groups 3, 4 and 13. In 2020, S. Kühn performed initial investigations on the reactivity of heteroleidiide salts **K₂[22]** towards Group 15 dihalides. Within those studies, the focus was on the reactivity of germelediide salt **K₂[31]** towards organodichlorophosphanes, targeting the synthesis of phospho-germapentafulvenes **32**. Phosphanes, however, are isolobal to donor stabilised tetrylenes, mentioned above (Figure 15).

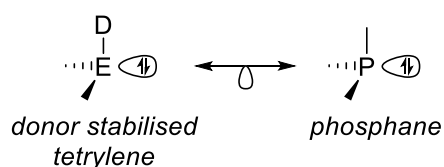
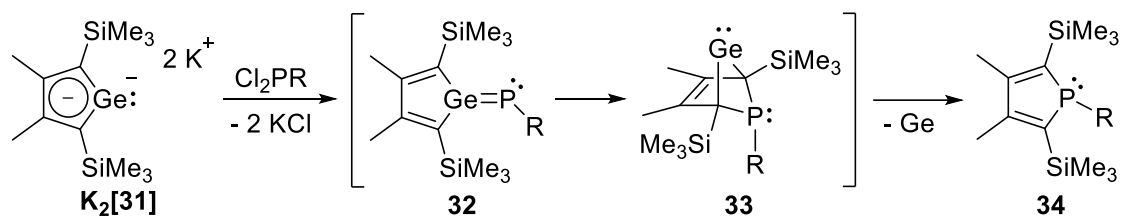


Figure 15 – Isolobal relation between donor stabilised tetrylenes and phosphanes.

The studies were mostly computational, concentrating on possible (other) products and the electronic effect of different substituents at the phosphorus atom on the structures. In general, the preference of the BCH structure **33** over the heterofulvene structure **32** was suggested for various substituents ($\Delta E = -71$ to -135 kJ mol⁻¹).^[67] Some experimental approaches were carried out as well, indicating the presence of phospho-BCH-germylenes **33** in the reaction mixture. However, the synthesis was on the one hand not selective and on the other hand, the above described germanium elimination reaction was observed upon attempts to isolate the contained phospho-BCH-germylenes **33**. Finally, the respective phospholes **34** were isolated (Scheme 8).^[67]



Scheme 8 – Reported reactivity of dipotassium germylene **K₂[31]** towards organodichlorophosphanes.

2 Motivation and Objective

In search for more sustainable solutions, the replacement of transition metal complexes in bond activation reactions has gained attention and interest over the past decades. The substitution with less toxic, cheaper, more earth abundant main group compounds, however, is challenging as it requires suitable design and fine tuning of the main group compounds to mimic transition metal complexes.^[4, 68-70] Since the first reports on isolable low-coordinated main group compounds like tetrylenes and heteroalkenes were published, the knowledge on stabilisation strategies has greatly expanded, enabling their application in bond activation reactions. Today, there are numerous reports on the successful activation of small molecules by low-coordinated main group compounds. However, the greatest challenge remains the subsequent liberation of the substrates, which is essential for further processing.

Against this background, our group aims for the synthesis of new heterofulvenes and tetrylenes. The targeted heteronuclear heavier alkenes exhibit highly polarised element-element double bonds, generally suitable for bond activation reactions. Indeed, past studies have shown, that the synthesis of heterofulvenes **23**, derived from tetrolediide salts $K_2[22]$ and element dichlorides, is possible. Evidence for the presence of the heterofulvene was provided by low temperature NMR measurements.^[55] However, their isolation was not achieved. Instead, in agreement with the results of density functional calculations, rearrangement reactions occurred at ambient temperature to give the more stable isomers. Depending on the precursor chosen, BCH-tetrylenes **24** (Group 4 and Group 14) or element-heterole complexes **26** and **27** (Group 13) were obtained.^[54-55, 58, 61-62] Still, as those isomers exhibit stable low-coordinated main group atoms, they are interesting compounds themselves against the background considered here (Figure 16).

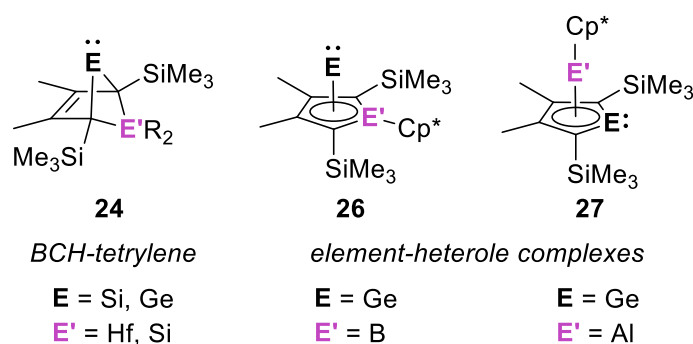
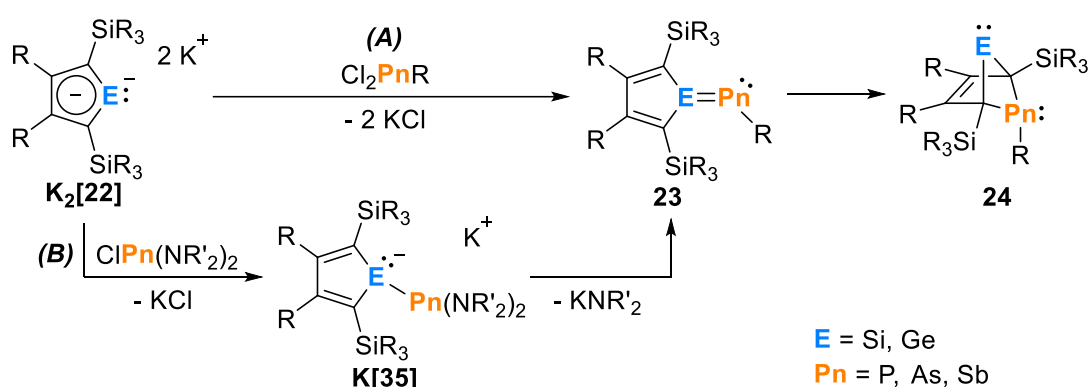


Figure 16 – Selected compounds obtained upon rearrangement reactions of heterofulvenes **23**.

Within the present work, the research on this field of chemistry will be expanded to the so far mostly unconsidered Group 15 based compounds. Using pnictogen dihalide precursors, the synthesis of heterofulvenes **23**, featuring $E=Pn$ double bonds is targeted. Starting with the combination of germanium and phosphorus-based precursors, the synthesis will then be extended to heavier and lighter Group 14 and 15 homologues: instead of germonolediide $K_2[31]$, also other heterole precursors will be used and phosphorus-based precursors will be complemented by arsenic- and antimony-based precursors, potentially giving a variety of new heterofulvenes **23**, which might rearrange and give the corresponding BCH-tetrylenes **24** (Scheme 9).



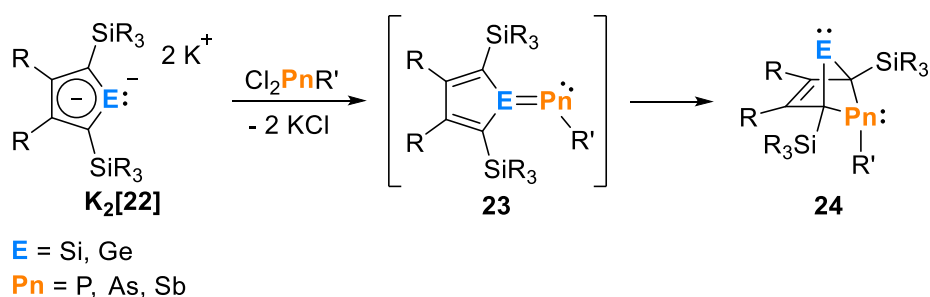
Scheme 9 – Targeted synthesis of pnicta-BCH-tetrylenes **24**.

Two synthetic strategies are scheduled. The first one **(A)** is the established double salt metathesis reaction, using dipotassium salts of tetrolediianions $K_2[22]$ and dichloro(organo)pnictogens as precursor. Strategy **(B)** is supposed to proceed via diaminopnictyltetrolide salts $K[35]$, synthesised from tetrolediide salts $K_2[22]$ and diaminopnictogen chlorides. Subsequent K elimination of potassium amide results in the formation of the heterofulvene **23**. Initial computational studies on this field predicted the rearrangement of the thereby obtained pnicta-tetrel-heterofulvenes **23** to the corresponding pnicta-BCH-tetrylenes **24** (Scheme 9).

Once successfully synthesised, the properties and the reactivity of this new compound class will be explored. Thereby, the ability to activate small molecules, as well as the ligating properties of the tetrylene onto transition metal complexes are of interest. Additionally, due to the second lone pair of electrons present at the pnictogen, bidentate coordination or the coordination of two different metal centers will be considered. The studies will be supported and complemented by quantum chemical computations.

3 Results and Discussion

In the present work, the reaction of 2,5-bis(trialkylsilyl)tetrolediide salts (**E** = Si, Ge) $K_2[22]$ towards organopnictogen dichlorides (**Pn** = P, As, Sb), targeting the synthesis of pnicta-BCH-tetrylenes **24**, is described (Scheme 10). However, the focus was set on the reaction of germolediide salts towards aminodichlorophosphanes. The resulting aminophospha-BCH-germylenes are introduced in Chapter 3.2. Here, their synthesis as well as their NMR spectroscopic and structural properties are analysed in detail. The transferability to heavier homologues (**Pn** = As and Sb) as well as the change from germole to silole (**E** = Si) are discussed in Chapter 3.3. Reactivity studies on aminophospha-BCH-germylenes are provided in Chapter 3.4.



Scheme 10 – General synthesis strategy for pnicta-BCH-tetrylenes **24** via double salt metathesis reaction.

Besides the above described reaction, the reactivity of germolediide salts towards diaminochlorophosphanes ($ClP(NR_2)_2$) was explored in a small project. The results are presented in Chapter 3.5.

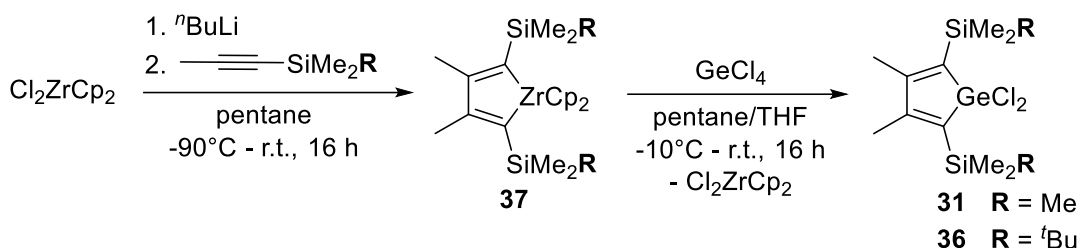
3.1 Synthesis of the Precursors

3.1.1 1,1-Dichloro-2,5-Bis(trialkylsilyl)tetroles and Their Tetrolediide Salts

The synthesis of 1,1-dichlorotetroles (**E** = Si, Ge) and their reduction by alkali metals, to give the corresponding tetrolediide salts, is well established in the literature^[59, 71-84] and will therefore not be discussed in great detail here. It was furthermore shown, using the example of a silolelediide, that the introduction of trialkylsilyl groups in the 2,5-position leads to a smaller HOMO-LUMO energy gap, which makes these compounds particularly reactive.^[59] Hence, 2,5-bis(trialkylsilyl)tetrolediide salts $K_2[22]$ are useful precursors for a variety of compounds, e.g. BCH-tetrylenes **24**.^[56]

Germoles

Within this work, mainly 1,1-dichloro-2,5-bis(trialkylsilyl)germole **31** (R = Me) and **36** (R = *t*Bu) were used as precursor. Their synthesis proceeds via element exchange reaction at a zirconacyclopentadiene **37**.^[71, 75] C. Reinhold introduced a one-pot synthesis for 1,1-dichloro-2,5-bis(trialkylsilyl)germole **31** and **36** where the zirconacyclopentadiene **37** is *in situ* reacted with germanium tetrachloride, which facilitated their synthesis (Scheme 11).^[85] Following this one-pot synthesis, the 2,5-bis(trimethylsilyl)germole **31** was obtained in good yields (79%). The 2,5-bis(*tert*butyldimethylsilyl)germole **36**, however, was obtained in a yield of 18%.^[59, 85]



Scheme 11 – Synthesis of 1,1-dichloro-2,5-bis(trialkylsilyl)germole **31** and **36** in a one-pot synthesis.^[85]

The synthesis of the 2,5-bis(*tert*butyldimethylsilyl)germole **36** was optimised. L. Bührmann showed that it proved to be reasonable to not do the one-pot synthesis described above, but to isolate the zirconacyclopentadiene **37** (R = *t*Bu) (89%^[86]). Afterwards, the element exchange reaction with germanium tetrachloride was carried out in THF only. After workup and recrystallization from pentane, germole **36** was isolated in 32% yield.^[86] The yield was again more than doubled within this work by the use of a mixture of pentane and diethyl ether (1:1), instead of only pentane, for the workup. Here, the crude product was obtained in a yield of 83%. Recrystallisation from pentane at -75°C gave germole **36** in a yield of 70%.

Silole

1,1-Dichloro-2,5-bis(triethylsilyl)silole **28** (Figure 17) was already available in the group from previous work. It was synthesised following an established multiple-step synthesis, refined by Reinhold^[85], which is based on work by Tamao *et al.*^[87]

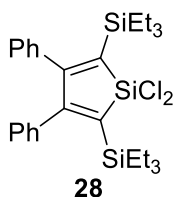
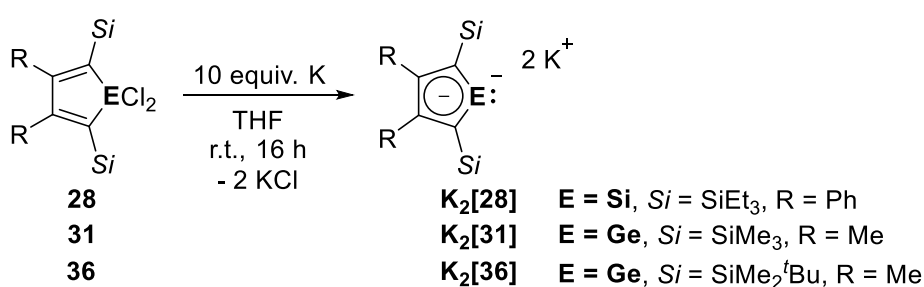


Figure 17 – 1,1-Dichlorosilole **28** used in this work.

Tetrolediide Salts

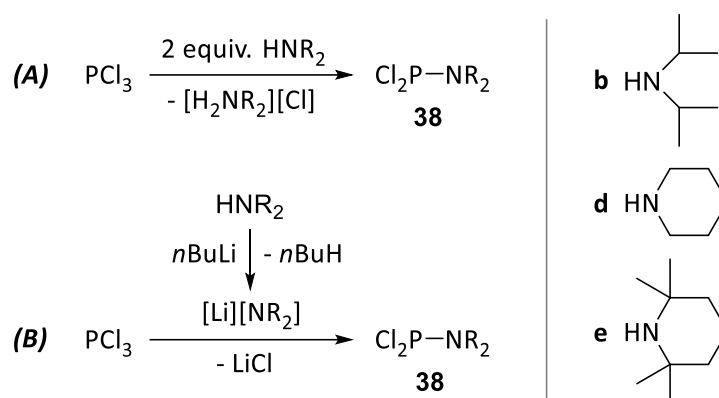
The reduction of 1,1-dichlorotetroles (**E** = Si, Ge) proceeds upon stirring with an excess of alkali metal.^[72-74, 84] For the herein used 2,5-bis(trialkylsilyl)tetroles **28** (**E** = Si), **31** (**E** = Ge) and **36** (**E** = Ge), the use of potassium was established.^[59] Carried out in THF or diethyl ether, the reduction takes 1-2 days. A colour change to dark red/greenish and the formation of a voluminous precipitate (KCl) indicates completion of the reaction. Full consumption of the dichlorotetrole can be ensured by NMR spectroscopy.^[59] Dipotassium tetrolediide solutions **K₂[28]** (**E** = Si), **K₂[31]** and **K₂[36]** (**E** = Ge) cannot be stored and should therefore be used *in situ* (Scheme 12).



Scheme 12 – Reduction of 1,1-dichloro-2,5-bis(trialkylsilyl)tetroles **28**, **31** and **36** using potassium metal.^[59]

3.1.2 Aminodichlorophosphanes

Within this work five aminodichlorophosphanes **38** were used, differing in sterical and electronic properties: dimethylamino- (**38a**), diisopropylamino (**38b**), dicyclohexylamino- (**38c**), piperidino- (Pip) (**38d**) and tetramethylpiperidinophosphane (TMP-phosphane) (**38e**). There are several known synthesis strategies for aminophosphanes. Aminodichlorophosphanes **38** are most commonly synthesised by addition of two equivalents of amine to one equivalent of trichlorophosphane. Under the formation of ammonium chloride, aminodichlorophosphanes **38** are formed (route **(A)** in Scheme 13).^[88-90] Alternatively, the amine can be deprotonated by addition of *n*-butyllithium (^{*n*}BuLi) to give the lithium amide which is then reacted with an equimolar amount of PCl₃ (route **(A)** in Scheme 13).^[90-91] This especially is advantageous or even required for more sterically demanding amines.



Scheme 13 – Synthetic routes (A) and (B) for aminodichlorophosphanes **38**.

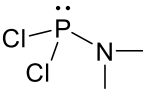
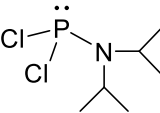
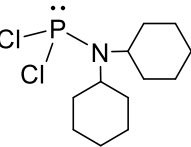
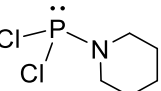
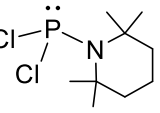
Diisopropylaminophosphane **38b** (78%; lit.: 68%^[89]) and piperidinophosphane **38d** (82%; lit.: 62%^[89]) were synthesised following route (A), while TMP-phosphane **38e** was synthesised via the lithium amide route (B). For this aminophosphane it can be noted that route (A) and (B) work equally well (88%; lit. (via route (A)): 90%^[89]). Dimethylaminophosphane **38a** was purchased from a commercial source. Dicyclohexylaminophosphane **38c** was used in previous works and was therefore already available in the group. The ³¹P NMR spectroscopic data of each aminodichlorophosphane is given in Table 1 for comparison. Those five amino-substituents were chosen as they exhibit slightly different electronic and steric properties, impacting the nucleophilicity of the phosphorus atom. To internally compare the aminodichlorophosphanes **38**, their buried volume as well as the substituent effect of the amino-function, compatible with Hammett σ constants, were calculated.

The buried volume was calculated via the *SambVca 2.1* web program^[92], using DFT optimised structures. The program calculates the sterical demand of electron donors based on coordination to a metal centre. It was originally designed to calculate the sterical demand of NHC's but can now be applied to all kinds of donors. The model assumes a metal that exhibits a fixed coordination sphere and a fixed ligand-metal distance. The program calculates the percentage of the spherical volume that is buried by the ligand (%V_{bur}).^[92-94] Here, the phosphorus atom of each aminodichlorophosphane **38** was coordinated to the metal centre. Within this series, dichloro(TMP)phosphane **38e** (%V_{bur} = 39.3) is predicted to be the most sterically demanding phosphane while dichloro(piperidino)phosphane **38d** (%V_{bur} = 27.3) is the least sterically demanding phosphane (Table 1).

The substituent constant (σ_p) of the amino function (NR₂) was calculated using the *Calculation of Substituent Properties* web program.^[95] Here, no structural optimisation was needed beforehand. The program was designed to calculate the electron donating or withdrawing ability

(according to Hammett σ constants) of substituents for which no experimental Hammett constants^[96] are available.^[95] For the series of amino-substituents used in this work counts: dicyclohexylamino (**c**) is the weakest ($\sigma_p = -0.15$) electron donating substituent, while TMP (**e**) is the strongest ($\sigma_p = -0.78$) electron donating substituent. Therefore, the latter enhances the nucleophilic character of the phosphane the most (Table 1).

Table 1 – Buried volume (% V_{bur}), substituent constant (σ_p) and ^{31}P NMR chemical shift (δ , recorded in benzene- d_6) of the aminodichlorophosphanes **38a-e** used in this work.

					
	38a	38b	38c	38d	38e
$\%V_{bur}$	28.1	35.3	29.8	27.3	39.3
σ_p	-0.69	-0.26	-0.15	-0.59	-0.78
$\delta^{31\text{P}}$	165.3	169.0	169.3	157.2	163.2

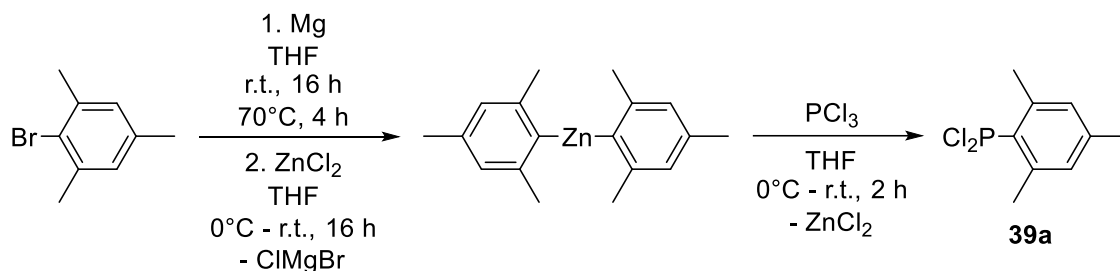
Comparing the ^{31}P NMR chemical shift of the different aminodichlorophosphanes **38** it can be noted that the phosphanes bearing a non-cyclic amino-substituent (NMe₂ (**a**), NⁱPr₂ (**b**), NCy₂ (**c**)) are shifted to lower frequencies than those bearing a cyclic amino-substituent (Pip (**d**), TMP(**e**)). However, no direct correlation of the sterical or electronic parameters to the ^{31}P NMR chemical shift was observed here.

3.1.3 Aryldichlorophosphanes

The synthesis of aryldichlorophosphanes **39** typically proceeds differently than that of aminodichlorophosphanes **38**. However, their synthesis is well known to the literature as well and is mostly, depending on the precursor, carried out via halogen metal exchange reactions. Within this work, two aryldichlorophosphanes **39a-b** were synthesised to explore their reactivity towards the heteroleidiide salts. Since it was shown in earlier studies^[67] that by using dichlorophenylphosphane, no clean or selective reaction was achievable, two dichlorophosphanes with more sterically demanding aryl substituents were synthesised: mesityl (Mes) (**a**) and 2,6-dimesitylphenyl (terphenyl; ^{Mes}Ter) (**b**).

Dichloro(mesityl)phosphane

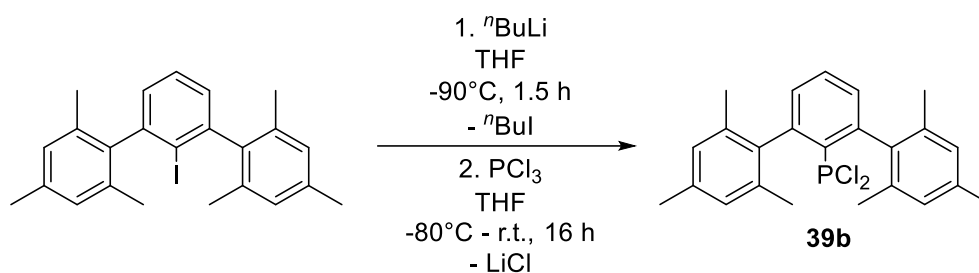
Dichloro(mesityl)phosphane **39a** was synthesised in a two-step reaction^[97-98]: Bromomesitylene was reacted with magnesium turnings to generate the Grignard reagent which was subsequently reacted with zinc(II) chloride. Then, upon element exchange reaction with trichlorophosphane, dichloro(mesityl)phosphane **39a** was obtained in a yield of 64% (lit.: 62%^[98]) (Scheme 14).



Scheme 14 – Synthesis of dichloro(mesityl)phosphane **39a** following an established procedure.^[97-98]

Dichloro(terphenyl)phosphane

Dichloro(terphenyl)phosphane (**39b**) was synthesised via a halogen metal exchange reaction. Iodoterphenyl, which was already available in the group, was reacted with ⁿBuLi to undergo the halogen metal exchange reaction which was followed by a salt metathesis reaction using trichlorophosphane. The product, dichloro(terphenyl)phosphane (**39b**), was obtained in a yield of 28% (lit.: 34%^[99]) (Scheme 15).



Scheme 15 – Synthesis of dichloro(terphenyl)phosphane **39b** via a literature procedure.^[99]

Both aryldichlorophosphanes **39** were characterised spectroscopically. The data is in good agreement with the literature.^[98-99] Interestingly, the ³¹P NMR signals of both compounds showed the isotope effect of the chloride substituents on the NMR chemical shift, which was not reported in the literature. Each product signal consists of three single signals of the approximate intensity ratio 100 : 64 : 10 (calculated values) (Figure 18). Within this work, these were the only two dichlorophosphanes where this effect was observed.

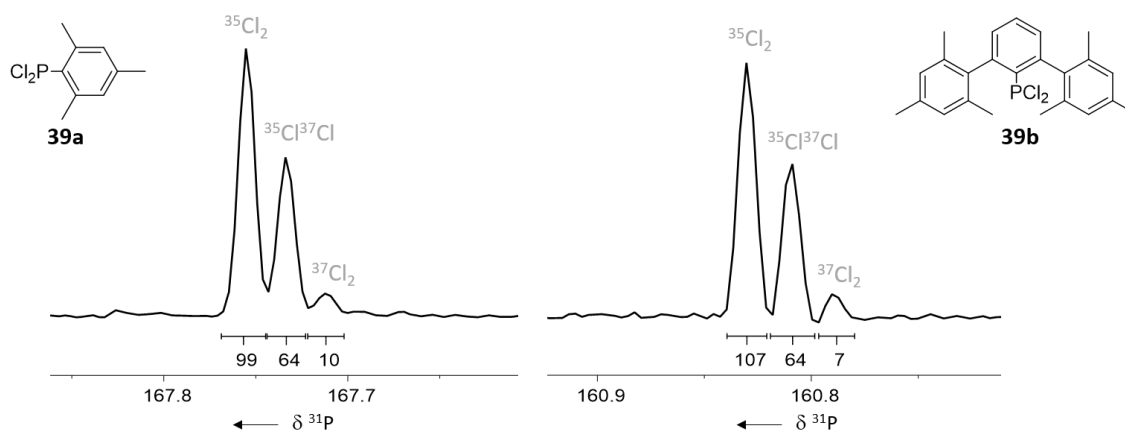


Figure 18 - Sections from the $^{31}\text{P}\{^1\text{H}\}$ NMR spectra (202.3 MHz, 305 K, benzene- d_6) showing each of the two aryldichlorophosphane **39** signals featuring the isotope effect of the chloride substituents on the NMR chemical shift.

3.1.4 Dichloroarsines

The aryldichloroarsines **40a-b** used within this work were kindly sent to us by A. Orthaber from Uppsala University, Sweden (Figure 19).^[100] The phenyl derivative **40a** can, for example, be prepared by comproportionation reactions of trichloroarsine and triphenylarsine. More selective reactions, however, are achieved using phenyl transfer reagents like tetraphenyl tin.^[101] Alternatively, it can be prepared from phenylarsonic acid, hydrochloric acid and sulfur dioxide.^[102-103]

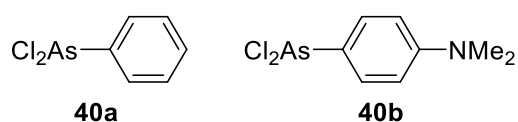


Figure 19 – Aryldichloroarsines **40** used within this work.^[100]

Note: Great care must be taken when working with these compounds as they are vesicants!^[102]

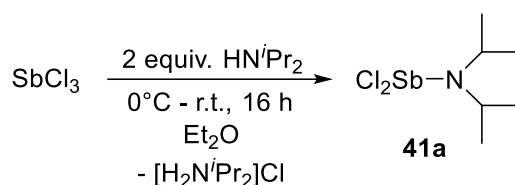
3.1.5 Dichlorostibanes

Going to even heavier homologues, two chlorostibanes **41** were synthesised. Here, one amino- (**a**) and one aryl-substituted (**b**) stibane were chosen.

Dichloro(diisopropylamino)stibane

Dichloro(diisopropylamino)stibane **41a** has not been reported on in the literature so far. Its synthesis was adapted from the synthesis of its lighter phospho- and arsa-homologues^[89, 104]: two equivalents of diisopropylamine were reacted with antimony trichloride (Scheme 16). After

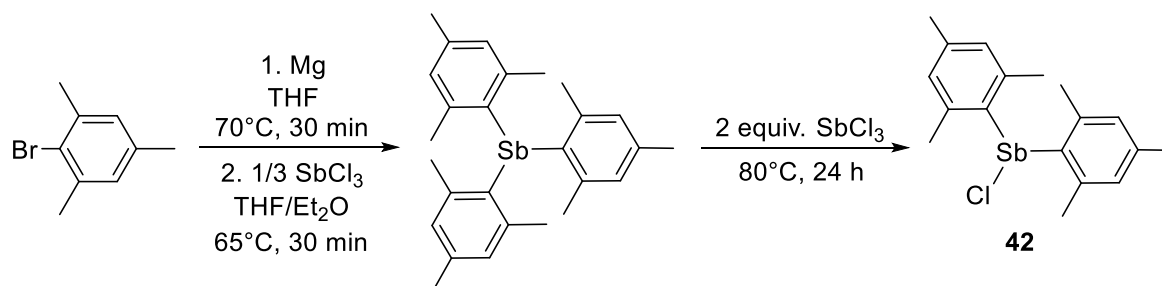
workup, the dichlorostibane was obtained in a yield of 32%. The product was characterised by NMR spectroscopy. It needs to be mentioned that it was also attempted to synthesise the product via the lithium amide route (see Scheme 13, **(B)**) as it is described for the related, literature known dichloro(*di**tert*butylamino)sibane.^[104] This however, lead to a product mixture of the mono- and di-substituted sibane, from which the dichlorostibane **41a** could not be isolated.



Scheme 16 – Synthesis of dichloro(*di*isopropylamino)sibane **41a**.^[89, 104]

Dichloro(mesityl)sibane

Dichloro(mesityl)sibane (**41b**) was attempted to be synthesised following literature procedures.^[105-106] Deviating from the mesitylphosphane **39a** synthesis, the heavier homologue cannot be directly synthesised. Here, trimesitylstibane was synthesised in a first step. Therefore, antimony trichloride was added to a freshly prepared solution of mesitylgrignard reagent (three equivalents). The product was then mixed with two equivalents of antimony trichloride. Heating the mixture of the two solids resulted in a comproportionation reaction and gave what was supposed to be dichloro(mesityl)sibane (**41b**), in a yield of 79% (lit.: 78%^[105]). The NMR spectroscopic data matches the literature.^[105-106] However, additional analysis by mass spectrometry was performed and it was found out that indeed, the chlorodimesitylstibane **42** was isolated.

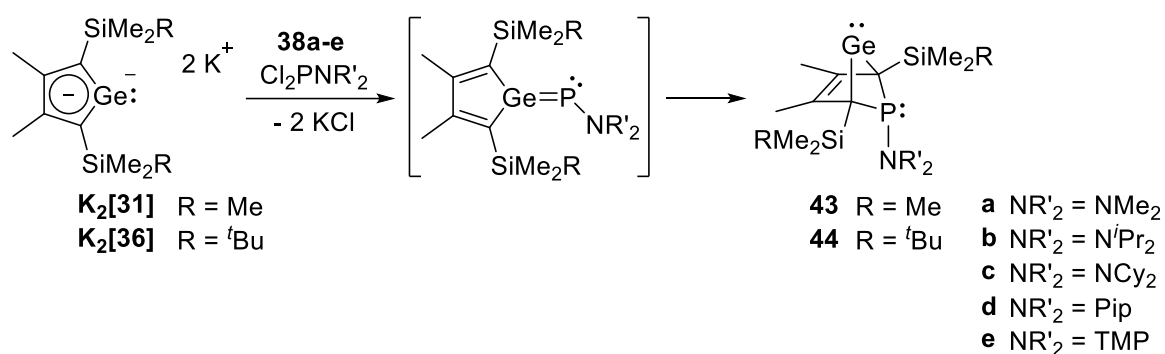


Scheme 17 – Two-step synthesis of chloro(*dimesityl*)sibane **42** via trimesitylstibane.^[105-106]

It was assumed that the sublimation of antimony trichloride on top of the reaction flask interfered with the equilibrium and drove the reaction towards the dimesitylstibane **42** instead of the targeted mesitylstibane **41b**.

3.2 Aminophospha-BCH-Germynes

Aminophospha-BCH-germylenes **43-44** (also referred to as *germylenes* in this work) are synthesised via a double salt metathesis reaction upon addition of aminodichlorophosphanes **38** to dipotassium germolediide solutions **K₂[31]** and **K₂[36]**. They exhibit interesting features, including two accessible lone pairs (P and Ge). Both, germylenes and phosphanes are commonly known ligands, potentially making this compound class an interesting bidentate or dual acting ligand for transition metal complexes. Herein, a facile, clean synthesis of this novel family of compounds is described (Scheme 18).

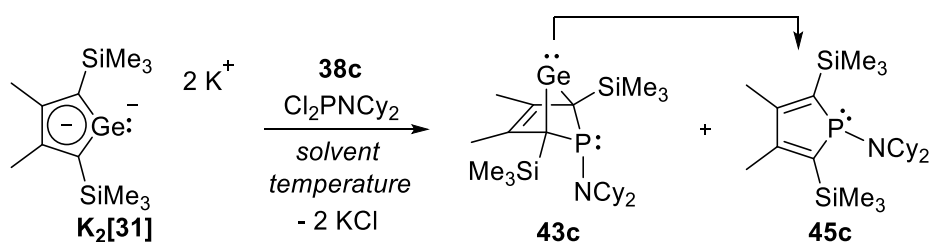


Scheme 18 – General synthesis of aminophospha-BCH-germylenes **43a-e** and **44a-e**.

3.2.1 Synthesis

3.2.1.1 Optimisations

To start off the synthesis of various aminophospha-BCH-germylenes **43-44**, the reaction of dipotassium 2,5-bis(trimethylsilyl)germolediide **K₂[31]** towards dicyclohexylamino-phosphane **38c** was studied representatively. The main focus here was to find conditions that suppress the formation of side products and minimise the formation of the follow-up product, the corresponding aminophospholes **45**. Therefore, suitable reaction conditions needed to be established, giving only the germylene **43c** (and its secondary product, phosphole **45c**) (Scheme 19).



Scheme 19 – Synthesis optimisations showcased for the reaction of dipotassium germolediide **K₂[31]** with dicyclohexylaminophosphane **38c**.

To analyse and compare the variations of solvent, temperature and sequence, $^{31}\text{P}\{^1\text{H}\}$ NMR spectra were recorded and the germylene **43c** and phosphole **45c** signals were integrated. The sum of each set of integrals was set to 100% to allow facile comparison of the reactions (phosphole to germylene ratio). If not otherwise stated in the text, the formation of byproducts was below 5%. A typical $^{31}\text{P}\{^1\text{H}\}$ NMR spectrum is shown in Figure 20. It displays the mixture obtained upon carrying out the reaction under conditions **A** (Table 2).

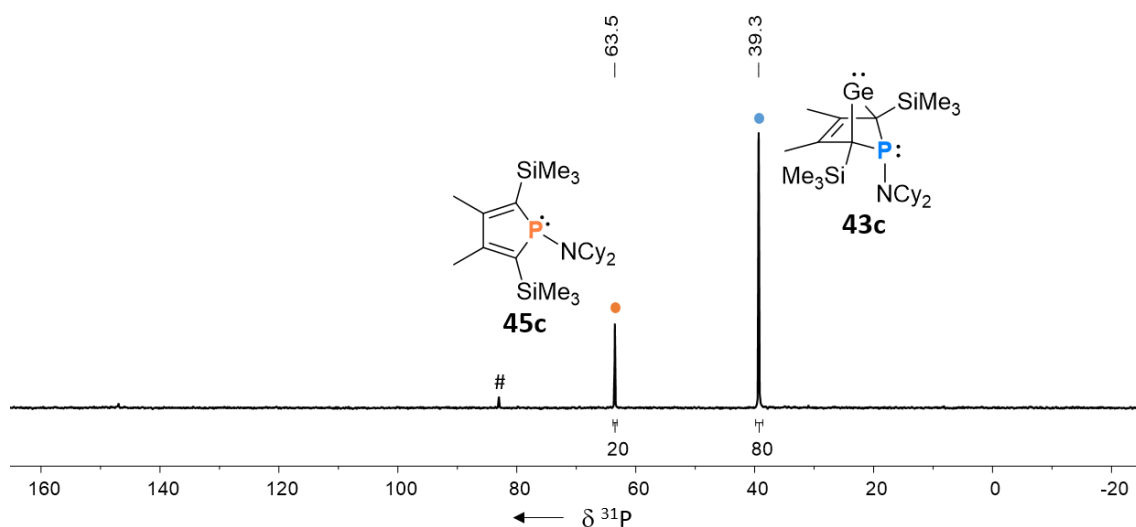


Figure 20 – $^{31}\text{P}\{^1\text{H}\}$ NMR spectrum (202.3 MHz, 305 K, THF) of the product mixture using conditions **A** (# = impurity).

Variation of the Temperature

Within the variations **A–D**, the temperature of the cold bath, cooling the germyliide [**31**] solution, was altered from room temperature to -80°C . Thereby, the aminophosphane **38c** solution was always added in one batch to the reaction flask: Carrying out the reaction at room temperature (**B**, ratio 73:27) was found to be the most ineligible variation, as it resulted in the formation of several byproducts additional to germylene **43c** and phosphole **45c**. It was assumed that the reaction proceeded too fast and therefore uncontrolled. Overall, the reaction proceeded much cleaner and yielded a better phosphole to germylene ratio at lower temperature (**A**, **C** and **D**). However, the reaction should also not proceed too slow, as concluded after lowering the reaction temperature to -80°C : the reaction seemed to be delayed at this temperature (**D**, ratio 52:48), which again favoured the formation of another unidentified compound with a ^{31}P NMR resonance at about $\delta^{31}\text{P} = 82$. To conclude this series of experiments, keeping the reaction temperature between -30°C (**C**, ratio 30:70) and -50°C (**A**, ratio 20:80) provided the most reaction control and the best phosphole to germylene ratio (Table 2).

Variation of the Solvent

The choice of solvents for reactions with dipotassium germolediides **K₂[31]** and **K₂[36]** is limited, as the precedent reduction of the dichlorogermole **31** works best in THF and diethyl ether.^[56] Still, there are differences in polarity which affect e.g. the solubility of salts like KCl and the germolediide salt **K₂[31]** and **K₂[36]** itself. Both salts are (partially) soluble in THF but not in diethyl ether. Therefore, using either the one or the other solvent can be expected to impact the reaction flow: Compared to the reaction in THF (**A**, ratio 20:80), the reaction carried out under the same conditions in diethyl ether (**E**) yields some side products at $\delta^{31\text{P}} = 30\text{-}35$ ppm and furthermore seems to enhance the rate of the formation of the phosphole **45c** (ratio 57:43) (Table 2). For those reasons, the reactions were carried out in THF.

Variation of the Sequence

To determine a suitable synthetic sequence for aminophospha-BCH-germylene **43c**, the order and speed of addition of the precursor solutions was varied (**F-H**): Dropwise addition of the aminophosphane **38c** solution to that of the germolediide **K₂[31]** was disadvantageous for the phosphole-to-germylene ratio (**F**, ratio 36:64) compared to the batch addition under the same conditions (**A**, ratio 20:80). Providing the germolediide salt **K₂[31]** and the aminophosphane **38c** as solids and dissolving in THF at -60°C (**G**, ratio 28:72) gives results similar to variation **C** (ratio 30:70), though there were small amounts of side products formed in the simultaneous approach. For variation **H**, the order was inverted: the germolediide **K₂[31]** solution was added to the aminophosphane **38c** solution, which was cooled in a cold bath. The result is the same as for variation **C** (ratio 30:70). This again demonstrates the delayed start of the reaction at lower temperature.

Table 2 – Variations **A-H** for finding optimal reaction conditions for the synthesis of germylene **43c**.

Variation	Temp.	Solvent	Addition	\int (45c)	\int (43c)
A	-50°C	THF	batch	20	80
B	r.t.	THF	batch	73	27
C	-30°C	THF	batch	30	70
D	-80°C	THF	batch	52	48
E	-50°C	Et ₂ O	batch	57	43
F	-50°C	THF	dropwise	36	64
G	-60°C	THF	simultaneous	28	72
H	-60°C	THF	inverted	30	70

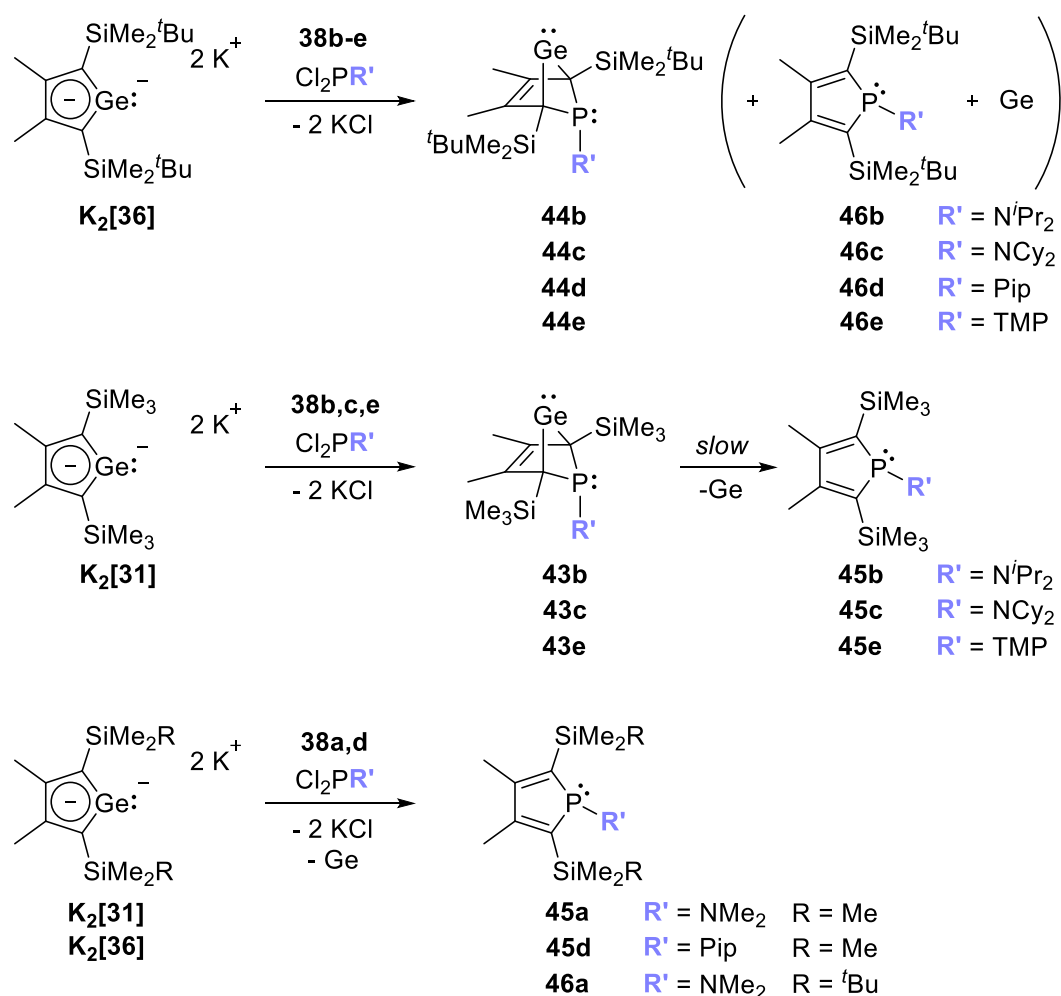
To summarise, for a successful synthesis of aminophospha-BCH-germylene **43c** it is crucial to work at temperatures between -30°C and -60°C and to provide stoichiometric amount of both reactants without time delay (batch addition).

3.2.1.2 Application onto Varying Precursors

Within this work, the five aminophosphanes **38**, shown in Chapter 3.1, were reacted with the germolediide salts **K₂[31]** and **K₂[36]**. As already discussed there, these amino-substituents slightly differ in size (see %V_{bur}-values^[92] in Table 1) and electron donating ability (see σ_p -values^[95] in Table 1) and thus behave differently regarding the reactivity towards germolediide salts **K₂[31]** and **K₂[36]**.

Regarding the formation and stability of aminophospha-BCH-germylenes **43-44**, it seems that not only the size of the silyl groups but also the nature of the amino substituent is of relevance. With two different germoles **31** and **36** and five different aminophosphanes **38a-e**, ten different reactions were examined. Comparing the results of those reactions points out the sensitivity towards sterical and electronic effects of the substituents. Scheme 20 displays the results of those ten reactions.

The diisopropylaminophosphane **38b** and the dicyclohexylaminophosphane **38c** behaved similar in the reaction towards both germolediide salts **K₂[31]** and **K₂[36]**. Overall, the mixtures of germylene **43b-c**, **44b-c** and phosphole **45b-c**, **46b-c** were obtained in good overall yields: With germole **31** as precursor, quantitative yields were obtained and about 80% yield were achieved with germole **36** as precursor. The formation of byproducts was usually not observed within these reactions and the amount of phosphole **45b-c**, **46b-c** was below 30% right after the reaction in all cases (Table 3). Similar results were obtained using the TMP-phosphane **38e** (Scheme 20). However, the reaction proceeded not as clean as with the non-cyclic aminophosphanes **38b** and **38c**. Moreover, the phosphole-to-germylene ratio (58 : 42 (**45e/43e**) and 15 : 85 (**46e/44e**)) is disadvantageous for the germylene (Table 3). At this point it may be anticipated that the enlarged steric bulk of the TMP-substituent (about 10% larger compared to the dicyclohexylaminophosphane) impacts the reaction rate, e.g. slows it down, possibly resulting in enhanced germanium elimination during the reaction.



Scheme 20 – Reaction of dipotassium germyliides **K₂[31]** and **K₂[36]** towards the different aminophosphanes **38**.

The reactions involving the piperidino- **38d** and dimethylamino-phosphanes **38a** differ from the other reactions. Compared to the aminophosphanes **38b** and **38c**, those precursors are smaller in size (% $V_{\text{bur}} = 27.3$ (**38d**), 28.1(**38a**)) but stronger electron donating ($\sigma_p = -0.59$ (**38d**), -0.69 (**38a**)) (Table 1). Using these two aminophosphanes, the respective aminophosphane-BCH-germylenes **43a+d**, **44a** were not obtained. Instead, only the respective phospholes **45a+d**, **46a** alongside other unidentified byproducts were identified by NMR spectroscopy. The formation of a dark precipitate furthermore indicated the elimination of germanium which presumably proceeds too fast to detect the germylene NMR spectroscopically. Here, a direct *germole to phosphole transformation*, similar to the *germole to silole transformation* reported by our group in 2018, seemed to take place.^[58] In addition, the reactions were mostly less selective. An exception was the reaction of germyliide salt **K₂[36]** with phosphane **38d**, which yielded 93% of germylene **44d** according to integration (Table 3). It needs to be noted that working with the piperidino-substituent, the formation of byproducts could, regardless of the germole used, distinctively be reduced by carrying out the reaction in diethyl ether.

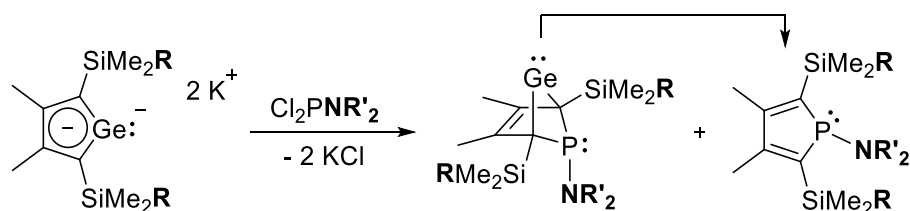


Table 3 – Overview of the obtained phosphole : **germylene** ratio for each reaction. The overall yield is given in parenthesis. (* = The reaction was only carried out once. # = The crude product was filtered over silica gel before the yield was determined. + = The product mixture contains impurities that could not be removed.)

		a (NMe ₂)	b (N ⁱ Pr ₂)	c (NCy ₂)	d (Pip)	e (TMP)
45 / 43	ratio	100 : 0	30 : 70	25 : 75	100 : 0	58 : 42
(R = Me)	(yield)	(50%) ^{#+}	(100%)	(95%)	(95%) ⁺	(n.d.) ⁺
46 / 44	ratio	100 : 0	3 : 97	2 : 98	7 : 93	15 : 85 [*]
(R = ^t Bu)	(yield)	(70%) ^{#+}	(79%)	(78%)	(71%) ⁺	(73%) ⁺

3.2.2 Structural Features of Aminophospha-BCH-Germynes

A pentane solution of germylene **43b** and phosphole **45b** was kept at -20°C for several days to afford colourless crystals of germylene **43b**, suitable for single crystal XRD analysis (Figure 21).

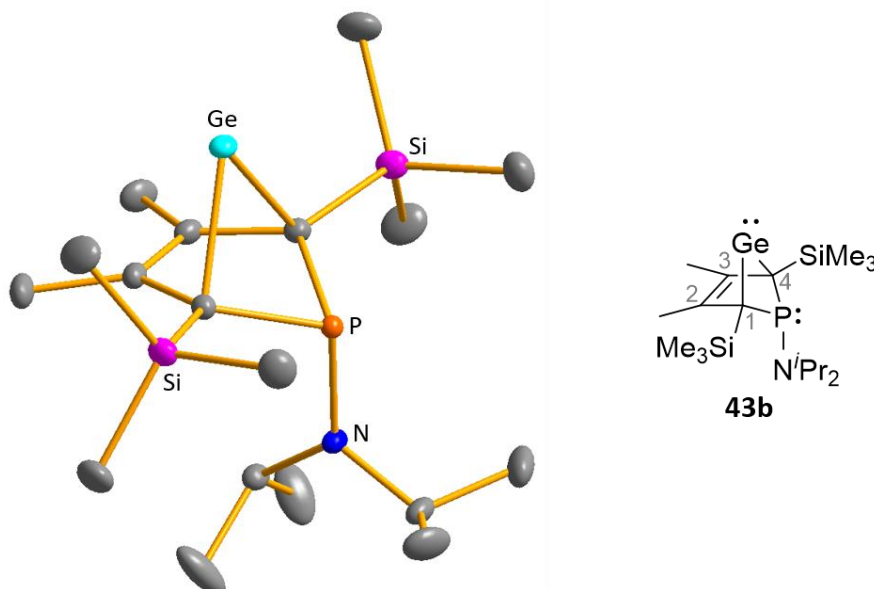


Figure 21 – Molecular structure of germylene **43b** in the crystal. Space group Pnma. Thermal ellipsoids at 50% probability. Hydrogen atoms are omitted for clarity.

The molecular structure is symmetric featuring a mirror plane spanned by the Ge, P and N atoms. The structural features confirm the analysis done by NMR spectroscopy: germylene **43b** possesses a bicyclohexene structure. The C²-C³ bond (142.3 pm) is shorter than the C¹-C² bond

(146.5 pm), but still longer than a typical C=C double bond (134 pm).^[107] The values however, are almost identical to those of the related hafnocena-BCH-germylene (Table 4).^[54] The Ge-C¹ bond of germylene **43b** (216.3 pm) is elongated compared to the sum of the single bond radii (196 pm).^[108] The Ge-C² distance (219.6 pm) is only slightly larger than the Ge-C¹ distance (216.3 pm), suggesting interaction of the C²-C³ double bond and the germanium atom as well. This so called homoconjugation, the delocalisation of π -electrons into the vacant germanium p-orbital (Figure 22), was also suggested for the hafnocena-BCH-germylene, though in that case, the Ge-C¹ bond is shorter (210.0 pm) and the Ge-C² distance is significantly larger (226.7) (Table 4).^[54]

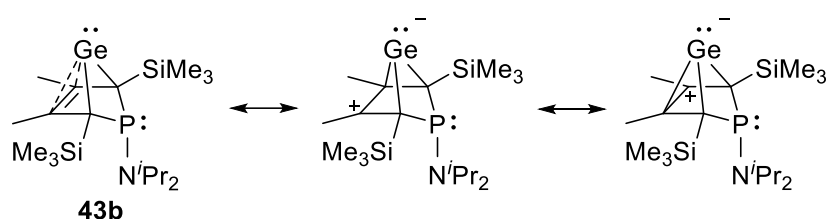


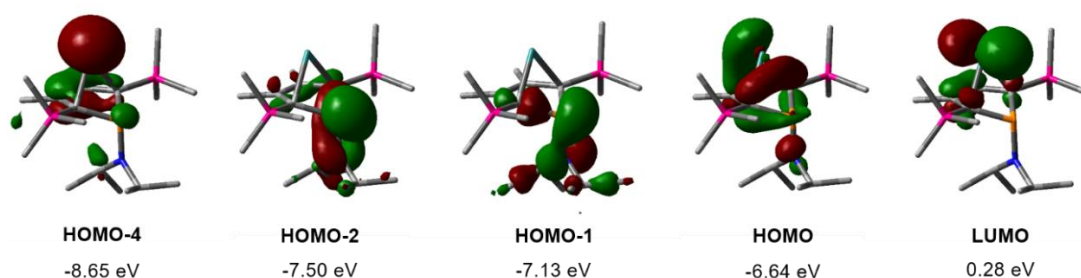
Figure 22 – Resonance structures of **43b**, describing the homoconjugative interaction in phospho-BCH-germylenes.

The C¹-Ge-C⁴ angle in germylene **43b** is $\alpha(\text{Ge}) = 70.3^\circ$ which is a rather acute angle compared to other cyclic germylenes^[16, 109-110], which are more in the range of the hafnocena-BCH-germylene **21** ($\alpha(\text{Ge}) = 85.0^\circ$)^[54] or even wider. The P-C^{1/4} bonds are within the expected range of phosphorus-carbon single bonds (186 pm^[108]). The phosphorus atom is, as typical for trivalent coordinated phosphorus atoms, pyramidalised ($\Sigma(\text{P}) = 302.3^\circ$), underlining the the lack of delocalisation of its lone-pair electrons into the backbone. The observed planarisation of the nitrogen atom in germylene **43b** (360.0°) as well as the short P-N bond (170.1 pm) can be assigned to negative hyperconjugation as studied and described by Haaland *et al.*^[111-112] (Table 4).

Table 4 – Selected bond lengths and bond angles of the molecular structure of germylene **43b**, the corresponding calculated structure and those of hafnocena-BCH-germylene **21**^[54].

	43b	43b (calc)	21 ^[54]
bond lengths [pm]			
C ¹ –C ²	146.53(6)	146.2	148.3(8)
C ² –C ³	142.33(8)	142.0	142.5(8)
C ¹ –Ge	216.32(4)	216.3	210.0(7)
C ² –Ge	219.64(5)	220.6	226.7(6)
C ¹ –P	184.11(4)	186.0	-
P–N	170.18(7)	172.6	-
bond angles [°]			
α(Ge)	70.347(14)	70.1	85.0(2)
Σ(P)	302.3	300.1	-
Σ(N)	360.0	358.3	-

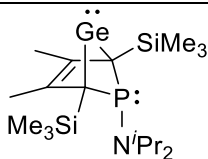
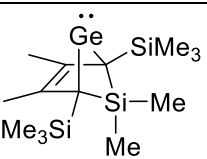
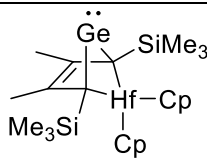
In general, the molecular structure and the optimised structure of germylene **43b** are in good agreement. The calculated bond lengths deviate from those found in the molecular structure by 1.5% or less, showing that the experimental structure is well represented by the calculated one. Selected frontier molecular orbitals of germylene **43b** are shown in Figure 23. The delocalisation of π -electrons of the C²=C³ bond to the germanium atom is depicted by the HOMO (homoconjugation). The above-mentioned interaction of the nitrogen lone pair with the antibonding P–C^{1/4} orbital is indicated by the HOMO-2. Both, the HOMO-2 and the HOMO-1 show contribution from the phosphorus lone pair. The HOMO-4 represents the lone pair at germanium as it shows large contributions from the germanium atom. With regards to ligating properties of phospho-BCH-germylenes **43-44** to transition metal centers, bidentate coordination, as considered in the beginning, might not be possible as those two orbitals are oriented in an angle of approximately 60° to each other. Coordination onto two (different) metal centers might nevertheless be possible (Figure 23).

**Figure 23** – Frontier molecular orbitals of germylene **43b** (M06-2X/6-311+G(d,p); isodensity value 0.04).

The properties of germylene **43b** were compared to those of related compounds: the hafnocena-BCH-germylene **21** and a hypothetical sila-BCH-germylene **47**. In that respect, the hafnocena-BCH-germylene **21** was optimised within these studies on the herein used method and basis set (M06-2X/6-311+G(d,p)). The HOMO-LUMO energy gap, the singlet-triplet energy gap (Table 5) and the extent of the homoconjugation (Table 6) were analysed, pursuing conclusions about the reactivity of the germylene moiety. With regards to e.g. small molecule activation, a small HOMO-LUMO energy gap is required.

The singlet-triplet energy gap (ΔE_{ST}) decreases in the order phospho-BCH-germylene **43b** (3.49) > sila-BCH-germylene **47** (3.22) > hafnocena-BCH-germylene **21** (2.63). The decrease from phospho- **43b** to hafnocene-BCH-germylene **21** aligns with the less acute C-Ge-C bond angle in the latter ($\Delta(\text{C-Ge-C}) = 15^\circ$; see Table 4). Furthermore, the calculated HOMO-LUMO energy gaps ($\Delta E_{\text{HOMO-LUMO}} = 6.92$ eV (**43b**), 6.25 eV (**47**), 5.69 (**21**)) as well as the relative energy level of each HOMO ($E(\text{HOMO}) = -6.64$ eV (**43b**), -6.37 eV (**47**), -6.00 eV (**21**)) follow the same trend. Overall, this predicts increasing reactivity or ability to undergo bond activation reactions going from phospho- **43b** to sila- **47** to hafnocene-BCH-germylene **21** (Table 5).

Table 5 – Calculated singlet-triplet gap [eV] and HOMO-LUMO gap [eV] of the phospho- **43b**, hafnocena- **21** and sila-BCH-germylenes **47** (M06-2X/6-311+G(d,p) (Ge, Si, N, C, H), def2-tzvp (Hf)).

			
	43b	47	21*
ΔE_{ST}	3.49	3.22	2.63
$E(\text{HOMO})$	- 6.64	- 6.37	- 6.00
$\Delta E_{\text{HOMO-LUMO}}$	6.92	6.25	5.69

*The values reported by Müller and coworkers (M06-2X/def2-tzvp) are similar: $\Delta E(\text{ST}) = 2.49$ eV^[55], $\Delta E(\text{HOMO-LUMO}) = 5.85$ eV^[54].

The extent of the homoconjugative interaction in those three different BCH-germylenes was compared on the basis of calculated (using model compounds) isodesmic reaction energies according to equation **(A)** (Figure 24). Thereby, the obtained values (ΔE_A) are proportional to the energy gain resulting from the stabilisation of the germylene by donation of electrons from the $\text{C}^2=\text{C}^3$ double bond. It furthermore needs to be taken into account that the element atom (**E**) interacts with the germylene as well. Therefore isodesmic equation **(B)** was set up (Figure 24).

This assessment was introduced by Müller and coworkers.^[54] The reaction energy of equation **(B)** is smallest for sila-BCH-germylene **47'** ($\Delta E_B = -5 \text{ kJ mol}^{-1}$), which exhibits a coordinatively saturated **E** atom. The reaction energy is largest for hafnocena-BCH-germylene **21'** ($\Delta E_B = -37 \text{ kJ mol}^{-1}$), which we traced back to the contribution of d-orbitals of the hafnium atom. The interaction of the phosphorus lone pair to the germylene is suggested to be weaker (ΔE_B (**43'**) = -17 kJ mol^{-1}) than the interaction of the hafnium atom with the germylene moiety. For comparative analysis of the homoconjugative interaction, it seemed reasonable to subtract the term **(B)** from the homoconjugation term **(A)** to give a corrected reaction energy $\Delta E_{\text{corr}} = \Delta E_A - \Delta E_B$ (Table 6). The obtained values are in a range of $\Delta E_{\text{corr}} = -90$ to -103 kJ mol^{-1} . However, the calculated values do not necessarily represent the homoconjugation only, as the calculation of isolated stabilising effects in larger molecules cannot be achieved. Here, it can therefore be concluded, that the extent of the homoconjugative interaction in BCH-germylenes is generally not strongly depending on the heteroatom **E** (Table 6).

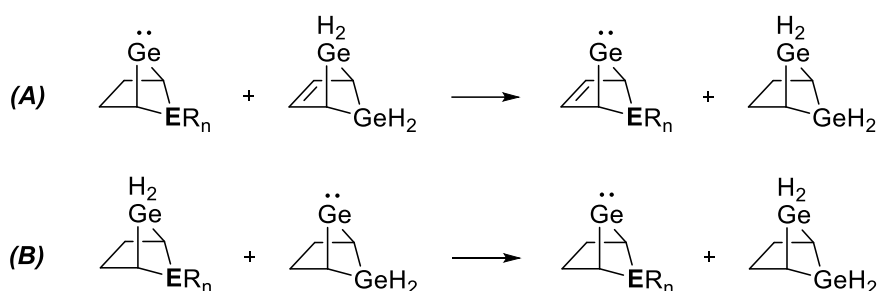


Figure 24 – Isodesmic equations used for comparison of the homoconjugative interaction as well as the element-germanium interaction in phosha- **43'**, sila- **47'** and hafnocena-BCH-germylenes **21'**. Calculations were carried out using model compounds (marked by ').

Table 6 – Data calculated according to the isodesmic equations **(A)** and **(B)** (M06-2X/6-311+G(d,p) (H, C, N, Si, P), def2-tzvp (Hf)).

	43' ER _n = PNMe ₂	47' ER _n = SiMe ₂	21' ER _n = HfCp ₂ *
ΔE_A	-119	-108	-127
ΔE_B	-17	-5	-37
ΔE_{corr}	-102	-103	-90

* Data reported by Müller and coworkers.^[54]

3.2.3 Structural Features of Aminophosholes

Phosphole **45e** was also analysed by single crystal XRD. The crystals were obtained, keeping a concentrated pentane solution of the phosphole at -30°C overnight. Its molecular structure is similar to that of phosphole **45c**, which was reported on by Kühn in antedate work^[67], and to that of diisopropylaminophosphole **48** by Hydrio *et al.*^[113]

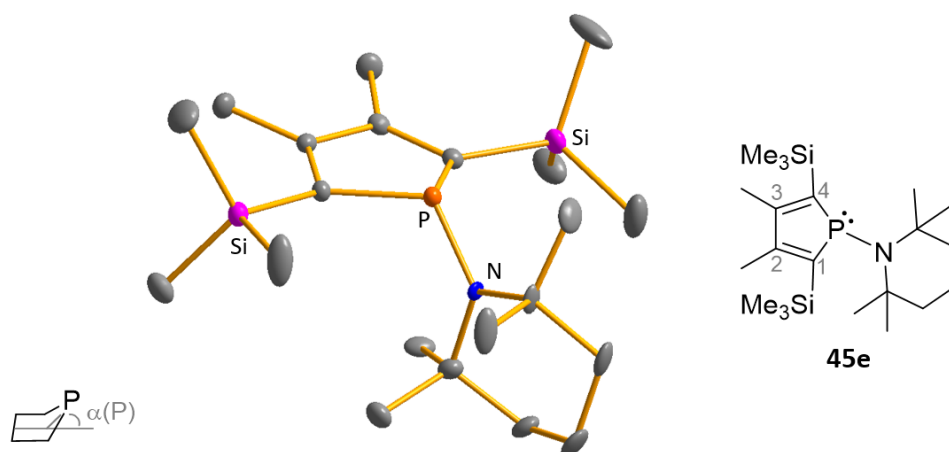
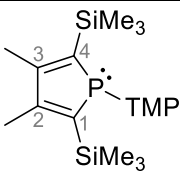
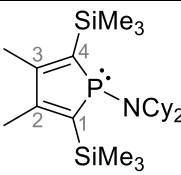
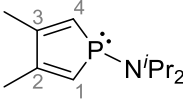


Figure 25 – Molecular structure of phosphole **45e** in the crystal. Disordered structure. Only the main structure (75%) is shown. Thermal ellipsoids at 50% probability level. Hydrogen atoms are omitted for clarity.

All three phospholes named above possess a slightly folded five-membered ring with flap angles $\alpha(\text{P})$ between 11.2° and 15.3° . The phosphorus atom is, as typical for phospholes, pyramidalised and the backbone consists of two slightly elongated C=C double bonds ($\text{C}^1=\text{C}^2 = 138.3 \text{ pm}$, 137.3 pm)^[108] and a slightly shortened C-C single bond ($\text{C}^2-\text{C}^3 = 145.2 \text{ pm}$, 146.4 pm)^[107]. The localisation of the π -electrons and the pyramidalisation of the phosphorus atom correlate with the high *s*-character of the phosphorus orbital occupying the lone pair electrons. For the two 2,5-bissilyl-substituted phospholes **45c** and **45e**, the pyramidalisation of the phosphorus atom is less distinct ($\Sigma\text{P} = 325.3^{\circ}$, 323.5°) than in the 2,5-hydrogen substituted phosphole **48** ($\Sigma\text{P} = 306.1^{\circ}$) and the above analysed phospho-BCH-germylene **43b** ($\Sigma(\text{P}) = 302.3^{\circ}$, Table 4). Similar to germylene **43b**, the nitrogen atom is planar in all three phospholes and the P-N bonds are, as expected for aminophosphanes, shortened ($\text{P}-\text{N} = 166.9\text{-}169.9 \text{ pm}$) compared to typical P-N single bonds (182 pm)^[108, 111-112]. Moreover, the dihedral angle of the amino group to the phosphole ring is almost perpendicular for the non-cyclic amino groups ($\alpha(\text{N}) = 91.5^{\circ}$ (**45c**), 91.7° (**48**)) and close to perpendicular for the TMP-phosphole **45c** ($\alpha(\text{N}) = 118.6^{\circ}$) (Table 7).

Table 7 – Selected bond lengths and bond angles of the aminophospholes **45e**, **45c**^[67] and **48**^[113].

			
	45e	45c ^[67]	48 ^[113]
bond lengths [pm]			
P–N	168.97(21)	168.08(9)	166.9(2)
P–C ¹	179.61(16)	180.06(8)	179.3(2)
C ¹ –C ²	138.31(22)	137.34(14)	n.a.
C ² –C ³	145.28(22)	146.37(11)	n.a.
angles [°]			
ΣP	325.3	323.5	306.1
α(P)	15.3	14.1	11.2
ΣN	359.1	358.3	n.a. (planar)
α(N)	118.6	91.5	91.7

3.2.4 NMR Spectroscopic Analysis of Mixtures

Due to their characteristic NMR pattern with clearly separated signals, the identification and analysis of germynes and phospholes, even in mixtures containing more than those two compounds, can unerringly be carried out. Besides the characteristic ³¹P NMR chemical shifts, here, the ¹H¹³C HMBC and the ¹H³¹P HMBC 2D-NMR spectra are of particular importance. This kind of analysis is especially useful and will be applied to product mixtures within reactivity studies later in this work. An exemplary analysis is shown in this chapter for the mixture of germylene **43b** and phosphole **45b**.

The ¹H NMR spectrum of the mixture shows two sets of signals for each functionality: trimethylsilyl protons (SiMe₃), isopropyl-methyl protons (N(CHMe₂)₂), backbone-methyl protons (C^{2/3}-Me) and isopropyl-methine protons (N(CHMe₂)₂). Characteristic for the phosphole **45b** is the splitting of the backbone-methyl protons into a doublet due to coupling to the phosphorus nucleus. No such coupling can be observed in the BCH-germylene **43b** (Figure 26).

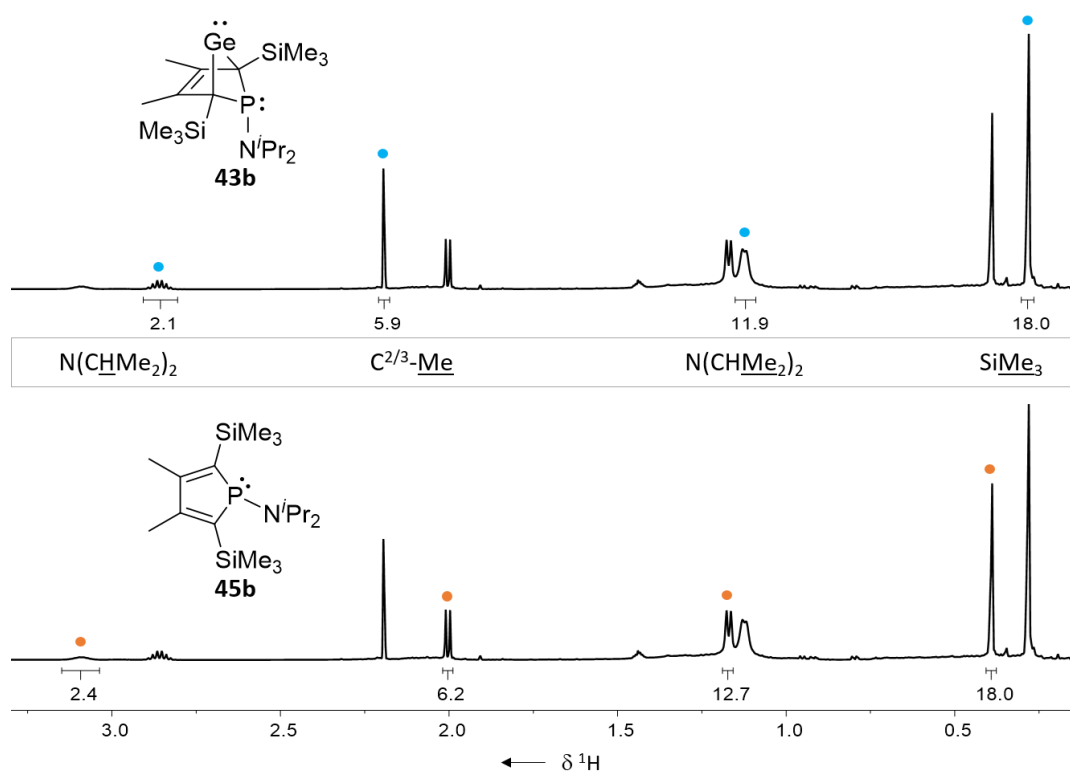


Figure 26 – ^1H NMR spectrum (500.1 MHz, 305 K, benzene- d_6) of a mixture of phospho-BCH-germylene **43b** (highlighted in blue, top) and phosphole **45b** (highlighted in orange, bottom).

The structure of the backbone can be determined via $^1\text{H}^{13}\text{C}$ HMBC NMR spectroscopy. Due to coupling of the $\text{C}^{1/4}$ carbons to the trimethylsilyl protons (SiMe_3) and the methyl protons ($\text{C}^{2/3}\text{-Me}$), as well as coupling of the $\text{C}^{2/3}$ carbons to the methyl protons ($\text{C}^{2/3}\text{-Me}$), triangular patterns are displayed in the $^1\text{H}^{13}\text{C}$ HMBC spectrum. The chemical shift of the $\text{C}^{1/4}$ carbon atoms allows the facile differentiation between the bicyclohexene and the butadiene backbone. The signals of sp^3 hybridised carbon atoms are shifted to lower frequency than those of sp^2 hybridised carbon atoms.^[114] Applied to this example, the bicyclohexene structures can be identified due to their bridgehead atoms that are sp^3 hybridised and therefore shifted to higher field ($\delta^{13}\text{C} = 60\text{-}80$; here: $\delta^{13}\text{C} = 74.1$ (**43b**)) (Figure 27). Furthermore, the $^2J_{\text{C,P}}$ coupling constants are typically larger in the phospholes (here: $^2J_{\text{C,P}} = 19$ Hz (**45b**)) than in the phospho-BCH-germylenes (here: $^2J_{\text{C,P}} = 8$ Hz (**43b**)) (Figure 28).

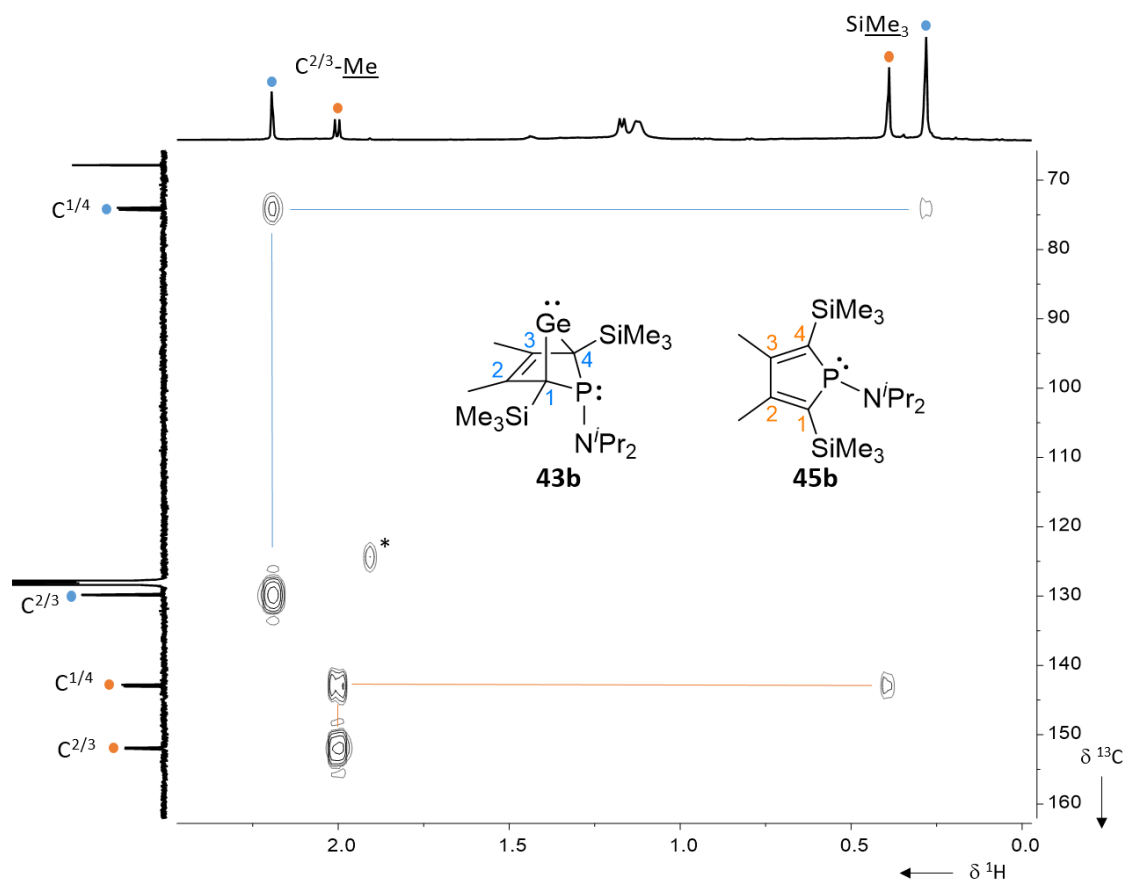


Figure 27 – Section from the $^1\text{H}/^{13}\text{C}$ HMBC NMR spectrum (500.1 MHz, 305 K, benzene- d_6) of a mixture of phospho-BCH-germylene **43b** (blue) and phosphole **45b** (orange) showing the characteristic triangular backbone patterns (*impurity).

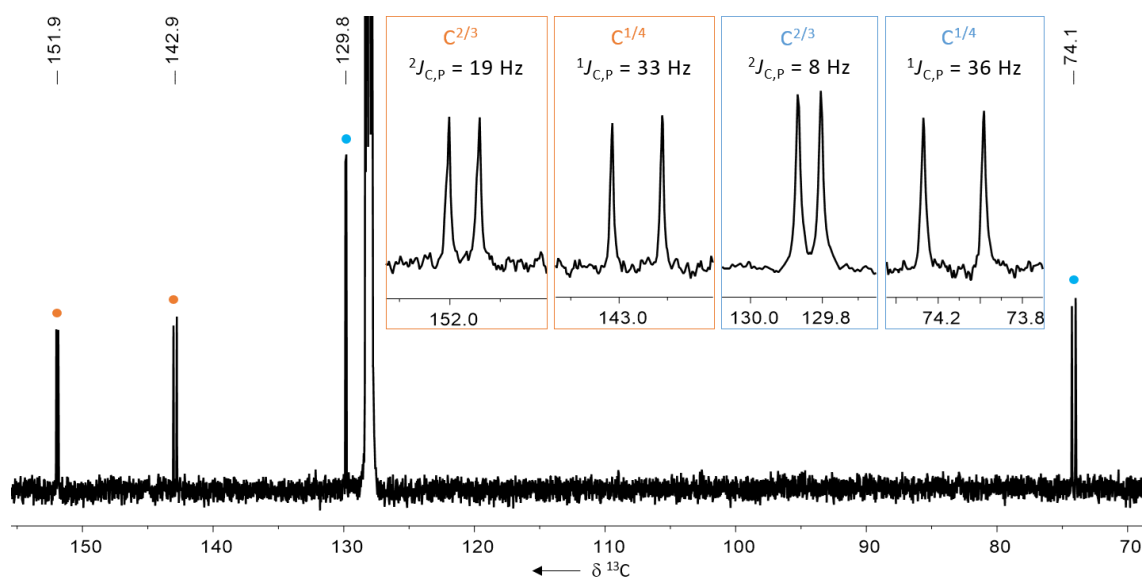


Figure 28 – Extract from the $^{13}\text{C}\{^1\text{H}\}$ NMR spectrum (125.8 MHz, 305 K, benzene- d_6) with zooms of the backbone carbon atom signals of Phospho-BCH-germylene **43b** (blue) and phosphole **45b** (orange).

Using $^1\text{H}^{31}\text{P}$ HMBC NMR spectroscopy, the ^1H NMR signals can be assigned to the different phosphorus species. The characteristic ^{31}P NMR chemical shifts enable facile and fast overview of the product mixtures. Generally, the phosphole signal is shifted to higher frequency than the corresponding phospho-BCH-germylene signal (here: $\delta^{31}\text{P} = 35.2$ (**43b**), 65.7 (**45b**)) (Figure 29).

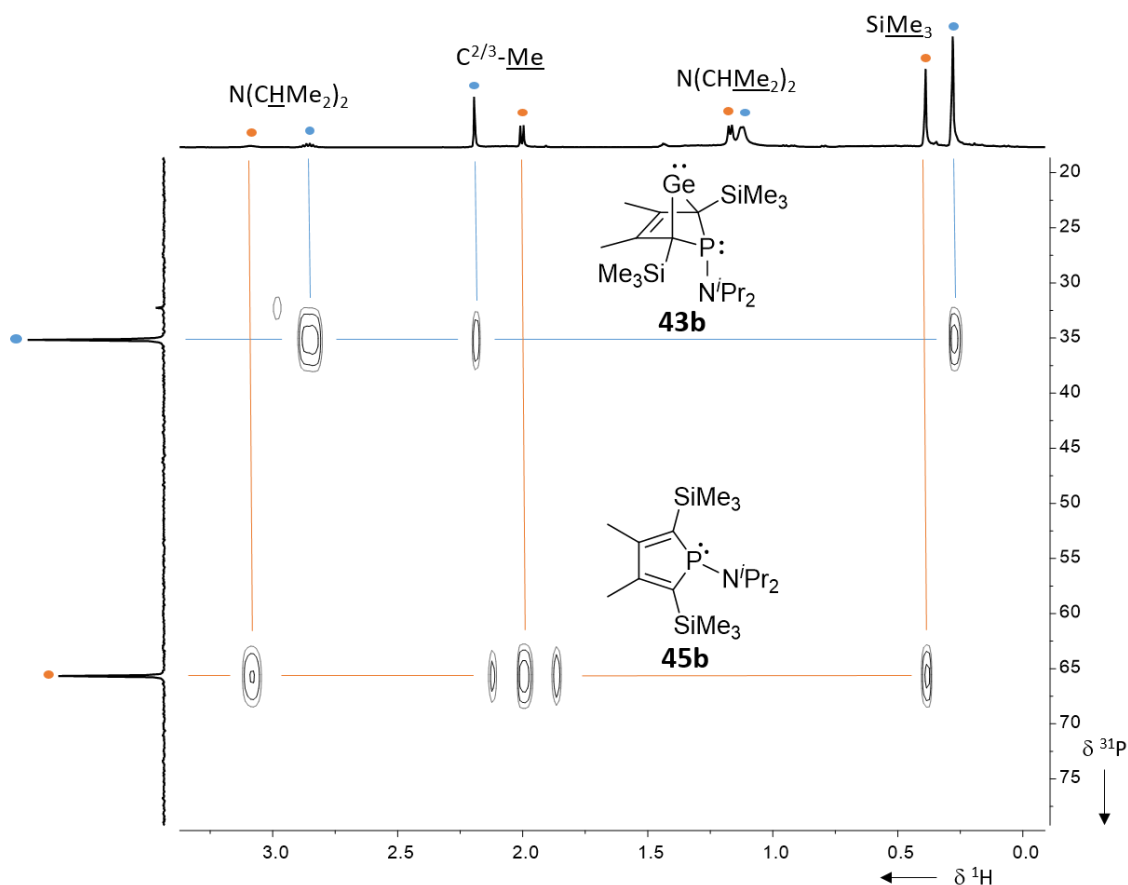


Figure 29 – $^1\text{H}^{31}\text{P}$ HMBC NMR spectrum (500.1 MHz, 305 K, benzene- d_6) of a mixture of phospho-BCH-germylene **43b** (blue) and phosphole **45b** (orange).

The $^{29}\text{Si}\{^1\text{H}\}$ INEPT NMR signals can be assigned to each phosphorus species based on their coupling constants. Due to coupling with the phosphorus nucleus, the $^{29}\text{Si}\{^1\text{H}\}$ NMR signals appear as doublets. The same coupling constant can, for most of the compounds, also be found in the $^{31}\text{P}\{^1\text{H}\}$ NMR spectrum, depicted as satellites to the respective phosphorus signal. Here, the silicon-phosphorus coupling in the phosphole **45b** is $^3J_{\text{Si,P}} = 25$ Hz (Figure 30).

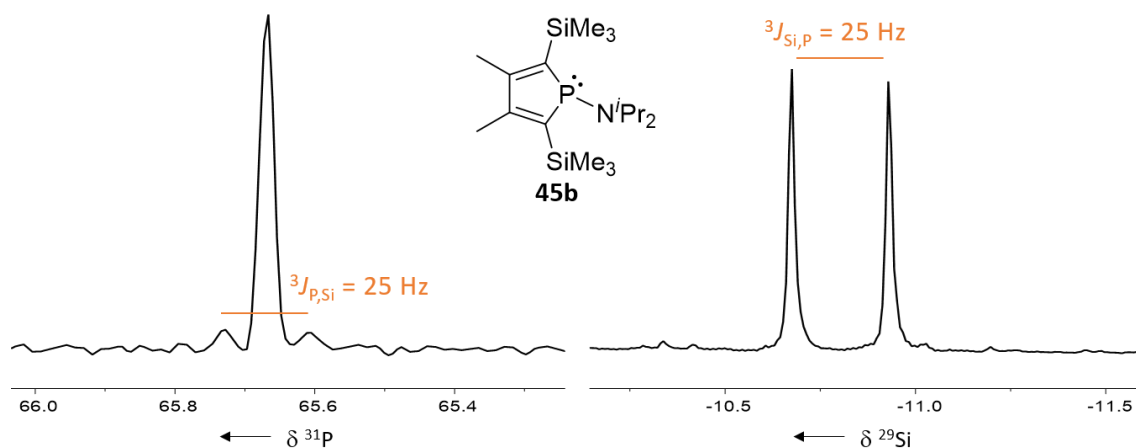


Figure 30 – Sections from the $^{31}\text{P}\{^1\text{H}\}$ NMR spectrum (202.3 MHz, 305 K, benzene- d_6) and the $^{29}\text{Si}\{^1\text{H}\}$ INEPT NMR spectrum (99.3 MHz, 305 K, benzene- d_6) of the reaction mixture, showing the signals assigned to phosphole **45b**.

3.2.5 Comparative Analysis of the NMR Spectroscopic Data

The NMR spectroscopic data, obtained for all aminophospha-BCH-germylenes **43-44** and aminophospholes **45-46** was considered in a comparative analysis to gain knowledge about the effects, arising from the properties of the amino-substituent as well as from the two different silyl-substituents. Especially for the tuning of the stability and for the reactivity of the herein introduced phospha-BCH-germylenes, this is of interest. Selected NMR spectroscopic data is summarised in Table 8. It seemed most suitable to focus on the ^{13}C NMR signals of the backbone-carbon atoms ($\text{C}^{1/4}$ and $\text{C}^{2/3}$), the ^{29}Si NMR signals as well as the respective coupling constant to the phosphorus atom, and on the ^{31}P NMR signals for the comparative analysis. In summary, both, the silyl groups (**R**) and the amino substituents (**R'**) slightly impact the electronic structure of the backbone and cause two main trends observable in the NMR spectroscopic data (Table 8).

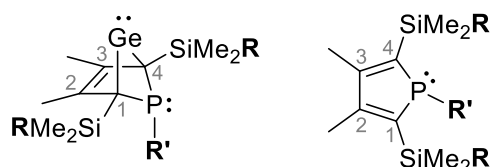


Table 8 – Selected NMR spectroscopic data of the synthesised germylenes **43-44** and phospholes **45-46**. All spectra were recorded in benzene- d_6 .

	R	R'	$\delta^{13}\text{C}$		$\delta^{29}\text{Si}$	$\delta^{31}\text{P}$
			C ^{1/4} ($^1J_{\text{C,P}}$ [Hz])	C ^{2/3} ($^2J_{\text{C,P}}$ [Hz])	($^2J_{\text{Si,P}}$ [Hz])	
Germylenes						
43b	Me	N ⁱ Pr ₂	74.4 (36)	129.9 (8)	-7.6 (21)	35.4
43c	Me	NCy ₂	74.7 (36)	129.8 (8)	-7.6 (21)	39.4
43e	Me	TMP	81.9 (48)	134.1 (8)	-7.4 (21)	30.8
44b	^t Bu	N ⁱ Pr ₂	72.8 (41)	131.1 (7)	-0.2 (18)	53.8
44c	^t Bu	NCy ₂	73.0 (41)	131.1 (7)	-0.2 (18)	57.7
44e	^t Bu	TMP	81.6 (53)	135.1 (8)	0.2 (22)	39.7
44d	^t Bu	Pip	73.4 (37)	130.4 (8)	0.4 (17)	59.8
Phospholes						
45b	Me	N ⁱ Pr ₂	143.0 (33)	151.9 (19)	-10.8 (25)	65.6
45c	Me	NCy ₂	143.0 (33)	151.6 (20)	-10.8 (25)	63.8
45e	Me	TMP	142.7 (34)	147.0 (26)	-9.8 (25)	54.2
45d	Me	Pip	142.9 (32)	154.3 (16)	-11.0 (25)	92.2
45a	Me	NMe ₂	143.6 (31)	153.4 (18)	-10.9 (25)	94.3
46b	^t Bu	N ⁱ Pr ₂	140.7 (36)	154.0 (16)	-3.1 (22)	71.7
46c	^t Bu	NCy ₂	141*	154*	-3.1 (23)	69.7
46e	^t Bu	TMP	139.7 (38)	148.9 (23)	-1.3 (22)	61.2
46d	^t Bu	Pip	140.2 (34)	155.1 (16)	-2.9 (22)	95.9
46a	^t Bu	NMe ₂	141.2 (31)	154.2 (17)	-2.5 (22)	98.5

*Data extracted from the $^1\text{H}^{13}\text{C}$ HMBC NMR spectrum.

Impact of the Silyl Groups (R)

In the former case, formally exchanging the trimethylsilyl groups for *tert*butyldimethylsilyl groups leads to a significant lowfield shift of the ^{31}P NMR signals of all phospholes and phospho-BCH-germylenes. The differences comprise about $\Delta(\delta^{31}\text{P}) = 9\text{-}18$ ppm for the germylenes with the same amino-substituent and about $\Delta(\delta^{31}\text{P}) = 4\text{-}6$ ppm for the phospholes with the same

substituent (Table 8). Figure 31 visualises this effect for the diisopropylamino-substituted germylenes **43b/44b** and phospholes **45b/46b**.

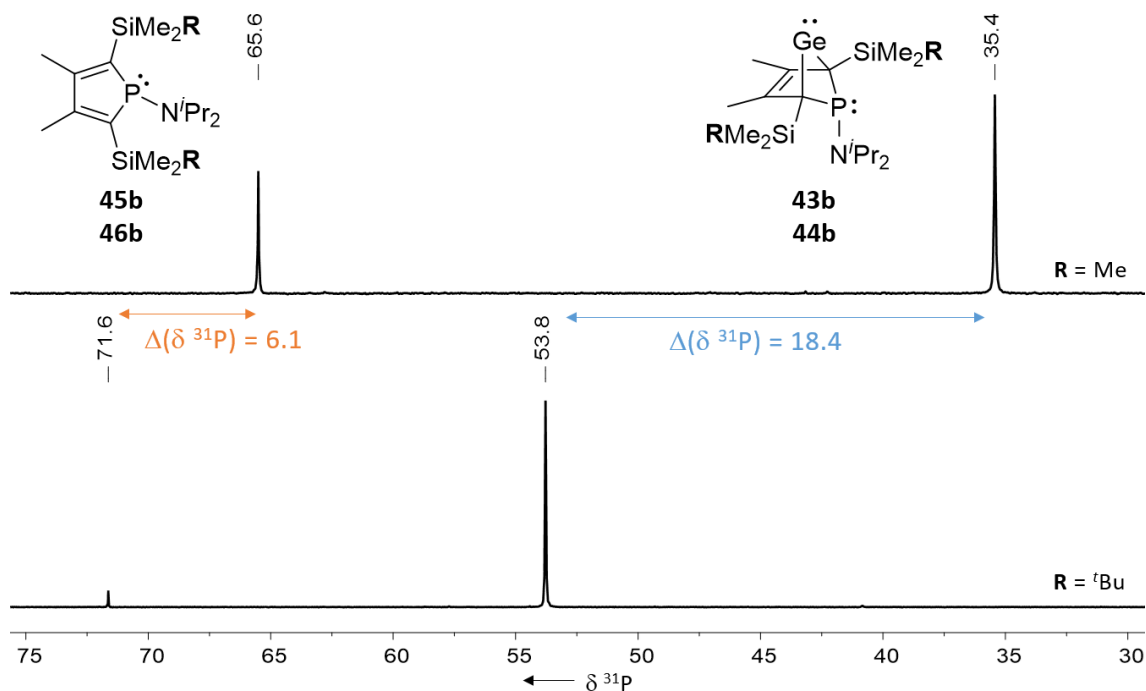


Figure 31 – $^{31}\text{P}\{^1\text{H}\}$ NMR spectra (202.3 MHz, 305 K, benzene- d_6) of the phosphole/germylene pairs **45b/43b** (top) and **46b/44b** (bottom), visualising the effect of the silyl groups on the ^{31}P NMR chemical shift.

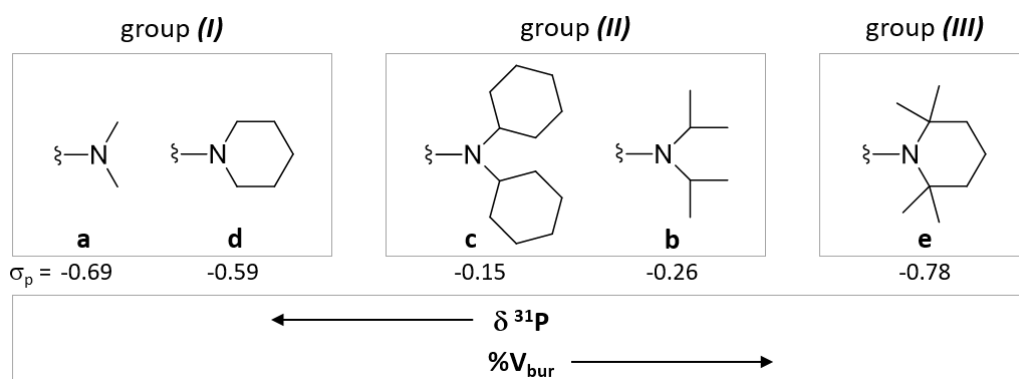
Additionally, indication was found that the rotation around the $\text{C}^{1/4}\text{-Si}$ bonds is hindered in all *tert*butyldimethylsilyl substituted germylenes (but not in the phospholes): In the ^1H NMR spectra, the methyl groups are split into two signals. Therefore, the influence of the orientation of the *tert*butyl moiety on the ^{31}P NMR chemical shift was examined in more detail for the germylenes **43b** and **44b** (see also Chapter 3.2.6). In this respect, two germylene **44b** isomers were optimised: one with the *tert*-butyl moiety oriented downwards (**A**) and one with it oriented upwards (**B**) (Table 9). Isomer **B** is predicted to be favoured by $\Delta E = -9 \text{ kJ mol}^{-1}$, which, at 298 K, accounts for a Boltzmann population of the isomers **A** and **B** of 3% and 97%, respectively. With the *tert*butyl group oriented downwards (**A**), the calculated NMR chemical shift is close to the experimental value of germylene **43b** ($\Delta(\delta^{31\text{P}}) = 3$) but much more unlike the experimental value of germylene **44b** ($\Delta(\delta^{31\text{P}}) = 16$). The calculated value of the predominant isomer **B** on the other hand, is closer to the experimental value of germylene **44b** ($\Delta(\delta^{31\text{P}}) = 6$). Since the ^{31}P NMR chemical shift is influenced by change in the Tolman cone angle^[115], we assume that the lowfield shift of the germylenes upon introduction of the larger silyl groups arises from the retained orientation of the *tert*butyl group (Table 9).

Table 9 – Examination of the impact of the silyl group on the ^{31}P NMR chemical shift of phospho-BCH-germylenes.

	43b	44b (A)	44b (B)
<i>Boltzmann population</i>	-	3%	97%
$\delta^{31}\text{P}_{\text{calc}}$	31	38	48
$\delta^{31}\text{P}_{\text{exp}}$	35.4	(53.8)	53.8
$\Delta(\delta^{31}\text{P})$	4	16	6

Impact of the Amino-Substituent (R')

Based on similarities observed in the reaction pattern of the aminodichlorophosphanes **38a-e** towards the germediide salts $\text{K}_2[\mathbf{31}]$ and $\text{K}_2[\mathbf{36}]$, as well as based on great similarity of the NMR spectroscopic data of the respective aminophospholes **45-46** and aminophospha-BCH-germylenes **43-44**, the products and aminophosphanes can be categorised into three groups: dimethylamino and piperidino group (*I*), diisopropylamino and dicyclohexylamino group (*II*), and tetramethylpiperidino (*III*). Following the row (*I*) \rightarrow (*III*), the ^{31}P NMR resonances are shifted to lower frequency and the buried volume of the aminophosphane ($\%V_{\text{bur}}$) increases. In the literature, the influence of changes in the Tolman cone angle on the ^{31}P NMR chemical shift is documented.^[115] The calculated electron donating ability (σ_p) of the amino substituents, on the other hand, does not match the presented order, indicating ancillary impact of the slightly varying electron donating properties of the amino substituent on the compounds discussed here. Still, within each group, the amino groups possess very similar calculated sigma constants (Figure 32).

**Figure 32** – Categorisation of the germylenes **43-44** and phospholes **45-46** into three groups.

Within each group, not only the ^{31}P NMR spectroscopic data is similar, but also the ^{13}C NMR spectroscopic data. The ^{13}C NMR chemical shift of the $\text{C}^{2/3}$ carbon atoms of the phospholes are shifted to higher field, following the row (I) \rightarrow (III). The trend is most distinctive for the trimethylsilyl substituted phospholes **45a-45e**. Also, the $^2J_{\text{C,P}}$ coupling constant increases in the same order (I) \rightarrow (III). However, an impact of the amino group on the ^{13}C NMR chemical shift of the $\text{C}^{1/4}$ carbon atoms was not observed. For the germylenes, the trend is different: The ^{13}C NMR signals of the $\text{C}^{1/4}$ carbon atoms as well as the $\text{C}^{2/3}$ carbon atoms of the TMP-substituted compounds (III) are shifted to lower field. Here, especially the $^1J_{\text{C,P}}$ coupling constant increases whilst the $^2J_{\text{C,P}}$ coupling constant remains unchanged. In general it was noted that the ^{29}Si NMR chemical shift as well as the $^2J_{\text{Si,P}}$ coupling constant are virtually independent from the amino-substituent (Table 8).

The aminophospha-BCH-germylenes **43a+d** and **44a** of group (I) were not obtained. Additionally, the NMR spectra of all four group (I) phospholes (**45a+d** and **46a+d**) needed to be recorded at lower temperature for full analysis. Due to the small size of the piperidino (d) and dimethylamino (a) groups, rotation around the P-N bond was too fast to detect averaged NMR signals of the amino groups at room temperature. However, at -40°C sharpening of the corresponding signals was observed. Exemplary ^1H NMR spectra of phosphole **45a** are shown in Figure 33. This again points out the difference of these amino groups compared to the diisopropylamino (b), dicyclohexylamino (c) and tetramethylpiperidino group (e).

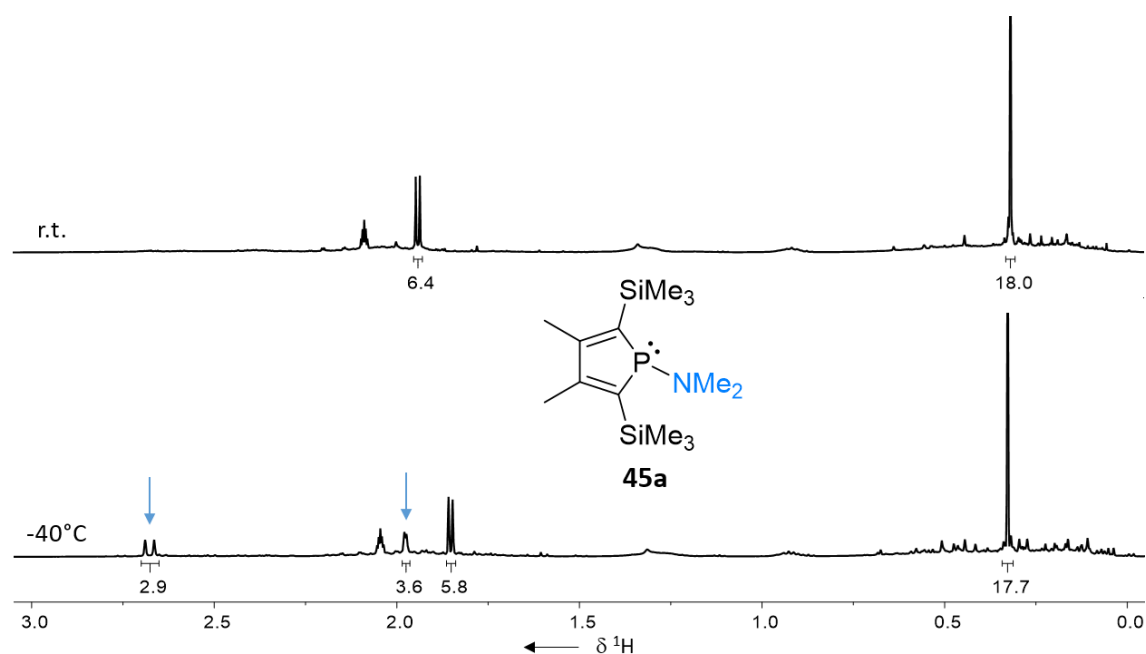


Figure 33 – ^1H NMR spectra (499.9 MHz, 305 K / 233 K, toluene- d_8) of phosphole **45a** at room temperature (top) and -40°C (bottom).

In summary, the observed trends match the results presented in Table 3 (Chapter 3.2.1): the steric properties of the amino substituent as well as of the silyl groups align with the observed stability or instability of the respective phospho-BCH-germylene. The connection of the steric properties of aminophospha-BCH-germylenes **43-44** to their stability will be further explained at a later point in this work (Chapter 3.2.7).

3.2.6 Replication of the ^{31}P NMR Spectroscopic Data

To support the conclusions drawn regarding the impact of the sterical and electronic properties of the substituents on the trends observed in the recorded ^{31}P NMR spectroscopic data, the ^{31}P NMR chemical shifts were replicated using DFT calculations. The calculations for germylene **43c** and phosphole **45c** were done by S. Kühn within antedate studies.^[67]

Firstly, the conformity of the optimised structures and the molecular structures should be ensured. The optimised structures of phosphole **45e** and phosphole **45c** were compared to the corresponding molecular structures in the crystal (Table 10). Such a comparison has already been made for germylene **43b** in Chapter 3.2.2, finding great similarity of the two structures. However, selected data is given here again, with focus on the phosphane moiety (Table 10).

Table 10 - Selected bond lengths and angles of molecular structures of germylene **43b**, phosphole **45e** and phosphole **45c** and the corresponding optimised (*cursive*) structures. Data of phosphole **45c** was retrieved from initial studies.^[67]

	43b		45e		45c	
	exp	calc	exp	calc	exp ^[67]	calc ^[67]
$\text{C}^1\text{-P} (\varnothing)$ [pm]	184.11(4)	185.0	179.61(16)	180.9	180.06(8)	181.8
P-N [pm]	170.18(7)	172.6	168.97(21)	171.2	168.08(9)	170.3
ΣP [°]	302.3	300.1	325.3	322.6	323.5	318.6
ΣN [°]	360.0	358.3	359.1	357.9	358.3	359.4

As already noted for germylene **43b**, the optimised structures are in overall good agreement with the molecular structures: The calculated bond length deviate from the measured bond length by about 2 pm, whereas the calculated lengths are always longer than the measured

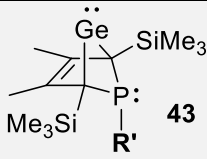
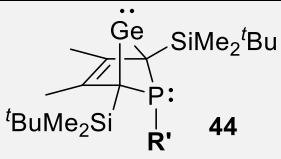
lengths. Deviation of the angular sum around the phosphorus and the nitrogen atom of the calculated structure from the molecular structure is largest for phosphole **45c** with $\Delta(\Sigma P) = 4.8^\circ$. The deviation of the other parameters is even smaller (Table 10). Hence, it can be concluded that the optimised structures represent the molecular structures appropriately.


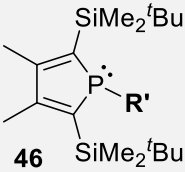
Secondly, the accuracy of the calculated ^{31}P NMR signals was studied. Therefore, the data measured in benzene- d_6 was compared to the calculated data. Overall, the calculated ^{31}P NMR chemical shifts are in satisfying agreement with the experimental values. The difference between calculated and experimental values does mostly not exceed $\Delta(\delta^{31}\text{P}) = 10$ ppm for all considered germynes and phospholes. An exception is phosphole **46b**, where the difference is $\Delta(\delta^{31}\text{P}) = 16$ ppm. Thereby, the calculated ^{31}P NMR signals are slightly shifted to higher frequencies than the experimental signals. The most accurate calculations were obtained for the SiMe_3 -substituted germynes. The arithmetic mean of the deviation to the experimental values is 3 ppm (Table 11). The correlation of the calculated and experimental data is additionally illustrated in Figure 34.

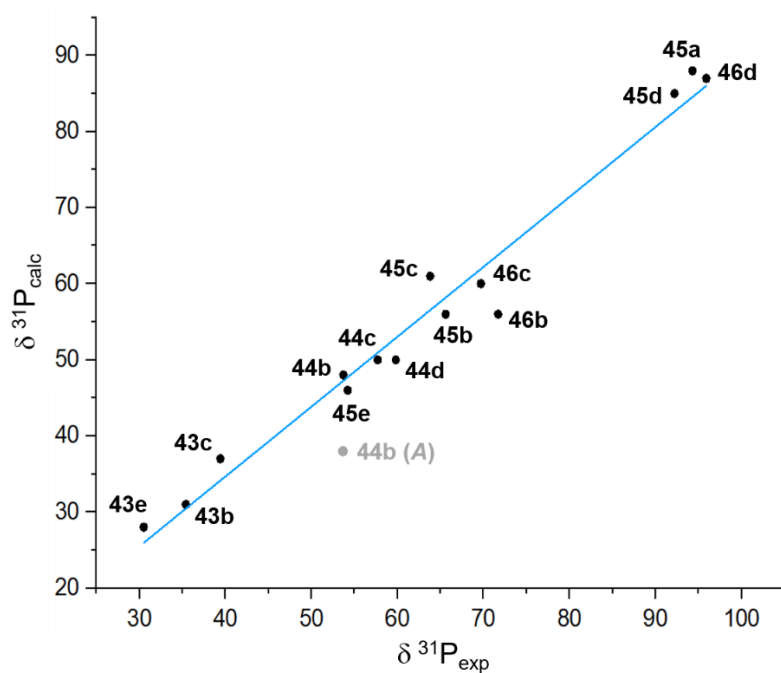
Though the ^{31}P NMR chemical shift of the herein considered compounds cannot exactly be predicted, the calculations allow rough estimation of trends like the shift to lower or higher frequency in comparison to related compounds. With the introduction of the larger silyl groups of germynes **44**, for example, the high field shift of the ^{31}P NMR signals, observed in the experiments, is replicated. The predicted high field shift for the ^{31}P NMR signals of the TMP substituted compounds (**e**) as well as the lowfield shift of about 30 ppm of the phospholes **45a+d** and **46a+d**, compared to the other phospholes, agrees well with the experimental data, too (Table 11).

However, the calculations did not suggest any influence of the silyl groups on the ^{31}P NMR chemical shift of the phospholes **45** vs. **46** (Table 11). This was interpreted as reflecting the above mentioned free rotation around the $\text{C}^{1/4}\text{-Si}$ bonds in the phospholes **46**, which further indicates the orientation of the *tert*butyl group in the respective germynes **44** to be responsible for the lowfield shift of their ^{31}P NMR signals in comparison to germynes **43** (Table 9).

Table 11 – Overview of the experimental (measured in benzene- d_6) and calculated ^{31}P NMR chemical shifts.

Germynes							
R'	$\delta^{31}\text{P}_{\text{exp}}$	$\delta^{31}\text{P}_{\text{calc}}$	$\Delta(\delta^{31}\text{P})$	$\delta^{31}\text{P}_{\text{exp}}$	$\delta^{31}\text{P}_{\text{calc}}$	$\Delta(\delta^{31}\text{P})$	
b	N^iPr_2	35.4	31	4	53.8	48	6
c	NCy_2	39.4	37	2	57.7	50	8
e	TMP	30.8	28	3	39.7	-	-
d	Pip	-	50	-	59.8	50	10

Phospholes							
R'	$\delta^{31}\text{P}_{\text{exp}}$	$\delta^{31}\text{P}_{\text{calc}}$	$\Delta(\delta^{31}\text{P})$	$\delta^{31}\text{P}_{\text{exp}}$	$\delta^{31}\text{P}_{\text{calc}}$	$\Delta(\delta^{31}\text{P})$	
b	N^iPr_2	65.6	56	10	71.7	56	16
c	NCy_2	63.8	61	3	69.7	60	10
e	TMP	54.2	46	8	61.2	-	-
d	Pip	92.2	85	7	95.9	87	9
a	NMe_2	94.3	88	6	98.5	-	-

**Figure 34** - Correlation of experimental (x axis) and calculated (y axis) ^{31}P NMR chemical shifts of the aminophospha-BCH-germylenes **43-44** and aminophospholes **45-46** (Table 11). Linear regression:

$$\delta^{31}\text{P}_{\text{calc}} = (2.054 \pm 2.94) + (0.918 \pm 0.04) \delta^{31}\text{P}_{\text{exp}}. \text{ Germylene } \mathbf{44b} \text{ (A) (Table 9) was not included in the regression.}$$

3.2.7 Germanium Elimination from Phospha-BCH-Germylenes

Even though germylene **43b** was crystallised, redissolving caused elimination of elemental germanium and formation of phosphole **45b**. The process was visible through colour change from colourless to black, caused by precipitation of the germanium that tarnished the solution over time. NMR spectra, recorded in THF- d_8 immediately after dissolving the crystals, already showed trace amounts (3%) of phosphole **45b** (marked in orange, ^1H line, Figure 35).

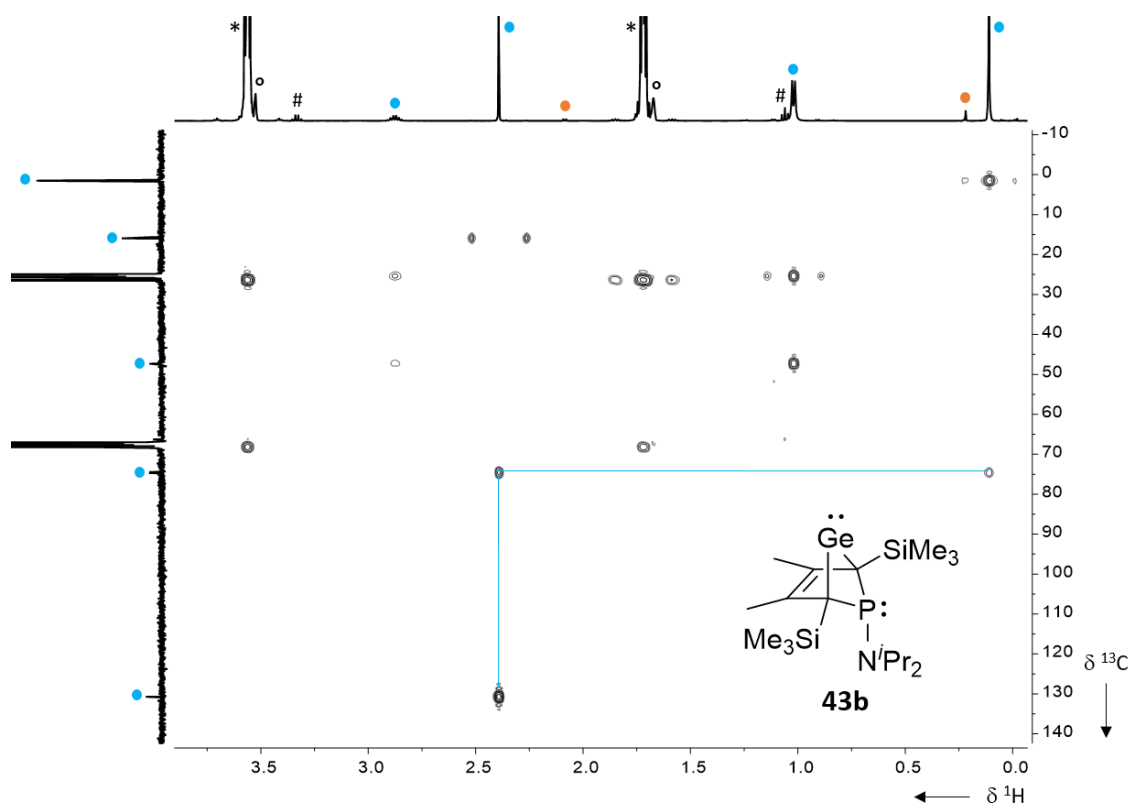
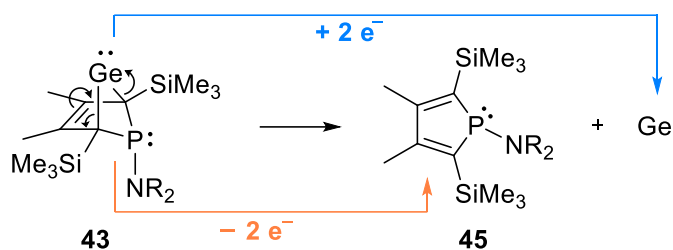


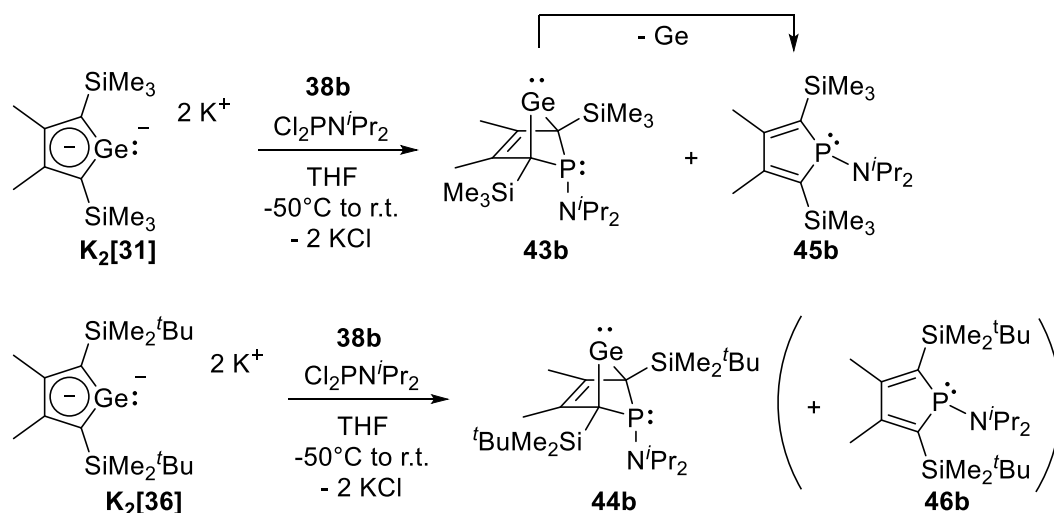
Figure 35 – $^1\text{H}/^{13}\text{C}$ HMBC NMR spectrum (500.1 MHz, 305 K, THF- d_8) of dissolved crystals of germylene **43b** (*THF- d_8 , °THF, #Pentane).

Within this work, the process of the decomposition reaction of phospha-BCH-germylenes **43** to give the corresponding phosphole **45** and elemental germanium is referred to as *reductive elimination of germanium*. Despite the fact that the term *reductive elimination* is used differently in the literature^[116], it is used here because the germanium atom is reduced within this process while the carbon backbone is oxidised (Scheme 21). This type of elimination reaction has previously been reported for similar BCH-germylenes by our group.^[58]



Scheme 21 – Reductive elimination of germanium from phospho-BCH-germylenes **43**.

It was found that the change from trimethylsilyl ($R = \text{Me}$, **43**) to *tert*butyldimethylsilyl ($R = \text{tBu}$, **44**) substituents has a strong impact on the stability of the respective germylene. Comparing the ^{31}P NMR spectra of reactions of each dipotassium germyliide $\text{K}_2[\mathbf{31}]$ and $\text{K}_2[\mathbf{36}]$ towards diisopropylaminophosphane **38b**, illustrates the differences. Both reactions were carried out at -50°C in THF and were stirred for one hour while slowly warmed to room temperature. Afterwards, the salts were removed by filtration in pentane. NMR spectra were recorded right after the workup in benzene- d_6 . While with the smaller silyl groups (germylene **43b**) already about 30% phosphole **45b** were formed (Scheme 22 and Figure 36, top), only a trace amount of about 3% phosphole **46b** was formed with the larger silyl groups (germylene **44b**) (Scheme 22 and Figure 36, bottom).



Scheme 22 – Impact of the silyl groups on the stability of germylenes **43b** and **44b**.

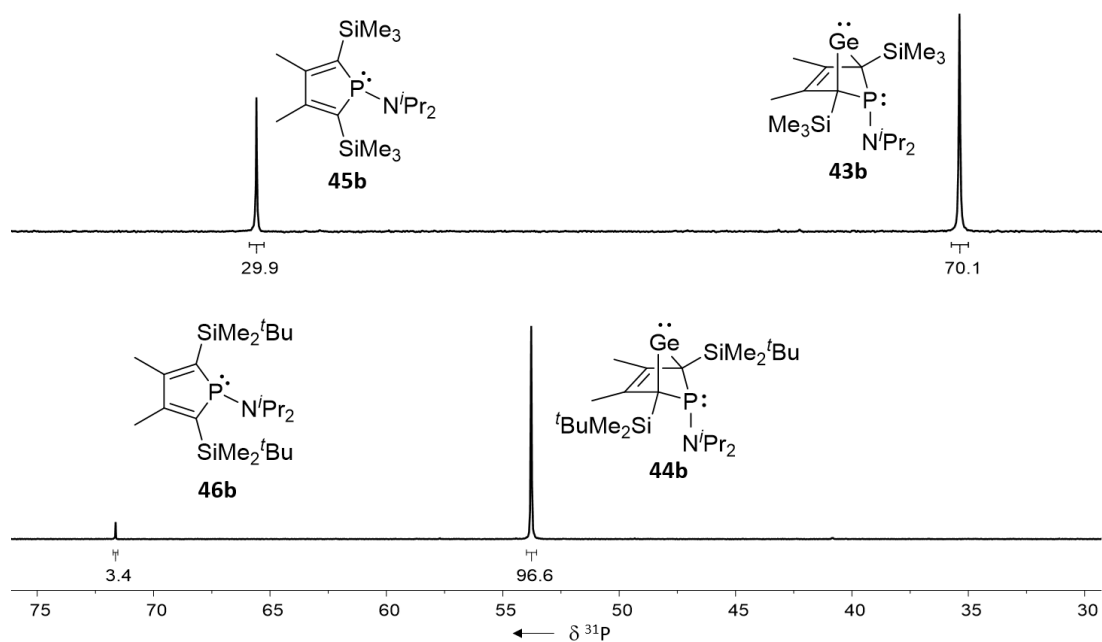


Figure 36 – $^{31}\text{P}\{^1\text{H}\}$ NMR spectra (202.3 MHz, 305 K, benzene- d_6) of the mixtures of germylene and phosphole **43b/45b** (top) and **44b/46b** (bottom) directly after their synthesis.

As indicated in Scheme 22, the reductive elimination from germylene **43b** continues over time until full conversion into the phosphole **45b** is achieved. This especially stands out regarding the NMR sample taken of the crystalline germylene **43b**. Three weeks after the first NMR measurement (Figure 37, top), a dark precipitate had formed and accumulated at the bottom of the NMR tube. NMR spectra of the colourless solution on top displayed pure phosphole **45b** (Scheme 37, bottom). In contrast, no further elimination takes place from germylene **44b** over time.

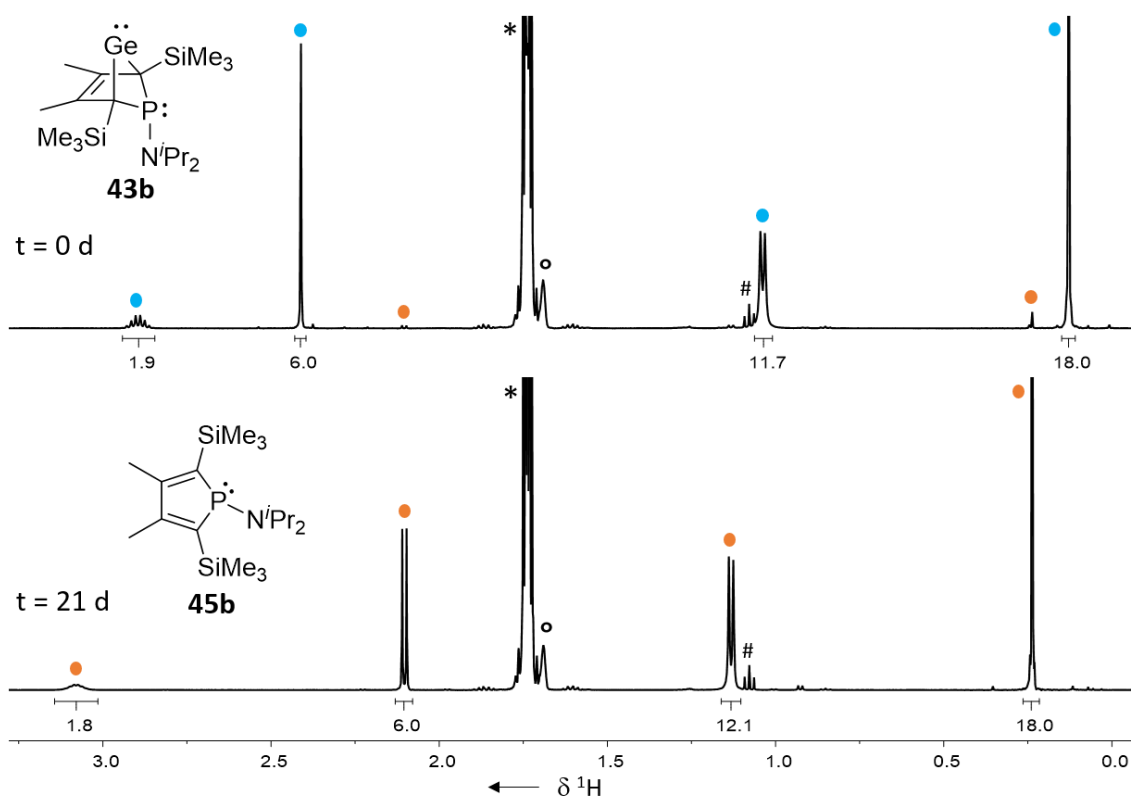


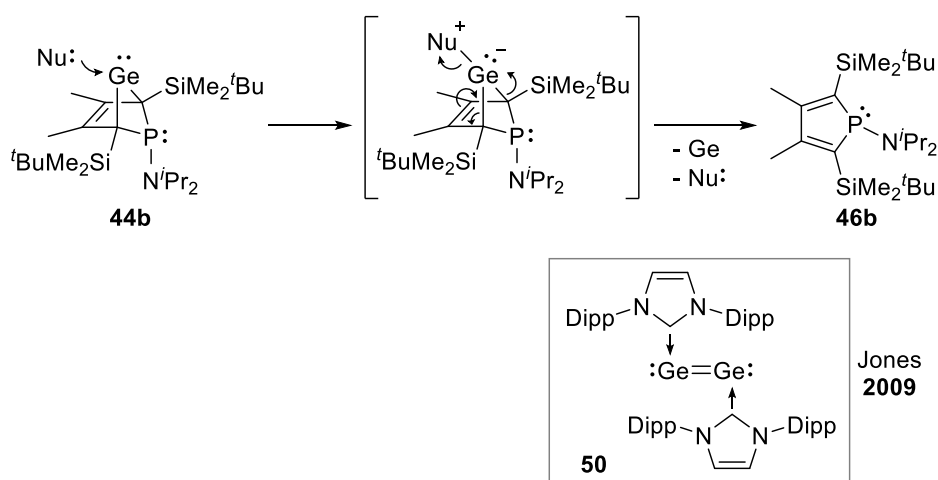
Figure 37 – ^1H NMR spectra (500.1 MHz, 305 K, THF-d_8) of the crystalline germylene **43b** after dissolving (top) and after three weeks (bottom) (* THF-d_8 , $^\circ\text{THF}$, #Pentane).

Additional experiments were carried out, showing that the germanium elimination from the larger germylene **44b** cannot be forced by higher temperature, nor can it be induced by common solvents used within the synthesis and workup: germylene **44b** is stable in pentane, benzene, toluene, diethyl ether and THF. It furthermore does not decompose when heated to 100°C in toluene for several hours. Similar experiments were also carried out for the smaller germylene **43b**. Here, the problem was that the germanium elimination depends on another factor which consistently caused slow germanium elimination. Therefore, the elimination took place while testing the external factors even if they were not responsible for the elimination. However, higher temperature and change of solvent did not influence the elimination rate.

3.2.7.1 Nucleophile Induced Germanium Elimination

Due to the independence from external factors like temperature and solvent, we postulated a bimolecular process to cause the germanium elimination from phospho-BCH-germylenes **43**. To transfer this hypothesis to the stable germynes **44**, their reactivity towards nucleophiles was studied. Upon addition of $^{\text{Me}}\text{NHC}$ **49** to a solution of germylene **44b** at room temperature, colour change to brownish red as well as a red precipitate were observed. Control NMR spectra

displayed a mixture of germylene **44b**, larger amount of phosphole **46b** and free $^{\text{Me}}\text{NHC} **49**, suggesting selective germanium elimination. Completion of the reaction took seven days with an equimolar amount of $^{\text{Me}}\text{NHC} **49** and three days with two equivalents of $^{\text{Me}}\text{NHC} **49**. Therefore, the bimolecular reaction mechanism is postulated as displayed in Scheme 23: nucleophilic attack of the $^{\text{Me}}\text{NHC} **49** at the germanium atom (vacant p-orbital; LUMO) initiates the elimination. Though no proof could be provided, it was taken into account that the red precipitate formed during the reaction was not elemental germanium but an NHC stabilised digermanium, similar to that reported by Jones and coworkers (**50**) (Scheme 23).^[117]$$$$



Scheme 23 – Postulated nucleophile induced germanium elimination from germylene **44b** (Nu = $^{\text{Me}}\text{NHC} **49**) and NHC-stabilised digermanium **50** by Jones and coworkers (Dipp = 2,6-diisopropylphenyl).^[117]$

As $^{\text{Me}}\text{NHC} **49** is, based on the calculated buried volume and the *Tolman Electronic Parameter*^[118-119] respectively, a relatively small and strong nucleophile (% V_{bur} = 25.8; TEP = 2051.7 cm^{-1}), the reactivity of germylene **44b** towards the smaller and weaker electron donating DMAP **51** (% V_{bur} = 20.0; TEP = 2065.8 cm^{-1}) and the more sterically demanding but strong nucleophile $^{\text{Dipp}}\text{NHC} **52** (% V_{bur} = 44.0; TEP = 2050.5 cm^{-1}) was studied. In both cases, no reaction was observed. This led to the assumption that the elimination reaction is limited by both, sterical and electronic properties of the nucleophile. This furthermore provides an explanation for the inability of donor solvents like THF (TEP = 2081.2 cm^{-1}) to trigger the elimination, as this is an even weaker electron donor (Table 12).$$

Table 12 – Tolman Electronic Parameter of selected molecules.

	52	49	51	
TEP [cm⁻¹]	2050.5 ^[118-119]	2051.7 ^[118-119]	2065.8 ^[118]	2081.2 ^[118]
	Cl₃P:	(Me₂N)₃P:	Cl₂P^tBu	Cl₂P^{Ph}
TEP [cm⁻¹]	2097.0* ^[118]	2061.9* ^[120]	2087.9 ^[120]	2092.1* ^[120]

* = experimental value.

Transferring this knowledge to the reaction mixtures when synthesising phospho-BCH-germylenes **43-44**, it emerges that there are many nucleophilic compounds involved, that can potentially initiate the germanium elimination reaction. Those are the phospho-BCH-germylenes **43-44** themselves (P and Ge site), the phospholes **45-46** as well as the precursors, the germole dianions **[31]** and **[36]** and the aminodichlorophosphanes **38**. To internally compare the steric demand of those compounds to the nucleophiles studied experimentally, their buried volume was calculated using the *SambVca 2.1* web program^[92]. The calculated values can be found in Figure 38, ordered by ascending steric demand. In each case, the coordinating atom is highlighted in colour.

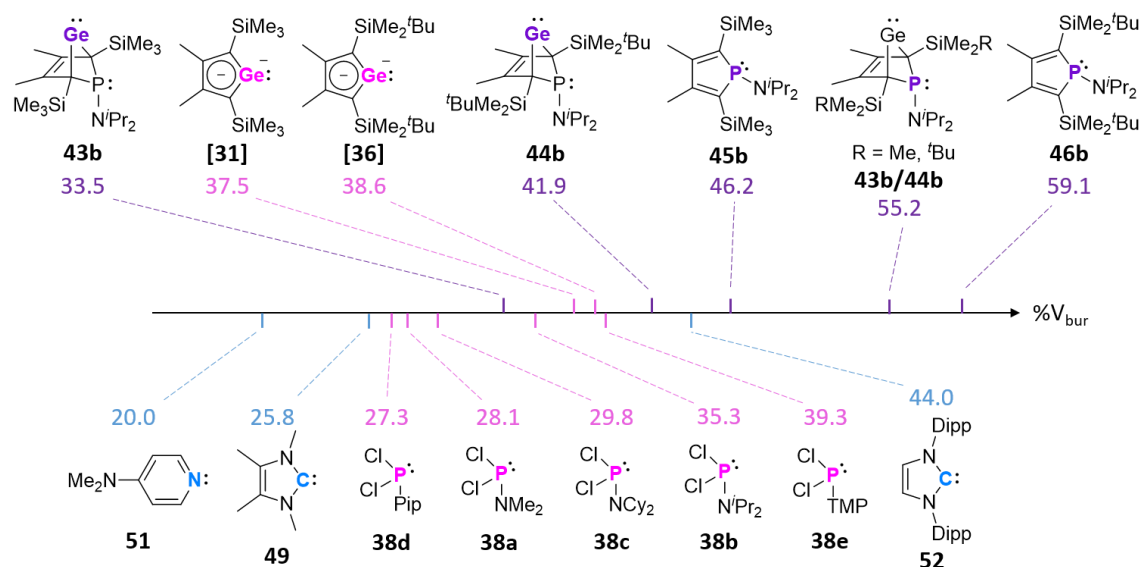


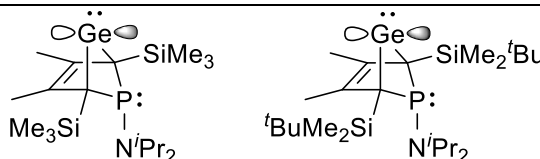
Figure 38 – Buried volume (% V_{bur}) of selected compounds used in this work. The donating atom is highlighted in colour: products (purple), precursors (pink) and other nucleophiles (blue). Description of the procedure for determination of the buried volume is provided in the appendix.

It needed to be considered that not only the steric demand of the nucleophile but also that of the electrophile is of importance, regarding the mechanism of the germanium elimination. It therefore seemed reasonable to add the buried volume of the nucleophile ($\%V_{\text{bur}}(\text{Nu})$) and that of the electrophile ($\%V_{\text{bur}}(\text{E})$) together (Equation 1). A similar idea was described by Zapf *et al.*^[121]

$$\%V_{\text{bur}}(\text{total}) = \%V_{\text{bur}}(\text{Nu}) + \%V_{\text{bur}}(\text{E}) \quad (1)$$

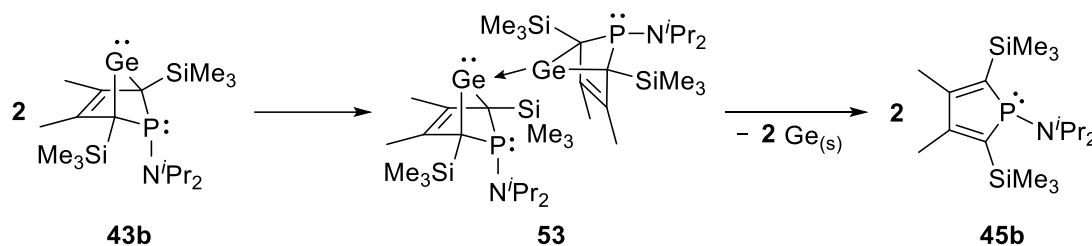
Here, the buried volume of the electrophilic part, the vacant p-orbital at the germanium atom of phospho-BCH-germylenes (LUMO), is $\%V_{\text{bur}}(\text{E}) = 33.5$ (**43b**), 41.9 (**44b**). Due to the different size of the silyl groups, the buried volume of germylene **44b** is about 20% larger than that of germylene **43b**. With regards to Equation 1, this means that smaller nucleophiles are required to induce the elimination reaction on germylene **44b**. The total buried volume ($\%V_{\text{bur}}(\text{total})$) for all possible nucleophile-electrophile combinations is given in Table 13.

Table 13 – Overview of the total buried volumes ($\%V_{\text{bur}}(\text{total})$) calculated based on Equation 1.

nucleophile (coord. atom)		
	43b as electrophile	44b as electrophile
^{Me} NHC 49 (C)	59.3	67.7
^{Dipp} NHC 52 (C)	77.5	85.9
germylene 43b (Ge)	67.0	-
germoleidiide [31] (Ge)	71.0	-
germylene 44b (Ge)	-	83.8
germoleidiide [36] (Ge)	-	80.5
phosphole 45b (P)	79.7	-
phosphole 46b (P)	-	88.1
germylene 43b/44b (P)	88.7	97.1
Cl ₂ PPip 38d (P)	60.8	69.2
Cl ₂ PNMe ₂ 38a (P)	61.6	70.0
Cl ₂ PNCy ₂ 38c (P)	63.3	71.7
Cl ₂ PN ⁱ Pr ₂ 38b (P)	68.8	77.2
Cl ₂ PTMP 38e (P)	72.8	81.2

Calculated values which can be used for comparison are the experimentally confirmed ones: the elimination reaction takes place for the pair of germylene **44b** and ^{Me}NHC **49** (%V_{bur}(total) = 67.7). It does not take place for the pairs of germylene **44b** and phosphole **46b** (%V_{bur}(total) = 88.1), germylene **44b** and germylene **44b** (%V_{bur}(total) = 83.8 (Ge), %V_{bur}(total) = 97.1 (P)) as well as for the pair of germylene **44b** and ^{Dipp}NHC **52** (%V_{bur}(total) = 85.9).

Based on the herein introduced approach, considering the calculated buried volume of the nucleophiles and the electrophiles in the context of the germanium elimination, the postulated self-induced elimination reaction of germylene **43b** is reinforced (Scheme 24). The total buried volume of the pair of germylenes **43b** and germylene **43b** is %V_{bur}(total) = 67.0. This is very similar to the total buried volume calculated for the pair of germylene **44b** and ^{Me}NHC **49** (%V_{bur}(total) = 67.7), for which it was experimentally shown that the elimination reaction proceeds. It can furthermore be concluded, that indeed, the larger size of the silyl groups of germylene **44b** prevents the self-induced elimination reaction (%V_{bur}(total) = 83.8). This value is similar to the total buried volume calculated for the pair of germylene **44b** and ^{Dipp}NHC **52** (%V_{bur}(total) = 85.9), for which it was experimentally shown that the elimination reaction does not take place (Table 13).

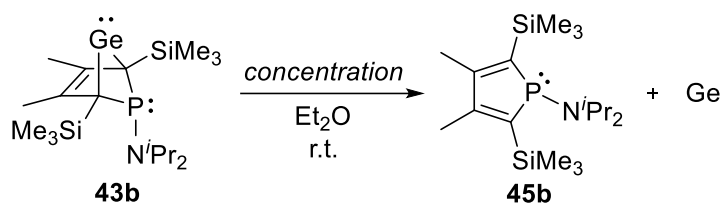


Scheme 24 – Proposed mechanism for the self-induced germanium elimination of phospho-BCH-germylene **43b**.

Regarding the synthesis of the germylenes, it should be considered that unreacted germole dianion as well as unreacted aminodichlorophosphane might also be able to initiate the germanium elimination from already formed germylenes. However, it cannot be expected that the aminodichlorophosphanes **38** are strong enough donors to initiate the elimination, as suggested based on the comparison of TEP values reported for related phosphanes (Table 12).^[118, 120] As there cannot be a critical %V_{bur}(total)-value determined but only values assigned for which the elimination proceeds (%V_{bur}(total) = 67.7) or does not proceed (%V_{bur}(total) = 85.9), predictions regarding the role of the dianions **[31]** (%V_{bur}(total) = 71.0) and **[36]** (%V_{bur}(total) = 80.5), as well as of phosphole **45b** (%V_{bur}(total) = 79.7) do not seem reasonable. The corresponding %V_{bur}(total)-values are somewhere in between those values (Table 13).

3.2.7.2 Dependence on the Concentration

The postulated bimolecular elimination process implies a concentration-dependent reaction rate (Scheme 25). Therefore, the kinetics of the elimination reaction were studied: A freshly prepared solution of germylene **43b** in diethyl ether ($c = 0.05 \text{ mol L}^{-1}$) was separated into two equal parts. One part was diluted to $c = 0.01 \text{ mol L}^{-1}$. The solutions were stirred at room temperature and NMR samples were taken over time. The starting ratio of germylene **43b** to phosphole **45b** was 73:24. The mixture additionally contained 3% of an unidentified compound ($\delta^{31\text{P}} = 79.0$) (Figure 39, top).



Scheme 25 – Investigations on the reaction kinetics of the germanium elimination reaction.

After three days, only trace amounts of germylene **43b** (1.3%) were left in the more concentrated solution and the mixture mostly contained phosphole **45b**. The percentage of the unidentified compound did not change (3%) (Figure 39, middle). After the same time, the diluted solution contained about 30% germylene **43b** and about 37% phosphole **45b**. Here, however, multiple sideproducts had formed. One of the main compounds (20%) features a ^{31}P NMR signal at $\delta^{31\text{P}} = 94.4$ (Figure 39, bottom). A side reaction like this had previously not been observed. However, no such highly diluted solutions of phospho-BCH-germylenes **43** have been handled until this point. The experiment was carried out a second time using the same concentration and gave identical results. The compound with the signal at $\delta^{31\text{P}} = 94.4$ could not be identified using NMR spectroscopy.

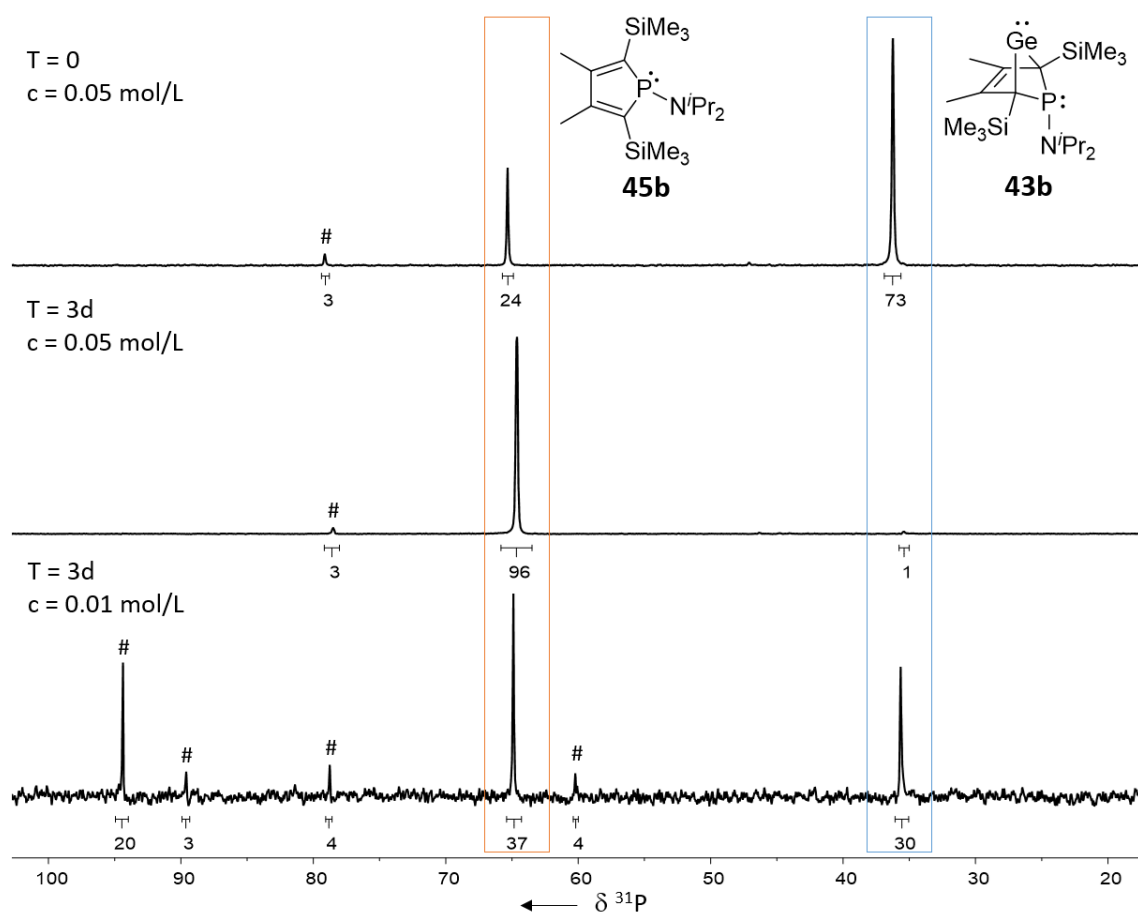


Figure 39 – $^{31}\text{P}\{^1\text{H}\}$ NMR spectra (202.3 MHz, 305 K, Et_2O) before the experiment (top), in after three days in $c = 0.05 \text{ mol L}^{-1}$ (middle) and after three days in $c = 0.01 \text{ mol L}^{-1}$ (bottom).

Despite the side reactions that took place in the diluted solution, it could be shown that the germanium elimination from phospho-BCH-germylenes proceeds faster in solutions of higher concentration. The dependence on the starting concentration suggests a second order reaction, which is coherent with the assumption of a bimolecular elimination process (Scheme 24).

3.2.7.3 DFT Calculations

To further support the postulated self-induced elimination mechanism (Scheme 24), DFT calculations were performed using the realistic system, starting with phospho-BCH-germylene **43b**. As isolated structures were optimised, it can be assumed that the entropy term is overestimated. Though the relative Gibbs free enthalpy difference ΔG for each step described in the following was incorporated in Figure 40, the focus will be on the calculated relative energy difference ΔE . The initialising step of the elimination reaction is the coordination of one germylene **43b**, acting as nucleophile, to another which is acting as electrophile. The optimised adduct **53** exhibits a Ge-Ge distance of 371 pm which is significantly larger than a Ge-Ge single

bond (242 pm^[108]), but within the sum of their van der Waals radii ($\Sigma(\text{vdW}) = 422 \text{ pm}^{[122]}$), indeed suggesting interaction between the two germynes. The adduct was found to be $\Delta E = -36 \text{ kJ mol}^{-1}$ lower in energy than the two separated germynes **43b**. As next step, it seemed reasonable to assume that upon formation of adduct **53**, the germanium elimination takes place and finally ends in the formation of two equivalents of phosphole **45b** and precipitation of two equivalents of germanium. Compared to the starting material, two equivalents of germylene **43b**, the elimination and precipitation of the germanium is predicted to be favoured by $\Delta E = -223 \text{ kJ mol}^{-1}$. For the calculation of this step, it was assumed, that triplet digermanium ($^3\text{Ge}_2$) is eliminated from the adduct **53**, which then dissociates and precipitates. The calculated dissociation energy of Ge_2 is $D^0(\text{calc}) = +252 \text{ kJ mol}^{-1}$, which is smaller than the value reported in the literature ($D_0 = +263.5 \text{ kJ mol}^{-1}^{[123]}$), but in an acceptable range. The sublimation enthalpy is $\Delta H_s(\text{Ge}_{(\text{g})} \rightarrow \text{Ge}_{(\text{s})}) = -371.7 \text{ kJ mol}^{-1}^{[123]}$. The intermediate steps are predicted to be high in energy ($\Delta E = +269$ and $+521 \text{ kJ mol}^{-1}$) (Figure 40). Still, the herein performed analysis based on DFT calculations supports the postulated mechanism (Scheme 24), as the formation of the initial germylene-germylene adduct **53** seems feasible. However, it can be concluded that the precipitation of germanium is the driving force in this reaction.

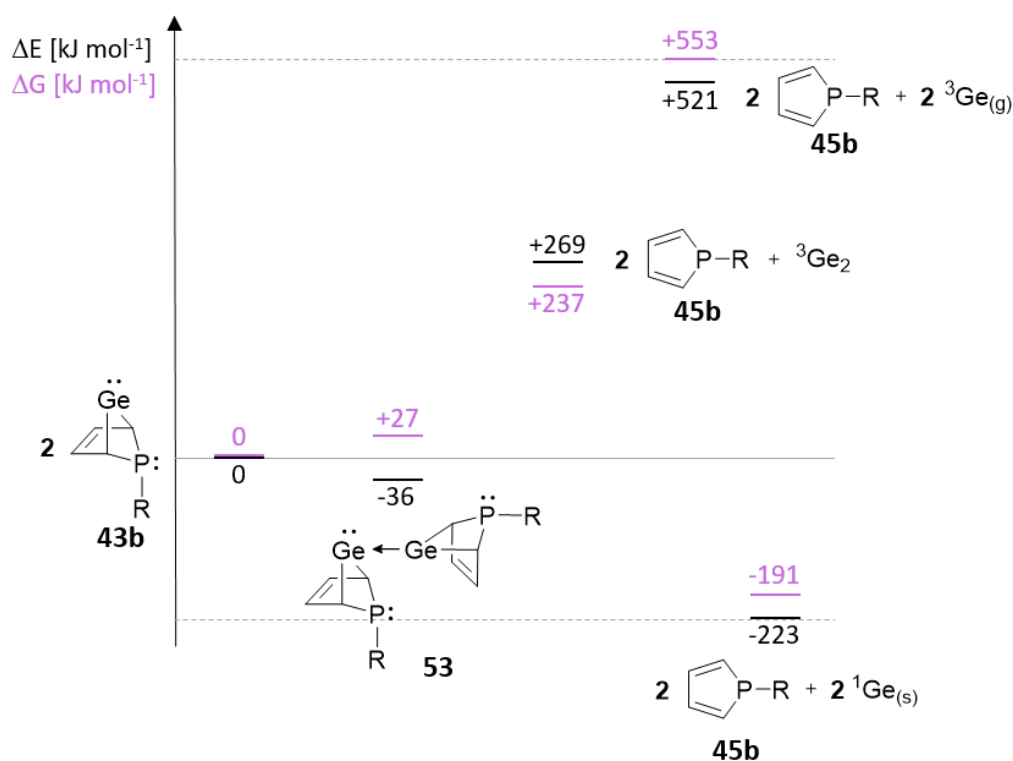


Figure 40 – Energy chart displaying the calculated overall energy gain of the self-induced germanium elimination from phospho-BCH-germylene **43b** (M06-2X/6-311+G(d,p)). The substituents of the backbone are omitted for clarity in this figure. $\text{R} = \text{N}^i\text{Pr}_2$. All structures shown are local minima.

3.3 Attempting to Expand the Scope: Pnicta-BCH-Germylenes

The potential and the limits of pnictogen-based bicyclic tetrylenes (pnicta-BCH-tetrylenes), like the herein introduced phospho-BCH-germylenes **43-44**, should be further explored. Considering heavier and lighter homologues of the precursors used up to this point, the experimental scope should be expanded. Therefore, following the established synthetic procedure of phospho-BCH-germylenes **43-44**, dipotassium tetrolediides, obtained upon reduction of dichlorotetroles by potassium metal, were reacted with dichloro organopnictogen precursors. An overview of the precursors applied in these scope-expanding studies, is given in Figure 41.

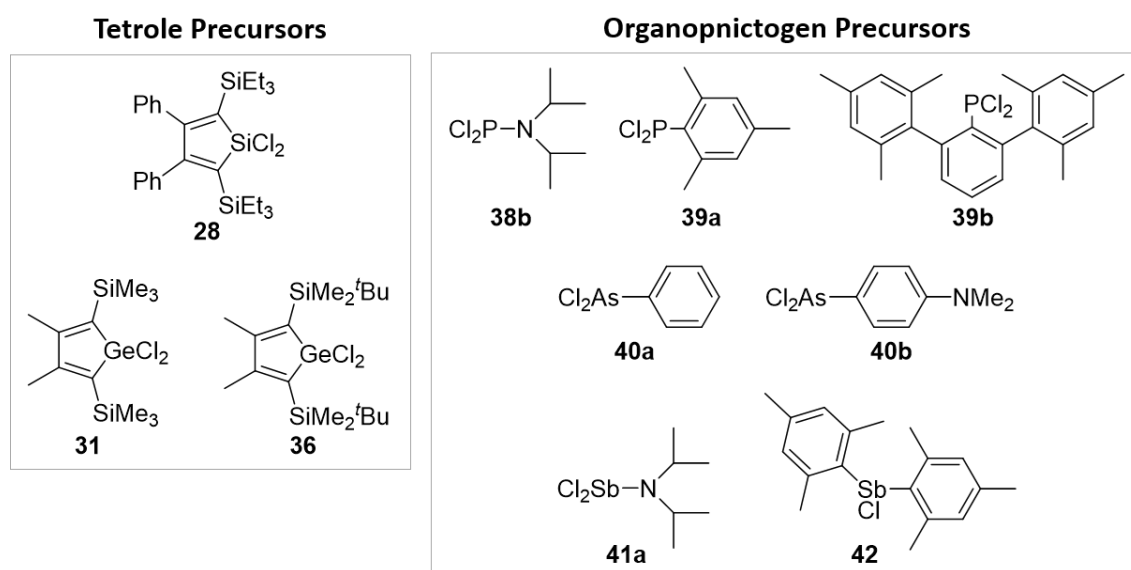
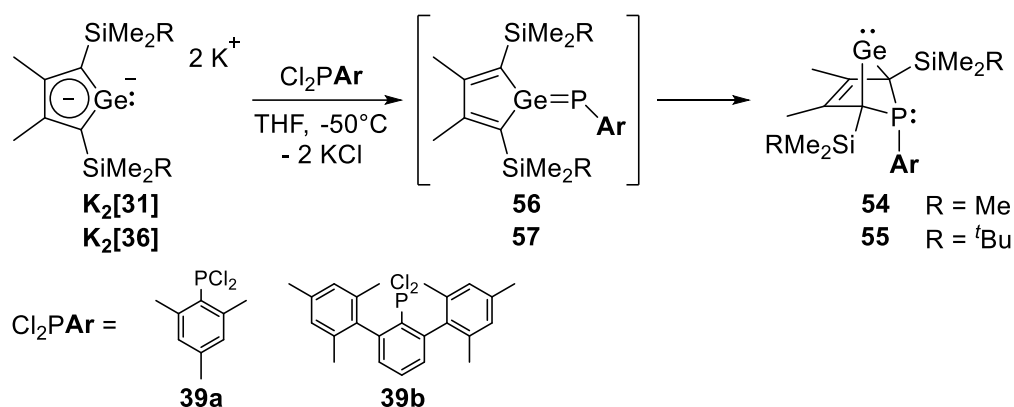


Figure 41 – Precursors used for the attempted syntheses of different pnicta-BCH-tetrylenes.

3.3.1 Arylphospha-BCH-Germylenes

Attempts were made formally exchanging the aminosubstituents of aminophospha-BCH-germylenes **43-44** for arylsubstituents to obtain the respective arylphospha-BCH-germylenes **54-55**. Therefore, the dipotassium germolediides $K_2[31]$ and $K_2[36]$ were reacted with two different aryldichlorophosphanes, Cl_2PMes **39a** and $Cl_2P^{Mes-Ter}$ **39b** (Scheme 26). The reactions were carried out using the established reaction conditions synthesising aminophospha-BCH-germylenes **43-44**: the arylphosphane **39** was added to a THF solution of the germolediide salt $K_2[31]$ or $K_2[36]$ at $-50^\circ C$.



Scheme 26 – Attempted synthesis of arylphospha-BCH-germylenes **54** with the sterically demanding mesityl- **39a** and 2,6-dimesitylphenyl-phosphanes **39b**.

Using the germole diide salt $\text{K}_2[\mathbf{31}]$ as precursor, complex product mixtures were obtained. On the other hand, with the *tert*butyldimethylsilyl-substituted germole diide salt $\text{K}_2[\mathbf{36}]$, the formation of one main product was indicated by the recorded NMR spectra. Integration of the corresponding signals in the ^1H NMR spectrum suggests a structure that consists of equal parts of the germole and the mesitylphosphane. The ^{13}C NMR signals of the backbone carbon atoms were detected in the typical sp^2 region ($\delta^{13}\text{C}(\text{C}^{1/4}) = 137.7$ and $\delta^{13}\text{C}(\text{C}^{2/3}) = 163.7$). This was indicative for either the respective phosphole or the phosphagermafulvene **57**. However, the detected compound exhibits a remarkably highfield shifted ^{31}P NMR signal ($\delta^{31}\text{P} = -144.2$) (Figure 42). This is not only distinctively different from all herein discussed compounds but also not in the expected region for phospholes ($\delta^{31}\text{P} > 0$) or phosphagermafulvene structures ($\delta^{31}\text{P} > 100$).^[124]

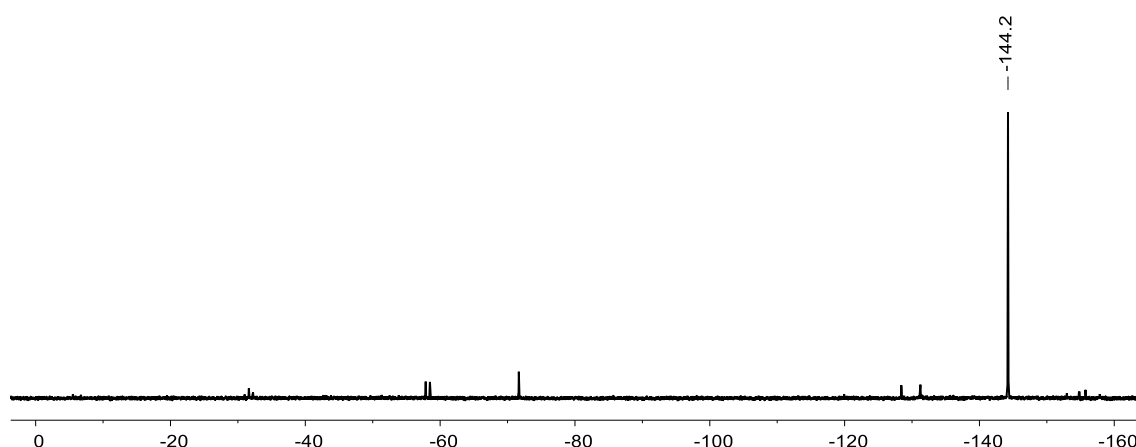
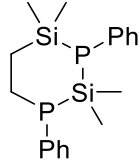
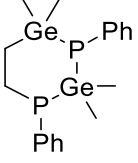
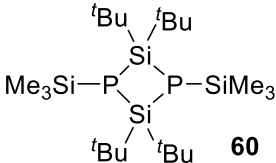


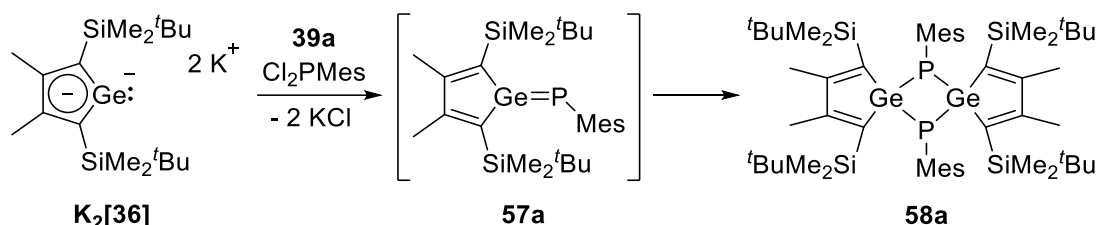
Figure 42 – $^{31}\text{P}\{^1\text{H}\}$ NMR spectrum (202.3 MHz, 305 K, benzene- d_6) of the product mixture obtained from the reaction of germole diide salt $\text{K}_2[\mathbf{36}]$ and mesitylphosphane.

Highfield ^{31}P NMR resonances, as the observed one at $\delta^{31}\text{P} = -144.2$, are reported in the literature e.g. for small phosphorus-containing rings and rings systems, containing a phosphorus atom located between two heavier group 14 elements ($\text{E} = \text{Si}, \text{Ge}$) (Table 14).^[124-127]

Table 14 – Cyclic compounds, containing P and Si or Ge atoms, reported in the literature.^[125-127]

			
	Couret <i>et al.</i> ^[125]	Escudie <i>et al.</i> ^[126]	Fritz <i>et al.</i> ^[127]
$\delta^{31}\text{P}$	-144.5 (Si-P-Si) -75.0 (Si-P-C)	-126.2 (Ge-P-Ge) -74.3 (Ge-P-C)	-226

We therefore suggest that indeed the intended double salt metathesis reaction took place upon addition of the mesitylphosphane **39a** to the germalediide salt $\text{K}_2[\mathbf{36}]$. However, the thereby formed phosphagermafulvene **57a** did not rearrange to give the phospho-BCH-germylene **55a** but dimerised to give the dimeric compound **58a**, featuring a four-membered Ge-P-Ge-P ring (Scheme 27). The presence of the dimer **58a** was furthermore indicated using high resolution mass spectrometry (calculated: $m/z = 1064.4326$, found (EI): $m/z = 1064.4311$).



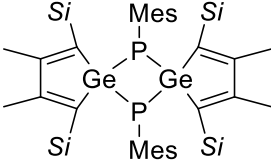
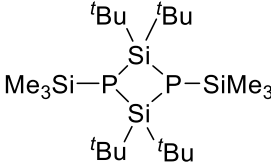
Scheme 27 – Postulated dimerisation of two phosphagermafulvenes **57a** giving the dimeric structure **58a** featuring a four-membered P-Ge-P-Ge ring.

Indication was found that by using dichloro(terphenyl)phosphane ($\text{Cl}_2\text{P}^{\text{MesTer}}$) **39b** as precursor, a similar reaction takes place. The spectra are more cluttered, however, one of the main ^{31}P NMR signals is in the similar range ($\delta^{31}\text{P} = -126.6$). Furthermore, matching crosspeaks were detected in the $^1\text{H}^{31}\text{P}$ HMBC NMR spectrum, indicating the presence of fulvene-dimer **58b**.

DFT calculations were performed on the herein suggested structure, substituted with the smaller SiMe₃ groups (**59a**) and the larger SiMe₂^tBu groups (**58a**), as well as on compound **60** reported by Fritz *et al.*^[127] Whereas the predicted ^{31}P NMR chemical shift of the four-membered

Si-P-Si-P ring (**60**) is close to the reported ^{31}P NMR chemical shift ($\Delta(\delta^{31}\text{P}) = 20$ ppm), the calculated value for the herein discussed four-membered Ge-P-Ge-P ring (**58a**) is shifted to lower field by $\Delta(\delta^{31}\text{P}) = 80\text{-}90$. We do not attribute this discrepancy to the different sized silyl groups as becomes clear by comparison of the data calculated for the different silyl groups ($\Delta(\delta^{31}\text{P}) = 14\text{-}16$) (Table 15).

Table 15 – Calculated ^{31}P NMR chemical shifts (M06L/6-311+G(2d,p)//M06-2X/6-311+G(d,p)) of the phosphagermafulvene dimer **58a** and **59a** and of compound **60** by Fritz *et al.*^[127]

	 58a/59a	 60
$\delta^{31}\text{P}_{\text{calc}}$	-55, -66 (59a , Si = SiMe ₃) -41, -50 (58a , Si = SiMe ₂ ^t Bu)	-246
$\delta^{31}\text{P}_{\text{exp}}$	-144.5 (58a , Si = SiMe ₂ ^t Bu)	-226 ^[127]
$\Delta(\delta^{31}\text{P})$	80–100 ppm	20 ppm

However, due to detection of the corresponding exact mass, it still was assumed that the dimeric fulvene **58a** is the species present in solution. Therefore, this field offers potential for further studies.

3.3.2 Pnicta-BCH-Silylenes

Exchanging germole for silole, in theory, is a rather small change that comes with an interesting feature: it provides another NMR active nucleus in the targeted molecule, giving hints on the electronic environment of the synthesised compound. The switch from germylene to silylene has successfully been achieved by Müller and coworkers: corresponding to the hafnocena-BCH-germylene **21**^[54], the authors reported on the synthesis of the analogous hafnocena-BCH-silylene **61**. It exhibits a remarkable highfield ^{29}Si NMR shift of $\delta^{29}\text{Si} = -155.2$.^[55] Another example from the group is the related sila-BCH-silylene **62**. Its silylene silicon atom exhibits an even more highfield shifted ^{29}Si NMR signal ($\delta^{29}\text{Si} = -210.6$)^[58] (Figure 43). The highfield shift of both compounds (**61**) and (**62**), compared to other two-coordinate silylenes, was assigned to the higher coordination number caused by the homoconjugative interaction.^[58] The effect becomes even more clear regarding the five-coordinated silicon(II) borole complexes **63** and **64** of

Bührmann and Sindlinger and coworkers, exhibiting ^{29}Si NMR chemical shifts of $\delta^{29}\text{Si} = -337.5$ and -349.4 , respectively.^[86, 128]

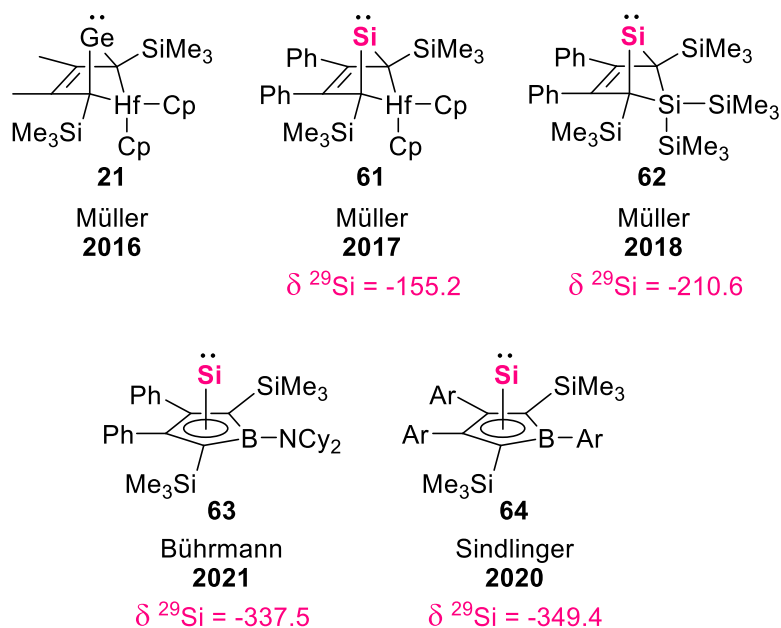
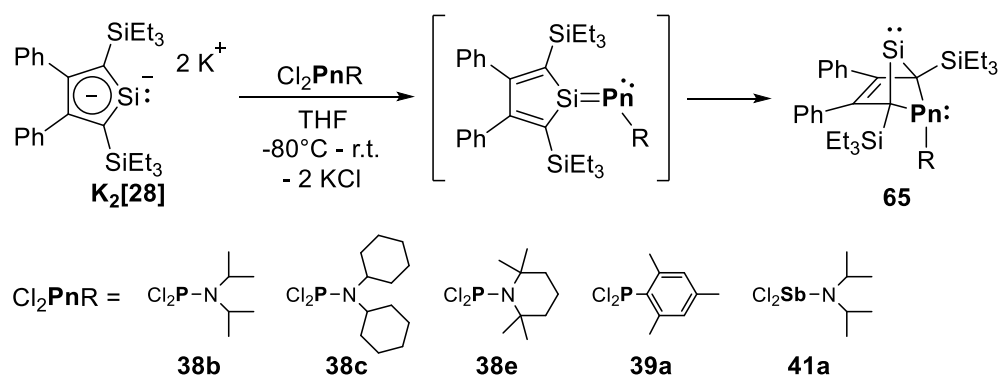


Figure 43 – Selected examples of germylenes and silylenes reported in the literature
 (Ar = 3,5-*tert*butylphenyl).^[54-55, 58, 86, 128]

With this in mind, the synthesis of pnicta-BCH-silylenes **65** was attempted, as comparative analysis of their ^{29}Si NMR chemical shift could potentially give insight into the homoconjugative interaction in pnictogen-based BCH-silylenes and furthermore, would give insight into the differences that arise from exchange of the pnictogen-substituents as well as from the pnictogen itself. Herein, the 2,5-bis(triethylsilyl)-substituted silole diide salt **K₂[28]**, obtained upon reduction of the respective dichlorosilole **28** with potassium metal, was reacted with three aminodichlorophosphanes (**38b**, **38c**, **38e**), dichloro(mesityl)phosphane **39a** and (diisopropylamino)dichlorostibane **41a** (Scheme 28).

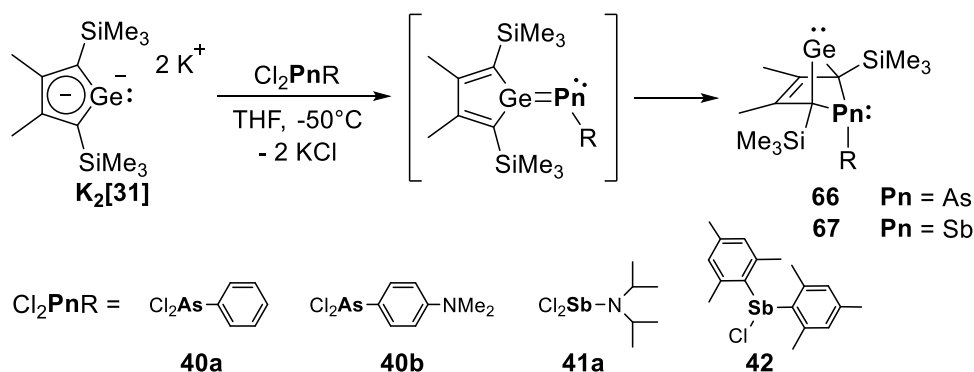


Scheme 28 – Intended synthesis of pnicta-BCH-silylenes.

The reactions did not meet the expectations as described in Scheme 28 and furthermore, did not proceed selectively. Independent from the dichloro organopnictogen precursor used, complex product mixtures were obtained. Attempts to optimise the reaction conditions, mainly through temperature control, as successfully applied on the aminophospha-BCH-germylenes **43-44**, did not result in remarkable change of the outcome. Therefore, this topic was not pursued any further within these studies.

3.3.3 Arsa- and Stiba-BCH-Germylenes

Attempts were made expanding the chemistry of pnicta-BCH-germylenes from phospho- to their arsa- (**66**) and stiba-derivatives (**67**). Therefore, dipotassium germoldiide **K₂[31]** was reacted with two different aryldichloroarsanes **40a-b**, aminodichlorostibane **41a** and diarylchlorostibane **42**. The reactions were carried out in THF between -50°C and room temperature (Scheme 29).



Scheme 29 – Intended synthesis of arsa- **66** and stiba-BCH-germylenes **67**.

The recorded NMR spectra of the obtained reaction mixtures showed unidentifiable product mixtures. Variation of the reaction time and the temperature did not enhance the selectivity of the reaction. As these test reactions did not seem to lead to promising results, this topic was not pursued any further. However, we were later given the hint, that going from phosphorus-based reagents to arsenic- and antimony-based reagents, it might be helping to carry the reaction out in unpolar solvents like hexane.^[129] Due to limited time, this was not tested within these studies.

3.3.4 Digression to Group 16: Germaselenone

A digression from group 15 to group 16 precursors was made with the intended goal to synthesise germaselenone **68**, a germafulvene analogon. Preliminary DFT calculations using model compounds **68'**-**70'**^[130] suggested its energetical favouring over the rearranged bicyclohexene structure **69'** ($\Delta E = -113 \text{ kJ mol}^{-1}$). Moreover, a remarkable energy gain was predicted upon dimerisation of the germaselenone **68'**, giving the dimeric compound **70'** ($\Delta E = -260 \text{ kJ mol}^{-1}$) (Figure 44).

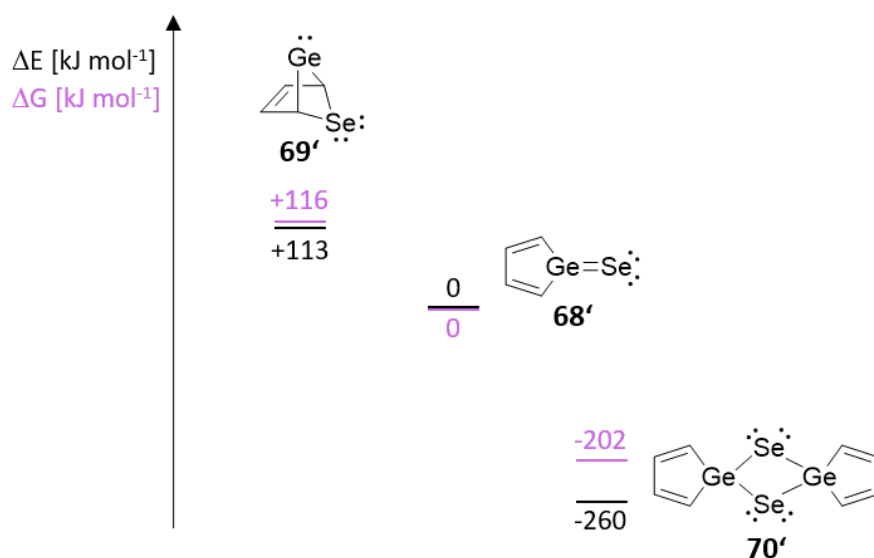
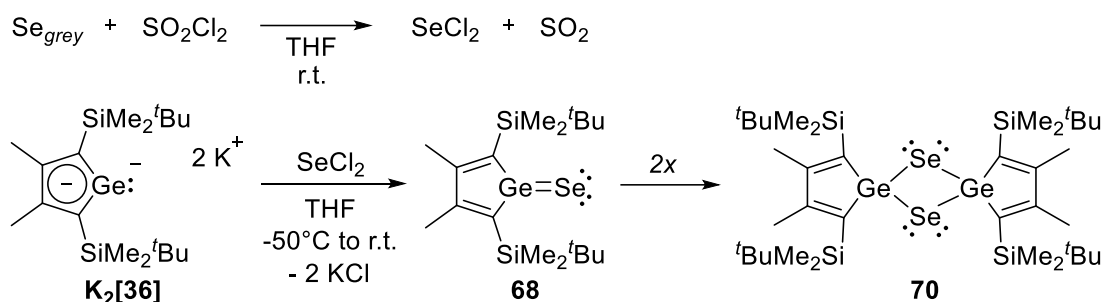


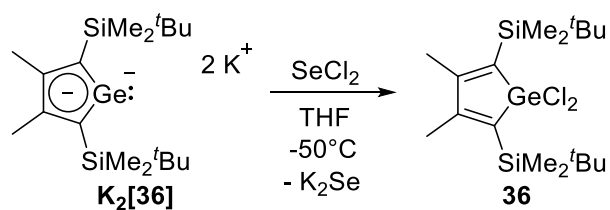
Figure 44 – Calculated relative energies of the germaselenone **68'**, its BCH isomer **69'** and its dimerisation product **70'** (M06-2X/def2-tzvp).^[130]

To synthesise the germaselenone, seleniumdichloride was synthesised following a literature procedure^[131]: The THF solution of seleniumdichloride was synthesised *in situ* from grey selenium and sulfurylchloride (Scheme 30). Product formation was indicated by colour change from yellowish to red and could be confirmed by ⁷⁷Se NMR spectroscopy. The recorded spectra showed one signal at $\delta^{77}\text{Se} = 1828.2 \text{ ppm}$ in accordance with the literature.^[131] The reaction with dipotassium germolediide **K₂[36]** was carried out at low temperature by addition of the seleniumdichloride solution to a THF solution of the germolediide salt (Scheme 30).



Scheme 30 – Synthesis of seleniumdichloride and intended reaction with dipotassium germolediide.

The reaction proceeded not as expected or intended. The recorded NMR spectra displayed a complex reaction mixture. The dichlorogermole **36** was identified as main product amongst several other unidentified compounds. The results were reproducible which eliminates the possibility of an incomplete reduction of the dichlorogermole **36** to the germolediide salt **K₂[36]** in the first place. Therefore, we assume that the germolediide was oxidised by seleniumdichloride so that under formation of potassiumselenide, the dichlorogermole **36** was formed (Scheme 31).



Scheme 31 – Reaction pathway of dipotassium germolediide towards seleniumdichloride, assumed on the basis of the products found.

3.4 Reactivity Studies on Aminophospha-BCH-Germynes

Against the background of the reductive germanium elimination (Chapter 3.2.7), the properties of the germylene moiety of aminophospha-BCH-germylenes **43-44** have already been discussed. There, the postulated self-induced elimination mechanism with the germylene acting as electrophile and nucleophile at the same time, pointed out its amphiphilic properties. Within this chapter, the reactivity of aminophospha-BCH-germylenes **43-44** will be further explored. Though the previous discussion mainly focussed on the germylene part of this compound class, it offers additional reaction sites to potentially react with electrophilic substrates: Figure 45 displays the frontier molecular orbitals of germylene **43b** as an exemplary representative of the herein examined compound class, exhibiting three lone pairs, located at the germanium atom (HOMO-4), the phosphorus atom (HOMO-2) and at the nitrogen atom (HOMO-1), as well as delocalised electron density in its backbone (HOMO).

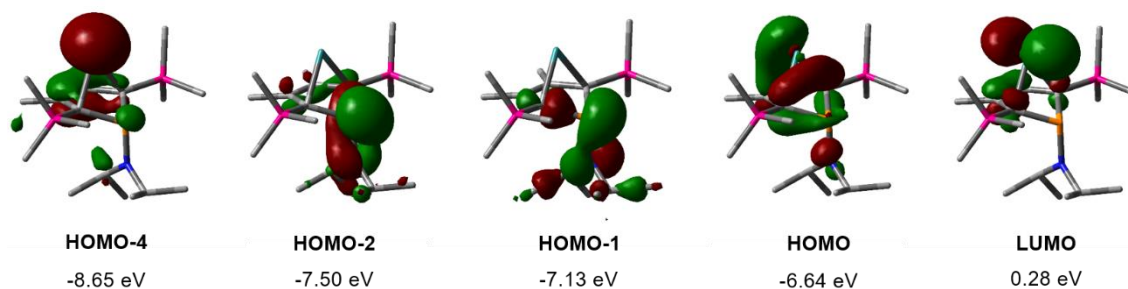


Figure 45 – Frontier molecular orbitals of germylene **43b** (M06-2X/6-311+G(d,p); isodensity value 0.04).

All reactivity studies presented in the following chapters were carried out using the diisopropylamino-substituted germynes **43b** and **44b** as well as the dicyclohexylamino-substituted germynes **43c** and **44c** as precursors (Figure 46).

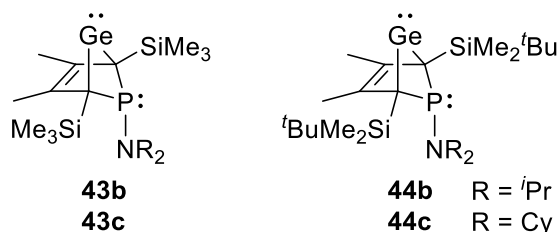
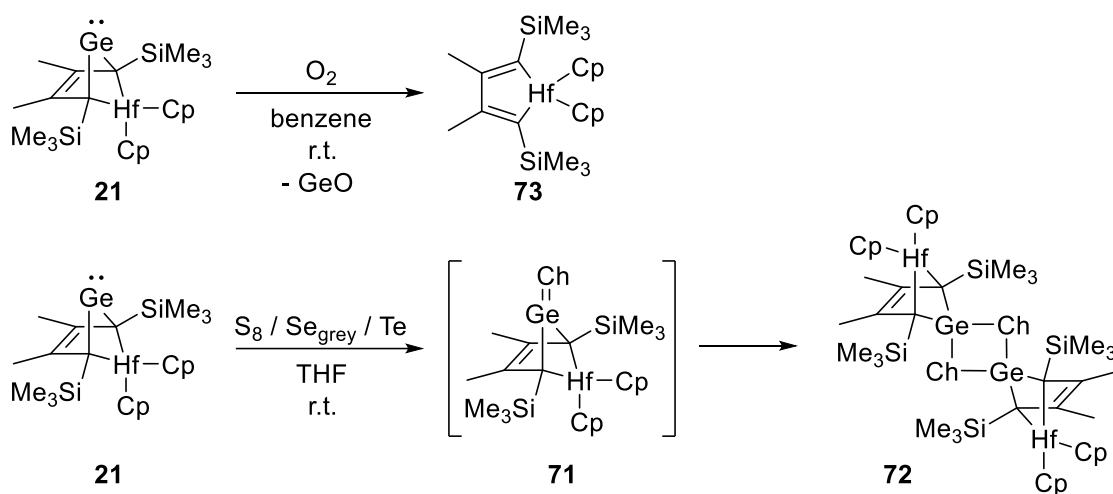


Figure 46 – Phospha-BCH-germylenes **43b+c** and **44b+c** used as starting material in the reactivity studies.

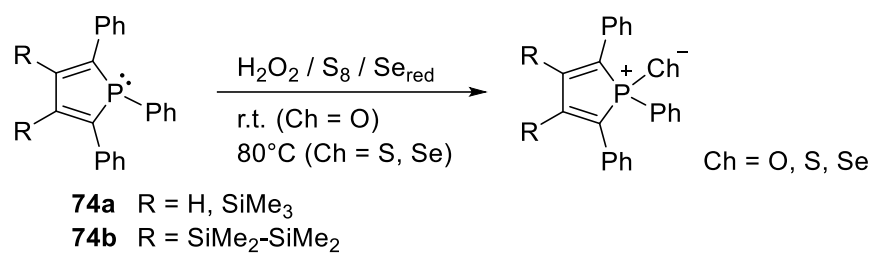
3.4.1 Oxidation Reactions

First, the reactivity of phospho-BCH-germylenes **43-44** towards elemental chalcogens was examined. Dong *et al.* reported on the reactivity of the related hafnocena-BCH-germylene **21** towards elemental chalcogens, targeting heavier ketones. Instead of the heavier ketones **71**, their dimerisation products, digermetanes **72**, featuring four-membered Ge-Ch-Ge-Ch rings for Ch = S, Se and Te, were obtained (Scheme 32, bottom).^[132] Upon exposure to oxygen (O₂), decomposition was observed, giving the corresponding hafnocenacyclopentadiene **73** and germanium monoxide (Scheme 32, top).^[54]



Scheme 32 – Reactions of hafna-BCH-germylene **21** towards elemental chalcogens.^[54, 132]

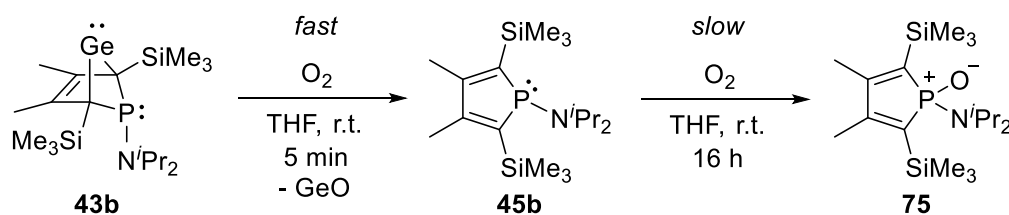
In the present study, the reaction at the phosphorus site should be considered as well. Trivalent phosphorus atoms, e.g. in phosphanes and phospholes, are likely to be oxidised by chalcogens.^[133-135] Scheme 33 displays a representative example from Pietschnig and coworkers.^[134] The authors reported on the oxidation of the phosphorus atom of two sterically demanding phospholes **74a-b**. In phosphole chemistry, typically oxygen transfer reagents like hydrogen peroxide are used to introduce oxygen into the phosphole.^[134, 136] The reactions with sulfur and selenium are mostly, as also reported by Pietschnig and coworkers, carried out at elevated temperature. Furthermore, it must be noted that typically red selenium is required to oxidise the phosphorus atom.^[137]



Scheme 33 – Exemplary reaction of phospholes **74a-b** towards chalcogens or chalcogen transfer reagents, described by Pietschnig and coworkers.^[134]

3.4.1.1 Reactivity Towards Oxygen (O₂)

Phospha-BCH-germylene **43b** was exposed to oxygen by running air through a column filled with phosphorous pentoxide (Scheme 34). This resulted in a rapid colour change of the THF solution from orange-brownish to yellow. Furthermore, a colourless precipitate was observed. As deduced by NMR spectroscopy, after five minutes of oxygen exposure, germylene **43b** was fully consumed.



Scheme 34 – Two-step reaction between germylene **43b** and oxygen.

The recorded ³¹P NMR spectrum displays a signal assigned to the phosphole **45b** ($\delta^{31}\text{P} = 65.0$) and an additional signal with a share of 18% at $\delta^{31}\text{P} = 64.6$ (Figure 47, middle). Stirring under oxygen exposure was continued overnight. This resulted in full consumption of the phosphole **45b**. The obtained product, featuring the ³¹P NMR signal at $\delta^{31}\text{P} = 64.6$ (in THF; $\delta^{31}\text{P} = 63.0$ in benzene-d₆), was identified as the phosphole oxide **75** (Figure 47, bottom). The observations suggest a two-step reaction between germylene **43b** and oxygen: in a first step, analogously to the reported reaction of hafna-BCH-germylene **21** towards oxygen^[54], germanium monoxide is eliminated. Then, in a second step, the phosphorus atom of the resulting phosphole **45b**, is oxidised. Here, the latter reaction seemed to proceed quite slow. Indeed, it was possible, to prevent the oxidation of the phosphorus atom and to really separate the two steps by carrying out the reaction at lower temperature (-50°C).

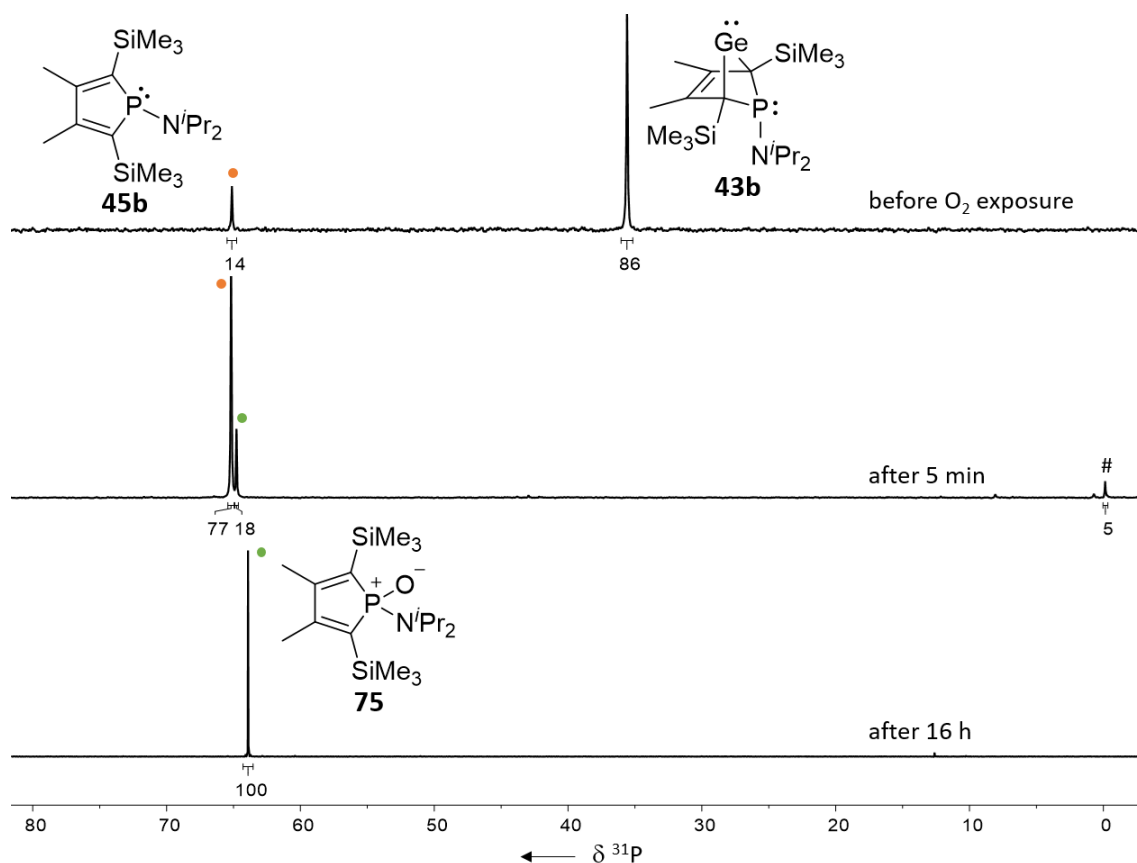


Figure 47 – $^{31}\text{P}\{^1\text{H}\}$ NMR spectra (202.3 MHz, 305 K) before oxygen exposure (top, in THF), after 5 min (middle, in THF) and 16 h (bottom, in benzene- d_6) of oxygen exposure at room temperature (● = phosphole **45b**, ● = phosphole oxide **75**, # = impurity).

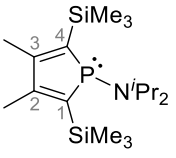
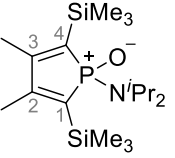
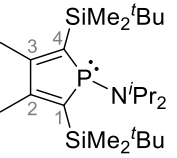
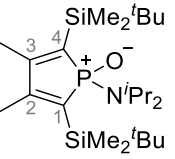
Although their ^{31}P NMR chemical shifts are very similar, phosphole **45b** and phosphole oxide **75** can clearly be differentiated by NMR spectroscopic analysis. Upon oxidation and quarternisation of the phosphorus atom, the $\text{C}^{1/4}$ carbon atoms are shifted to higher field ($\Delta(\delta^{13}\text{C}) = -7.5$ ppm) and the $\text{C}^{2/3}$ carbon atoms are shifted to lower field ($\Delta(\delta^{13}\text{C}) = +8.1$ ppm) than those in phosphole **45b**. Furthermore, the coupling constants to the phosphorus atom become larger ($\Delta(^1J_{\text{C,P}}) = 38$ Hz; $\Delta(^2J_{\text{C,P}}) = 7$ Hz). Especially the more than doubled in size $^1J_{\text{C,P}}$ coupling is striking. Concurrently, the $^2J_{\text{Si,P}}$ coupling constant decreases by $\Delta(^2J_{\text{Si,P}}) = 9$ Hz and the corresponding ^{29}Si NMR signal is shifted to lower field ($\Delta(\delta^{29}\text{Si}) = 0.9$ ppm) (Table 16).

For comparison, a toluene solution of the larger phospho-BCH-germylene **44b** was exposed to oxygen as well. After five minutes, a colour change from orange to yellow and the formation of a colourless precipitate was observed. The solution was exposed to oxygen for additional 30 minutes. The recorded NMR spectra revealed that again, the germylene **44b** was fully consumed. However, different from the previously described reaction, the solution contained only a trace amount (3%) of the corresponding phosphole oxide **76**, which is significantly less

than the 18% of phosphole oxide **75** obtained after only 5 minutes of reaction time. It was therefore assumed, that the second step, the oxidation of the phosphorus atom, is much slower for the larger phosphole **46b** than for the smaller one **45b**. The experiment was not carried out until full conversion into the phosphole oxide **76** was achieved.

The obtained NMR spectroscopic data of phosphole oxide **76** resembles that obtained for the smaller phosphole oxide **75**. The ^{13}C NMR shift of the backbone carbon atoms ($\delta^{13}\text{C} = 135$ ($\text{C}^{1/4}$), 160 ($\text{C}^{2/3}$)) is basically the same. As observed for phosphole oxide **75**, compared to its precursor phosphole **45b**, the ^{29}Si NMR signal of phosphole oxide **76** is shifted to lower field ($\Delta(\delta^{29}\text{Si}) = 0.8$ ppm) and the $^2J_{\text{Si,P}}$ coupling constant decreases as well (Table 16). The ^{31}P NMR chemical shift of both phosphole oxides **75** ($\delta^{31}\text{P} = 63.0$) and **76** ($\delta^{31}\text{P} = 63.7$) is in the expected range of about $\delta^{31}\text{P} = 20\text{--}70$ for R_3PO compounds.^[124]

Table 16 – Selected NMR spectroscopic data of the phospholes **45b** and **46b** as well as of the phosphole oxides **75** and **76**.

					
		45b	75	46b	76
$\delta^{13}\text{C}$	$\text{C}^{1/4}$ ($^1J_{\text{C,P}}$)	143.0 (33)	135.5 (71)	140.7 (36)	135*
	$\text{C}^{2/3}$ ($^2J_{\text{C,P}}$)	151.9 (19)	160.0 (26)	154.0 (16)	160*
$\delta^{29}\text{Si}$	($^2J_{\text{Si,P}}$)	-10.8 (25)	-9.9 (16)	-3.1 (22)	-2.3 (14)
$\delta^{31}\text{P}$		65.6	63.0	71.7	63.7

*Data was retrieved from the $^1\text{H}^{13}\text{C}$ HMBC NMR spectrum.

Phosphole oxide **75** was furthermore characterised by single crystal XRD analysis. Its solid state structure is very similar to those reported for other phosphole oxides. Here, it is compared to the 1,2,5-triphenylphosphole oxide **77** by Kumaravel *et al.*^[138] and the 1,2,5-triphenyl-3-trimethylsilylphosphole oxide **74a** by Klintuch *et al.*^[134]. As expected for a butadiene system, the $\text{C}^1\text{-C}^2$ bond (135.4 pm) is shorter than the $\text{C}^2\text{-C}^3$ bond (151.4 pm). These bond lengths are within the expected range of C-C double and single bonds, respectively^[107], and are similar to the reported ones. However, the $\text{C}^2\text{-C}^3$ bond in phosphole oxide **75** is longer than that reported by Kumaravel *et al.* ($\Delta(\text{C}^2\text{-C}^3) = 4.8$ pm). The P- C^1 (180.5 pm) and the P-O (148.8 pm) bonds lengths in phosphole oxide **75** are almost identical to the corresponding bond lengths of the literature known phosphole oxides **77** and **74a** (Table 17).

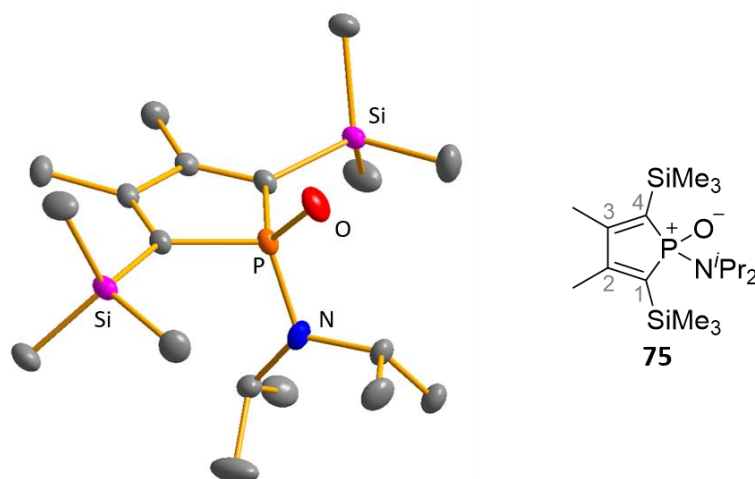


Figure 48 – Molecular structure of phosphole oxide **75** in the crystal. Hydrogen atoms are omitted for clarity. Thermal ellipsoids at 50% probability level. Space group: $P2_1/n$.

Table 17 – Selected structural data of the herein synthesised phosphole oxide **75** and phosphole oxides **77** and **74a** described in the literature.^[134, 138]

	 75	 77 Kumaravel <i>et al.</i> ^[138]	 74a Klintuch <i>et al.</i> ^[134]
P–O	148.78(6)	149.3	148.4
P–C ¹	180.46(8)	181.8	181.5-182.8
C ¹ –C ²	135.42(10)	135.5	134.9
C ² –C ³	151.37(11)	146.6	n.a.

The formation of stable phosphole oxides with both, the smaller and the larger phosphole **45b** and **46b** precursor, underlines their relatively large steric demand. Phosphole oxides with less sterically demanding substituents readily undergo Diels-Alder like dimerisation reactions upon formation (Scheme 35).^[113, 137, 139]



Scheme 35 – Exemplaric [4+2] Diels-Alder cycloaddition of a phosphole oxide, typically giving the endo dimer.^[137, 139]

DFT Calculations

The formation of the phosphole oxide **75** was additionally examined using DFT calculations. The initial elimination of germanium oxide, presumably via intermediate formation of the germanone **78** ($\Delta E = -165 \text{ kJ mol}^{-1}$), which provides an energy gain of $\Delta E = -189 \text{ kJ mol}^{-1}$. The second step of the observed reaction, which was found to proceed slow in the experiment, brings the greater energy gain of $\Delta E = -709 \text{ kJ mol}^{-1}$ (Figure 49). We correlated this energy gain to the P-O bond formation (407 kJ mol^{-1}).^[140]

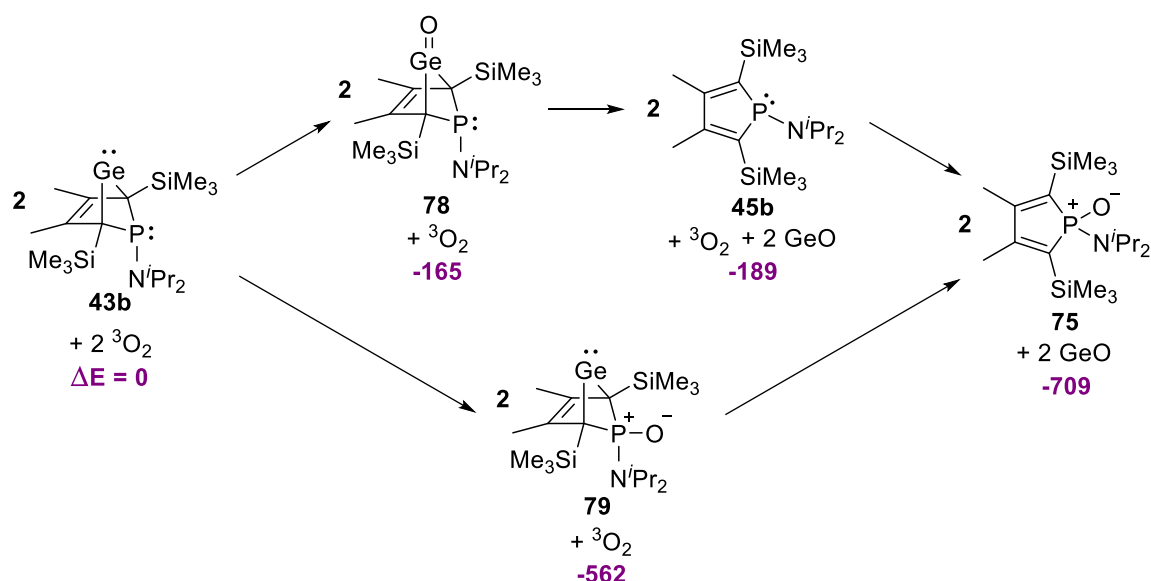
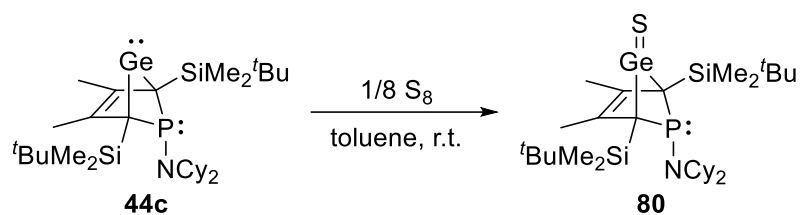


Figure 49 – DFT calculations (M06-2X/6-311+G(d,p)) corresponding to the reaction of oxygen towards germylene **43b**, ΔE in [kJ mol^{-1}].

However, the calculations did not suggest the reaction to proceed as observed. Instead, the initial formation of the P-O bond (phosphane oxide **79**) was calculated to be more favoured ($\Delta E = -562 \text{ kJ mol}^{-1}$). It is reasonable to assume that the latter reaction is kinetically inhibited. The oxidation of phosphanes by oxygen (O₂) is typically slow; most phosphanes are also manageable in air. This is due to the triplet groundstate of oxygen (³O₂) which generally reacts slowly with compounds with paired electrons (singlet state). Therefore, the analysis done based on DFT calculations is coherent with the experimental results.

3.4.1.2 Reactivity Towards Sulfur (S₈)

Targeting the synthesis of the germathione **80** or its dimerisation product, analogously to the reaction reported by Dong *et al.*^[132], an equimolar amount of cyclooctasulfur was added to a toluene solution of germylene **44c** (Scheme 36).



Scheme 36 – Intended synthesis of germathione **80** upon treatment of germylene **44c** with sulfur.

After 20 min of stirring at room temperature, a voluminous yellow precipitate had formed (GeS). NMR spectra recorded of the solution suggested the presence of four different compounds. Two of them were identified as the known phosphole **46c** ($\delta^{31\text{P}} = 69.9$) and the germylene **44c** ($\delta^{31\text{P}} = 57.7$), respectively. The remaining two sets of signals were assigned to the phospho-BCH-germylene sulfide **81** ($\delta^{31\text{P}} = 87.3$) and the phosphole sulfide **82** ($\delta^{31\text{P}} = 95.8$) (Figure 50). Evidence for the formation of germathione **80** or its dimerisation product, was not found.

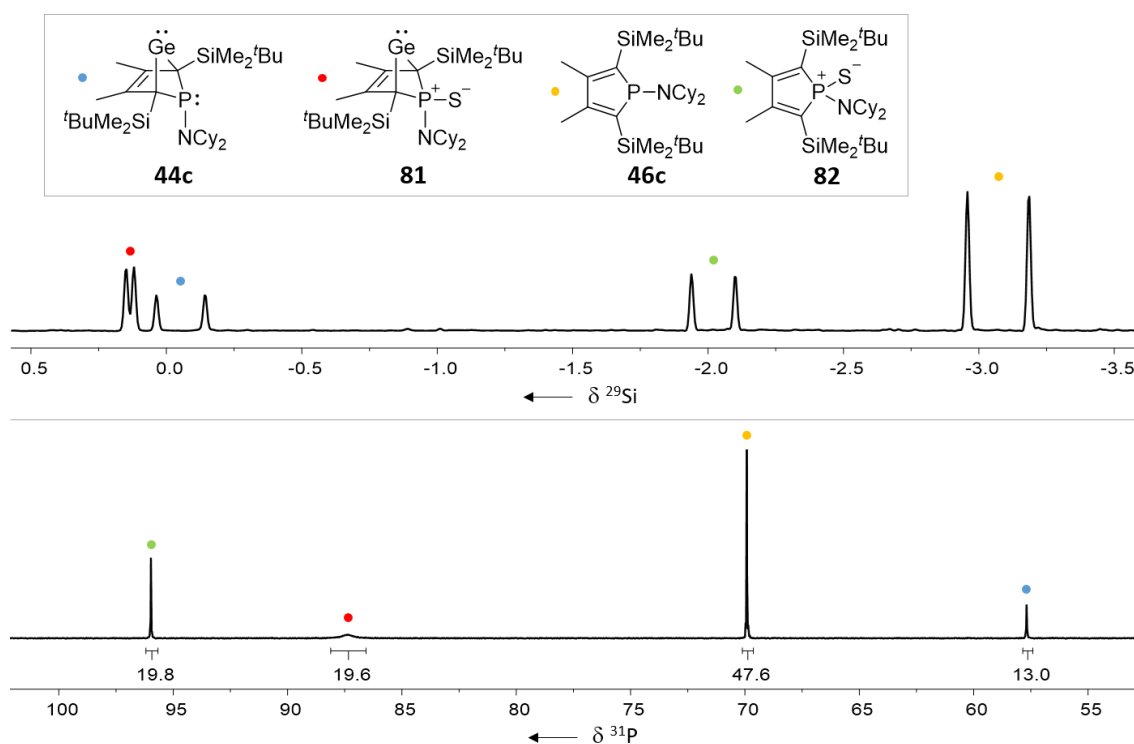
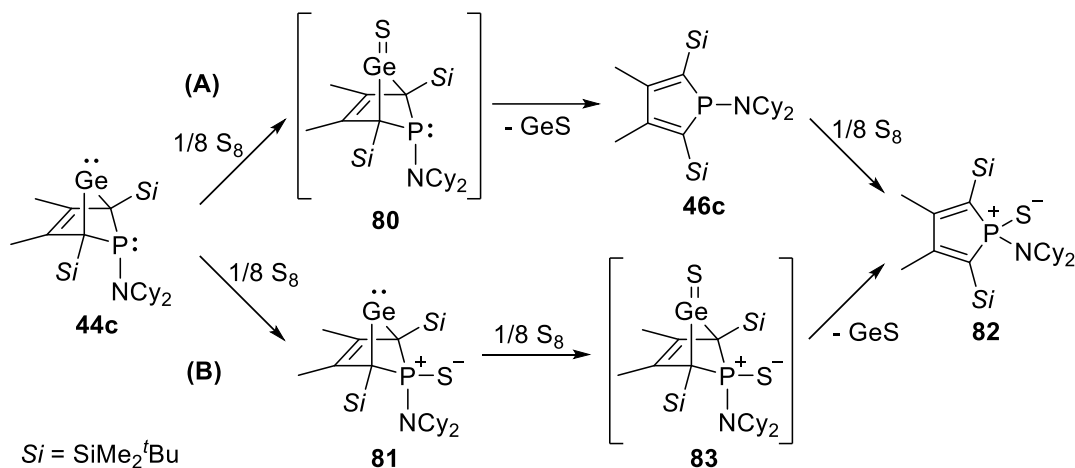


Figure 50 – Extract from the $^{29}\text{Si}\{^1\text{H}\}$ INEPT NMR spectrum (99.3 MHz, 305 K, chlorobenzene- d_5) and the $^{31}\text{P}\{^1\text{H}\}$ NMR spectrum (202.3 MHz, 305 K, chlorobenzene- d_5) showing the four products contained in the reaction mixture after 20 minutes reaction time.

Based on these results we suggest that, differently to the above described reaction towards oxygen, here both reaction pathways are accessible: **(A)** the formation of germathione **80** as the initial step, followed by elimination of germaniumsulfide and formation of phosphole **46c**, and **(B)** the oxidation of the phosphorus atom to give the phospho-BCH-germylene sulfide **81**, from

which germanium sulfide is eliminated in a second step, upon formation of the germathione **83** (Scheme 38). The calculated energy difference between the two initially formed isomers, **80** vs. **81**, was calculated to be $\Delta E = 54 \text{ kJ mol}^{-1}$ in favour of **81** (calculated at the M06-2X/6-311+G(d,p) level of theory). However, pathway (A) still seems to be favoured, as the mixture contained phosphole **46c** as the main product (47%) (Scheme 37).

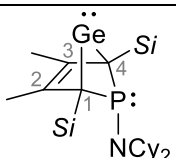
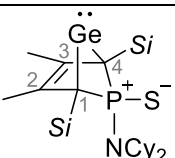
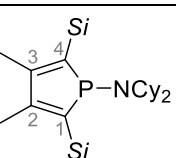
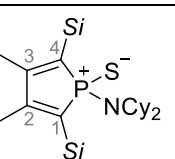


Scheme 37 – Suggested competing reaction pathways of phospho-BCH-germylene **44c** towards sulfur.

To complete the reaction, more cyclooctasulfur was added to the mixture and stirring was continued for several days. A yellow precipitate, germanium sulfide, had again formed. NMR spectroscopic analysis revealed completion of the reaction, as only the phosphole sulfide **82** was detected. It can be assumed that the crucial factor, enabling pathway (B) is the singlet state of the sulfur precursor. Different to the reaction with oxygen (O₂), no triplet-singlet transition needs to take place here.

NMR spectroscopic analysis of all four compounds in the mixture was enabled using 2D NMR spectroscopy again. As expected, the trends observed upon oxidation of the phosphorus atom by oxygen can also be observed upon oxidation with sulfur: The ¹³C NMR signals of the backbone carbon atoms of the germylene sulfide **81** are, compared to germylene **44c**, slightly shifted to lower and higher field, respectively ($\Delta(\delta^{13}\text{C}(\text{C}^{1/4})) = +4 \text{ ppm}$; $\Delta(\delta^{13}\text{C}(\text{C}^{2/3})) = -3 \text{ ppm}$). The trend, however, is inverted compared to the phosphole **46c** and the corresponding phosphole sulfide **46c** ($\Delta(\delta^{13}\text{C}(\text{C}^{1/4})) = -4 \text{ ppm}$; $\Delta(\delta^{13}\text{C}(\text{C}^{2/3})) = +4 \text{ ppm}$). On the other hand, the ²⁹Si NMR signals of both sulfides **81** and **82** are shifted to lower field compared to their respective precursor ($\Delta(\delta^{29}\text{Si}) = 0.2 \text{ ppm}$, 1.0 ppm) and the ²J_{Si,P} coupling constant is significantly reduced upon quarternisation of the phosphorus atom ($\Delta(^2J_{\text{Si,P}}) = 15 \text{ Hz}$, 7 Hz) (Table 18).

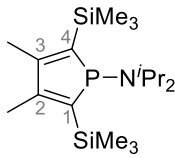
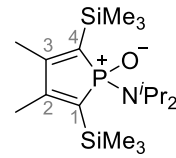
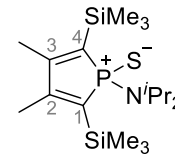
Table 18 – Selected NMR spectroscopic data of phospho-BCH-germylene sulfide **81** and the phosphole sulfide **82** in comparison with phospho-BCH-germylene **44c** and phosphole **46c**. Spectra recorded in chlorobenzene-*d*₅. ¹³C NMR spectroscopic data retrieved from the ¹H¹³C HMBC NMR spectrum. Si = SiMe₂tBu.

					
		44c	81	46c	82
$\delta^{13}\text{C}$	C ^{1/4}	73	77	141	137
	C ^{2/3}	131	129	154	158
$\delta^{29}\text{Si}\{\text{H}\}$	(² J _{Si,P})	-0.1 (18)	0.1 (3)	-3.1 (23)	-2.1 (16)
$\delta^{31}\text{P}\{\text{H}\}$		57.7	87.3	69.9	95.8

For comparative reasons, germylene **43b** was reacted with sulfur, too. Here, two equivalents of the latter were added to a toluene solution of the germylene and the suspension was stirred overnight to achieve full conversion. This, indeed was achieved and the phosphole sulfide **84** was isolated in a yield of 88% after workup.

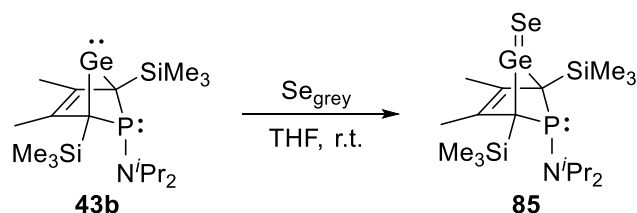
The NMR spectroscopic data obtained for the phosphole sulfide **84** is compared to that obtained for the corresponding oxide **75** and the precursor phosphole **45b** (Table 19): In accordance with the literature, the ³¹P NMR signal of the sulfide **84** is shifted to lower field than that of the respective oxide **75** ($\Delta(\delta^{31}\text{P}) = +29$ ppm).^[113, 134] In contrast, the impact on the ¹³C NMR chemical shift of the backbone carbon atoms is stronger in the oxide than in the sulfide when each compared to the phosphole **45b** ($\Delta(\delta^{13}\text{C}(\text{C}^{1/4})) = -7.5$ vs. -4.1 ; $\Delta(\delta^{13}\text{C}(\text{C}^{2/3})) = +8.1$ vs. $+4.9$).

Table 19 – Selected NMR spectroscopic data of the phosphole **45b**, the phosphole oxide **75** and the phosphole sulfide **84**. Spectra recorded in benzene-*d*₆.

				
		45b	75	84
$\delta^{13}\text{C}\{\text{H}\}$	C ^{1/4} (¹ J _{C,P})	143.0 (33)	135.5 (71)	138.9 (52)
	C ^{2/3} (² J _{C,P})	151.9 (19)	160.0 (26)	156.8 (22)
$\delta^{29}\text{Si}\{\text{H}\}$	(² J _{Si,P})	-10.8 (25)	-9.9 (16)	-9.3 (18)
$\delta^{31}\text{P}\{\text{H}\}$		65.6	63.0	92.0

3.4.1.3 Reactivity Towards Selenium

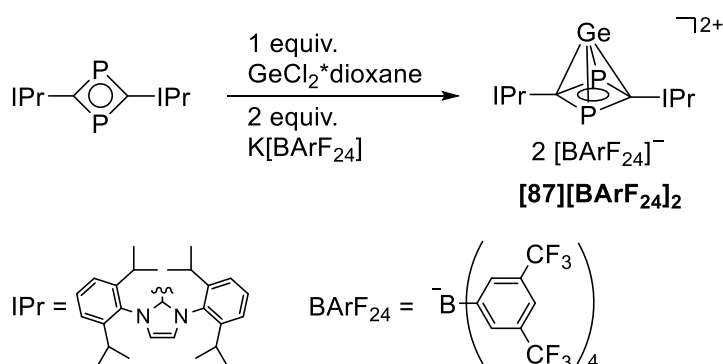
Next, the reactivity of phospho-BCH-germylene **43b** towards the heavier congener, selenium, was studied. Using grey selenium, the synthesis of the germaselenone **85** was targeted (Scheme 38). Logically consistent with the literature, the oxidation of the phosphane moiety was not expected.^[137] However, upon addition of grey selenium to a THF solution of germyle **43b** and stirring for two days, no reaction was observed. No further experiments were carried out in this regard.



Scheme 38 – Attempted synthesis of germaselenone **85**.

3.4.1.4 Reactivity Towards Nitrilium Antimonate

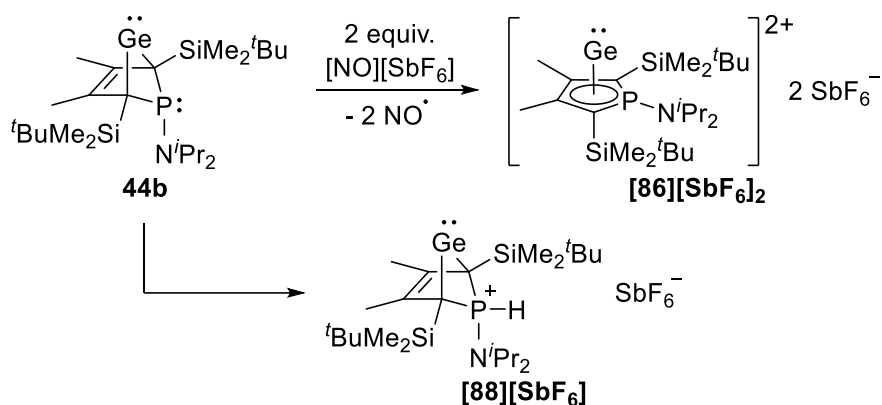
Additionally, instead of using oxidising reagents that form bonds with the substrate and oxidise a single site of the phospho-BCH-germylene **44b**, attempts were made oxidising the latter by abstraction of two electrons. Here, the synthesis of a germanium complex **[86]**, isolobal to e.g. germanium borole complexes **26**^[62], was targeted. This idea was inspired by a report from Coburger *et al.* where the authors describe the synthesis of a germapyramidane **[87]**, which can also be seen as a dicationic η^4 Ge complex (Scheme 39).^[141]



Scheme 39 – Synthesis of the germapyramidane **[87]** by Coburger *et al.*^[141]

Targeting a dicationic phospholium η^5 germanium complex **[86]**, phospho-BCH-germylene **44b** was reacted with two equivalents of nitrilium hexafluoroantimonate (Scheme 40, top). The targeted product **[86][SbF₆]₂** was not observed, however, based on NMR spectroscopy, a

phosphonium-BCH-germylene antimonate **[88b][SbF₆]** was identified as main product (Scheme 40, bottom).



Scheme 40 – Attempted oxidation of germylene **44b** (top) and the actually observed main product (bottom).

The phosphonium salt was identified by its characteristic large P-H coupling ($^1J_{\text{P-H}} = 587$ Hz, Figure 51). Furthermore, its structure was analysed by single crystal X-ray diffraction (Figure 54). Though it was dried *in vacuo*, it was assumed that the proton source in this case was a trace amount of water left in the nitrilium salt.

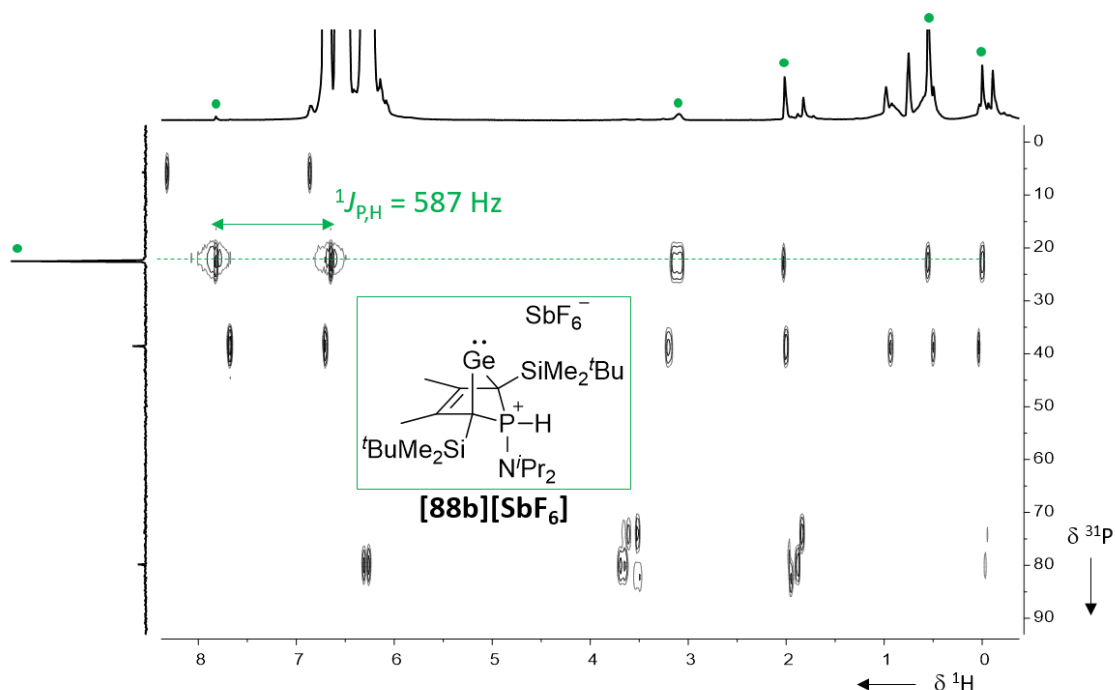
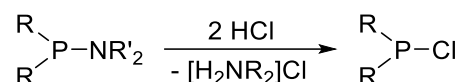


Figure 51 – $^1\text{H}^{31}\text{P}$ HMBC NMR spectrum (500.1 MHz, 305 K, ortho-difluorobenzene) of the product mixture obtained upon addition of nitrilium antimonate to phospho-BCH-germylene **44b**. Signals assigned to the phosphonium salt **[88b][SbF₆]** are highlighted in green.

3.4.2 Reactivity Towards Small Electrophiles

3.4.2.1 Unusual Proton Affinity

The surprising discovery of the aminophosphonium ion **[88b]** described above (Scheme 40) has drawn attention as commonly, the nitrogen atom is protonated in aminophosphanes and not the phosphorus atom (Scheme 41).^[90, 142] Therefore, the synthesis was aimed to be repeated purposefully.



Scheme 41 – Common exchange reaction on aminophosphanes.^[90, 142]

The protonation reaction was examined from the theoretical point of view, using DFT calculations. Comparison of the relative energies of four possible isomers of phosphonium-BCH-germylene **[89b]** (protonated at each of the four nucleophilic sites) revealed, that in accordance with the commonly reported reaction, the nitrogen atom is the favoured protonation site. Compared to the phosphonium ion **[89b]**, the ammonium ion **[89-N]** is favoured by $\Delta E = 31 \text{ kJ mol}^{-1}$ ($\Delta G = 35 \text{ kJ mol}^{-1}$). Protonation at the backbone double bond (carbocation **[89-C]**) and at the germanium atom (germylium ion **[89-Ge]**) are disadvantaged by $\Delta E = 99 \text{ kJ mol}^{-1}$ ($\Delta G = 100 \text{ kJ mol}^{-1}$) and $\Delta E = 131 \text{ kJ mol}^{-1}$ ($\Delta G = 118 \text{ kJ mol}^{-1}$), respectively (Figure 52).

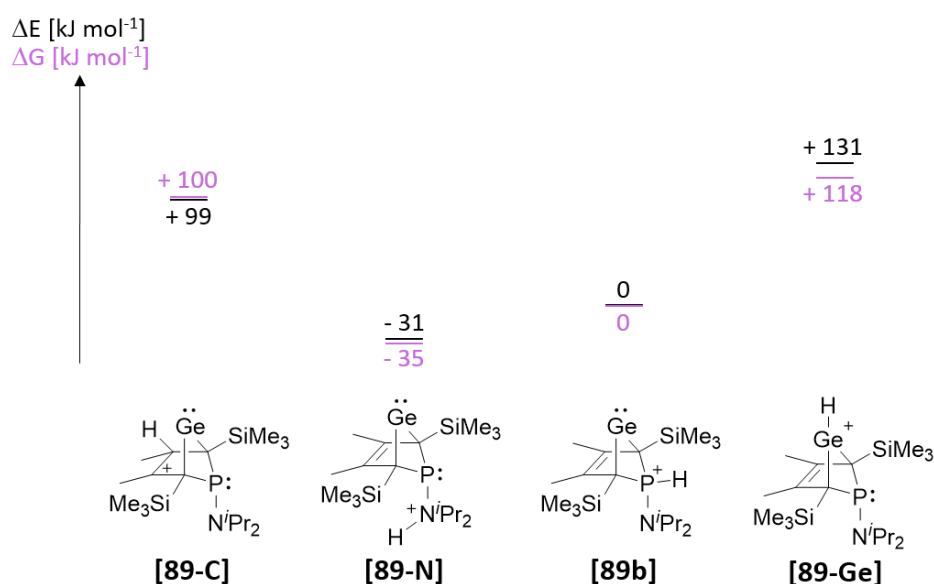
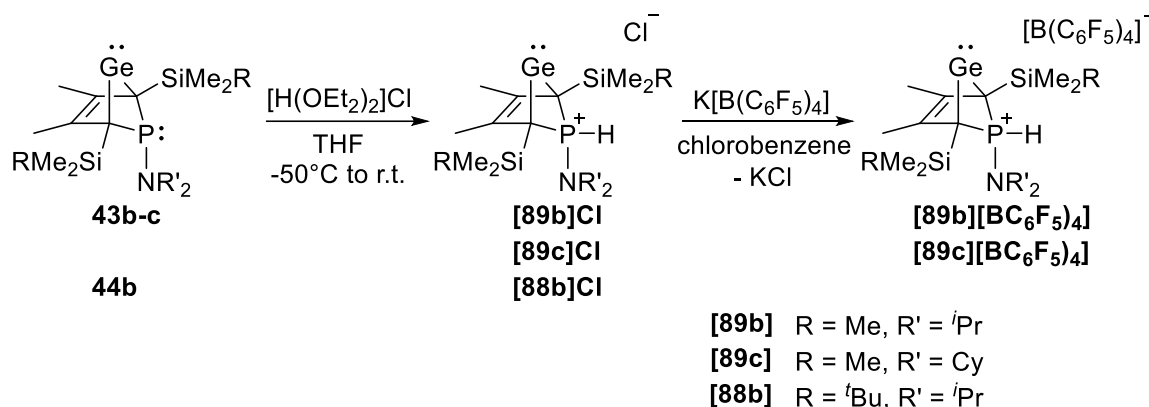


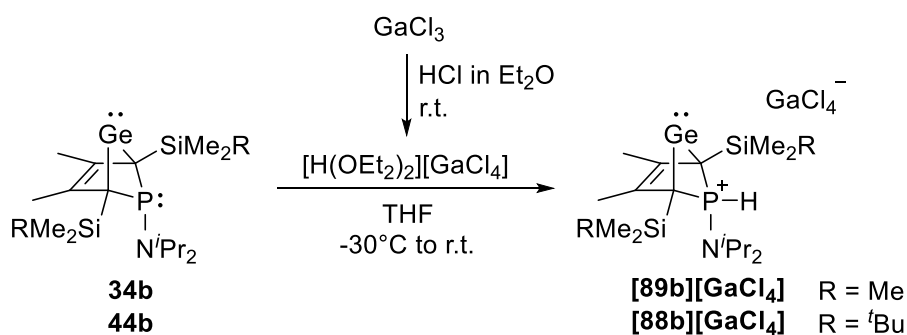
Figure 52 – Calculated relative energies (M06-2X/6-311+G(d,p)) for the different protonation sites.

To aim for the purposeful protonation of any nucleophilic site of phospho-BCH-germylenes, germynes **43b+c** and **44b** were treated with hydrochloric acid in diethyl ether. Interestingly, the protonation occurred selectively at the phosphorus atom, giving phosphonium-BCH-germylene salts **[88b]Cl**, **[89b]Cl** and **[89c]Cl** (Scheme 42).



Scheme 42 – Synthesis of phosphonium salts **[88b]Cl**, **[89b][B(C₆F₅)₄]** and **[89c][B(C₆F₅)₄]**.

Due to slow decomposition of the phosphonium salt into the respective phospho-BCH-germylene, the phosphole and other byproducts, the chloride ion was exchanged for a weakly coordinating anion, perfluoroborate [B(C₆F₅)₄], immediately after the reaction (Scheme 42). This enabled isolation of the phosphonium-BCH-germylene borates **[89b][B(C₆F₅)₄]** and **[89c][B(C₆F₅)₄]** in good yields of up to 80%. The borate salts are storable for weeks in solution and in the solid state. Alternatively, the synthesis was carried out with tetrachlorogallate as counterion by reaction of the germylene **43b** or **44b** with [H(OEt₂)₂][GaCl₄]. The latter was synthesised *in situ* from hydrochloric acid in diethyl ether and gallium trichloride (Scheme 43).^[143] The phosphonium gallates **[88b][GaCl₄]** and **[89b][GaCl₄]** were purified by crystallisation. Phosphonium-BCH-germylene gallate **[89b][GaCl₄]** was furthermore analysed by single crystal X-ray diffraction (see Figure 54). However, the formation of the respective phospholium salts was not observed.



Scheme 43 – Synthesis of phosphonium gallates **[88b][GaCl₄]** and **[89b][GaCl₄]**.

Comparative NMR Spectroscopic Analysis

Characterisation of the products was unambiguously done using NMR spectroscopy. The characteristic large P-H coupling constants ($^1J_{P,H} = 400\text{-}1000\text{ Hz}^{[115]}$) can be found in the ^1H and the hydrogen coupled ^{31}P NMR spectra. Exemplary spectra for phosphonium-BCH-germylene gallate **[89b][GaCl₄]** are displayed in Figure 53. Here, the coupling is $^1J_{P,H} = 568\text{ Hz}$. The binding of the germanium atom to the $\text{C}^{1/4}$ atoms persisted as indicated by the corresponding ^{13}C NMR resonance at $\delta^{13}\text{C} = 59.7$, typical for sp^3 -carbon atoms in the sp^3 -region.^[114]

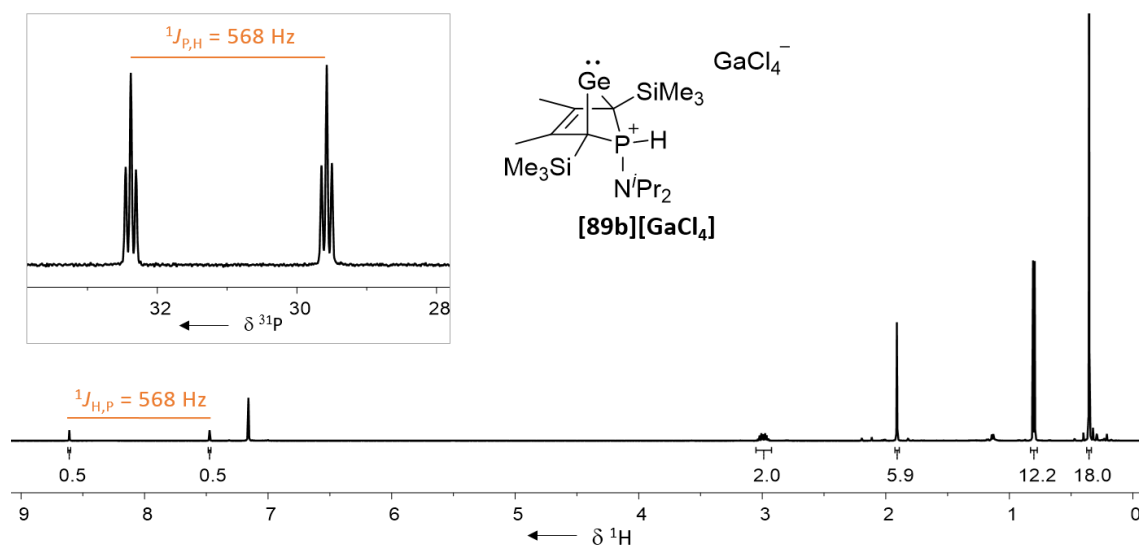


Figure 53 – $^1J_{P,H}$ coupling in phosphonium-BCH-germylene gallate **[89b][GaCl₄]** displayed in the ^{31}P NMR spectrum (202.3 MHz, 305 K, benzene- d_6) and the ^1H NMR spectrum (500.0 MHz, 305 K, benzene- d_6). The triplet signals in the ^{31}P NMR spectrum arise from the coupling to the *isopropyl*-methine hydrogen atoms ($^3J_{P,H} = 15\text{ Hz}$).

Compared to their precursors, the ^{31}P NMR signals of phosphonium-BCHGe salts are shifted to lower frequency. However, the ^{31}P NMR chemical shift is furthermore impacted by the solvent and by the presence of other compounds, here, namely the counterion.^[115] The impact of the solvent becomes clear when regarding the phosphonium borate **[89b][B(C₆F₅)₄]** that was recorded in chlorobenzene- d_5 and THF- d_8 : the ^{31}P NMR signal and the corresponding ^1H NMR signals are shifted to lower field when recorded in THF- d_8 ($\Delta(\delta^{31}\text{P}) = 13.7$ and $\Delta(\delta^1\text{H}(\text{P-H})) = 1.03$). It also becomes clear, that the impact is stronger on the cationic compound than on its neutral precursor **43b**. Regarding the presence of different anions it can be noted that smaller, more nucleophilic anions lead to a more lowfield shifted ^{31}P NMR signal of the phosphonium ion. Both observations can be explained by the coordinating properties of the counterion or the solvent. Here, THF and the chloride ion are coordinating substrates, especially when compared to benzene and the weakly coordinating borate anion. The stronger coordination to the cation causes the lowfield shift of the ^{31}P NMR chemical shift (Table 20).

Table 20 – Selected NMR spectroscopic data of different salts of phosphonium-BCH-germylenes **[88]** and **[89]**.

compound	R	R'	solvent	δ ¹ H	δ ³¹ P	δ ³¹ P
				P-H (¹ J _{H,P} [Hz])		precursor in C ₆ D ₆
[89b]Cl	Me	N ⁱ Pr ₂	C ₆ D ₆	8.06 (569.8)	28.9	35.4 (43b)
[89b][GaCl₄]	Me	N ⁱ Pr ₂	C ₆ D ₆	7.97 (569.1)	31.0	35.4 (43b)
[89b][B(C₆F₅)₄]	Me	N ⁱ Pr ₂	C ₆ D ₅ Cl	6.86 (568.8)	14.5	35.4 (43b)
[89b][B(C₆F₅)₄]	Me	N ⁱ Pr ₂	THF-d ₈	7.89 (565.8)	28.2	33.3* (43b)
[89c][B(C₆F₅)₄]	Me	NCy ₂	C ₆ D ₅ Cl	6.96 (567.0)	13.4	39.4 (43c)
[88b]Cl	^t Bu	N ⁱ Pr ₂	C ₆ D ₆	8.10 (577.5)	35.2	53.8 (44b)
[88b][GaCl₄]	^t Bu	N ⁱ Pr ₂	THF-d ₈	7.78 (580.3)	25.7	54.1 [#] (44b)
[88b][H(B(C₆F₅)₃)]	^t Bu	N ⁱ Pr ₂	toluene-d ₈	6.74 (570.7)	22.7	53.9 [°] (44b)

R and R' see Scheme 42. * Measured in THF-d₈. # Measured in THF. ° Measured in toluene-d₈.

Comparative Structural Analysis

The molecular structures of the phosphonium-BCH-germylene salts **[89b][GaCl₄]** and **[88b][SbF₆]** in the crystal show great similarity. In the following, those structures are compared to the molecular structure of germylene **43b** (Figure 54).

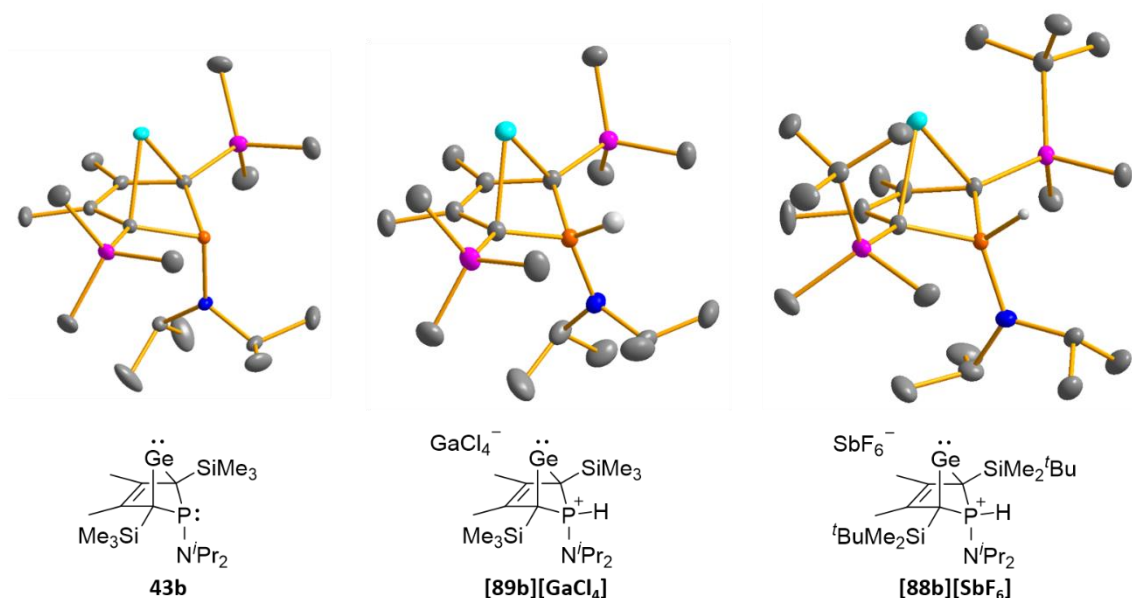
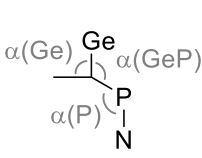
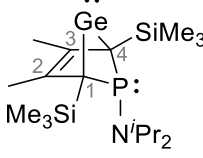
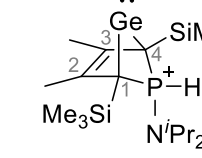


Figure 54 – Molecular structures of germylene **43b** (Pnma) and the phosphonium ions **[89b][GaCl₄]** (P₂₁/n) and **[89b][SbF₆]** (P₂₁/c) in the crystal. Thermal ellipsoids at 50% probability. Hydrogen atoms (except P-H) and the anions GaCl₄⁻ and SbF₆⁻ were omitted for clarity.

Upon protonation and quarternisation, the s-character of the orbitals involved in the bonds of the phosphorus atom towards the other atoms is enlarged, resulting in shortening of the P-C¹ and P-N bonds in the phosphonium ions **[89b]** and **[88b]** compared to germylene **43b**: The C¹-P bonds in the phosphonium salts are almost 7 pm (177.4/177.6 pm) shorter than in germylene **43b**. The P-N bond is shortened by 4-5 pm (163.9(8)/165.2(3) pm) and almost equals a formal P=N double bond here (162 pm^[107]). Additionally, the flap angle $\alpha(\text{P})$ is less acute upon quarternisation of the phosphorus atom ($\Delta(\alpha(\text{P})) = 20.9^\circ / 22.9^\circ$). The but-2-ene backbone of the molecule does not significantly change upon protonation. Both, the C¹-C² and the C²-C³ bonds are shortened by less than 1 pm compared to the precursor **43b**. The germanium-carbon distances, however, are enlarged by about 4 pm (C¹-Ge) and about 2 pm (C²-Ge), respectively (Table 21).

Table 21 – Selected bond lengths and angles of germylene **43b** and phosphonium-BCH-germylene **[89b]** and **[88b]**.

			
	43b	[89b]	[88b]
C ¹ -C ²	146.53(6)	147.69(18)	147.46(16)
C ² -C ³	142.33(8)	141.40(17)	141.87(17)
Ge-C ¹	216.32(4)	220.51(13)	220.89(13)
Ge-C ²	219.64(5)	222.41(12)	220.99(12)
P-C ¹	184.11(4)	177.91(14)	177.06(10)
P-N	170.18(7)	163.98(13)	165.23(10)
$\alpha(\text{Ge})$	82.012(7)	81.919(11)	82.429(9)
$\alpha(\text{GeP})$	127.121(12)	129.648(12)	130.000(21)
$\alpha(\text{P})$	114.914(23)	135.863(47)	137.807(43)

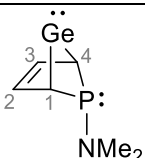
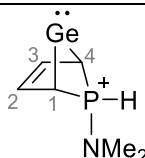
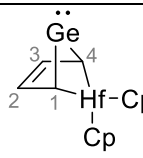
3.4.2.2 Homoconjugation in Phospha- and Phosphonium-BCH-Germylenes

Despite the fact that the Ge-C distances are larger in phosphonium-BCH-germylenes, they are significantly more stable than the corresponding phospha-BCH-germylenes. We initially assumed a stronger intramolecular interaction of the C²=C³ double bond with the vacant germanium p-orbital (C²=C³ → Ge; HOMO, Figure 45) to be the stability enhancing factor. For comparative analysis of the extent of the homoconjugation in both bicyclic germlyenes **43** and **[89]**, DFT calculations were carried out. For all herein performed calculations and analyses,

hydrogen-substituted model compounds (**43'** and **[89]'**) were used. The analysis procedure was inspired by that reported by Dong *et al.* for related hafnocena-BCH-tetrylenes.^[55]

In general, the structures of the optimised model compounds **43'** and **[89]'** are in good agreement with the experimental structures of **43b** and **[89b]** with less than 1% deviation of the respective bond lengths. Only the C¹-C² bonds of the calculated structures are shorter than the respective bonds in the experimental structures ($\Delta(\mathbf{43}') = 3.8 \text{ pm} = 2.6\%$ and $\Delta(\mathbf{[89]}') = 2.8 \text{ pm} = 1.9\%$). Nevertheless, in all compounds (experimental and calculated), the C¹-C² bonds are longer than the C²-C³ bonds and all C-C bonds are in between typical single and double bonds.^[107] Furthermore, natural bond orbital (NBO) analysis predicts higher Wiberg bond indices (WBI) for the C²-C³ bonds than for the C¹-C² bonds, indicating a but-2-ene backbone. The calculated values are comparable to those given for the hafnocena-BCH-germylene **21'** (Table 22). The Ge-C^{1/4} and Ge-C^{2/3} distances in the optimised structures are almost identical to the molecular structures in the crystal. The difference accounts 0.1 and 0.2 pm for germylene **43'**, and 0.6 and 0.5 pm for the phosphonium ion **[89]'** (Table 21). In general, upon protonation, the germanium atom moves further away from the but-2-ene backbone. Despite the increasing Ge-C distance, the by NBO analysis predicted WBI are very similar to those predicted for the phospho-BCH-germylenes **43'**, indicating comparably strong homoconjugative interaction in both compounds. This is contrary to the initial assumption (Table 22).

Table 22 – Selected results of the structure optimisations and NBO analysis of the model compounds **43'** and **[89]'** (M06-2X/def2-tzvp//M06-2X/6-311+G(d,p)), compared to the related hafnocena-BCH-germylene **21'** (M06-2X/def2-tzvp)^[54].

			
	43'	[89]'	21' ^[54]
C ¹ -C ² (WBI)	144.7 (1.21)	144.8 (1.21)	145.6 (1.27)
C ² -C ³ (WBI)	141.1 (1.36)	140.6 (1.39)	141.8 (1.38)
Ge-C ^{1/4} (WBI)	216.4 (0.58)	221.1 (0.50)	213.7 (0.54)
Ge-C ^{2/3} (WBI)	219.4 (0.34)	221.2 (0.31)	219.7 (0.27)
occupancy (p(Ge))	0.30 e	0.28 e	0.27 e

The calculated electron density of both model compounds, **43'** and **[89]'**, was analysed based on quantum theory of atoms in molecules (QTAIM).^[130] The interaction between the germanium atom and the four backbone-carbon atoms is of particular interest. For phospho-BCH-germylene **43'**, the calculated molecular graph displays a dicoordinated germylene with bonds between the germanium and the C¹ and C⁴ carbon atoms. The ring critical point (red dot) of the five-membered C₄-Ge ring is located between the C²-C³ bond and the germanium atom, indicating the C²=C³ → Ge interaction (Figure 55, left). The calculated graph of phosphonium-BCH-germylene **[89]'** is very similar to that of phospho-BCH-germylene **43'**, but displays an additional binding path. With regards to the homoconjugative interaction this can be seen as a T-shaped electron density distribution from the C²=C³ double bond to the germanium atom.^[144] The bond critical point (green dot) of the additional bond path is located approximately where the ring critical point in phospho-BCH-germylene **43'** is located. The ring critical points (red dots) of the two thereby emerging rings, however, are located close to the just mentioned bond critical point (Figure 55, right). This indicates great similarity of the electron density distribution in both compounds, **43'** and **[89]'**.

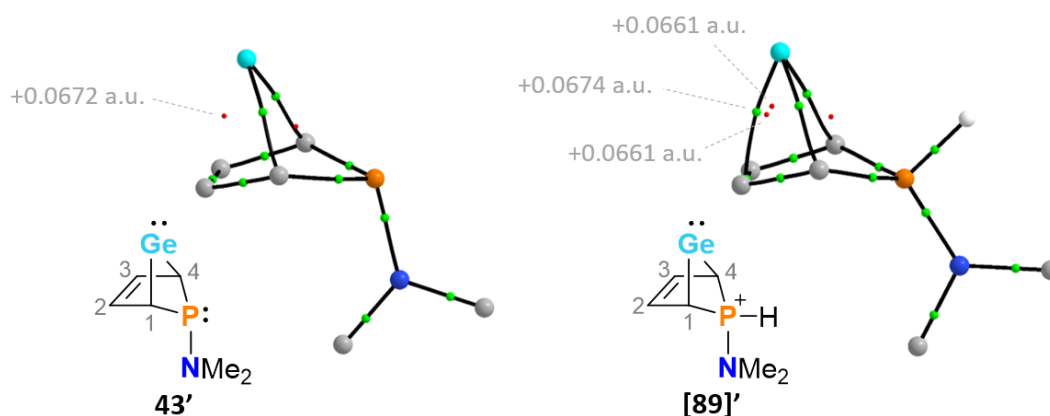
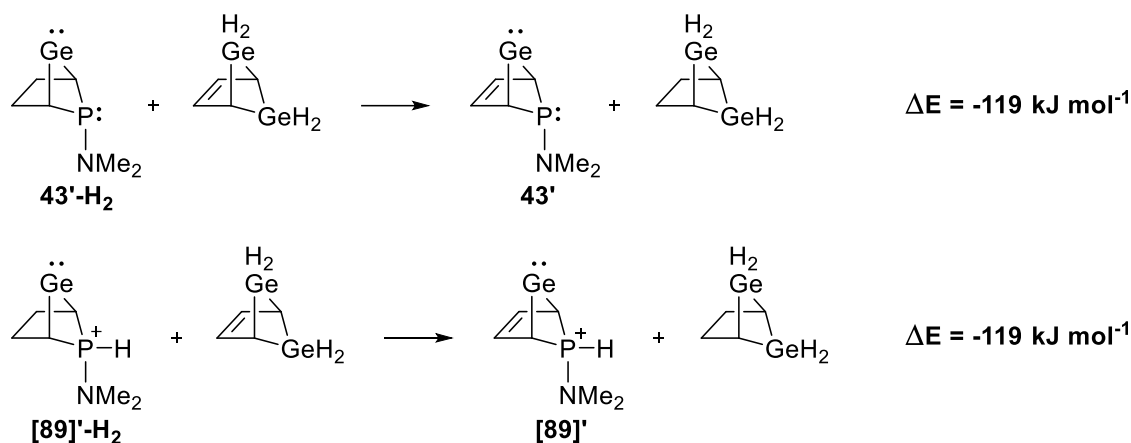


Figure 55 – Molecular graphs as part of the QTAIM analyses^[130] (M06-2X/def2-tzvp//M06-2X/6-311+G(d,p)) of model compounds of a phospho-BCH-germylene **43'** (left) and a phosphonium-BCH-germylene **[89]'** (right). Hydrogen atoms (except the P-H) are omitted for clarity. Red dots mark ring critical points. Green dots mark bond critical points. Selected values for the calculated electron density (ρ [a.u.]) are given and assigned to the corresponding points.

The assumption is consolidated by comparison of the electron density at the respective ring and bond critical points: the four values considered are very similar ($\rho = 0.06605 - 0.06738$ a.u.) (Figure 55). Comparing to the electron density at the bond critical points of the C¹-C² and C²=C³ bonds, respectively ($\rho(\mathbf{43}') = 0.2810$ a.u., 0.3058 a.u.; $\rho(\mathbf{[89]') = 0.2801$ a.u., 0.309 a.u.), it furthermore points out that the four discussed values are small.

Coherent with the results obtained from the QTAIM analysis, calculations of the isodesmic reaction energy for the reactions shown in Scheme 44 suggest identical strength of the homoconjugation in both compounds, phosphonium-BCH-germylene **[89]'** and phospha-BCH-germylene **43'**.



Scheme 44 – Isodesmic equations reflecting the extent of the homoconjugation in phospha-BCH-germylenes **43'** and phosphonium-BCH-germylenes **[89]'**.

The similarity is also illustrated regarding the frontier molecular orbitals of phospha-BCH-germylene **43'** and phosphonium-BCH-germylene **[89]'**. The type and shape of the highest occupied and the lowest unoccupied molecular orbitals of both compounds (HOMO and LUMO) are very similar. The difference emerges from the calculated energy level of the orbitals. The molecular orbitals of the phosphonium ion are lowered in energy, which we traced back to the positive charge. The respective germanium lone pair orbital (HOMO-4 and HOMO-2, respectively) is also significantly lowered in energy. The energy difference between the vacant p-orbital and the germanium lone pair orbital is larger in phosphonium-BCH-germylene **[89]'** ($\Delta E = 9.58$ eV vs. $\Delta E(\mathbf{43}') = 9.20$ eV) (Figure 56).

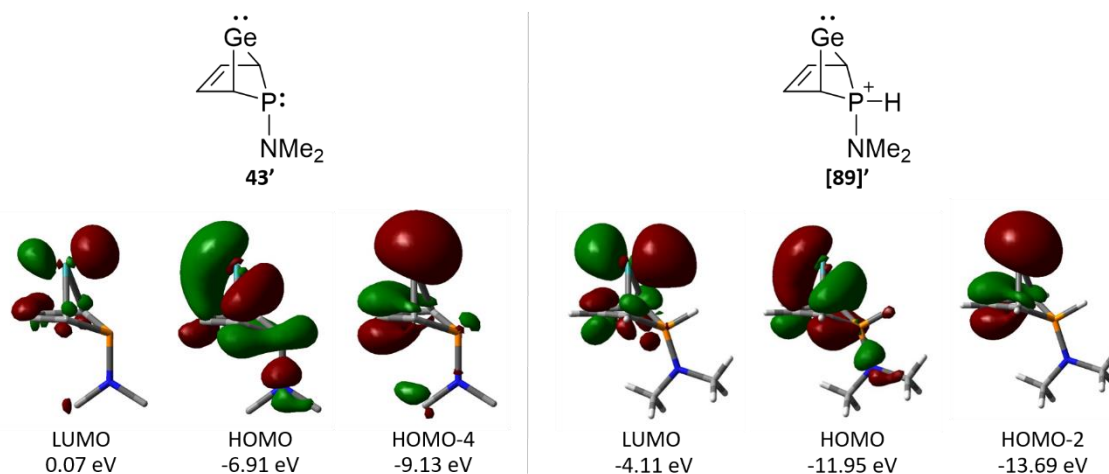


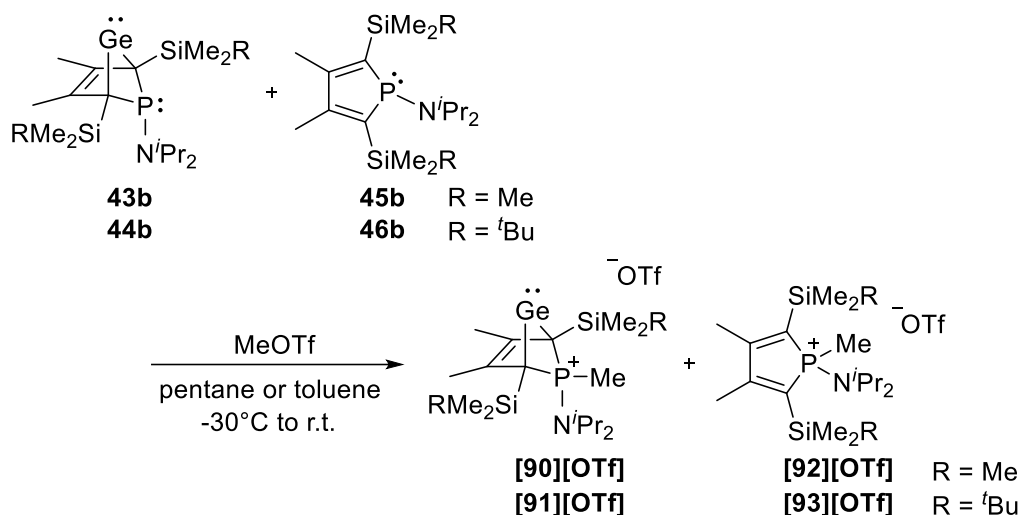
Figure 56 – Selected frontier molecular orbitals (M06-2X/def2-tzvp, at an isodensity value of 0.04) of phospho-BCH-germylene **43'** (left) and phosphonium-BCH-germylene **[89]'** (right).

The energetic lowering of the vacant p-orbital at the germanium atom (LUMO) enhances its Lewis acidic character, as it becomes a better electron pair acceptor. Concurrently, the energetic lowering of the lone pair orbital at the germanium (HOMO-2) reduces its nucleophilic character. We therefore assume the in Chapter 3.2.7 introduced mechanism of the germanium elimination not to be accessible for phosphonium-BCH-germylenes **[89]**: The enhanced Lewis acidic character of the germylene moiety should facilitate the initialisation of the elimination process, as electron donation into the LUMO now is energetically more favoured. However, it was also discussed in Chapter 3.2.7 that relatively strong nucleophiles are required to initialise the germanium elimination. We therefore traced the enhanced stability of phosphonium-BCH-germylenes **[89]**, compared to their corresponding phospho-BCH-germylenes **43**, back to the reduced nucleophilic character of the germylene moiety, which cannot initiate the bimolecular elimination process. In general, the reactivity of the germylene moiety of phosphonium-BCH-germylenes **[89]** and **[88]** towards nucleophiles is expected to be enhanced. Experiments, reinforcing this theoretical conclusion, have not been carried out. However, this would be an interesting question for future experiments.

3.4.2.3 Methylation

The successful and highly selective protonation of the phosphorus atom in phospho-BCH-germylenes **43-44** gave rise to the idea that methylation should proceed in the same fashion. Here, different to the typical reactivity of aminophosphanes towards proton sources, the alkylation of such compounds is expected to occur at the phosphorus atom.^[90, 136]

The treatment of phospho-BCH-germylenes **43b** and **44b** with methyl triflate, which was used as methyl cation source, resulted in the formation of methylphosphonium salts **[90][OTf]** and **[91][OTf]** (Scheme 45). It was furthermore noted, that the amount of phosphole **44b** or **46b** contained in the precursor solutions, reacted with the methyltriflate as well and gave the respective methylphospholium triflate **[92][OTf]** and **[93][OTf]** (2-6% share of the entirety). With the larger silyl groups (R = *t*Bu), the methylphosphonium-BCH-germylene triflate **[91][OTf]** was isolated in a yield of 60% after purification.



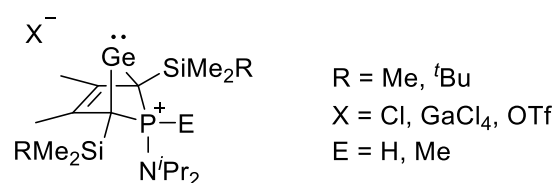
Scheme 45 – Synthesis of methylphosphonium-BCH-germylene triflates **[90][OTf]** and **[91][OTf]** and formation of the byproducts, methylphospholium triflates **[92][OTf]** and **[93][OTf]**.

The methylphosphonium and methylphospholium salts were characterised by NMR spectroscopy. In the ^1H NMR spectrum, the P-Me group of all compounds features a doublet signal at $\delta^1\text{H} = 2.03\text{-}2.35$, with a coupling constant of $^2J_{\text{P,H}} = 11.1\text{-}12.6$ Hz. Upon methylation, the ^{31}P NMR signals were, as expected, shifted to higher frequency compared to their precursors due to the $-I$ effect of alkyl substituents on the ^{31}P NMR chemical shift.^[115] The effect is much stronger for the SiMe_3 substituted compounds ($\Delta(\delta^{31}\text{P}) = 19.1$ (**43b**), 6.1 (**45b**)), than for the SiMe_2^tBu substituted ones ($\Delta(\delta^{31}\text{P}) = 3.7$ (**44b**), 3.5 (**46b**)). This is the opposite trend as observed for the salts of the protonated germylenes **[89]** and **[88]**, which were shifted to lower frequency (Table 23).

Table 23 – ^{31}P NMR chemical shift of methylphosphonium-BCH-germylene triflate **[90][OTf]** and **[91][OTf]** and methylphosphonium triflate **[92][OTf]** and **[93][OTf]** (measured in chlorobenzene- d_5) and their precursors **43b/45b** and **44b/46b** (measured in benzene- d_6).

R				
Me	35.4 (43b)	54.5 ([90][OTf])	65.6 (45b)	71.7 ([92][OTf])
^t Bu	53.8 (44b)	57.5 ([91][OTf])	71.7 (46b)	75.2 ([93][OTf])

Compared to the protonated phosphonium-BCH-germylene salts **[89b][GaCl₄]** and **[88b]Cl**, the coupling constant of the phosphorus atom to the ring carbon atoms increases for the methylphosphonium-BCH-germylene salts **[90][OTf]** and **[91][OTf]**. The increase is stronger for the $^1J_{\text{C,P}}$ coupling constant ($\Delta(^1J_{\text{C,P}}) = 9 \text{ Hz}$ ($\text{R} = \text{Me}$), 8 Hz ($\text{R} = {}^t\text{Bu}$)) than for the $^2J_{\text{C,P}}$ coupling constant ($\Delta(^2J_{\text{C,P}}) = 2 \text{ Hz}$ ($\text{R} = \text{Me}$), 3 Hz ($\text{R} = {}^t\text{Bu}$)). Larger coupling constants suggest stronger interaction of the phosphorus and the ring carbon atoms, however, the $\text{P}-\text{C}^{1/4}$ bond lengths are almost identical in both, the protonated and the methylated compounds, and only shortened compared to the precursors, germylenes **43b** and **44b**, respectively. Concurrently, the $^2J_{\text{Si,P}}$ coupling constant decreases by 16-18 Hz, indicating that the Si-P coupling is weaker in phosphonium-BCH-germylenes than in phospho-BCH-germylenes **43-44** (Table 24).



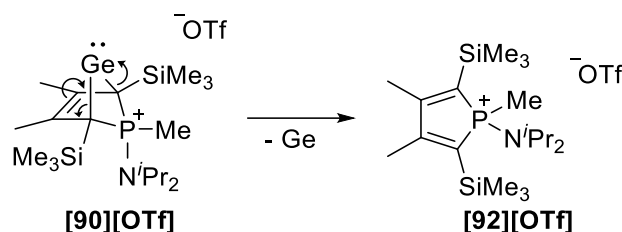
Scheme 46 – Phosphonium-BCHGe salts discussed in this chapter.

Table 24 – Selected NMR spectroscopic and structural data involving the phosphorus atom.

	R	E	$^1J_{\text{C,P}}$ ($\text{C}^{1/4}-\text{P}$) [Hz]	$^2J_{\text{C,P}}$ ($\text{C}^{2/3}-\text{P}$) [Hz]	$^2J_{\text{Si,P}}$ [Hz]	$\text{C}^{1/4}-\text{P}$ [pm]
43b	Me	-	36	8	21	184.1(1)
44b	^t Bu	-	40	7	18	184.4*
[89b][GaCl₄]	Me	H	48	9	3	177.4(4)
[88b]Cl	^t Bu	H	43	9	1	177.6(3)
[90][OTf]	Me	Me	57	11	5	177.9*
[91][OTf]	^t Bu	Me	51	12	2	-

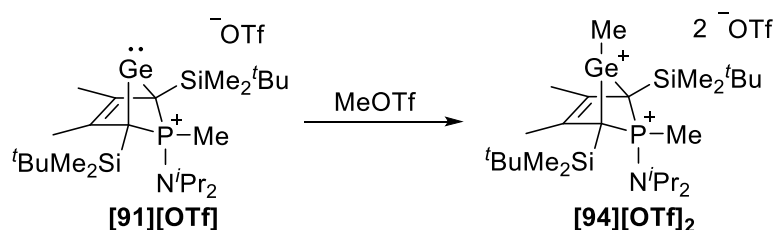
* Value calculated at the M06-2X/6-311+G(d,p) level of theory.

In individual cases, elimination of germanium from the otherwise storable methylphosphonium triflate **[90][OTf]** was observed. It is not known to date, what initiated the elimination (Scheme 47).



Scheme 47 – Elimination of germanium from methylphosphonium-BCH-germylene triflate **[90][OTf]** and **[91][OTf]**.

Treating the methylphosphonium triflate **[91][OTf]** with a second equivalent of methyl triflate did, as expected, not result in the formation of methylphosphonium-BCH-methylgermylium ditriflate **[94][OTf]₂** (Scheme 51). Instead, the precursor **[91][OTf]** was reisolated. This gave further evidence for the reduced nucleophilic character of the germylene moiety upon oxidation of the phosphorus atom, as discussed above (Chapter 3.4.2.2).



Scheme 48 – Attempted synthesis of the dicationic phosphonium-BCH-germylium ditriflate **[94][OTf]₂**.

3.4.3 Reactivity Towards Lewis Acids

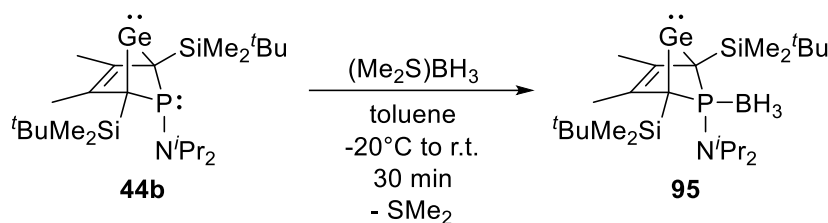
In this chapter, the reactivity of phospho-BCH-germylenes **42-43** towards different small Lewis acids is described. With regards to the HSAB concept^[145], the Lewis basic character of the within this work introduced compound class, phospho-BCH-germylenes, should be elaborated by reaction towards Lewis acids, varying in their acidic character. The Lewis acids chosen range from soft (BH_3) to hard (AlCl_3) Lewis acids.^[116, 145] The order aligns with the Lewis acid strength according to the calculated fluoride ion affinity (FIA). Additionally, the reactivity towards the sterically demanding tris(pentafluorophenyl)borane (BCF) was studied. Based on FIA values, the acid strength of BCF equals that of GaCl_3 (Figure 57).^[146]

	hard Lewis acid		soft Lewis acid		
	AlCl ₃	GaCl ₃	ZnCl ₂	BH ₃	B(C ₆ F ₅) ₃
FIA:	505	448	n.a.	279	448

Figure 57 – Lewis acids applied in the reactivity studies.^[116, 145] FIA values calculated in the gas phase.^[146]

3.4.3.1 Borane (BH₃)

Treatment of a toluene solution of germylene **44b** with borane-dimethylsulfide adduct resulted in the formation of the respective phosphorus-borane adduct **95** (Scheme 49). The reaction proceeded highly selective within 30 minutes, as suggested by control NMR spectra.



Scheme 49 – Reaction of germylene **44b** with (Me₂S)BH₃.

After workup and removal of excess borane, the adduct was characterised spectroscopically. The recorded NMR spectra displayed the adduct **95** ($\delta^{31\text{P}} = 81.2$, $\delta^{11\text{B}} = -33.3$) as well as small amounts (6%) of the respective phosphole-borane adduct **96** ($\delta^{31\text{P}} = 102.3$, $\delta^{11\text{B}} = -38.6$) (Figure 58). The amount equals the amount of phosphole **46b** contained in the starting material.

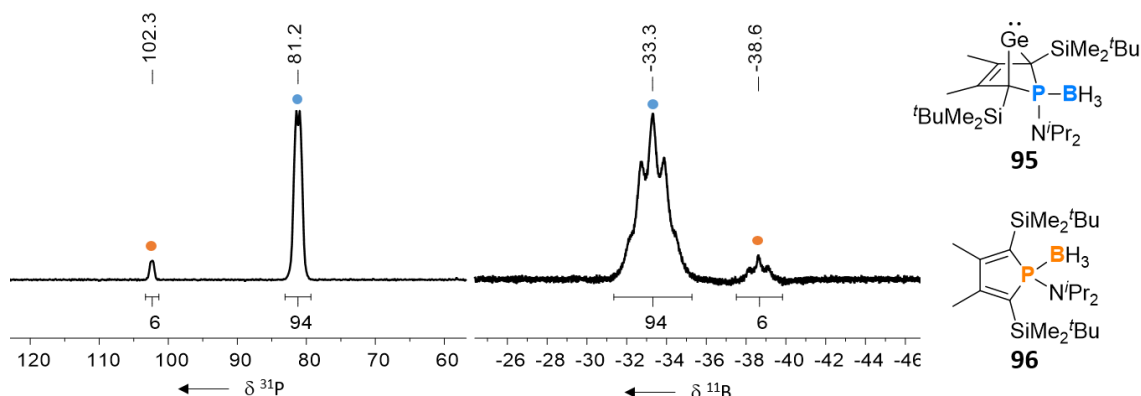


Figure 58 – ¹¹B (160.4 MHz, 305 K, toluene-d₈) and ³¹P (202.3 MHz, 305 K, toluene-d₈) NMR spectra of the germylene-borane adduct **95** (●) and the phosphole-borane adduct **96** (●).

Compared to their precursors, germylene **44b** ($\delta^{31\text{P}} = 53.8$) and phosphole **46b** ($\delta^{31\text{P}} = 71.6$), their borane adducts **95** and **96** are shifted to lower field. Characteristically, the $^{31\text{P}}$ NMR signals are broadened^[147-148] due to the neighbouring boron atom, which exhibits a nuclear spin of 3/2. The $^1J_{\text{P,B}}$ coupling constant ($^1J_{\text{P,B}} = 97$ Hz) is within the typical range of phosphorus-boron coupling constants of 10-180 Hz.^[124] The corresponding $^{11\text{B}}$ NMR signals ($\delta^{11\text{B}} = -33.3$ (**95**), -38.6 (**96**)) are in the typical range of four-coordinate boron compounds.^[149] Here, each signal appears as quintet, originating from two superimposed quartet signals, caused by coupling of the boron atom to the phosphorus atom (doublet) and the three hydrogen atoms (quartet) (Figure 58). As reported in the literature for comparable compounds, the resonances of the BH_3 moiety are very broad and can be found in the higher field of the ^1H NMR spectrum ($\delta^{1\text{H}} = 0.8\text{-}1.4$) (Figure 59).^[148]

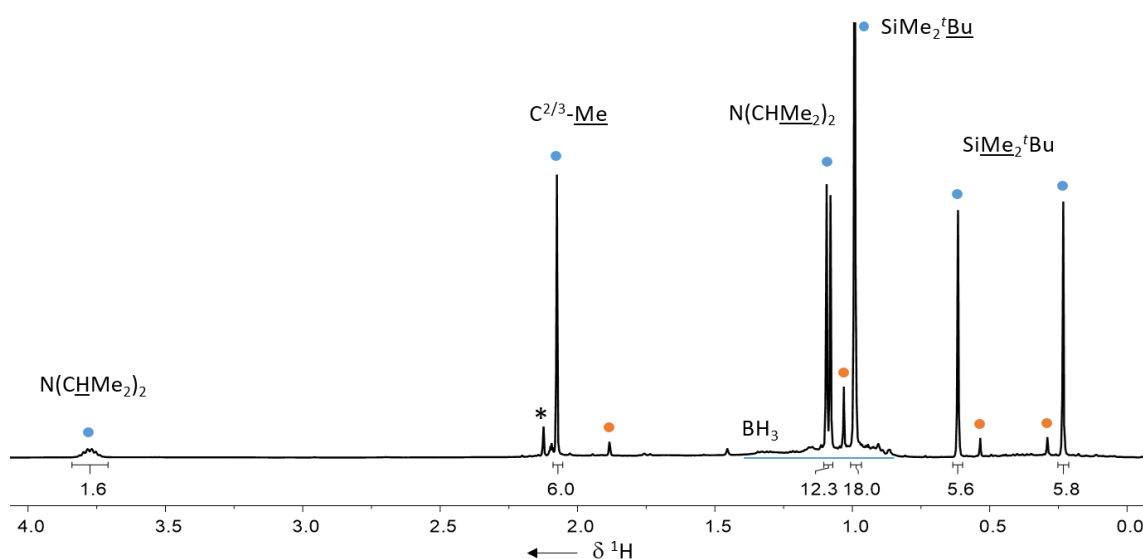
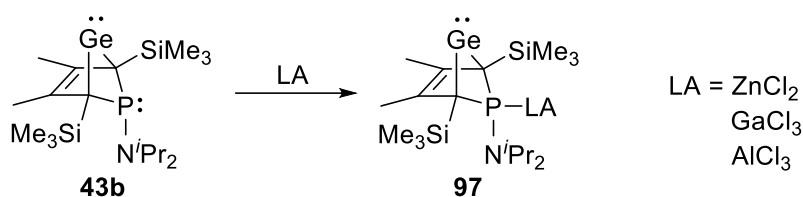


Figure 59 – ^1H NMR spectrum (500.0 MHz, 305 K, toluene- d_8) of the germylene-borane adduct **95** (●) and the phosphole-borane adduct **96** (●), * = solvent.

The selective coordination of the soft Lewis acid borane (BH_3) by the phosphorus atom of both, germylene **44b** and the phosphole **46b**, suggests that the phosphorus atom in the herein introduced phospho-BCH-germylenes **43-44** and phospholes **45-46** is best described as a soft Lewis base. This is coherent with the literature, as phosphanes (PR_3), including phospholes, are typically classified as soft Lewis bases.^[116, 145] Indication for the formation of the germanium-borane adduct of germylene **44b** was not found.

3.4.3.2 ZnCl₂, GaCl₃ and AlCl₃

Going from soft to harder Lewis acids, the reactivity of phospho-BCH-germylene **43b** towards zinc dichloride, a representative of medium hard Lewis acids, and gallium trichloride and aluminium trichloride as representatives for hard Lewis acids, was studied. In the literature, only few examples of triorganophosphane-trihalogenidotriels adducts (R₃P-EX₃ with E = Al, Ga) are known.^[150-152] To the best of our knowledge, no such phosphole adducts are known. Similar to the reaction with borane, the Lewis acids were each added to an *in situ* prepared, cooled THF solution of germylene **43b** (Scheme 50).

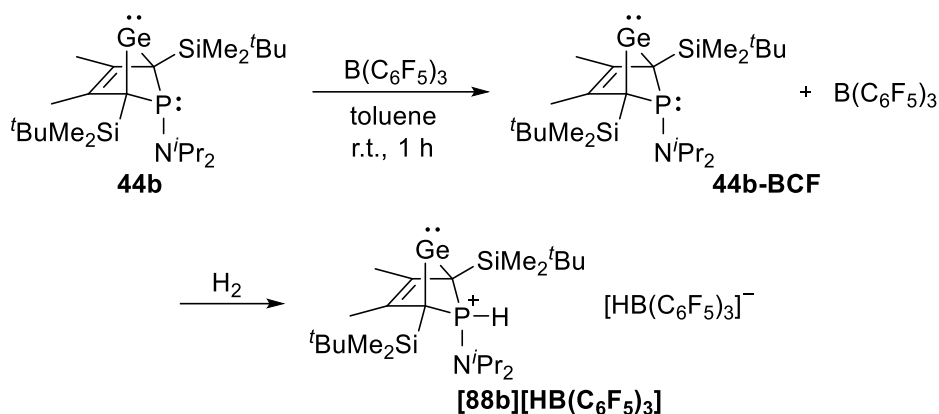


Scheme 50 – Attempted adduct formation of germylene **43b** with harder Lewis acids (LA).

Indeed, upon combination of phospho-BCH-germylene **43b** and the three Lewis acids, no donor-acceptor adduct (**97**) formation was observed. Instead, the starting material, a mixture of germylene **43b** and phosphole **45b** was reisolated. With the germylene site, however, no adduct formation was observed either.

3.4.3.3 Application in FLP Chemistry

As the herein introduced aminophospha-BCH-germylenes **44** have shown to be sterically demanding Lewis bases. For proof of principle, their application in FLP chemistry was studied. Therefore, tris(pentafluorophenyl)borane (BCF), a hard, sterically demanding Lewis acid, often used in FLP chemistry, was added to a toluene solution of germylene **44b**. As expected, no reaction was observed at first. Treatment of the degassed FLP solution with dihydrogen gas resulted in bond activation reaction of the latter (Scheme 51).



Scheme 51 – Dihydrogen activation with a phospho-BCH-germylene **44b** borane frustrated Lewis pair.

The formation of the respective phosphonium-BCH-germylene **[88b]** ($\delta^{31}\text{P} = 22.7$; $^1J_{\text{P,H}} = 570$ Hz) and the hydridoborate $[\text{HB}(\text{C}_6\text{F}_5)_3]^-$ ($\delta^{11}\text{B} = -23.7$) was noted in the recorded NMR spectra (Scheme 51). Upon dihydrogen activation, the ^{31}P NMR signal was shifted to higher field, to the typical range of phosphonium-BCH-germylenes (see Chapter 3.4.2.2). The corresponding ^{11}B NMR signal was shifted to higher field as well; from the three-coordinate to the four-coordinate boron region.^[149] While the respective P-H signal was also clearly depicted in the ^1H NMR spectrum, the B-H signal was very broad. According to integration, the phosphonium borate **[88b][HB(C₆F₅)₃]** made up about 40% of the reaction mixture. Inspired by work of Berke and coworkers, the main product ($\delta^{31}\text{P} = 108.9$, $\delta^{11}\text{B} = -13.1$) is suggested to be a follow-up product, either being another phosphonium borate salt or a Lewis acid-base adduct.^[153] However, its structure or nature could not be determined. Figure 60 displays the ^{31}P and ^{11}B NMR spectra before and after the reaction, respectively.

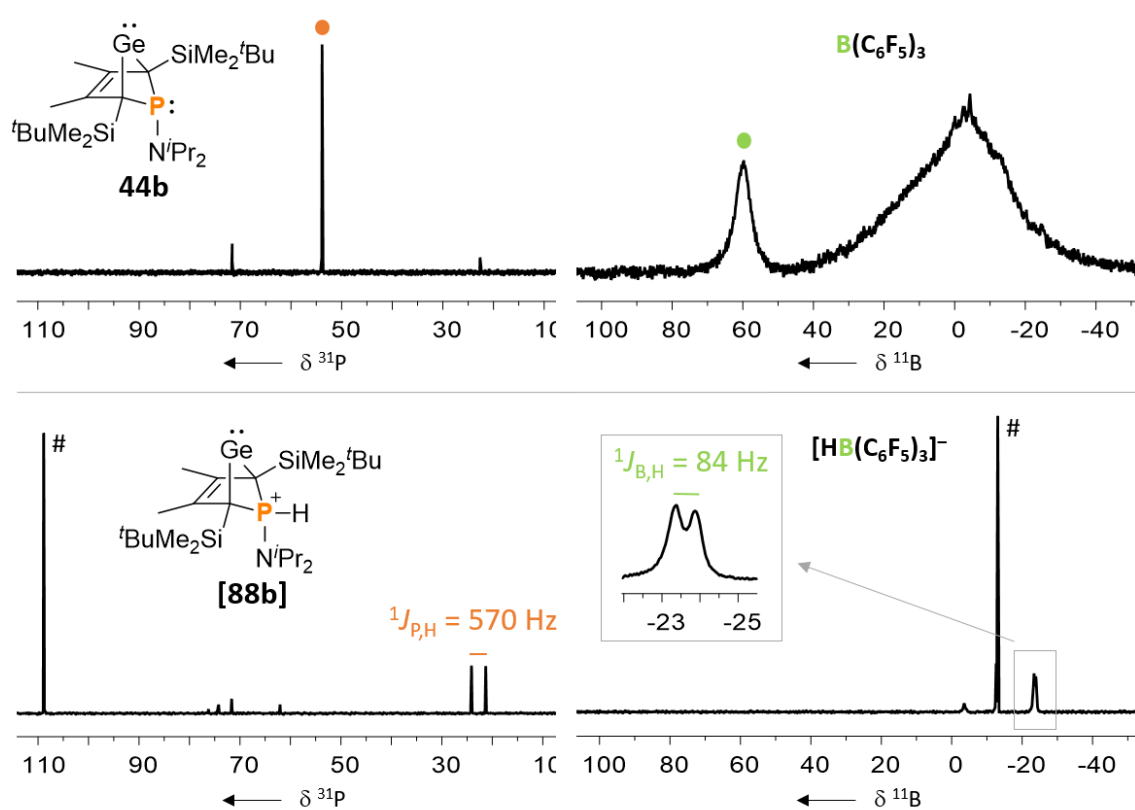


Figure 60 – ^{31}P (202.3 MHz, 305 K, toluene- d_8) and ^{11}B (160.4 MHz, 305 K, toluene- d_8) NMR spectra before (top) and after (bottom) the H_2 activation reaction (# = follow-up product).

As the colour did not remarkably change upon mixing of the acid and base as well as during the activation process, it may be assumed that the dihydrogen bond was not homolytically cleaved, but heterolytically. The radical pathway, by formation of radical ion pairs and homolytic bond cleavage, is usually indicated by intense colour change.^[21]

3.4.4 Reactivity Towards Transition Metal Complexes

The reaction of phospho-BCH-germylenes **43-44** towards various late transition metal complexes was studied to examine its suitability as ligand as well as its preferred coordination mode. In general, three coordination modes are possible: coordination of the phosphorus atom (**c1**), coordination of the germanium atom (**c2**) or bidentate coordination of the phosphorus and germanium atoms (**c3**). However, based on the previous analysis of the frontier molecular orbitals, the latter possibility (bidentate coordination mode **c3**) seems to be unfavoured due to the orientation of the orbitals, occupying the two lone pairs of electrons. Furthermore, based on the above discussed reactivity studies, coordination via the phosphorus atom (**c1**) was predicted (Figure 61).

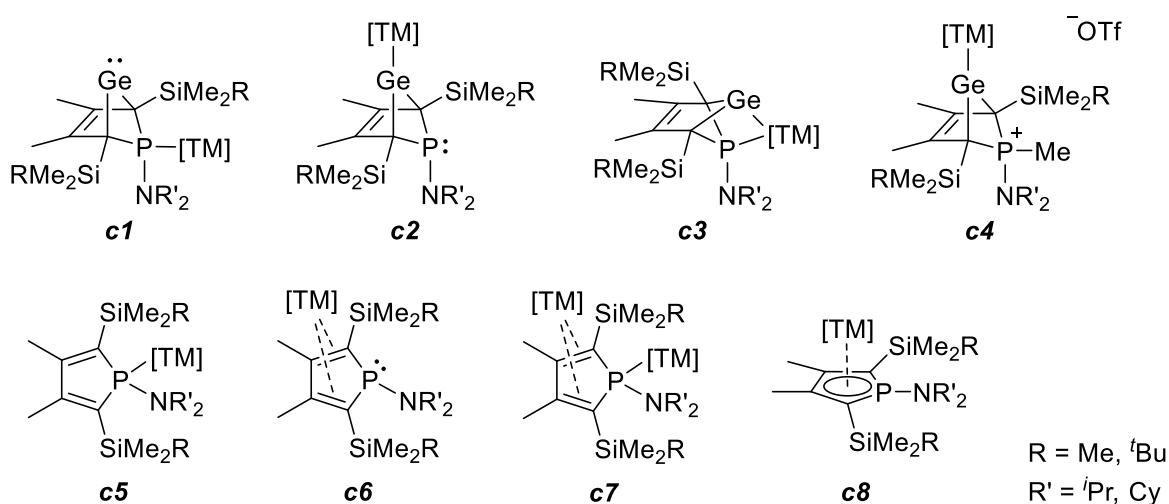
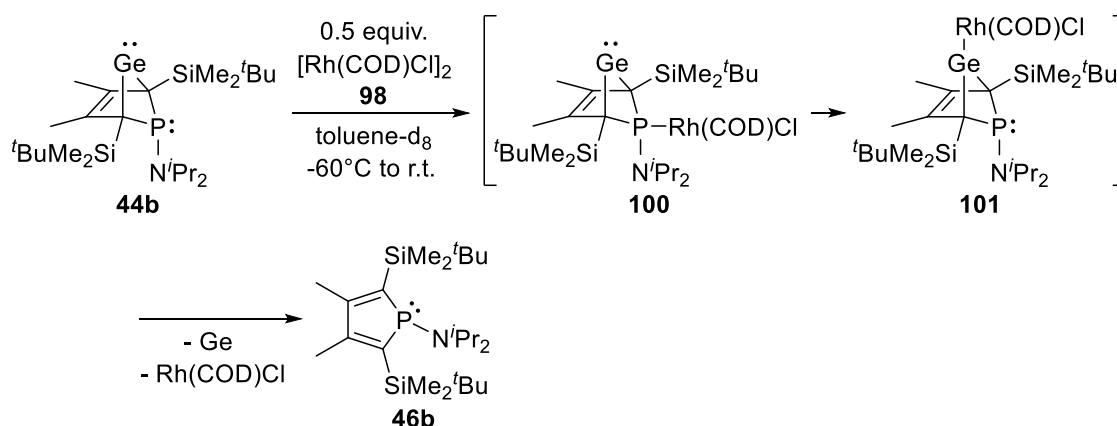


Figure 61 – Possible coordination modes of phospho-BCH-germylenes (**c1–c3**), phosphonium-BCH germylenes (**c4**), phospholes (**c5–c7**) and phospholyl anions (**c8**) to transition metal complexes [TM].^[154]

Additionally, the reactivity of methylphosphonium-BCH-germylene **[91]** and phospholes **45-46** towards transition metal complexes was studied. Using the phosphonium-BCH-germylene **[91]**, coordination via the germanium atom was targeted, as here, the phosphorus atom is already saturated (**c4**). For comparison, experiments using phospholes **45-46** as ligand for the metal were carried out. Theoretically, coordination via the phosphorus atom (**c5**) or coordination via the π-system (**c6**) is possible. The latter, however, is not commonly known to the literature. This type of coordination is usually reported for phosphole metal complexes, exhibiting enhanced butadiene reactivity, upon coordination to a second transition metal center (**c7**). Furthermore, it is known for phospholyl anions (**c8**) (Figure 61).^[154-155]

3.4.4.1 [Rh(COD)Cl]₂

Germylene **44b** was reacted with the dimeric cyclooctadiene-rhodium(I)chloride complex **98**. Here, the reactive species is the monomeric d⁸-ML₃ (14 VE) Rh(COD)Cl complex. Upon addition of a toluene solution of germylene **44b** to a toluene solution of the rhodium complex **98** at room temperature, the mixture turned green within five minutes. After additional five minutes of stirring the solution turned dark and a black precipitate was formed. The elimination of germanium and rhodium metal, as indicated by the formation of the black precipitate, was confirmed by analysis of NMR spectra, recorded from the crude reaction mixture: almost pure phosphole **46b** ($\delta^{31\text{P}\{^1\text{H}\}} = 71.6$) was obtained. Furthermore, signals of non-coordinated cyclooctadiene ($\delta^1\text{H}(\text{methine-H}) = 5.53$) were displayed in the ¹H NMR spectrum, showing that the rhodium complex **98** decomposed as well during the reaction. In a control experiment, however, it was shown that the phosphole **46b** does not react with [Rh(COD)Cl]₂ **98**.



Scheme 52 – Reaction of germylene **44b** towards the dimeric rhodium(I) complex **98**.

Based on the observed colour change, it was assumed that a phospho-BCH-germylene-rhodium complex was formed as an intermediate. To monitor the reaction and detect the intermediate complex, the reaction was carried out at -60°C. As no visible reaction took place at that temperature, the reaction mixture was stirred for 5 minutes at room temperature before a NMR sample was taken and measured at -50°C immediately. Spectra at -10°C and at room temperature were measured afterwards with 1 hour in between each temperature variation. The sample was kept at -60°C in the meantime. The ¹H NMR spectrum recorded at -50°C displayed signals that were assigned to germylene **44b**, the COD signals of complex **98** and small signals assigned to the phosphole **46b**. In the ³¹P{¹H} NMR spectrum, however, besides the germylene and phosphole signals ($\delta^{31\text{P}} = 53.9$ (**44b**), 71.6(**46b**)), additional signals were detected at $\delta^{31\text{P}} = 45\text{-}47$ and 120. The doublet signal at $\delta^{31\text{P}} = 120$ shows a coupling constant of $^1J_{\text{P,Rh}} = 163$ Hz which is in the range of reported $^1J_{\text{P,Rh}}$ coupling constants

($^1J_{\text{P,Rh}} = 110\text{-}210\text{ Hz}$).^[156-159] One particularly related example (**99**), reported by García *et al.*, is shown in Figure 62.^[157]

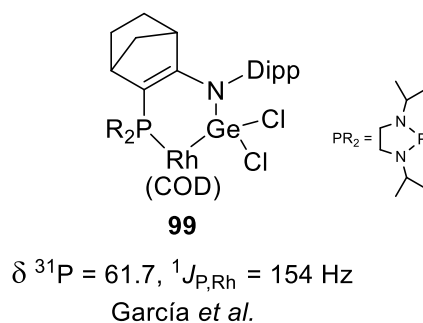


Figure 62 – Related Rh-P complex **99** reported by García *et al.*.^[157]

Therefore, the signal was assigned to a rhodium complex with a phosphorus ligand. As the phosphole does not react with the rhodium complex, it was assigned to the phospho-BCH-germylene-rhodium complex **100** in **c1** coordination (Figure 61). Going to higher temperature, the ratio of germylene **44b** to germylene-rhodium complex **100** to phosphole **46b** to the compound at $\delta^{31}\text{P} = 45\text{-}47$ changed (conversion from germylene **44b** to phosphole **46b**), depicting the ongoing reaction. Especially between the measurements at -10°C and room temperature, the formation of larger amounts of phosphole **46b** was visible as the sample darkened. Figure 63 shows the $^{31}\text{P}\{^1\text{H}\}$ NMR spectra recorded at different temperatures. The signals slightly shift upon warming to room temperature, as ^{31}P NMR spectroscopy is sensitive to temperature change.^[115]

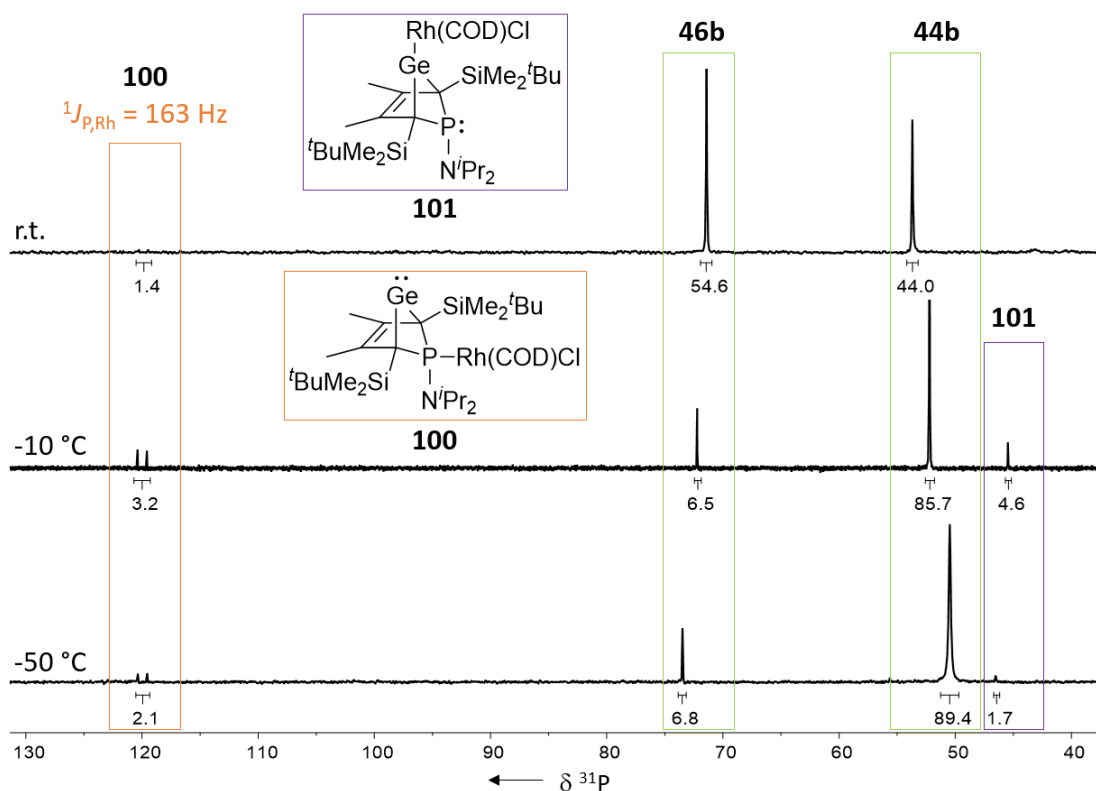


Figure 63 – Variable temperature $^{31}\text{P}\{^1\text{H}\}$ NMR spectra (202.3 MHz, toluene- d_8) of the reaction mixture: $-50\text{ }^\circ\text{C}$ (bottom), $-10\text{ }^\circ\text{C}$ (middle) and room temperature (top).

Using $^1\text{H}^{31}\text{P}$ HMBC and $^1\text{H}^{13}\text{C}$ HMBC NMR spectra, the bicyclic nature of complex **100**, with $\delta^{31}\text{P} = 120.0$, was confirmed. Furthermore, the additional singlet signal at $\delta^{31}\text{P} = 45.6$ could be assigned to another phosphagermylene-rhodium complex **101**. Both complexes exhibit sp^3 carbon atoms at $\delta^{13}\text{C} = 60$ (**100**) and $\delta^{13}\text{C} = 57$ (**101**), respectively. Because the ^{31}P NMR signal at $\delta^{31}\text{P} = 45.6$ did not show coupling to the rhodium centre, it was assigned to the **c2** coordination mode. At room temperature, the ^{31}P NMR signal intensity of those two compounds decreases, suggesting a short life time of the intermediate complexes (Figure 64).

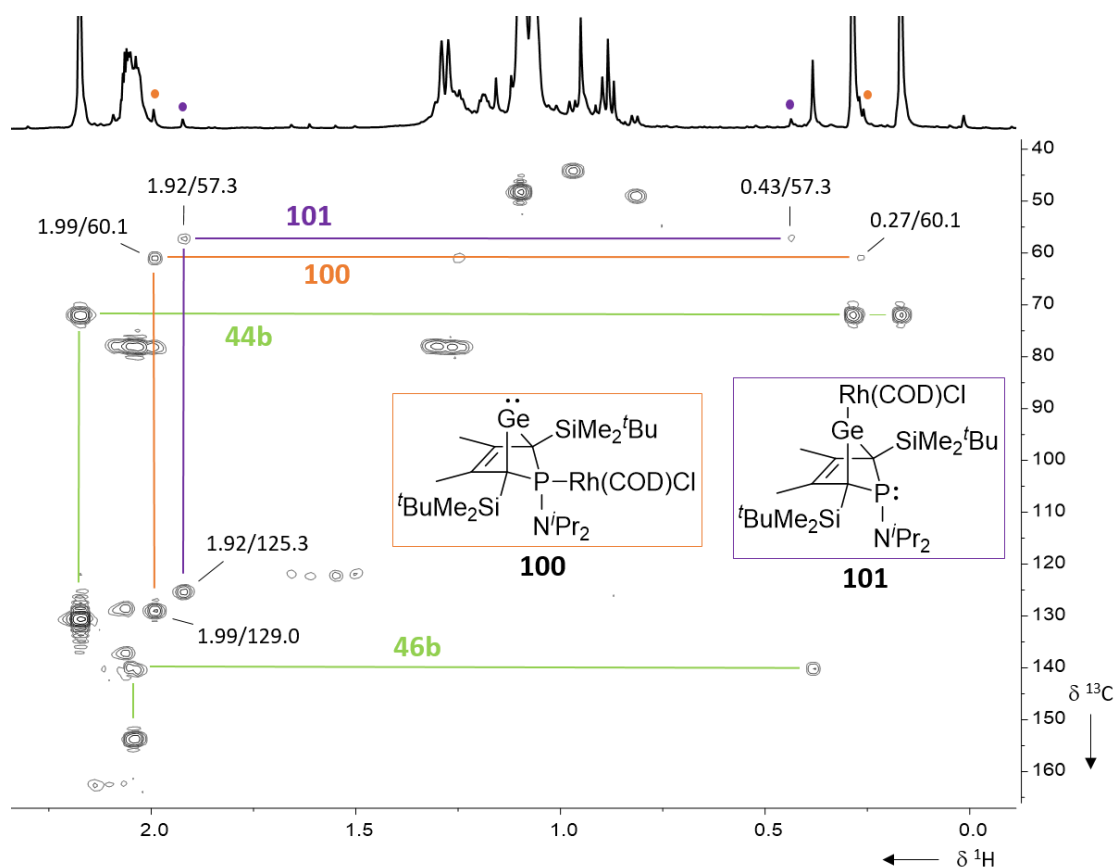


Figure 64 – $^1\text{H}^{13}\text{C}$ HMBC NMR spectrum (500.1 MHz, 263 K, toluene- d_8) showing the triangular patterns assigned to the germylene **44b**, phosphole **46b** (both green), the rhodium complexes **99** (**c1**, orange) and **100** (**c2**, purple).

Based on previous reactivity studies, we assume that germylene **44b** initially coordinates via the phosphorus atom (**100**) to the metal centre and then switches between coordination modes to coordination via the germanium atom (**101**). This isomerisation initiates the irreversible germanium elimination (Scheme 52).

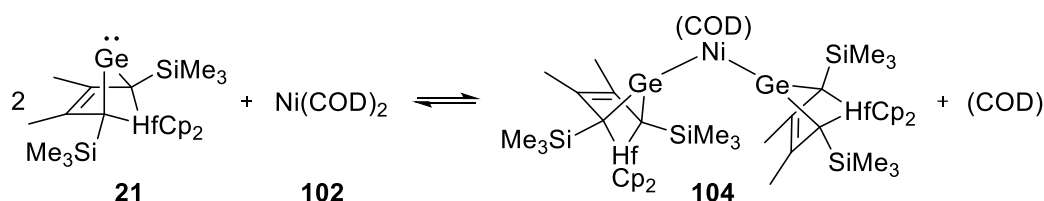
In addition to the experiments, DFT calculations were performed, comparing the relative energy difference between the two coordination modes **c1** and **c2** of germylene **43b** to the rhodium centre. The relative energy difference between complexes **100'** and **101'** is $\Delta E = 9 \text{ kJ mol}^{-1}$, whereas the coordination via the phosphorus atom (**100'**) is favoured (Figure 65). The small energy difference suggests the possibility for the proposed **c1** \rightarrow **c2** isomerisation. The reaction completes in the formation of the corresponding phosphole, as complex **101** decomposes irreversibly.



Figure 65 – Calculated relative energies for the two phospho-BCH-germylene-rhodium complexes **100'** and **101'** (M06-2X/6-311+G(d,p) (Ge, P, Si, N, C, H), def2-tzvp (Rh)).

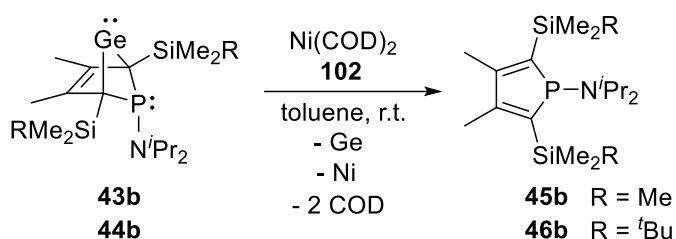
3.4.4.2 Ni(COD)₂ and Ni(CO)₂(PPh₃)₂

The reactivity of germylenes **43b** and **44b** towards two different nickel(0) complexes was studied. The complexes were chosen as one comprises relatively labile ligands (Ni(COD)₂) (**102**) and one comprises more strongly bonded ligands (Ni(CO)₂(PPh₃)₂) (**103**). The reactive species, however, in both cases is a d¹⁰-ML₂ (14 VE) complex: Ni(COD) and Ni(PPh₃)₂. It was shown before by Dong *et al.* that the germylene moiety of a hafnocene-BCH-germylene **21** reversibly reacts with Ni(COD)₂ (**102**). There, a bis-germylene nickel complex **104** was formed (Scheme 53). Upon removal of the non-coordinated COD, the complex **104** decomposed and gave germylene **21** back as well as complex **102** and elemental nickel.^[160]



Scheme 53 – Bis-germylene nickel complex **104** reported by Dong *et al.*^[160]

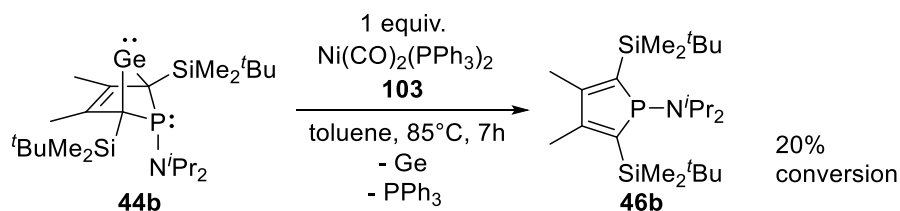
Formation of a complex like the one described by Dong *et al.* (Scheme 53) might have also been formed here, however, consistent with the reaction of the rhodium complex with germylene **44b**, the reaction of Ni(COD)₂ (**102**) with both germylenes, **43b** and **44b**, yielded the corresponding phosphole **45b** or **46b** and non-coordinated COD (Scheme 54). The metal accumulated as a shiny silver layer on the glass wall of the reaction vessel after 10 minutes reaction time. No variable temperature NMR experiments were carried out, though it may be assumed that the germanium elimination was initiated by transient germylene nickel complex formation (via the germanium atom, **c2**).



Scheme 54 – Reaction of germylenes **43b** and **44b** towards Ni(COD)₂.

In an independent experiment it was shown that, upon stirring at room temperature, phosphole **46b** does not form complexes with the nickel complex **102** in either fashion.

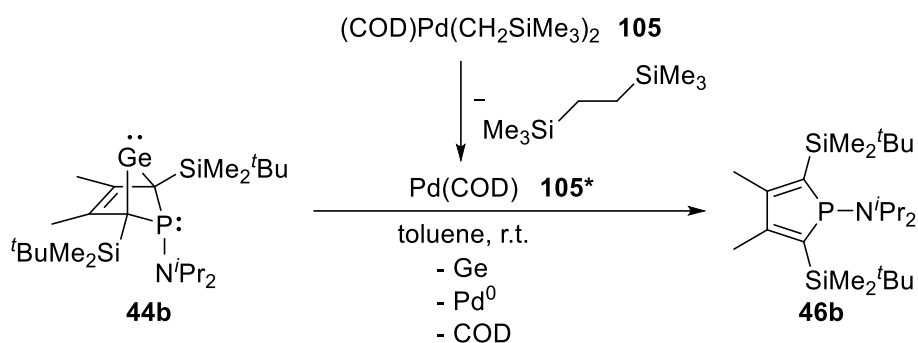
In contrast to the reaction with Ni(COD)₂ (**102**), addition of Ni(CO)₂(PPh₃)₂ (**103**) to germylene **44b** did not result in the formation of phosphole **46b**. Indeed, no reaction was observed at room temperature. Upon heating the toluene solution to 85°C for 7 hours, slow germanium elimination occurred (20% conversion). As it was shown that germylene **44b** does not decompose upon heating, this indicates reaction with the nickel complex **103** in the same or similar manner as observed with Ni(COD)₂ (**102**). The reaction, however, was not monitored until full conversion was achieved.



Scheme 55 – Temperature induced reaction of germylene **44b** with Ni(CO)₂(PPh₃)₂ (**103**).

3.4.4.3 Pd(CH₂SiMe₃)₂(COD)

Germylene **44b** was reacted with an equimolar amount of bis(trimethylsilyl(methyl))(cyclooctadiene)palladium(II) (**105**). The reactive species, however, is the d¹⁰-ML₂ (14 VE) Pd(COD) complex **105*** which is formed upon reductive elimination of bis(trimethylsilyl)ethane. The progress of the reaction can easily be monitored by ¹H NMR spectroscopy by integration of the trimethylsilyl moiety of the unreacted Pd(II) complex **105** and of the eliminated silylethane. Analogue to the previously discussed reaction, the phosphole **46b** was obtained (Scheme 56). The ³¹P NMR spectrum, however, displayed a second signal at δ ³¹P{¹H} = 104.9.



Scheme 56 – Reaction of germylene **44b** with the palladium complex **105***.

It was assumed that again, the germanium elimination was initiated by complex formation of the germylene with the metal. The intermediate germylene-palladium complex was not detected. It was furthermore noted that after 30 minutes, the germanium elimination was completed while only about 20% of the palladium(II) complex **105** (about 0.2 equivalents) was consumed. The recorded NMR spectra displayed phosphole **46b** and another sets of signals, featuring all typical phosphole backbone and substituent signals. The mixture contained the two compounds in a ratio of 3 : 1 after those 30 minutes (**A**, Figure 66). The reaction proceeded until the precursor palladium complex **105** was fully consumed. The ratio of phosphole **46b** to the unidentified compound was 1 : 1.7 (**B**, Figure 66).

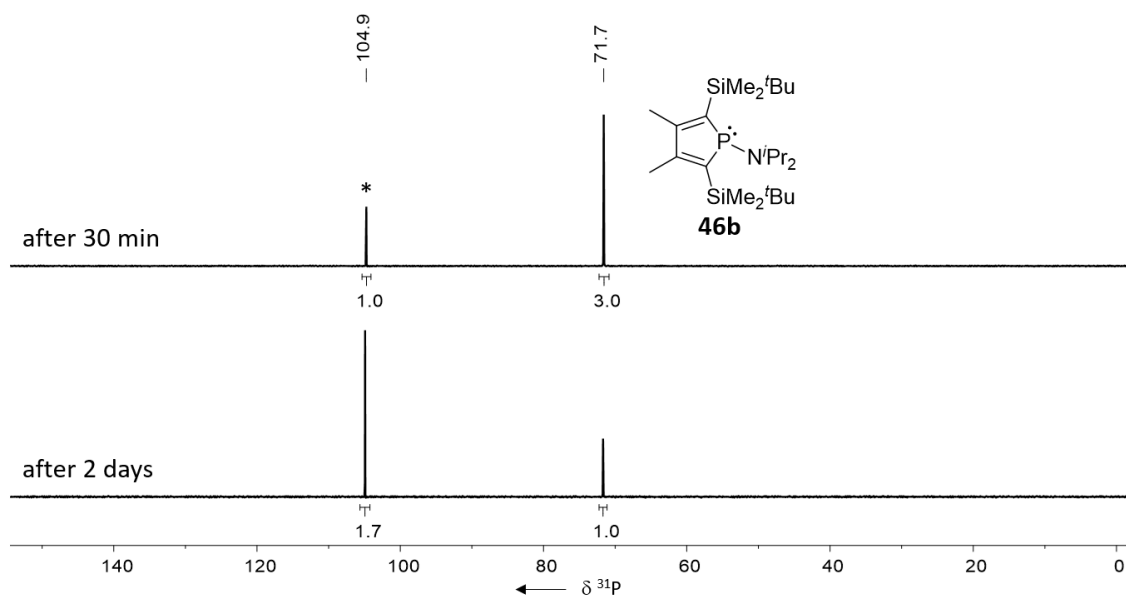
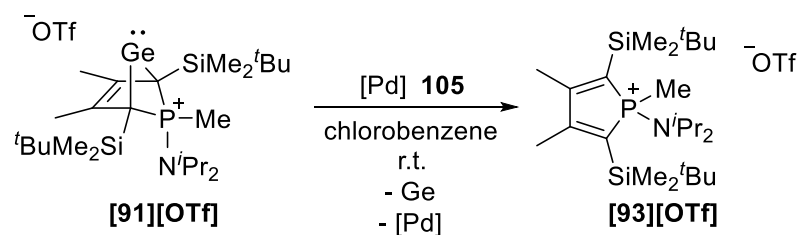


Figure 66 – ³¹P{¹H} NMR spectra (202.3 MHz, 305 K, benzene-d₆) of the reaction mixture after 30 minutes (top) and after two days (bottom), * = unidentified compound.

In addition, the reaction of methylphosphonium triflate **[91][OTf]** towards the palladium complex **105** was studied. Subsequent to the results described above, it resulted in the formation of methylphospholium triflate **[93][OTf]**. It might be assumed that the targeted coordination of the germylene moiety to the transition metal took place and initiated the germanium elimination. Complex formation with the phospholium ion **[93]** was not observed (Scheme 57). However, the reaction was slow. After 4 days in the NMR tube, only about 50% of phosphonium-BCH-germylene **[91]** were consumed (Figure 67).



Scheme 57 – Reaction of methylphosphonium triflate **[Me-BCH2b][OTf]** towards the palladium complex.

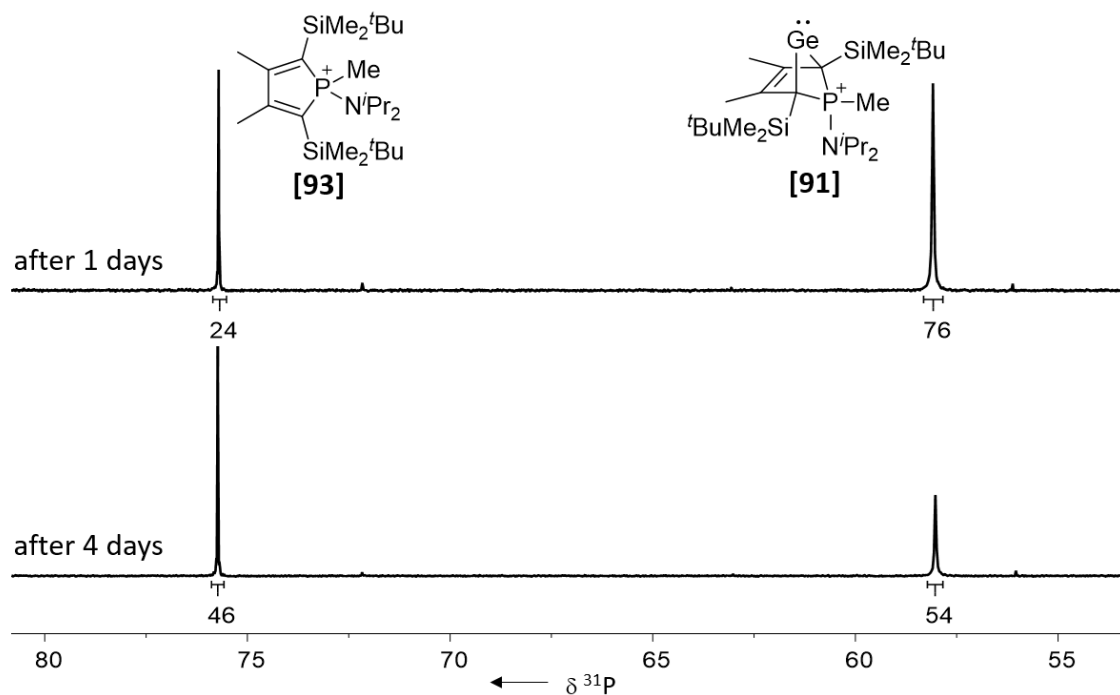
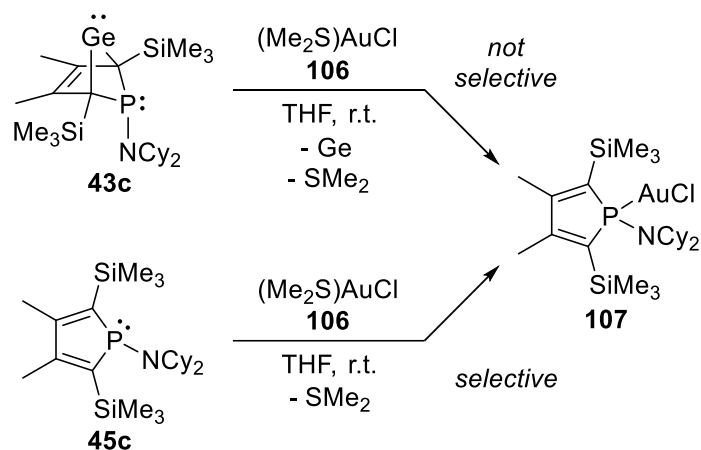


Figure 67 – $^{31}\text{P}\{^1\text{H}\}$ NMR spectra (202.3 MHz, 305 K, benzene- d_6) of the reaction mixture of phosphonium-BCH-germylene **[91]** and the palladium complex **105** after one day of stirring (top) and 4 days in the NMR tube (bottom).

3.4.4.4 (Me₂S)AuCl

The reactivity of germylene **43c** towards (dimethylsulfide)gold(I)chloride (**106**) was studied by addition of a toluene suspension of the gold complex **106** to a cooled, freshly prepared THF solution of germylene **43c** (Scheme 58). Here, the reactive species is a d¹⁰-ML₁ (12 VE) AuCl complex.



Scheme 58 – Reaction of germylene **43c** and phosphole **45c** towards (Me₂S)AuCl (**106**).

A control NMR spectrum was recorded after two hours, showing three main signals in the ³¹P NMR spectrum: δ ³¹P = 105.9, 77.4 and 63.3. The latter could be assigned to the phosphole **45c** (Figure 68, top). The reaction seemed to have continued as the ratio of the two unassigned signals (δ ³¹P = 105.9 and 77.4) had changed after workup (Figure 68, middle).

In an independent experiment, it was shown that phosphole **45c** can selectively be reacted with the gold complex **106** to form the phosphole-gold complex **107** (Scheme 58). Phosphole-gold(I) complexes are well known to the literature and are commonly synthesised in the same fashion.^[161-163] The NMR spectroscopic data of phosphole-gold complex **107** (Figure 68, bottom) matches that of one of the unknown compounds (δ ³¹P = 78) from the previously described reaction (Figure 68, middle and top).

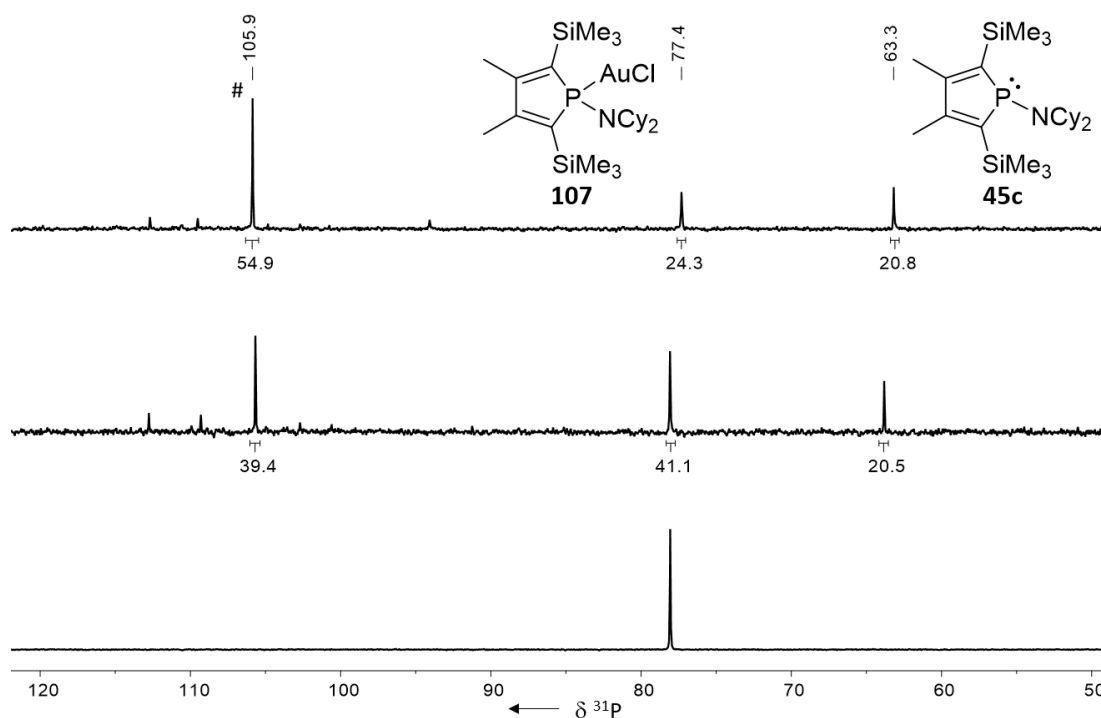


Figure 68 – $^{31}\text{P}\{^1\text{H}\}$ NMR spectra (202.3 MHz, 305 K) of the reaction mixtures with germylene **43b** as precursor (top (in THF) and middle (in benzene- d_6)) and phosphole **45c** as precursor (bottom (in benzene- d_6)), # = unidentified compound.

The typical triangular pattern for phosphole **45c** as well as for the respective gold complex **107** were observed in the $^1\text{H}^{13}\text{C}$ HMBC NMR spectrum (δ ^1H = 0.33 (SiMe $_3$), 1.71 (Me); δ ^{13}C = 136.9 (C $^{1/4}$), 160.3 (C $^{2/3}$)). Even though the compound at δ ^{31}P = 105.9 is the main compound, its structure could not be determined. The ^{31}P NMR signal of the complex **107** is shifted to lower field by about 14 ppm, compared to phosphole **45c** which is very similar to other reported phosphole/phosphole-gold complex pairs.^[162]

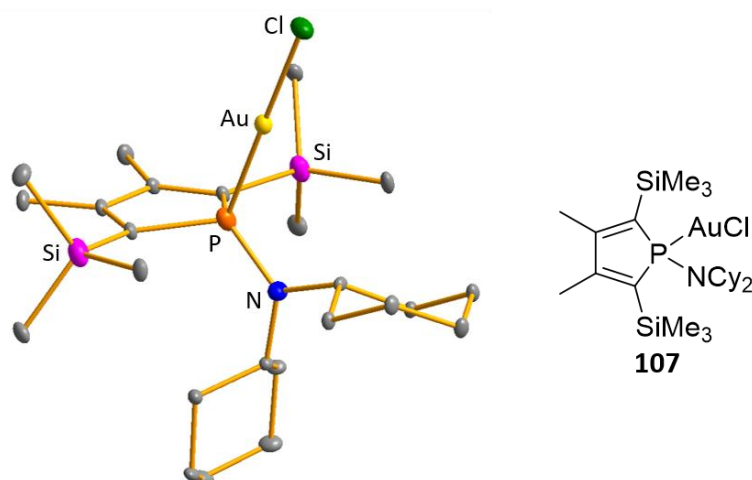
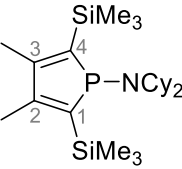
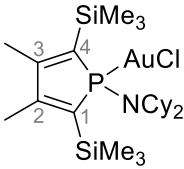


Figure 69 – Molecular structure of phosphole-gold complex **107** in the crystal. Space group $P2_1/c$. Thermal ellipsoids at 50% probability. The co-crystallised toluene molecule and all hydrogen atoms are omitted for clarity. Disordered structure, only the main structure (75%) is shown.

The phosphole-gold complex **107** was crystallised and analysed by X-ray diffraction (Figure 69). The phosphole moiety did not experience huge changes upon complexation: the bond lengths of its butadiene backbone did not significantly change compared to the precursor phosphole **45c** with $\Delta(C^{1/4}-C^{2/3}) = 1.3$ pm and $\Delta(C^2-C^3) = 2.5$ pm. The bonds around the phosphorus atom got slightly elongated by $\Delta = 1.6$ pm for the P-C^{1/4} bonds and $\Delta = 2.0$ pm for the P-N bonds. Furthermore, the coordination environment of the phosphorus atom remained the same. Excluding the bond to the gold atom, the phosphorus moiety flattened by less than $\Delta(\Sigma P) = 3^\circ$. As typical for phosphorus-gold(I) complexes, the P-Au-Cl moiety is almost linear with an angle of 179.0° . The P-Au (223.5 pm) and the Au-Cl (229.3 pm) bond lengths are within the typical range as well^[161-162] (Table 25).

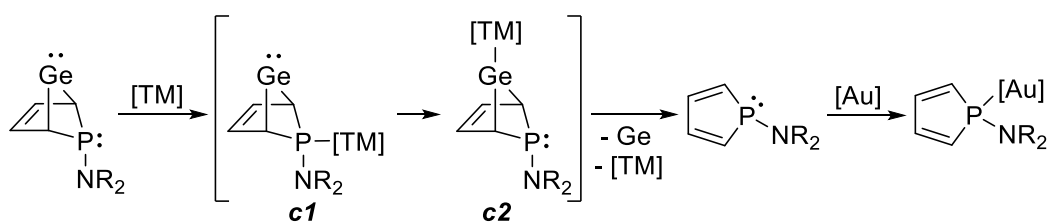
Table 25 – Selected bond lengths and angles of phosphole **45c**^[67] and the phosphole-gold complex **107**. The values listed for the bond lengths P-C^{1/4} and C^{1/4}-C^{2/3} are the respective arithmetic mean.

			
		45c ^[67]	107
bond lengths [pm]			
P-Au	-		223.53(6)
Au-Cl	-		229.34(14)
P-C ^{1/4}	180.06(8), 179.15(9)		181.4(1), 180.92(12)
C ^{1/4} -C ^{2/3}	137.34(14), 137.71(13)		136.07(14), 136.26(15)
C ² -C ³	146.37(11)		148.93(15)
P-N	168.08(9)		170.08(17)
angles [°]			
P-Au-Cl	-		179.037(44)
ΣP (excl. Au)	323.4		326.2

The reactivity of the complex **107** was not further examined, though it needs to be mentioned, that phosphine and phosphole gold complexes (upon reaction with silver antimonate) can be found as catalysts for e.g. alkyne activation^[162] or cycloisomerisation reactions^[163] in various literature reports.

3.4.4.5 Short Summary: Chapter 3.4.4

The reactivity of phospho-BCH-germylenes **43b+c** and **44b+c** towards several late transition metal complexes was studied. It was found that the main reaction is the reductive elimination of germanium from the bicyclic structure. The speed of the reaction depends on the transition metal complex used. The results from reactivity studies with two different nickel complexes **102** and **103** suggest that the rate-determining factor is not the metal centre but its ligands. Based on the examination of the reaction towards the rhodium(I) complex **98**, using variable temperature NMR experiments, it was possible to furthermore suggest a reaction mechanism: phospho-BCH-germylenes **43-44** initially coordinate via their phosphorus atom to the transition metal (**c1**). Upon isomerisation to **c2** coordination, the germanium atom is eliminated irreversibly to give the corresponding phosphole (Scheme 59). Based on reactivity studies of methylphosphonium-BCH-germylene triflate **[91][OTf]** towards the palladium complex **105**, it is assumed that upon quarternisation of the phosphorus atom, direct coordination of the germylene to the transition metal is possible as here, elimination of the germanium atom was observed, while the phosphorus atom remained in its quarternised coordination.

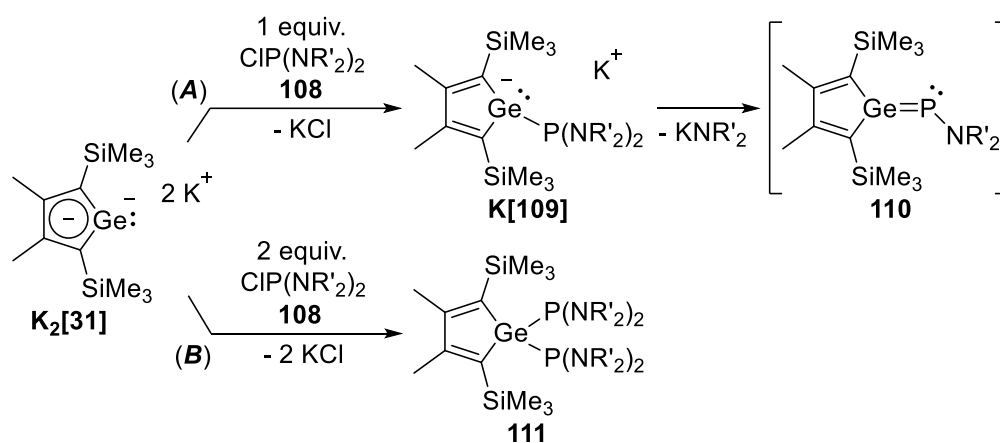


Scheme 59 – Postulated mechanism for the reaction of phospho-BCH-germylenes towards transition metal complexes [TM].

In most cases, the aminophospholes **45-46** did not react with the transition metal complexes. In case of the gold complex **106**, however, the corresponding complex **107** was obtained (Scheme 59).

3.5 Phosphanylgermolides and Diphosphanylgermoles

In a small project, the reactivity of dipotassium germolediide **K₂[31]** towards diaminochlorophosphanes **108a-c** was investigated. The goal was to synthesise potassium phosphanylgermolides **K[109]** via a single salt metathesis reaction in a first step. In a second step, a second salt metathesis was supposed to take place. Upon elimination of potassium amide from the phosphanylgermolide salt **K[109]** (**A**, Scheme 60), the thereby formed phosphagermafulvene **110** would be formed and potentially rearrange to give the known phospho-BCH-germylenes **43**. Another reaction that could possibly take place here is the reaction of two equivalents of chlorophosphane **108** with one equivalent of dipotassium germolediide **K₂[31]** to give the respective diphosphanylgermole **111** (**B**, Scheme 60).



Scheme 60 – Reactions of dipotassium germolediide **K₂[31]** towards diaminochlorophosphanes **108**.

Similar to the results discussed in the first part of this work, the choice of the amino substituents impacted the course of the reaction, here, driving the reaction more towards path (**A**) or (**B**).

3.5.1 Synthesis of Diaminochlorophosphanes

The reaction described above (Scheme 60) was carried out using three different diaminochlorophosphanes. *Bis*(diisopropylamino)chlorophosphane **108a** was purchased commercially. The mixed chloro(*diisopropylamino*)(piperidino)phosphane **108b** was not known in the literature but was synthesised in accordance to a literature procedure for a similar compound.^[164] Chlorodipiperidinophosphane **108c** was synthesised following literature-known procedures.^[165-166]

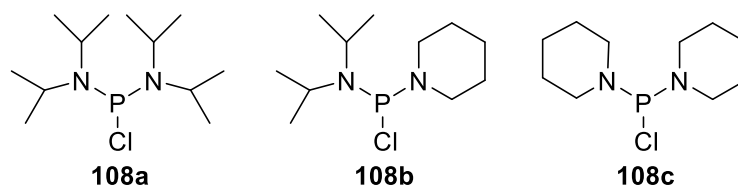
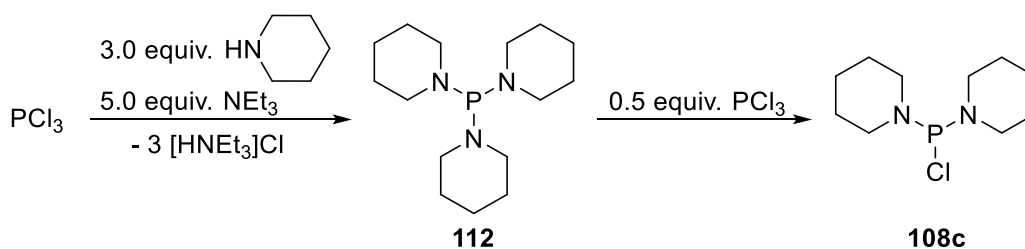


Figure 70 – Diaminochlorophosphanes **108a-c** used in this work.

Chloro(dipiperidino)phosphane

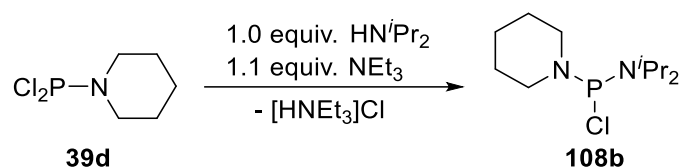
Chloro(dipiperidino)phosphane **108c** was synthesised in two steps. In a first step, tripiperidinophosphane **112** was synthesised from trichlorophosphane and piperidine, following a procedure by Bollinger *et al.*^[165] Here, triethylamine was used to compensate the released acid. The interstage product, tripiperidinophosphane, was obtained in 88% yield (Lit.: 76%^[165]). In a second step, a substituent comproportionation reaction was carried out by addition of half an equivalent of trichlorophosphane to the tripiperidinophosphane **112**. This step was described by Zeiß *et al.*^[166] After distillation, the product **108c** was obtained in a yield of 53% (Lit.: 75%^[166]) (Scheme 61). The NMR spectroscopic data of the interstage product **112** as well as of the final product **108c** matches the corresponding literature.^[165-166]



Scheme 61 – Synthesis of chlorodipiperidino)phosphane **108c** via tripiperidinophosphane **112**.^[165-166]

Chloro(diisopropylamino)(piperidino)phosphane

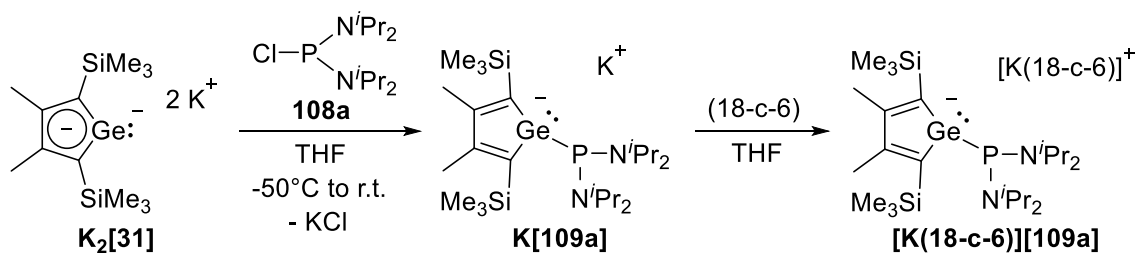
The mixed diaminochlorophosphane **108b** was synthesised from dichloropiperidino)phosphane **39d** (synthesis see Chapter 3.1.2) and diisopropylamine in accordance to a procedure by Bender *et al.* described for the related chloro(diisopropylamino)-(dimethylpiperidino)phosphane.^[164] It has proven to be useful to use triethylamine to compensate the within the reaction released hydrochloric acid instead of a second equivalent of diisopropylamine. As the reaction was not complete after 4 hours, the mixture was stirred for 3 days. Removal of the precipitates and the solvent gave the product, diisopropylamino(piperidino)phosphane **108b**, in quantitative yield (100%).

Scheme 62 – Synthesis of diisopropylamino(piperidino)phosphane **108b**.

The detailed synthesis and the analytical data of this newly reported compound can be found in the experimental part. It furthermore needs to be mentioned that the synthesis of this diaminochlorophosphane **108b** was not successful reacting dichloro(diisopropylamino)-phosphane **39b** with piperidine.

3.5.2 Reactions with Chloro(*bis*(diisopropylamino))phosphane

To synthesise the potassium phosphanylgermolide **K[109a]**, one equivalent of a freshly prepared THF solution of dipotassium germolediide **K₂[31]** was cooled to -50°C and one equivalent of a THF solution of diamino phosphane **108a** was added.

Scheme 63 – Synthesis of the phosphanylgermolide salt **[K(18-c-6)][109a]**.

After one hour of stirring, a bright red solution was obtained, containing the corresponding potassium phosphanylgermolide **K[109a]** as main product ($\delta^{31\text{P}} = 97.3$). The mixture contained two other compounds, identified as the disubstituted product, diphosphanylgermole **111a** ($\delta^{31\text{P}} = 111.3$) and tetrakis(diisopropylamino)diphosphane **113a** ($\delta^{31\text{P}} = 84.3$) (Figure 71). The diphosphane **113a** is known to the literature.^[167]

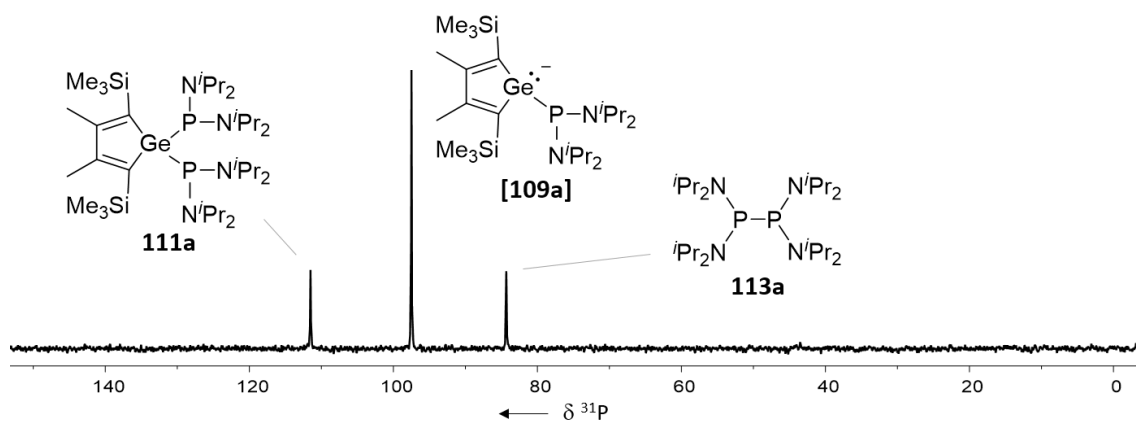


Figure 71 – $^{31}\text{P}\{^1\text{H}\}$ NMR spectrum (202.3 MHz, 305 K, THF) of the crude product mixture.

Due to decomposition of the potassium phosphanylgermolide **K[109a]** over time and to facilitate the crystallisation of the product, the potassium ion was complexed with crown ether (18-c-6) by addition of the latter to the crude product. Upon complexation of the potassium ion, the ^{31}P NMR signal of phosphanylgermolide **[109a]** was shifted to higher frequency ($\delta^{31}\text{P} = 101.9$, $\Delta(\delta^{31}\text{P}) = +4.6$), while the ^1H NMR signals remained mostly unchanged. The ^{13}C and ^{29}Si NMR spectra displayed broad signals. With the help low temperature NMR measurements (193 K), full NMR spectroscopic analysis of the phosphanylgermolide salt **[K(18-c-6)][109a]** was enabled. However, upon cooling, the ^{31}P NMR signal shifted to lower frequency ($\delta^{31}\text{P} = 93.2$, $\Delta(\delta^{31}\text{P}) = -8.0$), due to the sensitivity of ^{31}P NMR spectroscopy towards parameters like the temperature.^[115] The $^1\text{H}^{13}\text{C}$ HMBC NMR spectrum displayed an inverted triangular pattern (Figure 72), meaning that the $\text{C}^{1/4}$ carbon atoms ($\delta^{13}\text{C} = 160.7/164.1$) are shifted to lower frequency than the $\text{C}^{2/3}$ carbon atoms ($\delta^{13}\text{C} = 146.0/148.4$). This caught attention as usually, the typical triangular pattern is expected for non-aromatic compounds, e.g. as described for the phosphole **45b** (Chapter 3.2.4). Very similar chemical shifts and the inverted triangular pattern, however, have also been reported for the similar mesityl-germolide salt **[K(18-c-6)][114]** ($\delta^{13}\text{C} = 169.0$ ($\text{C}^{1/4}$), 146.1 ($\text{C}^{2/3}$)).^[60] In the respective study it was shown that switching between a localised and delocalised π -electron system (**[K(18-c-6)][114]** vs. **K[114]**), the chemical shift of the backbone carbon atoms is impacted (Table 26).^[60] Independent from the localisation or delocalisation of the π -electrons, however, the $\text{C}^{1/4}$ carbon NMR signals remain shifted to higher frequency compared to the $\text{C}^{2/3}$ carbon atoms, suggesting that the inversion of the triangular pattern does not necessarily correlate with the localisation or delocalisation of the π -electron system.

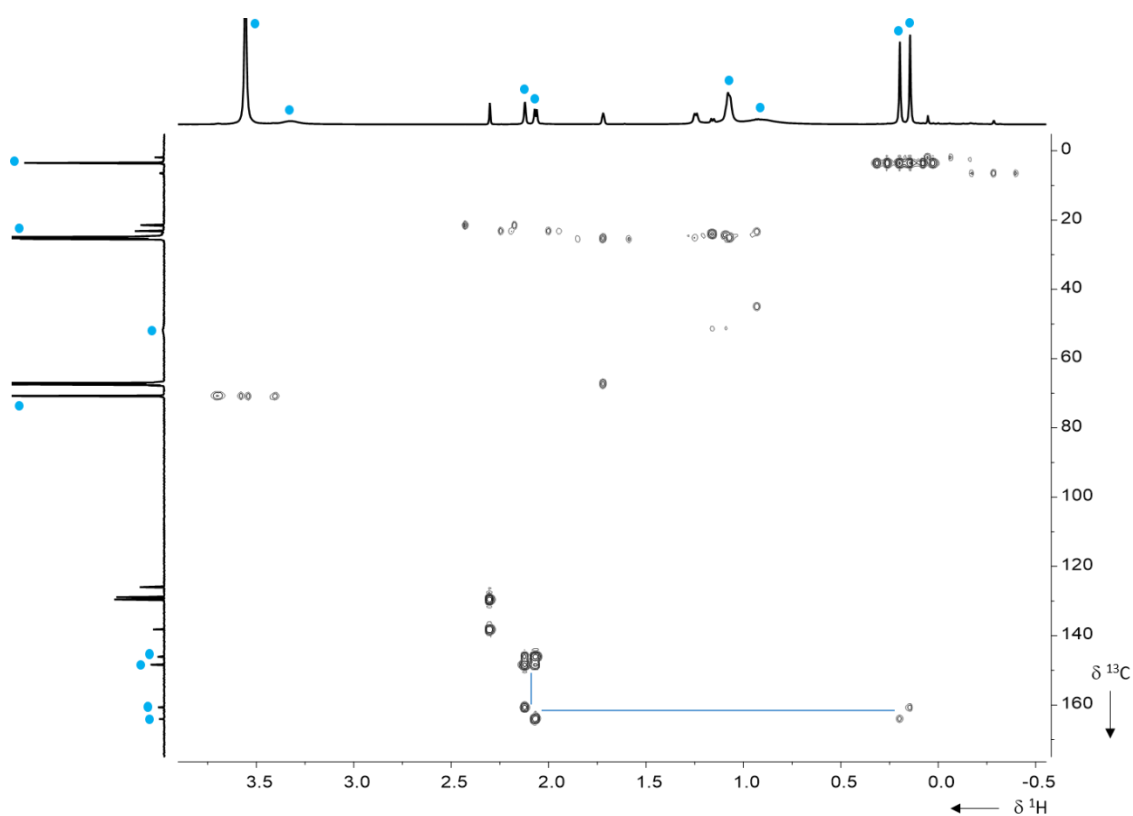
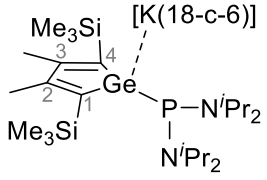
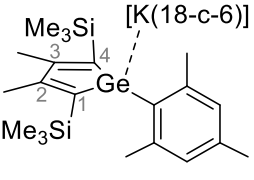
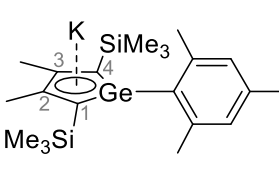


Figure 72 – $^1\text{H}^{13}\text{C}$ HMBC NMR spectrum (500.1 MHz, 193 K, THF-d_8) of the phosphanylgermolide salt **[K(18-c-6)][109a]**.

Table 26 – Selected NMR spectroscopic data of phosphanylgermolide salt **[K(18-c-6)][109a]** (measured in THF-d_8 at 193 K), and germolide salt **[K(18-c-6)][114]** and germolide salt **K[114]** (both measured in benzene- d_6 at 305 K).

			
	[K(18-c-6)][109a]	[K(18-c-6)][114] ^[60]	K[114] ^[60]
$\delta^{13}\text{C}$ ($\text{C}^{1/4}$)	160.7, 164.1	169.0	157.8
$\delta^{13}\text{C}$ ($\text{C}^{2/3}$)	146.0, 148.4	146.1	138.6
$\delta^{31}\text{P}$	93.2	-	-

The rotation around the Ge-P bond seems to be hindered as the asymmetry of the compound, displayed in its molecular structure (Figure 76), is also indicated in solution. Asymmetric, in this case, describes the parallel orientation of the phosphorus lone pair to the Ge-C¹ bond as described by the bisected Newman projection **P-2**, which describes the ground state of phosphanylgermolide **[109a]** (Figure 73). For each backbone carbon atom, a ^{13}C NMR signal was detected showing different $^1J_{\text{C,P}} / ^2J_{\text{C,P}}$ coupling constants for both sides of the germole backbone

(C¹ and C² vs. C³ and C⁴) (Figure 74). Furthermore, two sets of signals were also found for each substituent.

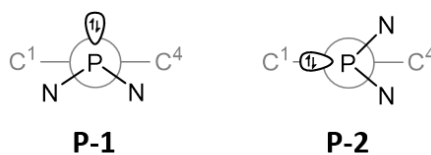


Figure 73 – Perpendicular (**P-1**) and bisected (**P-2**) Newman projections along the Ge-P bond of phosphanylgermolide **[109a]**.

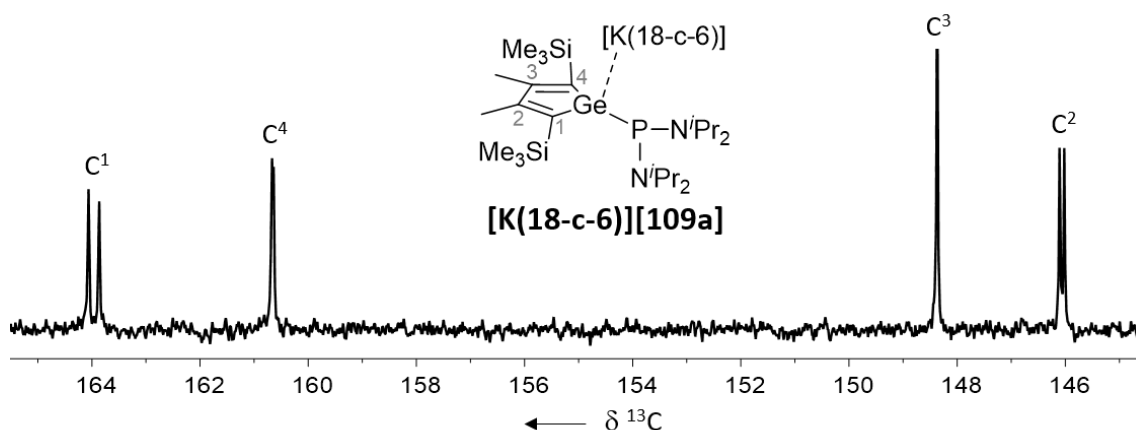


Figure 74 – Section from the $^{13}\text{C}\{^1\text{H}\}$ NMR spectrum (125.7 MHz, 193 K, THF- d_8) of phosphanylgermolide salt **[K(18-c-6)][109a]**, showing the signals assigned to the backbone carbon atoms.

To experimentally assess the extent of the rotational barrier, variable temperature ^1H NMR spectra of the dissolved crystalline germolide salt **[K(18-c-6)][109a]** were recorded in THF- d_8 from 305 K to 193 K. At room temperature, averaged broad signals were detected for the SiMe_3 and $\text{C}^{2/3}$ -Me groups, suggesting fast exchange, or here, fast rotation around the Ge-P bond. Upon cooling, sharpening and splitting of the broad signals was observed. At 193 K (-80°C), two separated signals were detected for the SiMe_3 and $\text{C}^{2/3}$ -Me groups, respectively, suggesting slow rotation around the Ge-P bond. The coalescence temperature was found to be 283 K (Figure 75). The energy barrier at the coalescence temperature was estimated using an equation based on an approximate solution and the Eyring equation.^[168] With a difference in the two resonance frequencies of $\delta\nu = 26.1$ Hz, the free enthalpy is $\Delta G^\ddagger = 59.6$ kJ mol⁻¹.

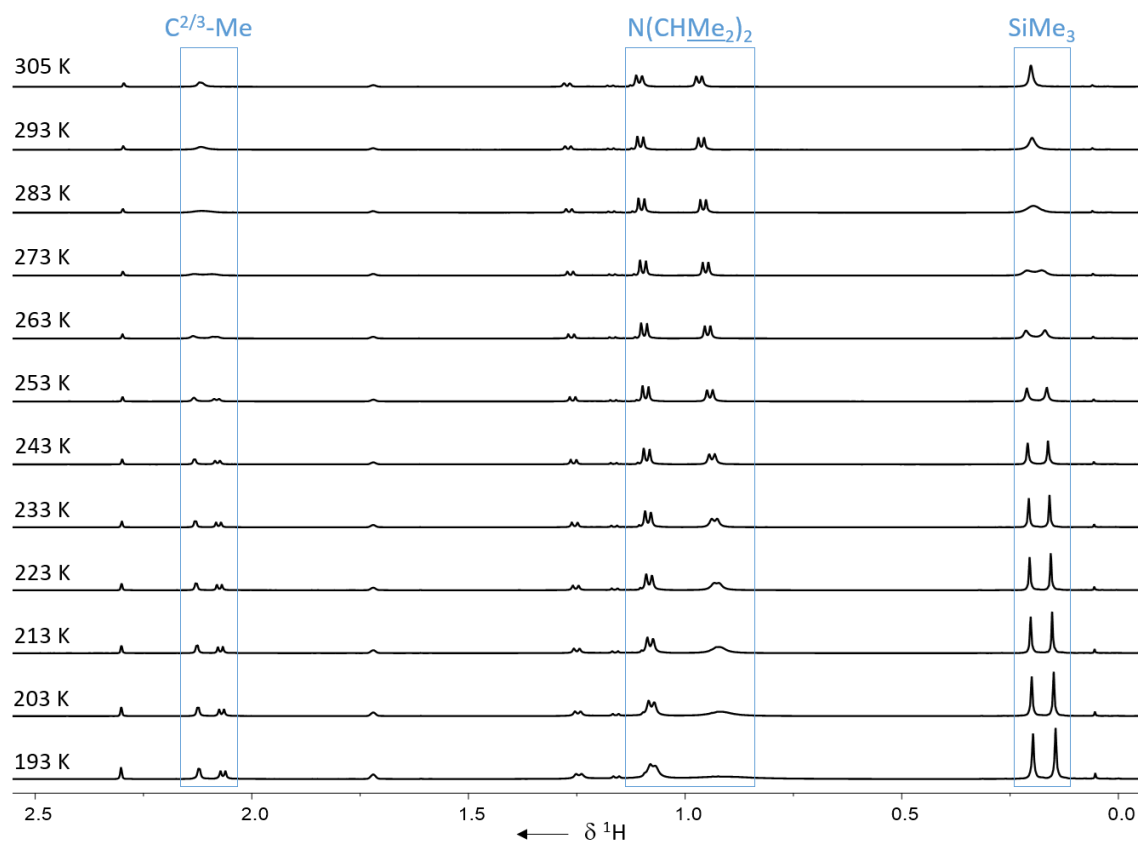


Figure 75 – ^1H VT NMR spectra (500.1 MHz, 305–193 K, THF-d_8) of phosphanylgermolide salt **[K(18-c-6)][109aa]**.

Keeping a toluene solution of phosphanylgermolide salt **[K(18-c-6)][109a]** at -20°C overnight resulted in the formation of red crystals, suitable for XRD analysis (Figure 76).

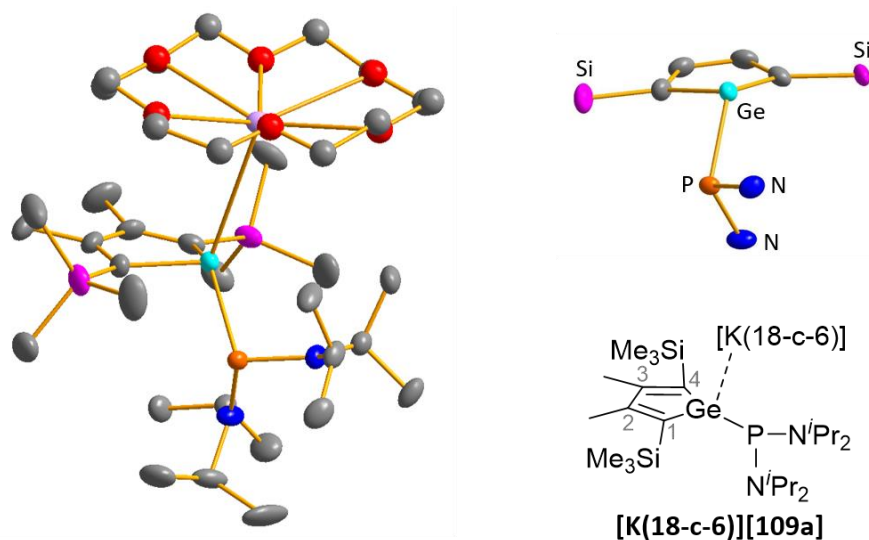
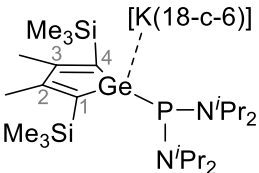
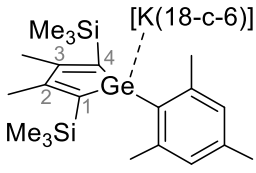
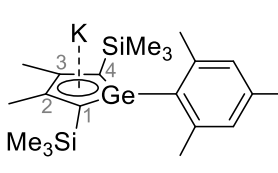


Figure 76 – Molecular structure of the phosphanylgermolide salt **[K(18-c-6)][109a]** in the crystal. Space group P1.

Thermal ellipsoids at 50% probability. Hydrogen atoms are omitted for clarity. On the right, the counterion **[K(18-c-6)]** as well as the substituent-carbon atoms are omitted as well. Disordered structure, only the main structure (52%) is shown.

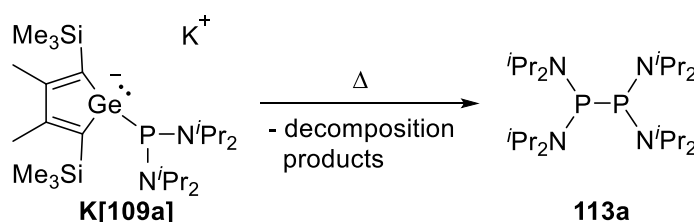
The molecular structure of phosphanylgermolide salt **[K(18-c-6)][109a]** was compared to the molecular structures of **[K(18-c-6)][114]** and **K[114]**, reported by Dong *et al.*^[60] The authors reported on a mesityl-germolide in an aromatic as well as a non-aromatic state, clearly distinguishable by the bond lengths in the germole ring and the coordination environment of the germanium atom: the bond lengths of the C¹-C² and the C²-C³ bonds of the aromatic germolide **K[114]** are almost equal ($\Delta(\text{C}^1\text{-C}^2 - \text{C}^2\text{-C}^3) = 1.2 \text{ pm}$), while those of the non-aromatic **[K(18-c-6)][114]** are shortened and elongated, respectively ($\Delta(\text{C}^1\text{-C}^2 - \text{C}^2\text{-C}^3) = -8.3 \text{ pm}$). The germanium atom in the non-aromatic compound **[K(18-c-6)][114]** is pyramidalised ($\Sigma(\text{Ge}) = 310.3^\circ$) and the Ge-C¹ bond is elongated compared to its aromatic isomer **K[114]**, and furthermore in the expected range for Ge-C single bonds.^[108] The considered bond lengths of the herein introduced germolide **[K(18-c-6)][109a]** only slightly deviate from those of germolide **[K(18-c-6)][114]**. Moreover, the germanium atom is pyramidalised as well ($\Sigma(\text{Ge}) = 313.1^\circ$). The Ge-P bond (Ge-P = 243.1 pm) is elongated compared to the sum of covalent radii by $\Delta(\text{Ge-P}) = 10 \text{ pm}$ (Table 27).^[108] Phosphanylgermolide **[109a]** is best described as a non-aromatic germolide. The germanium center is pyramidalised, featuring three (elongated) single bonds and a lone pair of electrons, thus being isolobal to phosphanes. It can therefore be assumed that phosphanylgermolide **[109a]** is a good σ -donor. However, its properties e.g. in complex formation with transition metals, were not tested within these studies.

Table 27 – Selected NMR spectroscopic data and structural parameters of the germolide salts **[K(18-c-6)][109a]**, **[K(18-c-6)][114]** and **K[114]**.^[60]

			
	[K(18-c-6)][109a]	[K(18-c-6)][114] ^[60]	K[114] ^[60]
C ¹ -C ² [pm]	137.62(26)	137.6(13)	142.9(4)
C ² -C ³ [pm]	146.14(23)	145.9(19)	141.7(5)
C ¹ -Ge [pm]	198.11(17)	197.0(10)	187.6(3)
$\Sigma(\text{Ge})$ [°]	313.1	310.3	355.1
Ge-P [pm]	243.14(7)	-	-

Attempted Potassium Amide Elimination

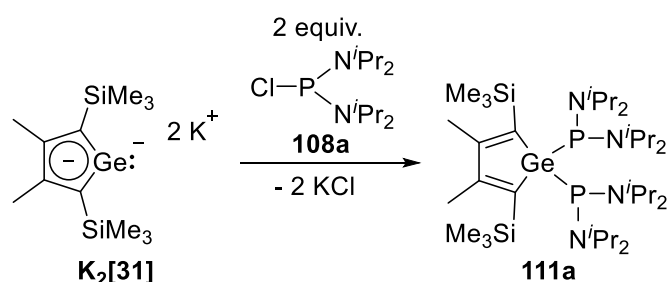
Heating a THF solution of the product mixture of germole **111a**, germolide salt **K[109a]** and diphosphane **113a** (see Figure 71) to 50°C for one hour did not cause significant changes in the composition of the mixture. After changing from THF to toluene and heating to 100°C for three hours, however, only the signal at $\delta^{31\text{P}} = 84.0$, assigned to diphosphane **113a**, remained. After removal of the precipitates, that had formed during the heating process, the remaining colourless solid was fully analysed by NMR spectroscopy. The obtained NMR spectroscopic data is in good agreement with data reported by Westerman *et al.*^[167] The formation of the diphosphane **113a** suggests, that the phosphanylgermolide **[109a]** as well as the diphosphanylgermole **111a** are not stable at elevated temperature, and it furthermore suggests that the P-N bonds are stronger than the P-Ge bond in phosphanylgermolide **[109a]**. Therefore, it can be assumed that the scheduled elimination of potassium amide from diamino-phosphagermolide salts **K[109]**, is not possible (Scheme 64).



Scheme 64 – Heat induced decomposition of potassium germolide **K[109a]**.

Synthesis of the Diphosphanylgermole

In an independent experiment, the diphosphanylgermole **111a** ($\delta^{31\text{P}}\{^1\text{H}\} = 111.3$) was synthesised. Addition of two equivalents of diaminochlorophosphane **108a** to the dipotassium germole diide **K₂[31]** resulted in the formation of a bright yellow solution of diphosphanylgermole **111a** (Scheme 65).



Scheme 65 – Synthesis of diphosphanylgermole **111a**.

Keeping the concentrated pentane solution at -30°C overnight afforded yellow crystals of *bis(bis(diisopropylamino)phosphanyl)germole* **111a**. The structural features will be discussed in Chapter 3.5.3. The ^1H and $^{13}\text{C}\{^1\text{H}\}$ NMR spectra, recorded of the dissolved crystalline compound **111a**, displayed sharp signals for the germole moieties and very broad signals for the *isopropylamino* groups. This might be drawn back to hindered rotation around the Ge-P bonds, due to the crowded arrangement of the $\text{P}(\text{N}^i\text{Pr}_2)_2$ groups. The $^{31}\text{P}\{^1\text{H}\}$ NMR spectrum displayed only one singlet signal for the compound (Figure 77).

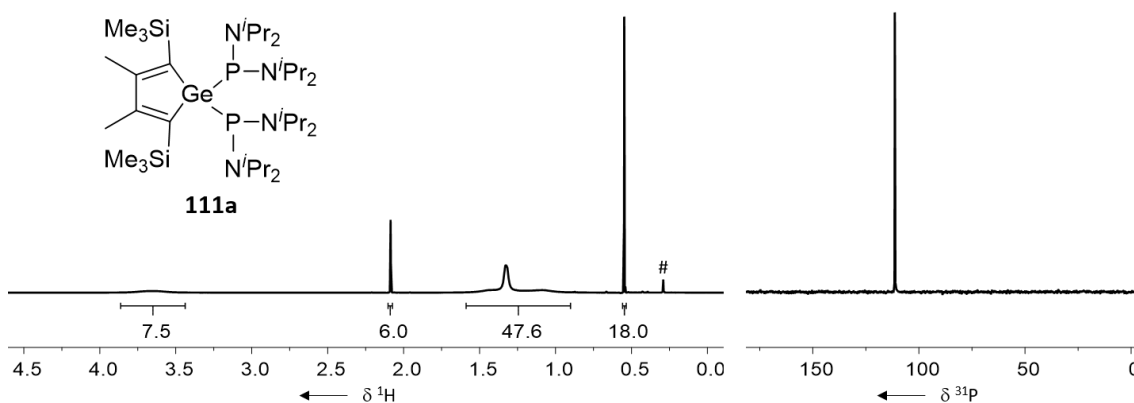
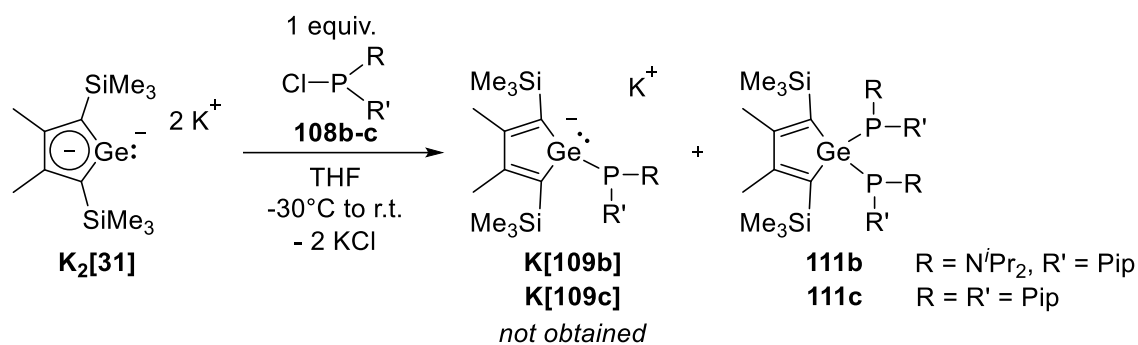


Figure 77 – ^1H NMR spectrum (500.1 MHz, 305 K, benzene- d_6) and $^{31}\text{P}\{^1\text{H}\}$ NMR spectrum (202.3 MHz, 305 K, benzene- d_6) of diphosphanylgermole **111a**.

3.5.3 Reactions with $\text{ClP}(\text{N}^i\text{Pr}_2)(\text{Pip})$ and $\text{ClP}(\text{Pip})_2$

Using the mixed diaminochlorophosphane **108b** and the chlorodipiperidinophosphane **108c** as precursor, the potassium phosphanylgermolides **K[109b]** and **K[109c]** were not isolated. In both cases, independent from the stoichiometry used, formation of the respective diphosphanylgermole **111b** or **111c** was favoured. This was visualised by consideration of the yield of the reaction of dipotassium germole diide **K₂[31]** with diaminochlorophosphane **108b**: using one equivalent of phosphane, the diphosphanylgermole **111b** was obtained in 34% yield (calculated based on the amount of germole used); using two equivalents of diaminochlorophosphane, the diphosphanylgermole **111b** was obtained in a yield of 90%.



Scheme 66 – Reaction of diaminochlorophosphanes **108b** and **108c** with dipotassium germolediide **K₂[31]**.

For the mixed diphosphanylgermole **111b**, two sets of signals in the ratio 1 : 0.6 were recorded. As this compound exhibits two stereogenic centres (the P atoms), the two resonances were assigned to two different diastereomers: *RR* (Figure 78, left) and *RS* (Figure 78, right). Two sets of signals, fitting the integration of 1 : 0.6 were also observed in the ^1H and $^{29}\text{Si}\{^1\text{H}\}$ INEPT NMR spectra. The *RR*-isomer ($\delta^{31}\text{P} = 102.2$) features only one signal for each moiety. For the *RS*-isomer ($\delta^{31}\text{P} = 101.2$), two signals were detected for each moiety. The *RR*-isomer is the predominant one and also the one that was analysed by single crystal x-ray diffraction (Figure 80). Figure 78 displays the $^{31}\text{P}\{^1\text{H}\}$ and the $^{29}\text{Si}\{^1\text{H}\}$ INEPT NMR spectra of the two diastereomers. The results are reproducible and always give the same ratio of 1 : 0.6.

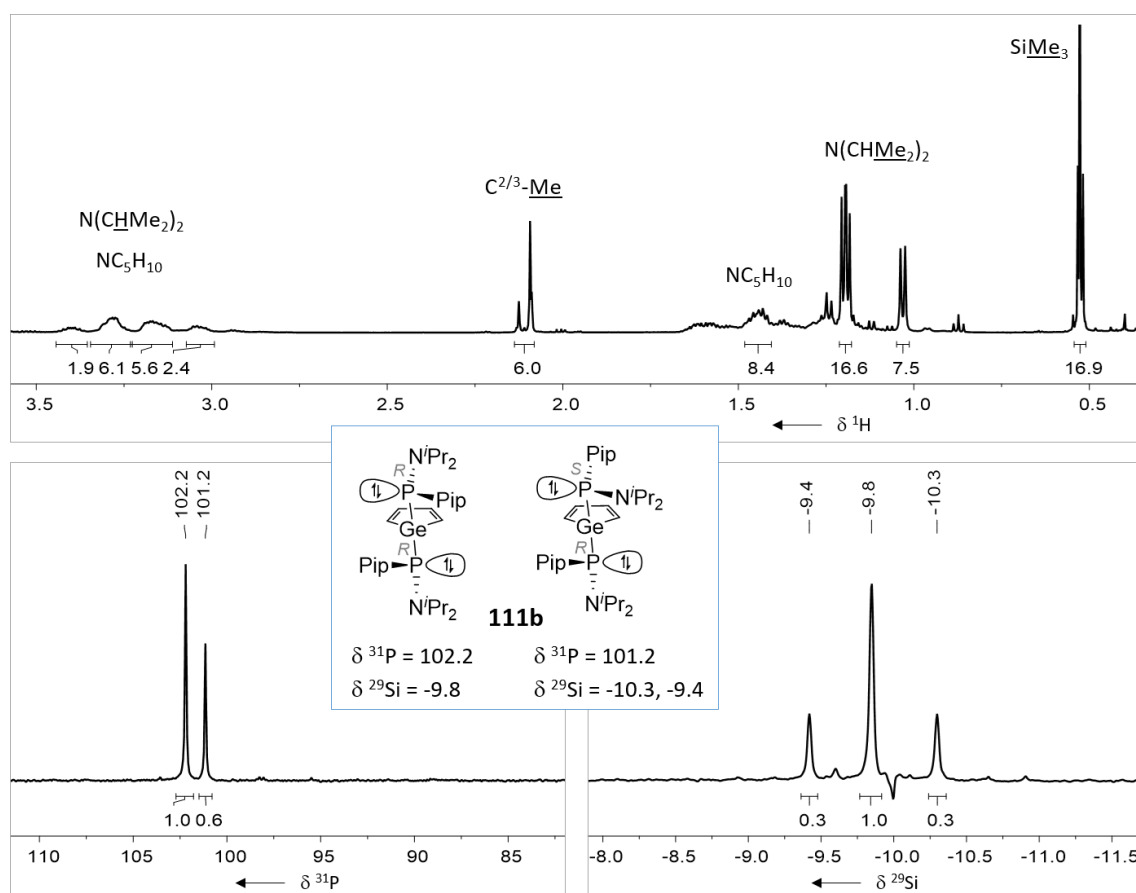
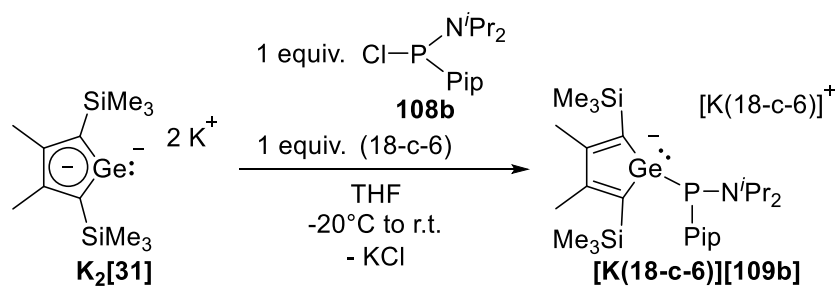


Figure 78 – ^1H NMR spectrum (500.1 MHz, 305 K, benzene- d_6), $^{31}\text{P}\{^1\text{H}\}$ NMR spectrum (202.3 MHz, 305 K, benzene- d_6) and $^{29}\text{Si}\{^1\text{H}\}$ INEPT NMR spectrum (99.3 MHz, 305 K, benzene- d_6) of the two diastereomers of the mixed diphosphanylgermole **111b**.

Though there was no evidence for the presence of the mixed potassium phosphanylgermole **K[109b]** found in the crude product NMR spectra, its isolation was achieved by immediate complexation of the potassium ion with crown ether (18-c-6). Therefore, the diamino phosphane **108b** and crown ether (18-c-6) were added simultaneously to the dipotassium germole diide **K₂[31]** solution (Scheme 67). The germole salt **[K(18-c-6)][109b]** was obtained as a red oily solid in 60% yield. The analogous reaction using dipiperidinophosphane **108c** was not carried out.



Scheme 67 – Synthesis of phosphanylgermole salt **[K(18-c-6)][109b]**.

Compared to the *bis*(diisopropylamino)phosphanylgermolide salt **[K(18-c-6)][Xa]** ($\delta^{31\text{P}} = 103.9$ in benzene- d_6 at room temperature), the $^{31\text{P}}$ NMR signal of the mixed aminophosphanylgermolide salt **[K(18-c-6)][Xb]** is shifted to lower field ($\Delta(\delta^{31\text{P}}) = 27.1$ ppm). An analogous lowfield shift was observed for the aminophospholes, comparing the diisopropylamino- **45b** and the piperidinophosphole **45d** ($\Delta(\delta^{31\text{P}}) = 26.6$ ppm; see Chapter 3.2.5). The $^{13\text{C}}$ NMR chemical shift of the backbone carbon atoms of the germolide salts **[K(18-c-6)][109a]** and **[K(18-c-6)][109b]** are very similar. A more detailed comparison of the NMR spectroscopic data is not indicated at this point, as the well resolved spectra were recorded in different solvents and at different temperatures. In both cases, however, the $\text{C}^{1/4}$ carbon atoms are shifted to lower field than the $\text{C}^{2/3}$ carbon atoms (Table 28).

Table 28 – Selected NMR spectroscopic data of the phosphanylgermolide salts **[K(18-c-6)][109a+b]** and the diphosphanylgermoles **111a-c**. Unless otherwise stated, spectra were recorded in benzene- d_6 at room temperature.

	$\delta^{13\text{C}}$		$\delta^{31\text{P}}$
	$\text{C}^{1/4}$ ($^2J_{\text{C,P}}$)	$\text{C}^{2/3}$ ($^3J_{\text{C,P}}$)	
Phosphanylgermolides			
[K(18-c-6)][109a]*	160.7 (d, 4 Hz) 164.1 (d, 25 Hz)	146.0 (d, 11 Hz) 148.4 (s)	93.2
[K(18-c-6)][109a]	161.4-161.8 (m) 163.4-164.0 (m)	147.7-148.2 (m) 150.0-150.5 (m)	103.9
[K(18-c-6)][109b]	164.4 (d, 9 Hz)	151.5 (d, 5 Hz)	131.0
Diphosphanylgermoles			
111a	146.2 (t, 8 Hz)	162.7 (t, 2 Hz)	111.3
111b	144.7-146.5 (m)	160.8-162.4 (m)	101.1, 102.2
111c	146.1 (t, 6 Hz)	160.7 (t, 2 Hz)	125.0

*Recorded in THF- d_8 at 193 K.

In comparison, the $^1\text{H}^{13\text{C}}$ HMBC NMR spectra of the three diphosphanylgermoles **111a-c** display the typical triangular pattern with the signals of the $\text{C}^{1/4}$ carbon atoms ($\delta^{13\text{C}} = 144$ -147) shifted to higher field than those of the $\text{C}^{2/3}$ carbon atoms ($\delta^{13\text{C}} = 160$ -163). Moreover, the chemical shift of the butadiene-carbon atoms $\text{C}^{1/4}$ and $\text{C}^{2/3}$, respectively, is very similar in all three compounds (Table 28). The $^{13\text{C}}$ NMR spectra are of higher order. The respective signals are pseudo triplet signals for the diphosphanylgermoles **111a** and **111c** (Figure 79). The resolution of the $^{13\text{C}}$ NMR spectrum of diphosphanylgermole **111b** is not good enough for a detailed analysis. Regarding the $^{31\text{P}}$ NMR resonances of the three compounds, no coherent trend was observed. The piperidino-diphosphagermole **111c** ($\delta^{31\text{P}} = 125.0$) is shifted to lower field

compared to the diisopropyl-diphosphanylgermole **111a** ($\delta^{31}\text{P} = 111.3$). The mixed amino-diphosphanylgermole **111b** ($\delta^{31}\text{P} = 101.1, 102.2$), however, is shifted to higher field. It is furthermore shifted to even higher field than its respective germolide salt **[K(18-c-6)][109b]** ($\delta^{31}\text{P} = 131.0$) (Table 28).

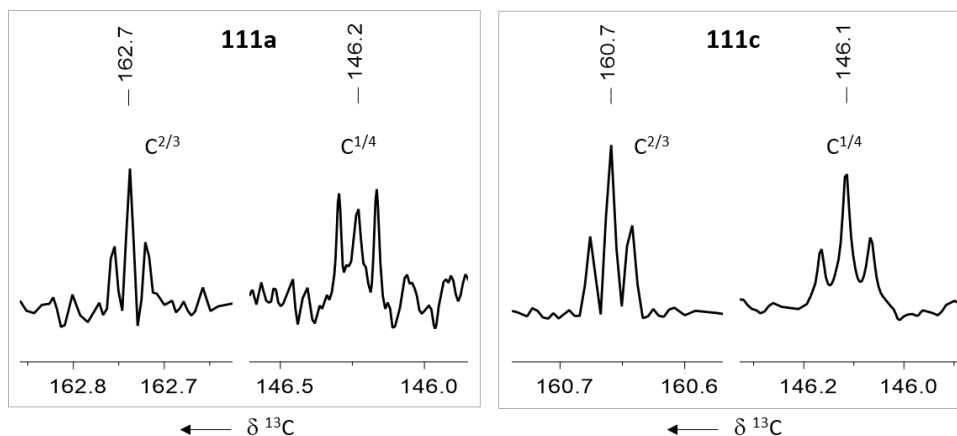


Figure 79 – Sections from the $^{13}\text{C}\{^1\text{H}\}$ NMR spectra (125.7 MHz, 305 K, benzene- d_6) of diphosphanylgermoles **111a** (left) and **111c** (right), showing the $\text{C}^{1/4}$ and $\text{C}^{2/3}$ signals.

The observed similarity of the NMR spectroscopic data of the germole backbone of the three diphosphanylgermoles **111a-c** also translates to their structural parameters. The molecular structures of all three diphosphanylgermoles **111a-c** are compared: The $\text{C}^{1/4}$ - $\text{C}^{2/3}$ bond lengths (135.6-136.0 pm) and the C^2 - C^3 bond lengths (149.6-149.9 pm) are similar in all three compounds with deviation between 0.1-0.4 pm. The Ge- $\text{C}^{1/4}$ bond lengths are slightly elongated in germole **111a** compared to germoles **111b+c** ($\Delta = 1.7/1.3$ pm). Still, all of the above named bond lengths are within the expected range.^[107] Larger differences were observed regarding the phosphorus moieties: The Ge-P bond lengths are similar in the germoles **111b** and **111c** ($\Delta = 1.7$ pm) but elongated by about $\Delta = 5$ pm in the germole **111a**. All Ge-P bond lengths are elongated compared to expected Ge-P single bond lengths (232 pm).^[108] Furthermore, the P-Ge-P bond angle is widest in germole **111a** (117.9°) and most acute in germole **111c** (104.7°). The order of both, the Ge-P bond lengths and the P-Ge-P bond angle, can be correlated to the decreasing sterical demand of the $\text{P}(\text{NR}_2)_2$ groups going from diisopropylamino to isopropylamino-piperidino to dipiperidino substitution. The P-N bonds are, independent from the amino-substituent (N^iPr_2 or Pip), slightly elongated by about 1 pm in germole **111b** (Table 29).

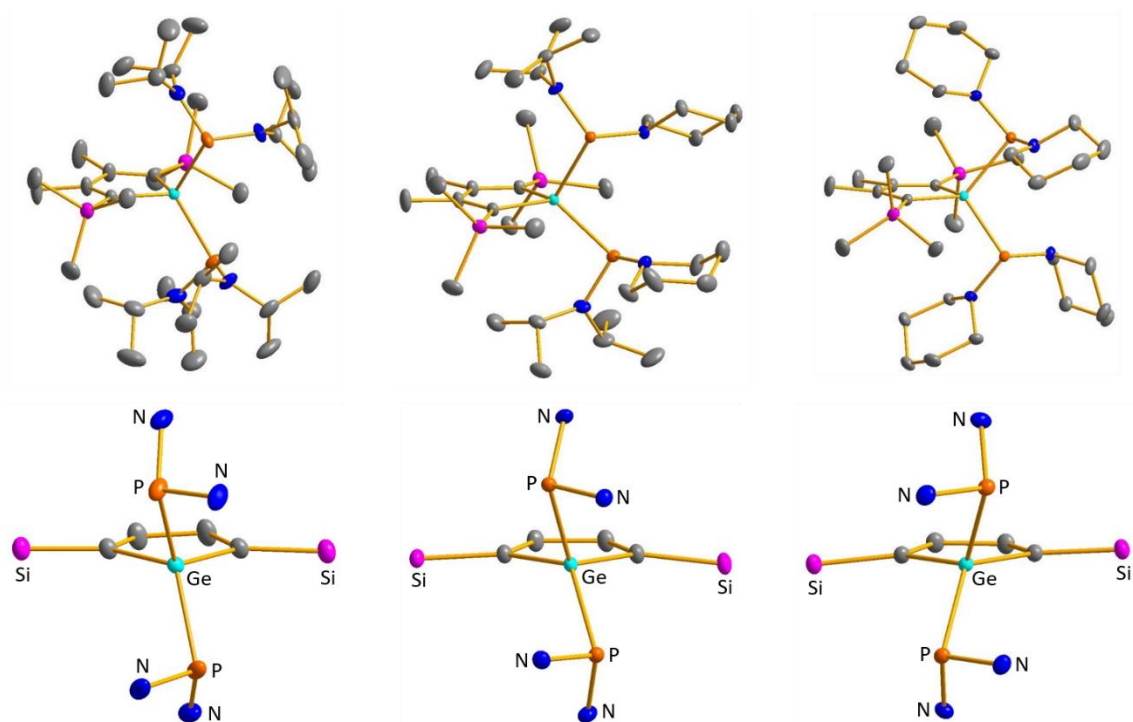


Figure 80 – Molecular structures of the diphosphanylgermole **111a** (left), **111b** *RR*-isomer (middle) and **111c** (right) in the crystal. Space group: $C2/c$ (**111a**), $P2_1/c$ (**111b**), $P2_1/n$ (**111c**). Thermal ellipsoids at 50% probability. Hydrogen atoms are omitted for clarity. In the lower row, the substituent-carbon atoms are omitted as well.

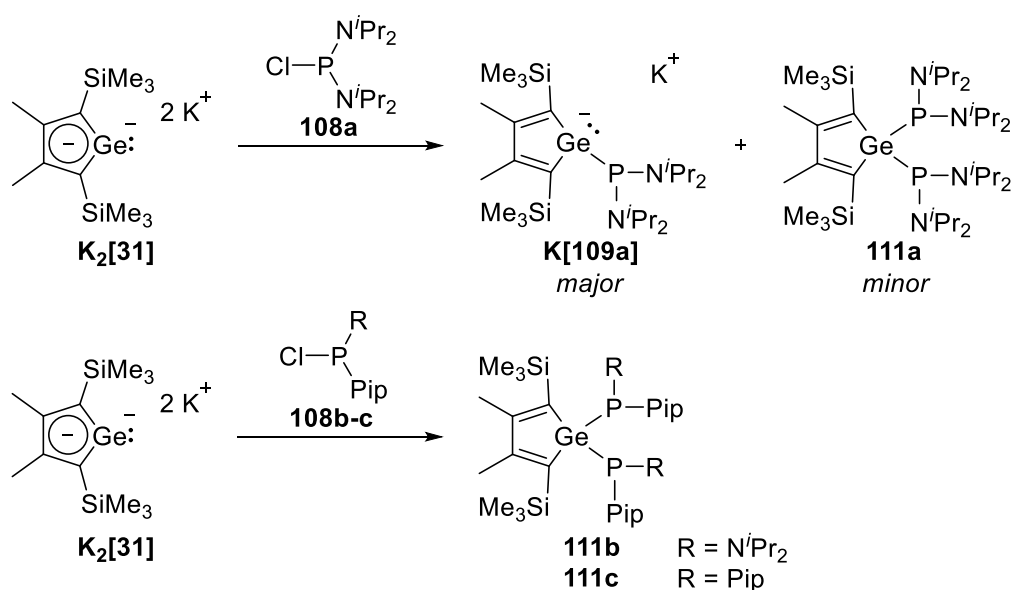
Table 29 – Selected bond lengths and angles of the three different diphosphanylgermole **111a-c**.

	111a	111b	111c
C^1-C^2 [pm]	135.63(17)	135.99(12)	136.03(9)
C^2-C^3 [pm]	149.63(23)	149.94(12)	149.79(8)
$Ge-C^1$ [pm]	198.61(12)	197.46(7)	197.60(8)
$Ge-P^1$ [pm]	240.22(4)	235.52(5)	234.00(7)
P^1-N^1/P^1-N^2 [pm]	169.75(15)	170.50(8)/171.26(9)	170.17(8)
$P-Ge-P$ [°]	117.963(12)	107.034(17)	104.792(13)

The structural differences noted regarding the $Ge-(P(NR_2)_2)_2$ moiety do not allow conclusions about the strikingly different ^{31}P NMR chemical shift of germole **111b** compared to the germole **111a+c**. However, the observed differences are in line with the observations and analyses made in the main part of this work (Chapters 3.2.5 – 3.2.7), corresponding to the steric properties of the amino substituents.

3.5.4 Short Summary: Chapter 3.5

Within this chapter, the synthesis of two phosphanylgermolide salts **[K(18-c-6)][109a+b]** and three diphosphanylgermoles **111a-c** was described. The compounds were analysed by NMR spectroscopy and single crystal x-ray diffraction, and were internally compared. Matching the observations made in the main part of this work, the stability of the intermediate product, the phosphanylgermolide, seems to be influenced by the steric properties of the amino substituent: more sterically demanding substituents favour the monosubstituted product, potassium phosphanylgermolide **K[109a]**, whereas introduction of less sterically demanding substituents favours the disubstituted product, diphosphanylgermole **111b+c** (Scheme 68). The initial goal, however, was not achieved: it was not possible to eliminate potassium amide from potassium phosphanylgermolide **K[109a]** to provide an alternative synthesis for phospho-BCH-germylene **43b**. Instead, upon heating of the germolide salt **K[109a]**, the Ge-P bond was broken and the corresponding tetraaminodiphosphane **113a** was obtained.

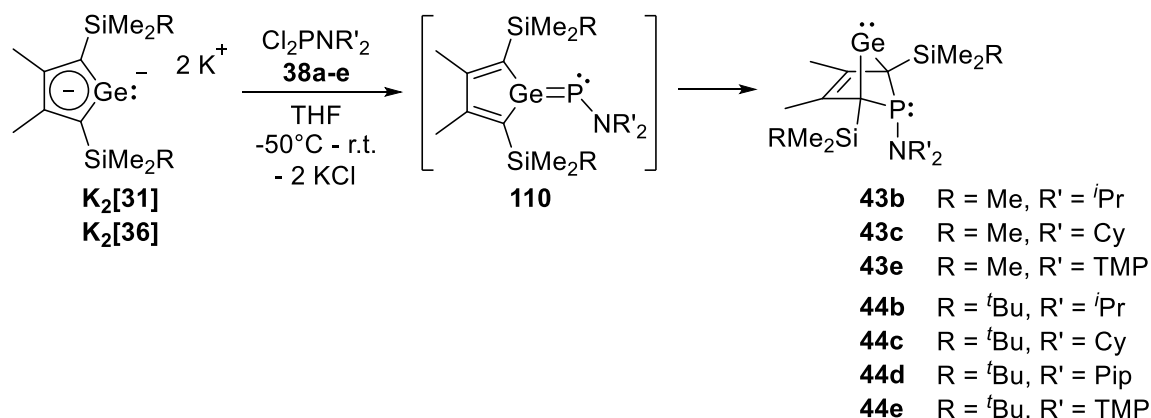


Scheme 68 – Summary of the reactions of dipotassium germolide **K₂[31]** towards the three different diaminophosphanes **108a-c**.

4 Summary & Outlook

Within this work, the reactivity of pnictogen dichlorides towards 2,5-bis(trialkylsilyl)-substituted tetrolediide salts was studied. With the idea of low-coordinated main group compound catalysed bond activation on hand, the main target was to synthesise new heavier alkene analogues and/or tetrylenes. As known from previous studies, dealing with related systems based on elements of the Groups 4 and 14, the respective heterofulvenes can selectively be obtained, however, it was shown that they are not stable at ambient temperature and rearrange to the more stable bicyclohexene (BCH) isomer. The latter, however, are tetrylenes, exhibiting orbitals generally suitable for bond activation reactions.

The major part of this work consist of studies on the reactivity of aminodichlorophosphanes **38a-e** towards dipotassium germolediide salts $K_2[31]$ ($R = Me$) and $K_2[36]$ ($R = tBu$). Though the corresponding aminophosphagermapentafulvenes **110** were not detected, the synthesis of aminophospha-BCH-germylenes **43-44** was optimised. The products were obtained alongside only one byproduct in good overall yields (>70%). Here, seven different aminophospha-BCH-germylenes **43b+c+e** and **44b-e** were introduced (Scheme 69).



Scheme 69 – Synthesis of aminophospha-BCH-germylenes **43b,c,e** and **44b-e**.

Using the diisopropylaminophospha-BCH-germylene **43b** as probe, this novel family of compounds was structurally characterised. Supported by detailed computational analysis (DFT), it was shown that aminophospha-BCH-germylenes **43-44** are, as their Group 4 and 14 relatives, stabilised by homoconjugation. The effect was furthermore found to be comparably strong (ΔE_{corr} (**43'**) = -102 kJ mol^{-1}) as in the related hafnocena-BCH-germylene **21** (ΔE_{corr} (**21'**) = -90 kJ mol^{-1}). Therefore, it was assumed that the germylene reactivity is dominated by nucleophilic properties (Figure 81).

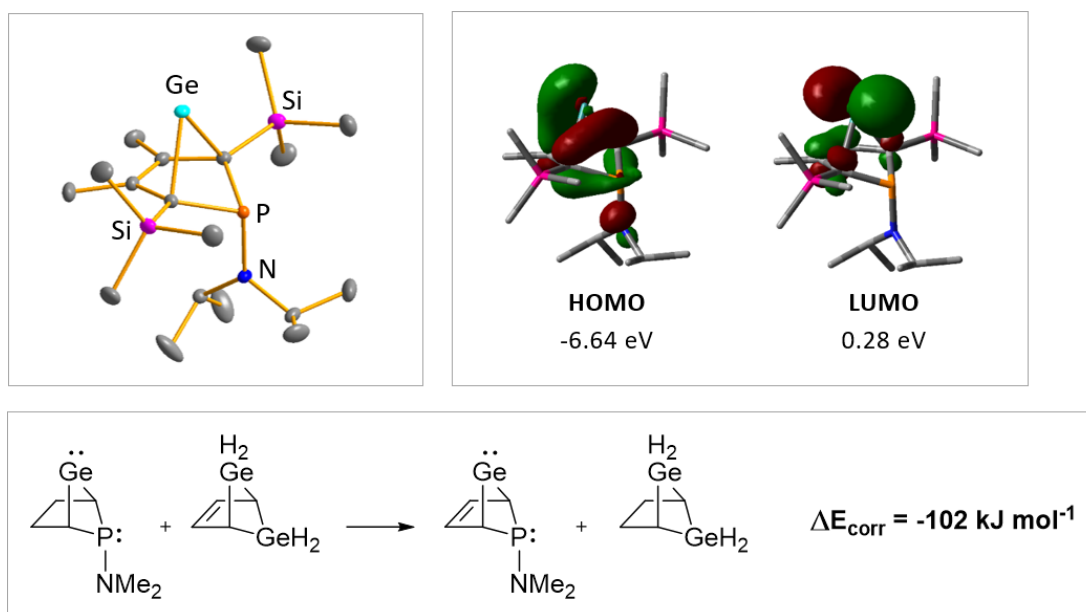
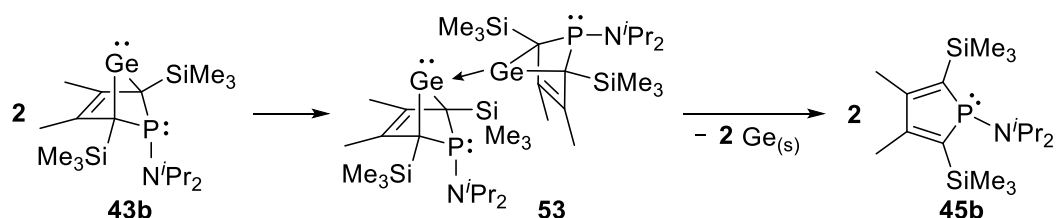


Figure 81 – Molecular structure and frontier molecular orbitals of germylene **43b** as representative for aminophospha-BCH-germylenes **43-44**, stabilised by homoconjugation.

However, it was shown that aminophospha-BCH-germylenes **43-44** exhibit unexpected reactivity. A key feature is the postulated bimolecular process for the elimination of germanium, which resulted in the formation of the corresponding aminophospholes **45**. The process, postulated to be initialised by nucleophilic attack of one germylene **43** on another. The concentration dependence of the reaction rate was demonstrated (Scheme 70). In agreement with general knowledge on stabilisation strategies for tetrylenes, it was shown that the stability of aminophospha-BCH-germylenes **43-44** depends on the sterical properties of the substituents. Here, the silyl groups in the 2,5-position of the germole and the amino substituent were identified as decisive factors. The *tert*butyldimethylsilyl substituted phospho-BCH-germylenes **44b-e** were stable in the solid state and in solution and did not undergo the elimination reaction.



Scheme 70 – Postulated bimolecular process for the elimination of germanium from germylene **43b**.

The postulated bimolecular process for the elimination of germanium underlines the amphiphilic character of the germylene. Experiments using other nucleophiles like NHCs,

support the postulated mechanism: The addition of small nucleophiles to phospho-BCH-germylene **44b** initiated the elimination of germanium. Despite the size of the nucleophile, its σ -donating strength was found to be a crucial factor for the initialisation. This allowed the conclusion that aminophospha-BCH-germylenes **44-45** are relatively strong σ -donors themselves. Overall, ten different aminophospholes **45a-e** and **46a-e** were detected (and characterised) within this work.

With the aminophospha-BCH-germylenes **44** (and **43**) on hand, their reactivity was studied. One of the main subjects was the cooperativity or competition of the two σ -donor sites, germanium and phosphorus. Examining the coordination properties towards different transition metal complexes, $\text{Ni}(\text{COD})_2$ (**102**), $\text{Ni}(\text{CO})_2(\text{PPh}_3)_2$ (**103**), $(\text{COD})\text{Pd}(\text{CH}_2\text{SiMe}_3)_2$ (**105**) and $(\text{Me}_2\text{S})\text{AuCl}$ (**106**), it was established that upon complex formation, decomposition of the transition metal complex and germanium elimination from the phospho-BCH-germylene **43-44** took place. However, using the dimeric rhodium(I) complex **98** allowed NMR spectroscopic insight into the coordination behaviour of the germylene: two short-lived complexes **100** and **101** were detected. Supported by DFT calculations ($\Delta E(\mathbf{100}' \text{ vs. } \mathbf{101}') = 9 \text{ kJ mol}^{-1}$), initial coordination via the phosphorus atom, followed by intramolecular shift to the germylene, which initiates the elimination of germanium, was postulated (Scheme 82). The final elimination reaction was attributed to electron donation into the vacant p-orbital (π -backdonation from the metal), similar to the nucleophile induced elimination reaction. It was additionally assumed, that simultaneous coordination (bidentate) of P and Ge is not possible due to the orientation of the respective orbitals.

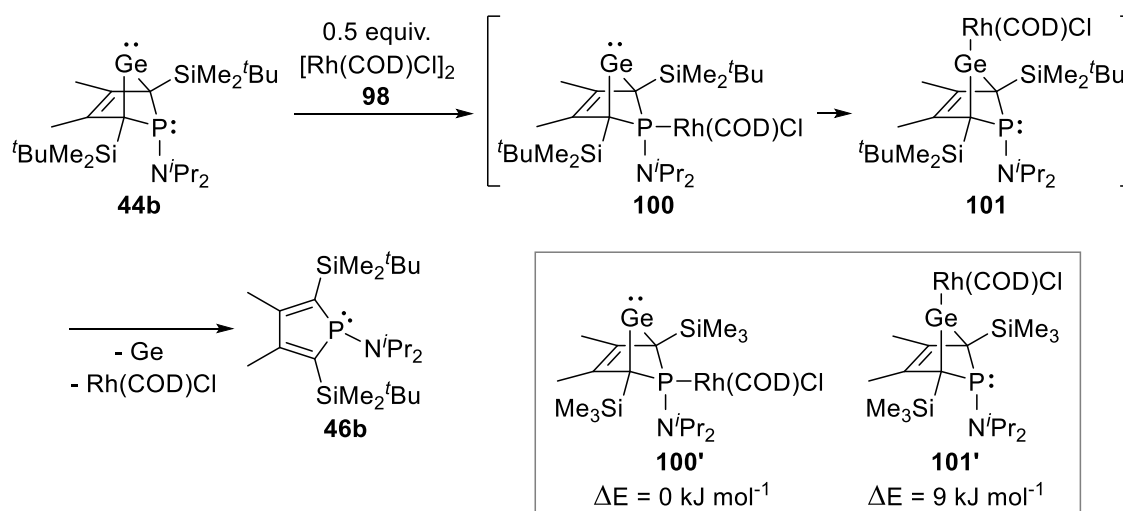
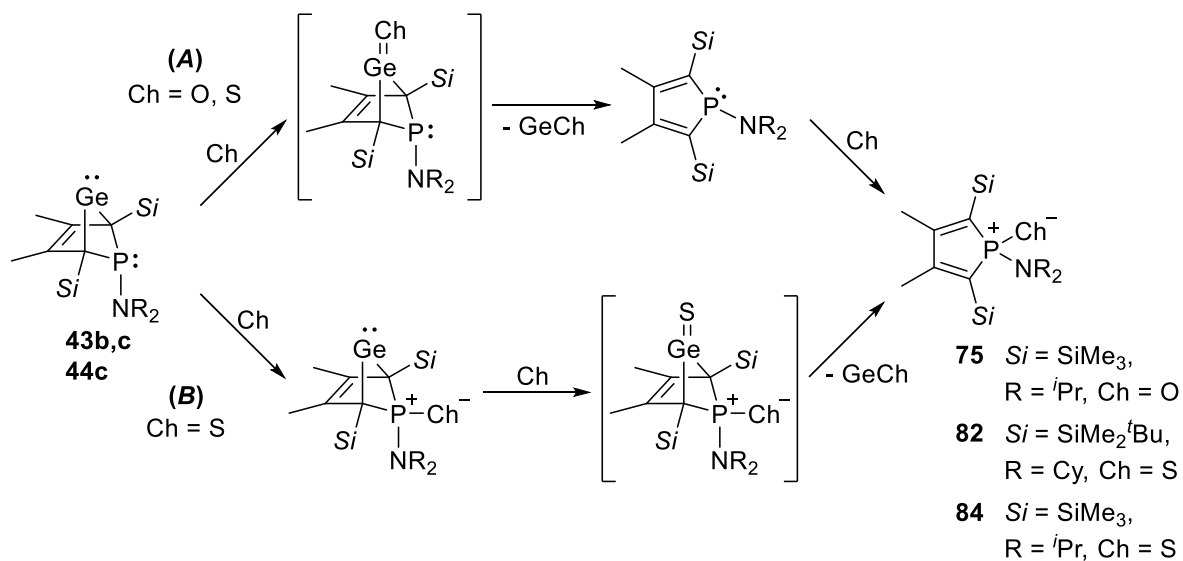


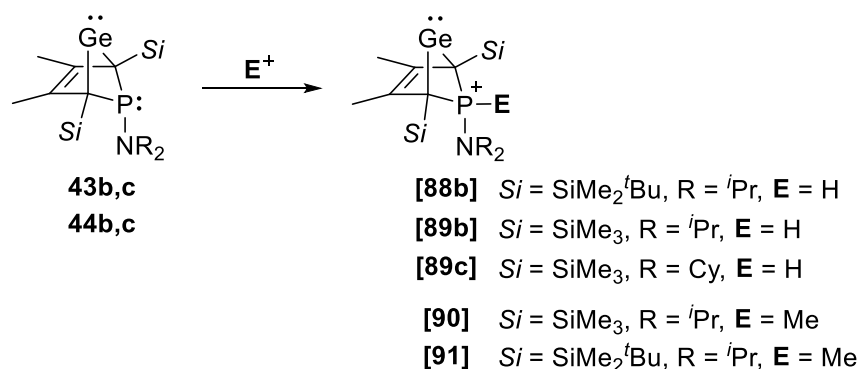
Figure 82 – Postulated reaction of aminophospha-BCH-germylenes **43-44** towards transition metal complexes, supported by DFT calculations, depicted for the reaction of germylene **44b** towards $[\text{ClRh}(\text{COD})]_2$ (**98**).

Treating aminophospha-BCH-germylenes **43b,c** and **44c** with elemental chalcogens, oxygen and sulfur, two-step reactions were observed. First, the germanium is oxidised and eliminated from the molecule. In the second step, the resulting phosphole is oxidised at the phosphorus atom. The phosphole oxide **75** and the phosphole sulphides **82** and **84** were characterised. Another, minor reaction path (**B**), leading to the same final product, was found for the reaction with sulfur: there, the phosphane is oxidised in a first step. The germylene is oxidised and eliminated from the germathione in the second step (Scheme 71).



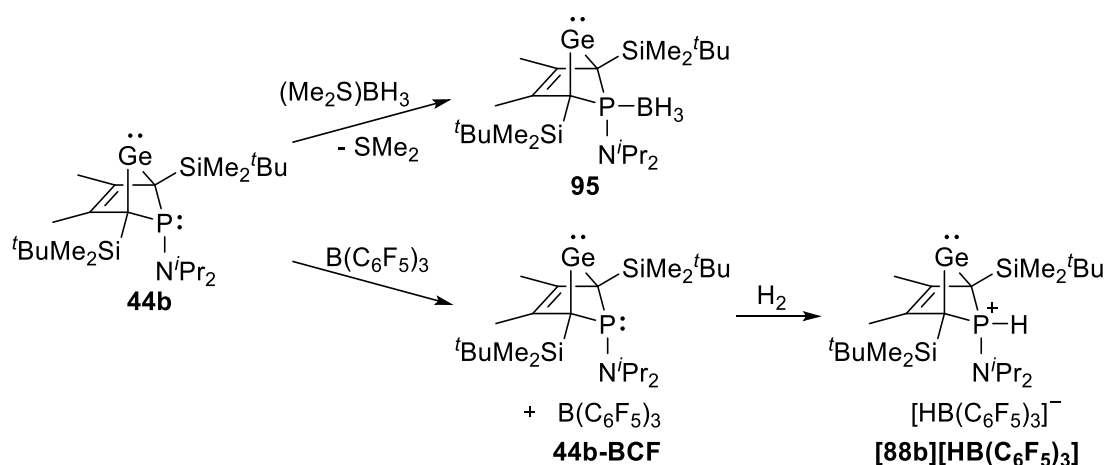
Scheme 71 – Reaction of aminophospha-BCH-germylenes **43b,c** and **44c** towards elemental chalcogens.

Aminophospha-BCH-germylenes **43b,c** and **44b** showed extraordinary reactivity towards small electrophiles. It was demonstrated that protonation as well as methylation occurred selectively at the phosphorus atom, giving the corresponding phosphonium ions **[88b]**, **[89b]**, **[98c]**, **[90]** and **[91]** (Scheme 72). This led to enhanced stability of the germylene as it effected energetic lowering of the frontier molecular orbitals. However, alongside the increased stability, the nucleophilicity of the germylene was lowered as well.



Scheme 72 – Reaction of aminophospha-BCH-germylenes **43b,c** and **44b** towards small electrophiles, giving salts of phosphonium-BCH-germylenes **[88b]**, **[89b]**, **[89c]**, **[90]** and **[91]**.

Finally, it was shown that germylene **44b** forms a classical Lewis acid-base adduct **95** with the small Lewis acid BH_3 , and a frustrated Lewis pair **44b-BCF** with the sterically demanding Lewis acid BCF. The FLP **44b-BCF** was shown to, presumably heterolytically, cleave dihydrogen (Scheme 73).



Scheme 73 – Reactivity of aminophospha-BCH-germylene **44b** towards selected Lewis acids.

In general, deep understanding of the structure and properties of aminophospha-BCH-germylenes **43-44** was gained. This novel family of compounds exhibits some interesting and unexpected features. Furthermore, the knowledge gained on the germanium elimination process might be transferred to related systems (e.g. sila-BCH-germylenes) and enable their isolation and studies.

Other pnicta-BCH-tetrylenes ($E = Si, Ge$; $Pn = As, Sb$) were not accessible within this work. However, the reaction of germolediide salt K_2 [**36**] towards aryldichlorophosphanes **39a-b** was found to be especially interesting. Using mesitylphosphane **39a** resulted in the highly selective

formation of the dimerisation product of two phosphagermapentafulvenes **57a**. The compound, containing a four-membered Ge-P-Ge-P ring **58a** (Figure 83), was obtained with some minor impurities in a yield of 95%. It was shown, that the formation of this kind of product again depends on the sterical properties of the germole as well as of the aryl substituent. Therefore, this field offers potential for further studies, varying the substituents, potentially enabling the isolation of other fulvene dimers or even the initially targeted phosphagermapentafulvenes. Additionally, trapping reactions could be performed.

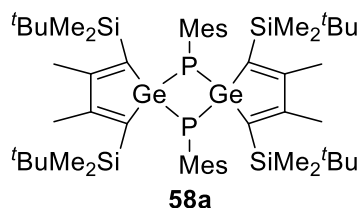
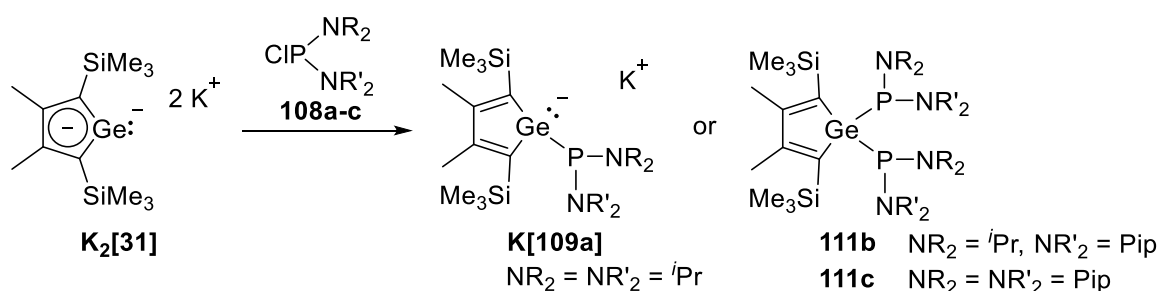


Figure 83 – Obtained aryl-substituted phosphagermapentafulvene dimer **58a**.

In another project, the synthesis of phosphagermapentafulvenes **110**, in two separated steps, was attempted. It was shown here, that the first step, the formation of phosphanylgermolide salts **K[109]**, can be performed. However, the success depends on the sterical properties of the amino substituents: using less crowded diaminephosphanes **108b+c**, bis(diaminophosphanyl)germoles **111b+c** were obtained instead of the mono-substituted products (Scheme 74). Though the second step, the elimination of potassiumamide, did not proceed as planned, the synthesis and characterisation of two phosphanylgermolide salts **[K(18-c-6)][109a+b]** was described. In further studies, the (donor) properties of these compounds, isolobal to phosphanes, could be examined.



Scheme 74 – Synthesis of phosphanylgermolide salt **K[109a]** and diphosphanylgermoles **111b+c**.

5 Experimental Part

5.1 Operational Methods and Tools

All operations were carried out under inert atmosphere using an MBraun glovebox filled with nitrogen and standard Schlenk technique. Glassware was stored in an oven at 160°C. It was evacuated and flushed with argon before use. Argon was run through a column filled with phosphorouspentoxide as drying agent.

THF, diethyl ether, *n*-hexane and *n*-pentane were dried over sodium-potassium alloy. Benzene, benzene-d₆, toluene, toluene-d₈ and tetrahydrofuran-d₈ were dried over sodium. Chlorobenzene and *ortho*-difluorobenzene were dried over calcium chloride. All solvents were distilled prior to use and stored over molecular sieve (4Å). Chlorobenzene-d₅, chloroform-d₃ and dichloromethane-d₂ were dried and stored over molecular sieve (4Å).

SbCl₃ and GaCl₃ were purified by sublimation prior to use. PCl₃ was distilled prior to use. Methyl triflate was stored over molecular sieve (4Å). Dichloro(phenyl)arsine **40a** and dichloro(*para*-dimethylaminophenyl)arsine **40b** were kindly send to us by the Orthaber group from Uppsala University, Sweden.^[100] Tris(pentafluorophenyl)borane (BCF), silole dichloride **28** and dichloro(dicyclohexylamino)phosphane (**38c**) were already available in the working group. All other chemicals are commercially available and were used without purification.

NMR Spectroscopy

Nuclear magnetic resonance (NMR) spectra were recorded on a *Bruker Avance III RMN 1Bay* spectrometer (500 MHz), a *Bruker Avance DRX* spectrometer (500 MHz), a *Bruker Avance III WB500* spectrometer (500 MHz), a *JEOL JNM-ECZL* (500 MHz) and a *Bruker Furier 300* spectrometer (300 MHz). Chemical shifts δ are given in ppm relative to tetramethylsilane as standard. Coupling constants *J* are given in Hertz. ¹H NMR spectra were referenced internally using the residual proton signal of the deuterated solvent. ¹³C{¹H} NMR spectra were also referenced internally using the central line of the solvent signal (Table 30). In case of more than one solvent signal, the most low-field shifted one was used for referencing. The spectra of all other nuclei were referenced to external standards which are given in Table 31.

Table 30 – Chemical shifts of the deuterated solvents (residual proton signals).

solvent	δ ¹ H		δ ¹³ C
toluene-d ₈	7.09	(C ₆ D ₃ H(CD ₃))	137.5
tetrahydrofuran-d ₈	3.58	(C ₄ D ₇ H _O)	67.2
benzene-d ₆	7.16	(C ₆ D ₅ H)	128.1
chlorobenzene-d ₅	7.14	(C ₆ D ₄ HCl)	134.2
chloroform-d ₃	7.26	(CHCl ₃)	77.2
dichloromethane-d ₂	5.35	(CDHCl ₂)	53.8
D ₂ O capillary	4.79	(HDO)	–

Table 31 – External NMR standards.

nucleus	δ	external standard
¹¹ B	0.0	BF ₃ ·Et ₂ O
¹⁹ F	0.0	CFCl ₃
²⁹ Si	11.1	Me ₂ SiHCl
³¹ P	0.0	H ₃ PO ₄ (85% in D ₂ O)
⁷¹ Ga	0.0	Ga(NO ₃) ₃ in C ₆ D ₆
⁷⁷ Se	0.0	SeMe ₂

Additional to the one-dimensional experiments shown above, the following two-dimensional NMR spectra were recorded to precisely assign all compound signals: ¹H¹³C HMQC, ¹H¹³C HMBC and ¹H³¹P HMBC. Furthermore, ²⁹Si{¹H} INEPT experiments were performed using the parameters d3 = 0.0068 s and d4 = 0.0313 s. The multiplicity of NMR signals was entitled as follows: s (singlet), d (doublet), t (triplet), q (quartet), sept (septet), dt (doublet of triplets) and dsept (doublet of septets).

Single Crystal X-Ray Diffraction

Single crystal X-ray diffraction analyses were carried out on a *Bruker AXS D8 Venture* diffractometer with Mo K α and Cu K α radiation, and a *Photon III CPAD* detector or on a *Bruker AXS Apex II CCD* diffractometer with Mo K α radiation and a *Bruker Apex II CCD* detector. Molecular structures were resolved and refined using *SHELXL-97*. For visualisation, *Diamond 4.0* was used.

Gas Chromatography-Mass Spectrometry

GC-MS spectra were recorded on an *Agilent GC 7890B* with a HP 5 MS ultra inert GC column and an *Agilent 5977B GC/MSD* detector.

UV/Vis Spectroscopy

UV/Vis spectra were recorded on a *SPECORD 200 PC* double-beam photometer from *Analytik Jena* with a wavelength range from 190-1100 nm.

High Resolution Mass Spectrometry

High resolution mass spectra (HR-MS) were recorded on a *Finnigan-LCG* or *Finnigan-MAT95* spectrometer.

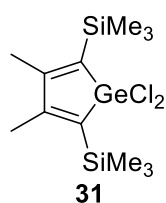
5.2 Experimental Procedures

5.2.1 Gerroles

5.2.1.1 1,1-Dichloro-2,5-bis(trimethylsilyl)-3,4-dimethylgermole (31)

Germole **31** was prepared following a literature known procedure.^[59]

Zirconocene dichloride (10.3 mmol, 3.00 g) was suspended in pentane (80 mL) and cooled to -90°C. *n*-Butyllithium (21.6 mmol, 13.5 mL) was added dropwise. The reaction mixture was stirred for one hour while it was kept at -90°C. Silylpropyne (21.6 mmol, 2.42 g), dissolved in pentane (5 mL), was then added dropwise at that temperature. It was stirred overnight and the mixture was allowed to warm to room temperature. For the element exchange reaction, first, THF (10 mL) was added and then germanium tetrachloride (10.3 mmol, 2.20 g) was slowly added at 0°C. The reaction mixture was kept at that temperature for one hour and was afterwards allowed to warm to room temperature overnight. The solvent was removed under reduced pressure. The residue was redissolved in pentane (50 mL) and filtered over a P4 frit to recover zirconocenedichloride. The solution was then filtered over silica. The solvent of the filtrate was removed under reduced pressure. Recrystallisation from pentane at -10°C yielded germole **31** (6.6 mmol, 2.44 g, 65%, Lit.: 79%^[59]) as colourless crystals. The NMR spectroscopic data matches the literature.^[59]



$^1\text{H NMR}$ (500.1 MHz, 305 K, C_6D_6) δ = 0.31 (s, 18H, 2 x SiMe_3), 1.65 (s, 6H, 2 x $\text{C}^{2/3}\text{-Me}$).

$^{13}\text{C}\{^1\text{H}\}$ NMR (125.7 MHz, 305 K, C_6D_6) δ = 0.2 (SiMe_3), 19.4 ($\text{C}^{2/3}\text{-Me}$), 132.9 ($\text{C}^{1/4}$), 160.9 ($\text{C}^{2/3}$).

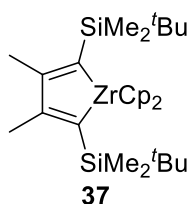
$^{29}\text{Si}\{^1\text{H}\}$ INEPT NMR (99.3 MHz, 305 K, C_6D_6) δ = -7.7.

5.2.1.2 2,5-Bis(*tert*-butyldimethylsilyl)-1,1-dichloro-3,4-dimethylgermole (**36**)

Germole **36** was prepared in a two-step reaction following literature known procedures.^[59, 75, 85]

The yield was significantly enhanced by improving the workup.

For the first step, zirconocenedichloride (17.8 mmol, 5.21 g) was suspended in pentane (150 mL) and cooled to -90°C . *n*-Butyllithium (37.4 mmol, 23.4 mL) was added dropwise. The reaction mixture was stirred for one hour while it was kept at -90°C . Silylpropyne (35.6 mmol, 5.50 g), dissolved in pentane (10 mL), was then added dropwise at that temperature. It was stirred overnight and the mixture was allowed to warm to room temperature. After filtration over a P4 frit, the solvent was removed under reduced pressure to give the zirconacyclopentadiene **37** (15.9 mmol, 8.44 g, 89%) as a red-brown solid.



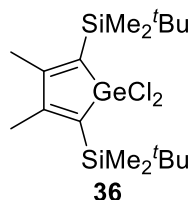
$^1\text{H NMR}$ (500.1 MHz, 305 K, C_6D_6): δ = 0.13 (s, 12H, 2 x SiMe_2^tBu), 1.10 (s, 18H, 2 x SiMe_2^tBu), 1.87 (s, 6H, 2 x $\text{C}^{2/3}\text{-Me}$), 5.97 (s, 10H, 2 x Cp).

$^{13}\text{C}\{^1\text{H}\}$ NMR (125.7 MHz, 305 K, C_6D_6) δ = -0.19 (SiMe_2^tBu), 19.0 (SiMe_2^tBu , C^4), 29.0 ($\text{C}^{2/3}\text{-Me}$), 29.2 (SiMe_2^tBu), 142.7 ($\text{C}^{2/3}$), 198.3 ($\text{C}^{1/4}$).

$^{29}\text{Si}\{^1\text{H}\}$ INEPT NMR (99.3 MHz, 305 K, C_6D_6): δ = -8.2.

For the second step, the element exchange reaction, zirconacycle **37** (1.50 g, 2.84 mmol) was dissolved in 50 mL THF and the solution was cooled to 0°C . Germaniumtetrachloride (0.61 g, 2.84 mmol) was slowly added via syringe. The reaction mixture was stirred for 1h at 0°C , followed by stirring at room temperature for several days. A few drops of water were added before the solvent was removed under reduced pressure. The residue was redissolved in pentane/diethyl ether (1:1) and filtered over a P4 frit to recover the zirconocenedichloride. The

solution was then filtered over silica gel. Removal of the solvent yielded the germole **36** (83% crude product) as a slightly yellow solid. Recrystallisation from pentane yielded the purified germole **36** (0.84 g, 1.86 mmol, 65%, Lit.: 18%^[59]) as colourless solid. The NMR spectroscopic data matches the literature.^[59]



¹H NMR (500.1 MHz, 305 K, C₆D₆) δ = 0.36 (s, 12H, 2 x SiMe₂tBu), 0.96 (s, 18H, 2 x SiMe₂tBu), 1.82 (s, 6H, 2 x C^{2/3}-Me).

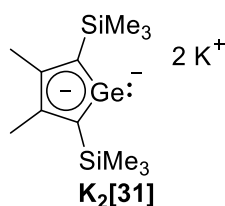
¹³C{¹H} NMR (125.7 MHz, 305 K, C₆D₆) δ = -3.2 (SiMe₂tBu), 19.1 (SiMe₂tBu, C⁴), 21.3 (C^{2/3}-Me), 27.6 (SiMe₂tBu), 132.2 (C^{1/4}), 161.7 (C^{2/3}).

²⁹Si{¹H} INEPT NMR (99.3 MHz, 305 K, C₆D₆) δ = 0.4.

5.2.1.3 Dipotassium Germolediides

A vial was equipped with dichlorogermole **31** or **36** (74 mg / 90 mg, 0.20 mmol) and potassium (2.00 mmol, 78 mg). THF (5 mL) was added and the suspension was stirred overnight. The solution was transferred into a Schlenk flask and was immediately used, as the compound is not suitable for storage. The NMR spectroscopic data given below matches the literature.^[59]

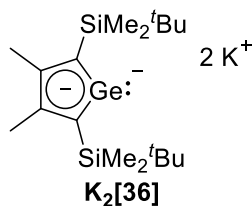
Dipotassium 2,5-bis(trimethylsilyl)-3,4-dimethylgermolediide (K₂[**31**])



¹H NMR (500.1 MHz, 305 K, THF/D₂O capillary) δ = 0.55 (s, 18H, 2 x SiMe₃), 2.66 (s, 6H, 2 x C^{2/3}-Me).

¹³C{¹H} NMR (125.7 MHz, 305 K, THF/D₂O capillary) δ = 4.8 (SiMe₃), 20.9 (C^{2/3}-Me), 130.9 (C^{2/3}), 156.1 (C^{1/4}).

²⁹Si{¹H} INEPT NMR (99.3 MHz, 305 K, THF/D₂O capillary) δ = -15.9.

Dipotassium 2,5-bis(*tert*-butyldimethylsilyl)-3,4-dimethylgermolediide (K₂[36])

¹H NMR (500.1 MHz, 305 K, THF/D₂O capillary) δ = 0.15 (s, 12H, 2 x SiMe₂tBu), 0.95 (s, 18H, 2 x SiMe₂tBu), 2.21 (s, 6H, 2 x C^{2/3}-Me).

¹³C{¹H} NMR (125.7 MHz, 305 K, THF/D₂O capillary) δ = 0.6 (SiMe₂tBu), 18.1 (SiMe₂tBu, C⁴), 22.2 (C^{2/3}-Me), 28.9 (SiMe₂tBu), 130.1 (C^{2/3}), 151.4 (C^{1/4}).

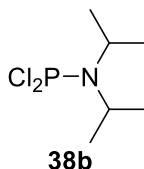
²⁹Si{¹H} INEPT NMR (99.3 MHz, 305 K, THF/D₂O capillary) δ = -5.9.

5.2.2 Aminodichlorophosphanes

The preparation of aminodichlorophosphanes **38** is well described in the literature.^[88-89] However, smaller changes regarding the solvent and the reaction time were made within this work. The procedures used are given below.

5.2.2.1 Dichloro(*diisopropylamino*)phosphane (38b)

A dropping funnel was loaded with pentane (20 mL) and *diisopropylamine* (2.04 g, 20.00 mmol). Afterwards, pentane (100 mL) and trichlorophosphane (1.37 g, 10.00 mmol) were added to a two-neck Schlenk flask which was then cooled to 0°C. The amine solution was slowly added. After 2 hours the ice bath was removed. A colourless precipitate was formed. The suspension was stirred overnight at room temperature before it was filtered over a glass frit. Removal of the solvent yielded dichloro(*diisopropylamino*)phosphane **38b** (1.57 g, 7.75 mmol, 78%, Lit.: 68%^[89]) as a light yellow oil. No further purification was needed. The NMR spectroscopic data is in good agreement with the literature.^[169]



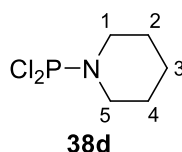
¹H NMR (500.1 MHz, 305 K, C₆D₆): δ = 0.96 (d, ³J_{H,H} = 6.9 Hz, 12H, N(CHMe₂)₂), 3.62 (m, 2H, N(CHMe₂)₂).

¹³C{¹H} NMR (125.7 MHz, 305 K, C₆D₆): δ = 23.2 (d, ³J_{C,P} = 8 Hz, N(CHMe₂)₂), 48.3 (d, ²J_{C,P} = 14 Hz, N(CHMe₂)₂).

³¹P{¹H} NMR (202.4 MHz, 305 K, C₆D₆): δ = 169.0.

5.2.2.2 Dichloro(piperidino)phosphane (38d)

A dropping funnel was loaded with pentane (70 mL) and piperidine (5.96 g, 70.00 mmol). Afterwards, pentane (100 mL) and trichlorophosphane (4.81 g, 35.00 mmol) were added to a two-neck Schlenk flask which was then cooled to 0°C. The piperidine solution was slowly added. After 30 minutes the ice bath was removed. A colourless precipitate was formed. The suspension was stirred overnight at room temperature before it was filtered over a glass frit. Removal of the solvent yielded Dichloro(piperidino)phosphane **38d** (5.35 g, 28.76 mmol, 82%, Lit.: 62%^[89]) as a colourless oil. No further purification was needed. The ³¹P NMR spectroscopic data matches the literature.^[89]



¹H NMR (500.1 MHz, 305 K, C₆D₆): δ = 1.06-1.16 (m, 6H, C^{2/3/4}-H), 2.82-2.90 (m, 4H, C^{1/5}-H).

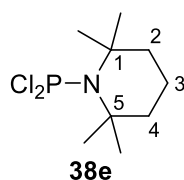
¹³C{¹H} NMR (125.7 MHz, 305 K, C₆D₆): δ = 24.0 (C³), 26.3 (d, ³J_{C,P} = 5 Hz, C^{2/4}), 47.4 (d, ²J_{C,P} = 20 Hz, C^{1/5}).

³¹P{¹H} NMR (202.4 MHz, 305 K, C₆D₆): δ = 157.2.

5.2.2.3 Dichloro(2,2,6,6-tetramethylpiperidino)phosphane (38e)

Deviating from the literature, dichloro(2,2,6,6-tetramethylpiperidino)phosphane was synthesised in a two-step reaction via the lithium amide.^[89, 91]

2,2,6,6-Tetramethylpiperidine (2.12 g, 15.00 mmol) was dissolved in THF (25 mL) and cooled to 0°C. *n*-Butyllithium (9.4 mL, 15.00 mmol) was added dropwise and the resulting solution stirred for 30 minutes. Afterwards, trichlorophosphane (6.20 g, 45.10 mmol) was added and the solution was stirred for one hour. The ice bath was removed and the mixture was stirred overnight. After filtration over a glass frit, the solvent was removed. The residue was redissolved in pentane and filtered over a glass frit. Removal of the solvent yielded dichloro(2,2,6,6-tetramethylpiperidino)phosphane **38e** (3.20 g, 13.20 mmol, 88%, Lit.: 90%^[89]) as orange-brown solid.



$^1\text{H NMR}$ (500.1 MHz, 305 K, C_6D_6): $\delta = 1.16\text{-}1.26$ (m, 6H, $\text{C}^{2/3/4}\text{-H}$), 1.42 (br s, 12H, 4 x Me).

$^{13}\text{C}\{^1\text{H}\}$ NMR (125.7 MHz, 305 K, C_6D_6): $\delta = 16.5$ ($\underline{\text{C}}^3$), 31.8 (br m, 4 x Me), 41.1 ($\underline{\text{C}}^{2/4}$), 61.7 (m, $\underline{\text{C}}^{1/5}$).

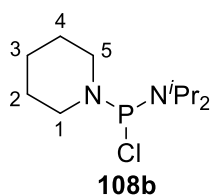
$^{31}\text{P}\{^1\text{H}\}$ NMR (202.4 MHz, 305 K, C_6D_6): $\delta = 163.2$.

5.2.3 Diaminochlorophosphanes

5.2.3.1 Chloro(diisopropylamino)(piperidino)phosphane (108b)

Chloro(diisopropylamino)(piperidino)phosphane (**108b**) was synthesised according to a procedure described by Niecke *et al.* for a similar unsymmetrically substituted diaminophosphane.^[164]

Dichloro(piperidino)phosphane (**38d**) (5.35 g, 28.76 mmol) and triethylamine (3.20 g, 31.64 mmol) were dissolved in diethyl ether (80 mL) in a two-neck Schlenk flask. In a dropping funnel, diisopropylamine (2.91 g, 28.76 mmol) was dissolved in diethyl ether (20 mL). The amine solution was slowly added to the flask at 0°C. After complete addition, the ice bath was removed and the reaction mixture stirred at room temperature for three days. It was filtered over a glass frit. The solvent was removed under reduced pressure to afford chloro(diisopropylamino)(piperidino)phosphane (**108b**) (7.20 g, 28.71 mmol, 100%) as a yellow oil without further purification.



$^1\text{H NMR}$ (499.9 MHz, 305 K, C_6D_6): $\delta = 1.04$ (d, $^4J_{\text{H,P}} = 6.7$ Hz, 6H, $\text{N}(\text{CHMe}_2)_2$), 1.23 (d, $^4J_{\text{H,P}} = 6.7$ Hz, 6H, $\text{N}(\text{CHMe}_2)_2$), 1.26-1.37 (m, 6H, NC_5H_{10}), 2.88-2.95 (m, 2H, NC_5H_{10}), 2.96-3.05 (m, 2H, NC_5H_{10}), 3.47-3.58 (m, 2H, $\text{N}(\text{CHMe}_2)_2$).

$^{13}\text{C}\{^1\text{H}\}$ NMR (125.7 MHz, 305 K, C_6D_6): $\delta = 23.1$ (d, $^3J_{\text{C,P}} = 12$ Hz, $\text{N}(\text{CHMe}_2)_2$), 24.4 (d, $J_{\text{C,P}} = 5$ Hz, NC_5H_{10}), 24.9 (NC_5H_{10} , $\underline{\text{C}}^3$), 26.7 (d, $J_{\text{C,P}} = 9$ Hz, NC_5H_{10} , $\underline{\text{C}}^{2/4}$), 47.2-47.6 (m, $\text{N}(\text{CHMe}_2)_2$, NC_5H_{10} , $\underline{\text{C}}^{1/5}$).

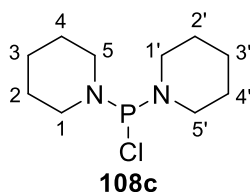
$^{31}\text{P}\{^1\text{H}\}$ NMR (202.4 MHz, 305 K, C_6D_6): $\delta = 145.3$.

5.2.3.2 Chloro(dipiperidino)phosphane (**108c**)

Chlorodipiperidinophosphane (**108c**) was prepared in a two-step reaction following literature known procedures.^[165-166]

Phosphorus trichloride (17.2 mmol, 1.5 mL) and triethylamine (86.2 mmol, 12.5 mL) were diluted in diethyl ether (100 mL). The solution was cooled to 0°C in an ice bath and piperidine (51.6 mmol, 5.1 mL) was slowly added via a syringe. Afterwards, the suspension was allowed to warm up to room temperature and was stirred overnight. After filtration over a P4 frit, the solvent was removed under reduced pressure to yield tripiperidinophosphane (**112**) (15.1 mmol, 4.29 g, 88%, Lit.: 76%^[165]) as a slightly yellow oil, that solidified after two days.

The tripiperidinophosphane (**112**) was then dissolved in diethyl ether (50 mL) and cooled to 0°C in an ice bath. Phosphorus trichloride (7.5 mmol, 0.7 mL) was added dropwise. After addition, the solution was heated to reflux for two hours and then stirred overnight at room temperature. The suspension was filtered over a P4 frit. The solvent was removed under reduced pressure and the oily yellow residue was distilled ($1 \cdot 10^{-3}$ mbar, 90°C) to give chloro(dipiperidino)phosphane (**108c**) (11.9 mmol, 2.80 g, 53%, Lit.: 75%^[166]) as colourless oil. The NMR spectroscopic data is in good agreement with the literature.^[166]



¹H NMR (499.9 MHz, 305 K, C₆D₆): δ = 1.05–1.20 (m, 12H, C^{2/3/4}-H), 2.66–2.84 (m, 8H, C^{1/5}-H).

¹³C{¹H} NMR (125.7 MHz, 305 K, C₆D₆): δ = 24.7 (C³), 26.6 (d, ³J_{C,P} = 7 Hz, C^{2/4}), 47.9 (d, ²J_{C,P} = 15 Hz, C^{5/5}).

³¹P{¹H} NMR (202.4 MHz, 305 K, C₆D₆): δ = 150.0.

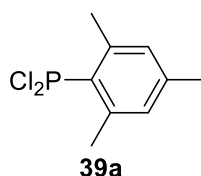
5.2.4 Aryldichlorophosphanes

5.2.4.1 Dichloro(mesityl)phosphane (**39a**)

Dichloromesitylphosphane (**39a**) was prepared according to literature procedures.^[97-98]

A THF solution (30 mL) of mesityl Grignard was prepared from bromomesitylene (4.98 g, 25.00 mmol) and magnesium turnings (0.63 g, 26.00 mmol). The solution was stirred at room temperature overnight and afterwards heated to reflux for 4 hours. It was then cooled to 0°C and a solution of zinc dichloride (4.09 g, 30.00 mmol) in THF (70 mL) was slowly added. After complete addition the solution was allowed to warm to room temperature and it was stirred overnight. It was again cooled to 0°C and a solution of trichlorophosphane (3.98 g, 29.00 mmol)

in THF (20 mL) was added dropwise. The mixture was allowed to warm to room temperature over 1.5 hours. The solvent was removed under reduced pressure and the residue was redissolved in hexane. Filtration over a glass frit and removal of the solvent yielded dichloro(mesityl)phosphane (**39a**) (3.53 g, 15.97 mmol, 64%, Lit.: 62%^[98]) as a colourless oil. The NMR spectroscopic data is in good agreement with the literature.^[98] However, the in the literature reported byproducts were not or only in trace amounts formed (ClBrPMes ($\delta^{31}\text{P} = 161.8$; 1.5%) and Br₂PMes (0%)).



¹H NMR (500.1 MHz, 305 K, C₆D₆): $\delta = 1.93$ (s, 3H, *para*-Me), 2.52 (d, ⁴J_{H,P} = 4.0 Hz, 6H, 2 x *ortho*-Me), 6.49-6.52 (m, 2H, 2 x *meta*-H).

¹³C{¹H} NMR (125.7 MHz, 305 K, C₆D₆): $\delta = 21.0$ (*para*-Me), 21.4 (d, ³J_{C,P} = 26 Hz, *ortho*-Me), 130.9 (d, ³J_{C,P} = 4 Hz, *meta*-CH), 132.3 (d, ¹J_{C,P} = 67 Hz, C^{ipso}), 143.3 (*para*-CMe), 143.6 (d, ²J_{C,P} = 27 Hz, 2 x *ortho*-CMe).

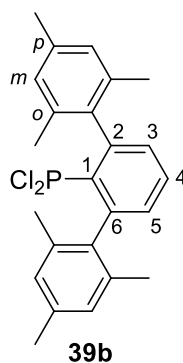
³¹P{¹H} NMR (202.4 MHz, 305 K, C₆D₆): δ (Cl₂-isotopic pattern) = 167.8 (90%, 58%, 9%).

GC-MS: t_R = 7.6 min, m/z (%) = 77 (12), 91 (29), 103 (11), 115 (16), 119 (43), 132 (10), 147 (18), 149 (42), 185 (100), 220 (90) [M⁺].

5.2.4.2 Dichloro-(2,6-dimesitylphenyl)phosphane (**39b**)

Dichloro-(2,6-dimesitylphenyl)phosphane (**39b**) was prepared according to a literature procedure by Pietschnig *et al.*^[99]

Deviating from the literature, a solution of 2,6-dimesitylphenyliodide (1.00 g, 2.27 mmol) in THF (30 mL) was cooled to -80°C and *n*BuLi (1.5 mL, 2.38 mmol) was slowly added. The mixture was stirred for 90 min before trichlorophosphane (0.94g, 6.81 mmol) was added dropwise. The mixture was allowed to warm to room temperature overnight. The solvent was removed under reduced pressure. The residue was then redissolved in toluene and filtered over a glass frit. Removal of the solvent gave the crude product **39b** (62%, Lit: 85%^[99]) as pale orange solid. Recrystallisation from toluene at -20°C yielded dichloro-(2,6-dimesitylphenyl)phosphane (**39b**) (262 mg, 0.63 mmol, 28%, Lit.: 34%^[99]) as slightly yellow solid. The NMR spectroscopic is in accordance with the literature.^[99]



$^1\text{H NMR}$ (500.1 MHz, 305 K, C_6D_6): δ = 2.09 (s, 12H, 4 x *ortho*-Me), 2.17 (s, 6H, 2x *para*-Me), 6.80 (d, $^3J_{\text{H,H}}$ = 7.6 Hz, 1H, $\text{C}^{3/5}$ -H), 6.81 (d, $^3J_{\text{H,H}}$ = 7.6 Hz, 1H, $\text{C}^{3/5}$ -H), 6.84 (s, 4H, 4 x *meta*-H), 7.10 (t, $^3J_{\text{H,H}}$ = 7.6 Hz, 1H, C^4 -H).

$^{13}\text{C}\{^1\text{H}\}$ NMR (125.7 MHz, 305 K, C_6D_6): δ = 21.2 (4 x *ortho*-Me), 21.6 (2 x *para*-Me), 128.6 (4 x *meta*-CH), 130.9 ($\text{C}^{3/5}$), 133.2 (C^4), 135.0 (d, $^1J_{\text{C,P}}$ = 72 Hz, C^1), 136.4 (d, $^3J_{\text{C,P}}$ = 8 Hz, C^{ipso}), 136.5 (d, $^4J_{\text{C,P}}$ = 3 Hz, *ortho*-CMe), 137.8 (*para*-CMe), 147.2 (d, $^2J_{\text{C,P}}$ = 29 Hz, $\text{C}^{2/6}$).

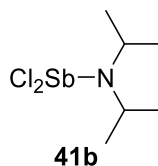
$^{31}\text{P}\{^1\text{H}\}$ NMR (202.4 MHz, 305 K, C_6D_6): δ (Cl_2 -isotopic pattern) = 160.8 (90%, 53%, 6%).

5.2.5 Stibanes

5.2.5.1 Dichloro(diisopropylamino)stibane (41a)

Dichloro(diisopropylamino)stibane (**41a**) is not known in the literature. It was synthesised similar to its lighter homologue dichloro(diisopropylamino)arsane, described by Scherer and Höntschi.^[104]

In a Schlenk flask, antimonytrichloride (1.95 g, 8.50 mmol) was diluted in diethyl ether (10 mL). The solution was cooled to 0° and a diethyl ether (10 mL) solution of diisopropylamine (1.73 g, 17.11 mmol) was added dropwise. A colourless precipitate was formed immediately. The suspension was stirred overnight at room temperature. The solvent was removed and the residue dissolved in pentane and filtered over a glass frit. Removal of the solvent yielded dichloro(diisopropylamino)stibane (**41b**) (0.80 g, 2.72 mmol, 32%) as a colourless solid. It is not storable and decomposes within days.



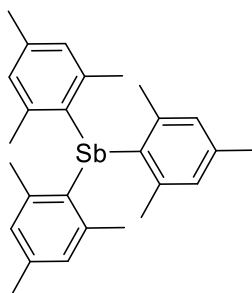
$^1\text{H NMR}$ (500.1 MHz, 305 K, C_6D_6): δ = 0.98 (d, $^3J_{\text{H,H}}$ = 6.8 Hz, 12 H, $\text{N}(\text{CHMe}_2)_2$), 3.99 (sept, $^3J_{\text{H,H}}$ = 6.8 Hz, 2H, $\text{N}(\text{CHMe}_2)_2$).

$^{13}\text{C}\{^1\text{H}\}$ NMR (125.7 MHz, 305 K, C_6D_6): δ = 26.7 ($\text{N}(\text{CHMe}_2)_2$), 49.6 ($\text{N}(\text{CHMe}_2)_2$).

5.2.5.2 Chloro(dimesityl)stibane (**42**)

Dichloro(mesityl)stibane (**41b**) was aimed to be synthesised in a two-step reaction following a procedure by Chalmers *et al.* and Ates *et al.*.^[105-106]

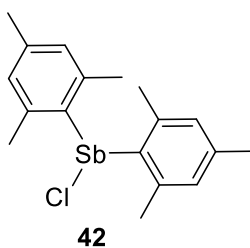
In a first step, trimesitylstibane was synthesised. Therefore, a Schlenk flask was equipped with magnesium turnings (1.09 g, 45.00 mmol) and one flake of iodine. THF (30 mL) was added. A THF-solution of bromomesitylene (6.9 mL, 45.00 mmol) was added dropwise to the flask. After complete addition, the mixture was heated to reflux for 30 minutes. To the mesitylgrignard solution, antimonytrichloride (3.43 g, 15.00 mmol), dissolved in diethyl ether (25 mL), was slowly added. The resulting solution was heated to reflux for 30 minutes. Afterwards, it was cooled to 0°C and water (12 mL) was added. The precipitates were filtered off and washed with diethyl ether. The combined organic layers were dried over magnesiumsulfate. Removal of the solvent gave an oily yellow residue. Addition of ethanol resulted in precipitation of a colourless solid. The solvent was removed by filtration to give trimesitylstibane (5.68 g, 11.84 mmol, 79%, Lit.: 78%). The NMR spectroscopic data matches the literature.^[105]



¹H NMR (500.1 MHz, 305 K, CDCl₃): δ = 2.28 (s, 9H, *para*-Me), 2.31 (s, 18H, *ortho*-Me), 6.85 (s, 6H, *meta*-H).

¹³C{¹H} NMR (125.7 MHz, 305 K, CDCl₃): δ = 21.0 (*para*-Me), 25.5 (*ortho*-Me), 129.0 (*meta*-C), 136.8 (*ortho*-C), 137.9 (*para*-C), 144.9 (C^{*ipso*}).

For the second step, a comproportionation reaction, trimesitylstibane (2.40 g, 5.00 mmol) and antimonytrichloride (2.57 g, 11.25 mmol) were added to a Schlenk flask and heated to 80°C for 24 hours. The residue was then dissolved in pentane/chloroform (1:1, 35 mL). The solution was restricted in volume and kept at -20°C overnight. The colourless precipitate was filtered off and dried *in vacuo*. The NMR spectroscopic data corresponds to dichloro(mesityl)stibane **41b**, as reported in the literature (53% yield).^[105-106] However, analysis by GC-MS revealed that instead, chlorodimesitylstibane **42** was obtained (2.56 g, 6.47 mmol, 86%).



$^1\text{H NMR}$ (500.1 MHz, 305 K, CDCl_3): δ = 2.30 (s, 3H, *para*-Me), 2.74 (s, 6H, *ortho*-Me), 6.97 (s, 2H, *meta*-H).

$^{13}\text{C}\{^1\text{H}\}$ NMR (125.7 MHz, 305 K, CDCl_3): δ = 21.4 (*para*-Me), 22.9 (*ortho*-Me), 130.7 (*meta*-C), 142.4 (*ortho*-C), 144.8 (*para*-C), 147.1 (*C*^{*ipso*}).

GC-MS: t_R = 12.6 min, m/z (%) = 119 (53), 275 (100), 358 (18), 396 (3) [M^+].

MS: calculated: m/z = 394.04; found (EI): m/z = 394 [M^+].

5.2.6 Selenium Dichloride

Seleniumdichloride was prepared following a procedure by Chivers *et al.*^[131]

To a Schlenk flask, equipped with grey selenium powder (79 mg, 1.00 mmol), sulfurylchloride (135 mg, 1.00 mmol) was added at room temperature. The suspension was stirred for 10 minutes before THF (2.5 mL) was added. It was stirred for one hour to give a red solution of seleniumdichloride (c = 0.4 mmol/mL). The formation was confirmed by NMR spectroscopy. The data matches the literature.^[131]



$^{77}\text{Se}\{^1\text{H}\}$ (95.5 MHz, 305 K, none): δ = 1828.2.

The compound is not suitable for storage and should be used within one day after preparation.^[131]

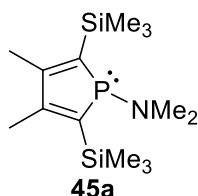
5.2.7 Phospha-BCH-Germylenes & Phospholes

5.2.7.1 Phospholes 45a and 46a

The THF solution (6 mL) of dipotassium germolediide K_2 [**31**] or K_2 [**36**], synthesised by the reduction of dichlorogermole **31** or **36** (74 mg / 90 mg, 0.20 mmol) with potassium, was cooled to -50°C . Dichloro(dimethylamino)phosphane **38a** (29 mg, 0.20 mmol) was added directly to the cooled solution. The reaction mixture was stirred for 30 minutes whilst it was allowed to warm to room temperature. The solvent was removed and the residue redissolved in pentane. It was filtered over silica gel. Removal of the solvent gave phosphole **45a** (29 mg, 0.10 mmol, 50%) and

phosphole **46a** (52 mg, 0.14 mmol, 70%) as yellow-orange oils containing minor impurities that could not be removed.

At room temperature, the signals of the dimethylamino moiety cannot be observed. Therefore, low temperature NMR measurements (-40°C) were performed. The NMR spectroscopic data of phosphole **45a** (at 305 K) correspond to those from previous work.^[67]



¹H NMR (499.9 MHz, 305 K, C₆D₆): δ = 0.34 (s, 18H, SiMe₃), 1.94 (d, ⁴J_{H,P} = 5.6 Hz, 6H, C^{2/3}-Me).

¹³C{¹H} NMR (125.7 MHz, 305 K, C₆D₆): δ = 0.5 (d, ³J_{C,P} = 3 Hz, SiMe₃), 17.8 (d, ³J_{C,P} = 6 Hz, C^{2/3}-Me), 143.6 (d, ¹J_{C,P} = 31 Hz, C^{1/4}), 153.4 (d, ²J_{C,P} = 18 Hz, C^{2/3}).

²⁹Si{¹H} INEPT NMR (99.3 MHz, 305 K, C₆D₆): δ = -10.9 (d, ²J_{Si,P} = 24 Hz).

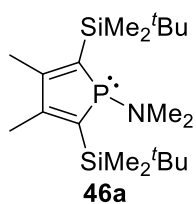
³¹P{¹H} NMR (202.4 MHz, 305 K, C₆D₆): δ = 94.3.

MS: calculated: m/z = 299.17; found (EI): m/z = 298.85 [M⁺].

Spectra recorded at -40°C:

¹H NMR (499.9 MHz, 233 K, toluene-d₈): δ = 0.33 (s, 18H, SiMe₃), 1.85 (d, ⁴J_{H,P} = 5.6 Hz, 6H, C^{2/3}-Me), 1.98 (d, ³J_{H,P} = 2.8 Hz, 3H, NMe₂), 2.68 (d, ³J_{H,P} = 12.3 Hz, 3H, NMe₂).

¹³C{¹H} NMR (125.7 MHz, 233 K, toluene-d₈): δ = 0.8 (d, ³J_{C,P} = 3 Hz, SiMe₃), 18.3 (d, ³J_{C,P} = 6 Hz, C^{2/3}-Me), 40.5 (d, ²J_{C,P} = 12 Hz, NMe₂), 44.5 (d, ²J_{C,P} = 39 Hz, NMe₂), 143.6 (d, ¹J_{C,P} = 30 Hz, C^{1/4}), 153.8 (d, ²J_{C,P} = 18 Hz, C^{2/3}).



¹H NMR (499.9 MHz, 305 K, C₆D₆): δ = 0.32 (s, 12H, SiMe₂^tBu), 1.04 (s, 18H, SiMe₂^tBu), 2.04 (d, ⁴J_{H,P} = 5.6 Hz, 6H, C^{2/3}-Me).

¹³C{¹H} NMR (125.7 MHz, 305 K, C₆D₆): δ = -3.4 (m, SiMe₂^tBu), 18.8 (SiMe₂^tBu, C⁴), 19.4 (d, ³J_{C,P} = 6 Hz, C^{2/3}-Me), 27.8 (m, SiMe₂^tBu), 141.2 (d, ¹J_{C,P} = 33 Hz, C^{1/4}), 154.2 (d, ²J_{C,P} = 17 Hz, C^{2/3}).

²⁹Si{¹H} INEPT NMR (99.3 MHz, 305 K, C₆D₆): δ = -2.5 (d, ²J_{Si,P} = 22 Hz).

³¹P{¹H} NMR (202.4 MHz, 305 K, C₆D₆): δ = 98.5.

MS: calculated: m/z = 383.26; found (EI): m/z = 383.08 [M⁺].

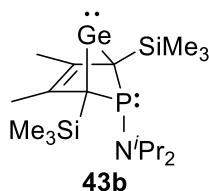
Spectra recorded at -40°C:

$^1\text{H NMR}$ (499.9 MHz, 233 K, toluene-d₈): δ = 0.21 (s, 6H, SiMe_2^tBu), 0.36 (s, 6H, SiMe_2^tBu), 1.00 (s, 18H, SiMe_2^tBu), 1.96 (d, $^3J_{\text{H,P}} = 2.2$ Hz, 3H, NMe_2), 1.98 (d, $^4J_{\text{H,P}} = 5.6$ Hz, 6H, $\text{C}^{2/3}\text{-Me}$), 2.67 (d, $^3J_{\text{H,P}} = 11.8$ Hz, 3H, NMe_2).

$^{13}\text{C}\{^1\text{H}\}$ NMR (125.7 MHz, 233 K, toluene-d₈): δ = -3.9 (SiMe_2^tBu), -2.6 (d, $^3J_{\text{C,P}} = 7$ Hz, SiMe_2^tBu), 19.3 (SiMe_2^tBu , C^4), 19.9 (d, $^3J_{\text{C,P}} = 6$ Hz, $\text{C}^{2/3}\text{-Me}$), 28.0 (SiMe_2^tBu), 40.7 (d, $^2J_{\text{C,P}} = 12$ Hz, NMe_2), 44.6 (d, $^2J_{\text{C,P}} = 40$ Hz, NMe_2), 141.4 (d, $^1J_{\text{C,P}} = 33$ Hz, $\text{C}^{1/4}$), 154.6 (d, $^2J_{\text{C,P}} = 17$ Hz, $\text{C}^{2/3}$).

5.2.7.2 Germylene **43b** and Phosphole **45b**

The THF solution (6 mL) of dipotassium germodiide **K₂[31]**, synthesised by the reduction of dichlorogermole **31** (74 mg, 0.20 mmol) with potassium, was cooled to -50°C. Dichloro(diisopropylamino)phosphane **38b** (40 mg, 0.20 mmol), dissolved in THF (3 mL), was added. The reaction mixture was stirred for 30 minutes whilst it was allowed to warm to room temperature. The solvent was removed. The product mixture contained phosphole **45b** and germylene **43b** in a mixture of 30 : 70, in an overall yield of 100%. The residue was redissolved in pentane. Storing the solution at -20°C for several days gave colourless crystals of germylene **43b** suitable for XRD analysis.



$^1\text{H NMR}$ (500.1 MHz, 305 K, C_6D_6): δ = 0.29 (s, 18H, 2 x SiMe_3), 1.13 (d, $^3J_{\text{H,H}} = 6.5$ Hz, 12H, $\text{N}(\text{CHMe}_2)_2$), 2.19 (s, 6H, 2 x $\text{C}^{2/3}\text{-Me}$), 2.83-2.91 (m, 2H, $\text{N}(\text{CHMe}_2)_2$).

$^{13}\text{C}\{^1\text{H}\}$ NMR (125.7 MHz, 305 K, C_6D_6): δ = 1.6 (d, $^3J_{\text{C,P}} = 7$ Hz, SiMe_3), 15.7 (d, $^3J_{\text{C,P}} = 4$ Hz, $\text{C}^{2/3}\text{-Me}$), 25.2 (m, $\text{N}(\text{CHMe}_2)_2$), 46.8 (m, $\text{N}(\text{CHMe}_2)_2$), 74.4 (d, $^1J_{\text{C,P}} = 36$ Hz, $\text{C}^{1/4}$), 129.9 (d, $^2J_{\text{C,P}} = 8$ Hz, $\text{C}^{2/3}$).

$^{29}\text{Si}\{^1\text{H}\}$ INEPT NMR (99.3 MHz, 305 K, C_6D_6): δ = -7.6 (d, $^2J_{\text{Si,P}} = 21$ Hz).

$^{31}\text{P}\{^1\text{H}\}$ NMR (202.4 MHz, 305 K, C_6D_6): δ = 35.4.

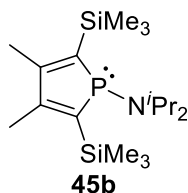
$^1\text{H NMR}$ (500.1 MHz, 305 K, THF-d₈): δ = 0.11 (s, 18H, 2 x SiMe_3), 1.01 (d, $^3J_{\text{H,H}} = 6.6$ Hz, 12H, $\text{N}(\text{CHMe}_2)_2$), 2.39 (s, 6H, 2 x $\text{C}^{2/3}\text{-Me}$), 2.83-2.93 (m, 2H, $\text{N}(\text{CHMe}_2)_2$).

$^{13}\text{C}\{^1\text{H}\}$ NMR (125.7 MHz, 305 K, THF-d₈): δ = 1.5 (d, $^3J_{\text{C,P}} = 6$ Hz, SiMe_3), 15.9 (d, $^3J_{\text{C,P}} = 5$ Hz, $\text{C}^{2/3}\text{-Me}$), 47.3 (m, $\text{N}(\text{CHMe}_2)_2$), 74.6 (d, $^1J_{\text{C,P}} = 36$ Hz, $\text{C}^{1/4}$), 130.7 (d, $^2J_{\text{C,P}} = 8$ Hz, $\text{C}^{2/3}$). $\text{N}(\text{CHMe}_2)_2$ signal hidden by the solvent signal.

$^{29}\text{Si}\{^1\text{H}\}$ INEPT NMR (99.3 MHz, 305 K, THF- d_8): $\delta = -9.3$ (d, $^2J_{\text{Si,P}} = 21$ Hz).

$^{31}\text{P}\{^1\text{H}\}$ NMR (202.4 MHz, 305 K, THF- d_8): $\delta = 33.3$.

The NMR spectroscopic data of phosphole **45b** correspond to those from previous work.^[67]



^1H NMR (500.1 MHz, 305 K, C_6D_6): $\delta = 0.40$ (s, 18 H, 2 x SiMe_3), 1.18 (d, $^3J_{\text{H,H}} = 6.6$ Hz, 12 H, $\text{N}(\text{CHMe}_2)_2$), 2.02 (d, $^4J_{\text{H,H}} = 6.5$ Hz, 6 H, 2 x $\text{C}^{2/3}\text{-Me}$), 3.05–3.15 (m, 2 H, $\text{N}(\text{CHMe}_2)_2$).

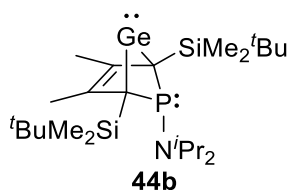
$^{13}\text{C}\{^1\text{H}\}$ NMR (125.7 MHz, 305 K, C_6D_6): $\delta = 1.4$ (d, $^3J_{\text{C,P}} = 3$ Hz, SiMe_3), 18.1 (d, $^3J_{\text{C,P}} = 6$ Hz, $\text{C}^{2/3}\text{-Me}$), 24.4 (d, $^3J_{\text{C,P}} = 8$ Hz, $\text{N}(\text{CHMe}_2)_2$), 51.1 (d, $^2J_{\text{C,P}} = 8$ Hz, $\text{N}(\text{CHMe}_2)_2$), 143.0 (d, $^1J_{\text{C,P}} = 33$ Hz, $\text{C}^{1/4}$), 151.9 (d, $^2J_{\text{C,P}} = 19$ Hz, $\text{C}^{2/3}$).

$^{29}\text{Si}\{^1\text{H}\}$ INEPT NMR (99.3 MHz, 305 K, C_6D_6): $\delta = -10.8$ (d, $^2J_{\text{Si,P}} = 25$ Hz).

$^{31}\text{P}\{^1\text{H}\}$ NMR (202.4 MHz, 305 K, C_6D_6): $\delta = 65.6$.

5.2.7.3 Germylene **44b** and Phosphole **46b**

The THF solution (6 mL) of dipotassium germodiide **K₂[36]**, synthesised by the reduction of dichlorogermole **36** (90 mg, 0.20 mmol) with potassium, was cooled to -50°C . Dichloro(diisopropylamino)phosphane **38b** (40 mg, 0.20 mmol), dissolved in THF (3 mL), was added. The reaction mixture was stirred for 30 minutes whilst it was allowed to warm to room temperature. The solvent was removed. The product mixture contained phosphole **46b** and germylene **44b** in a mixture of 3 : 97, in an overall yield of 79%.



^1H NMR (500.1 MHz, 305 K, C_6D_6) $\delta = 0.21$ (s, 6H, 2 x SiMe_2^tBu), 0.32–0.34 (m, 6H, 2 x SiMe_2^tBu), 1.11 (s, 18H, 2 x SiMe_2^tBu), 1.13 (d, $^3J_{\text{H,H}} = 6.8$ Hz, 12H, $\text{N}(\text{CHMe}_2)_2$), 2.23 (s, 6H, 2 x CH_3), 3.14–3.25 (m, 2H, $\text{N}(\text{CHMe}_2)_2$).

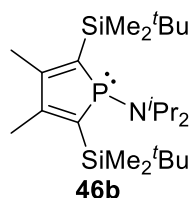
$^{13}\text{C}\{^1\text{H}\}$ NMR (125.7 MHz, 305 K, C_6D_6) $\delta = -2.5$ (d, $^3J_{\text{C,P}} = 5$ Hz, $\text{Si}(\text{Me}_2)^t\text{Bu}$), -2.1 (d, $^3J_{\text{C,P}} = 5$ Hz, $\text{Si}(\text{Me}_2)^t\text{Bu}$), 17.1 (d, $^3J_{\text{C,P}} = 4$ Hz, $\text{C}^{2/3}\text{-Me}$), 19.0 (d, $^4J_{\text{C,P}} = 2$ Hz, $\text{Si}(\text{Me}_2)^t\text{Bu}$), 25.4 (d, $^3J_{\text{C,P}} = 5$ Hz, $\text{N}(\text{CHMe}_2)_2$), 28.4 (d, $^3J_{\text{C,P}} = 3$ Hz, $\text{Si}(\text{Me}_2)^t\text{Bu}$), 48.7 (d, $^2J_{\text{C,P}} = 10$ Hz, $\text{N}(\text{CHMe}_2)_2$), 72.8 (d, $^1J_{\text{C,P}} = 41$ Hz, $\text{C}^{1/4}$), 131.1 (d, $^2J_{\text{C,P}} = 7$ Hz, $\text{C}^{2/3}$).

$^{29}\text{Si}\{^1\text{H}\}$ INEPT NMR (99.3 MHz, 305 K, C_6D_6) $\delta = -0.2$ (d, $^2J_{\text{Si,P}} = 18$ Hz).

$^{31}\text{P}\{^1\text{H}\}$ NMR (202.4 MHz, 305 K, C_6D_6) $\delta = 53.8$.

MS: calculated: $m/z = 513.24$; found (EI): $m/z = 514.29$ [M+H].

UV-Vis: λ_{max} [nm] = 272.



^1H NMR (500.1 MHz, 305 K, C_6D_6): $\delta = 0.42$ (s, 12H, 2 x SiMe_2tBu), 0.98 (s, 18H, 2 x SiMe_2tBu), 1.19 (d, $^3J_{\text{H,H}} = 6.4$ Hz, 12H, $\text{N}(\text{CHMe}_2)_2$), 2.09 (d, $^4J_{\text{H,P}} = 6.3$ Hz, 6H, 2 x $\text{C}^{2/3}\text{-Me}$), 3.02-3.13 (m, 2H, $\text{N}(\text{CHMe}_2)_2$).

$^{13}\text{C}\{^1\text{H}\}$ NMR (125.7 MHz, 305 K, C_6D_6): $\delta = -2.6$ (d, $^3J_{\text{C,P}} = 4$ Hz, SiMe_2tBu), 19.3 (SiMe_2tBu), 19.9 (d, $^3J_{\text{C,P}} = 6$ Hz, $\text{C}^{2/3}\text{-Me}$), 24.1–24.5 (m, $\text{N}(\text{CHMe}_2)_2$), 27.8 (d, $^3J_{\text{C,P}} = 3$ Hz, SiMe_2tBu), 50.8 (br, $\text{N}(\text{CHMe}_2)_2$), 140.7 (d, $^1J_{\text{C,P}} = 36$ Hz, $\text{C}^{1/4}$), 154.0 (d, $^2J_{\text{C,P}} = 16$ Hz, $\text{C}^{2/3}$).

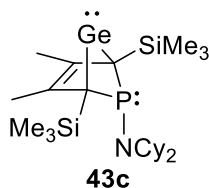
$^{29}\text{Si}\{^1\text{H}\}$ INEPT NMR (99.3 MHz, 305 K, C_6D_6): $\delta = -3.1$ (d, $^2J_{\text{Si,P}} = 22$ Hz).

$^{31}\text{P}\{^1\text{H}\}$ NMR (202.4 MHz, 305 K, C_6D_6): $\delta = 71.7$ ($^2J_{\text{P,Si}} = 22$ Hz).

MS: calculated: $m/z = 439.32$; found (EI): $m/z = 439.18$ [M^+].

5.2.7.4 Germylene 43c and Phosphole 45c

The THF solution (6 mL) of dipotassium germylene **31**, synthesised by the reduction of dichlorogermole **31** (74 mg, 0.20 mmol) with potassium, was cooled to -50°C . Dichloro(dicyclohexylamino)phosphane **38c** (56 mg, 0.20 mmol), dissolved in THF (3 mL), was added. The reaction mixture was stirred for 30 minutes whilst it was allowed to warm to room temperature. The solvent was removed and the residue dissolved in diethyl ether and filtered over a PTFE syringe filter. The solvent was removed. The product mixture contained phosphole **43c** and germylene **45c** in a mixture of 25 : 75, in an overall yield of 95%.



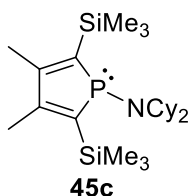
^1H NMR (500.1 MHz, 305 K, C_6D_6): $\delta = 0.39$ (s, 18H, 2 x SiMe_3), 2.34 (s, 6H, 2 x $\text{C}^{2/3}\text{-Me}$), 2.49 (br, 2H, $\text{NCy}_2\text{-C}^{\text{ipso}}\text{-H}$). Cyclohexyl signals can not be assigned due to overlap with the phosphole signals.

$^{13}\text{C}\{^1\text{H}\}$ NMR (125.7 MHz, 305 K, C_6D_6): $\delta = 1.6$ (d, $^3J_{\text{C,P}} = 6$ Hz, SiMe_3), 15.7 (d, $^3J_{\text{C,P}} = 4$ Hz, $\text{C}^{2/3}\text{-Me}$), 25.5 (NCy_2), 26.2 (NCy_2), 35.0 (NCy_2), 53.2 (NCy_2 , C^{ipso}), 74.8 (d, $^1J_{\text{C,P}} = 37$ Hz, $\text{C}^{1/4}$), 129.9 (d, $^2J_{\text{C,P}} = 8$ Hz, $\text{C}^{2/3}$).

$^{29}\text{Si}\{^1\text{H}\}$ NMR (99.3 MHz, 305 K, C_6D_6): $\delta = -7.6$ (d, $^2J_{\text{Si,P}} = 21$ Hz).

$^{31}\text{P}\{^1\text{H}\}$ NMR (202.4 MHz, 305 K, C_6D_6): $\delta = 39.4$.

The NMR spectroscopic data of phosphole **45c** correspond to those from previous work.^[67]



^1H NMR (500.1 MHz, 305 K, C_6D_6): $\delta = 0.43$ (s, 18H, 2 x SiMe_3), 0.99 (qt, $J_{\text{H,H}} = 13.1$ Hz, $J_{\text{H,H}} = 3.6$ Hz, 2 H, Cy), 1.16 (qt, $J_{\text{H,H}} = 13.1$ Hz, $J_{\text{H,H}} = 3.3$ Hz, 4 H, Cy), 1.43-1.54 (m, 6 H, Cy), 1.66-1.73 (m, 4 H, Cy), 2.04 (d, $^4J_{\text{H,P}} = 6.6$ Hz, 6H, 2 x $\text{C}^{2/3}\text{-Me}$), 2.10-2.16 (m, 4 H, Cy), 2.69-2.78 (m, 2 H, Cy, 2 x HC^{ipso}).

$^{13}\text{C}\{^1\text{H}\}$ NMR (125.7 MHz, 305 K, C_6D_6): $\delta = 1.5$ (d, $^3J_{\text{C,P}} = 3$ Hz, SiMe_3), 18.3 (d, $^3J_{\text{C,P}} = 6$ Hz, $\text{C}^{2/3}\text{-Me}$), 26.3 (Cy), 26.9 (Cy), 35.2 (d, 8 Hz, Cy), 60.9 (d, $^2J_{\text{C,P}} = 6$ Hz, Cy, C^{ipso}), 143.0 (d, $^2J_{\text{C,P}} = 33$ Hz, $\text{C}^{1/4}$), 151.6 (d, $^2J_{\text{C,P}} = 20$ Hz, $\text{C}^{2/3}$).

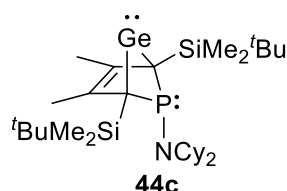
$^{29}\text{Si}\{^1\text{H}\}$ INEPT NMR (99.3 MHz, 305 K, C_6D_6): $\delta = -10.8$ (d, $^2J_{\text{Si,P}} = 25$ Hz).

$^{31}\text{P}\{^1\text{H}\}$ NMR (202.4 MHz, 305 K, C_6D_6): $\delta = 63.8$.

MS: calculated: $m/z = 435.29$; found (EI): $m/z = 435.13$ [M^+].

5.2.7.5 Germylene **44c** and Phosphole **46c**

The THF solution (6 mL) of dipotassium germodiide **K₂[36]**, synthesised by the reduction of dichlorogermole **36** (90 mg, 0.20 mmol) with potassium, was cooled to -50°C . Dichloro(dicyclohexylamino)phosphane **38c** (56 mg, 0.20 mmol), dissolved in THF (3 mL), was added. The reaction mixture was stirred for 30 minutes whilst it was allowed to warm to room temperature. The solvent was removed. The product mixture contained phosphole **46c** and germylene **44c** in a mixture of 2 : 98, in an overall yield of 78%.



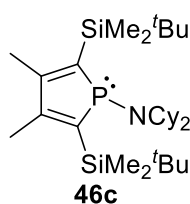
^1H NMR (500.1 MHz, 305 K, C_6D_6) δ = 0.21 (s, 6H, 2 x SiMe_2^tBu), 0.34–0.36 (m, 6H, 2 x SiMe_2^tBu), 1.11 (s, 18H, 2 x SiMe_2^tBu), 2.29 (s, 6H, 2 x CH_3). The NCy_2 signals are broad and overlay with other signals.

$^{13}\text{C}\{^1\text{H}\}$ NMR (125.7 MHz, 305 K, C_6D_6) δ = -2.5 (d, $^3J_{\text{C,P}} = 9$ Hz, $\text{Si}(\text{Me}_2)^t\text{Bu}$), -2.2 (d, $^3J_{\text{C,P}} = 5$ Hz, $\text{Si}(\text{Me}_2)^t\text{Bu}$), 17.0 (d, $^3J_{\text{C,P}} = 4$ Hz, $\text{C}^{2/3}\text{-Me}$), 19.1 (d, $^4J_{\text{C,P}} = 3$ Hz, $\text{Si}(\text{Me}_2)^t\text{Bu}$), 26.5 (NCy_2), 27.5 (NCy_2), 36.3 (br, NCy_2), 28.5 (d, $^3J_{\text{C,P}} = 3$ Hz, $\text{Si}(\text{Me}_2)^t\text{Bu}$), 59.0 (NCy_2 , $\underline{\text{C}}^{\text{ipso}}$), 73.0 (d, $^1J_{\text{C,P}} = 41$ Hz, $\text{C}^{1/4}$), 131.1 (d, $^2J_{\text{C,P}} = 7$ Hz, $\text{C}^{2/3}$).

$^{29}\text{Si}\{^1\text{H}\}$ INEPT NMR (99.3 MHz, 305 K, C_6D_6) δ = -0.2 (d, $^2J_{\text{Si,P}} = 18$ Hz).

$^{31}\text{P}\{^1\text{H}\}$ NMR (202.4 MHz, 305 K, C_6D_6) δ = 57.7.

MS: calculated: $m/z = 593.31$; found (EI): $m/z = 592.86$ [M^+].



^1H NMR (500.1 MHz, 305 K, C_6D_6): δ = 0.38 (SiMe_2^tBu), 2.14 (d, $^4J_{\text{H,P}} = 6.2$ Hz, $\text{C}^{2/3}\text{-Me}$). Due to low concentration, assignment of the NCy_2 signals was not possible.

$^{13}\text{C}\{^1\text{H}\}$ NMR (125.7 MHz, 305 K, C_6D_6): δ = 141 ($\text{C}^{1/4}$), 154 ($\text{C}^{2/3}$). Data retrieved from the $^1\text{H}^{13}\text{C}$ HMBC NMR spectrum. Assignment of the remaining signals was not possible due to low concentration of the phosphole.

$^{29}\text{Si}\{^1\text{H}\}$ INEPT NMR (99.3 MHz, 305 K, C_6D_6): δ = -3.1 (d, $^2J_{\text{Si,P}} = 23$ Hz).

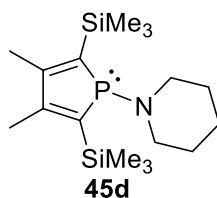
$^{31}\text{P}\{^1\text{H}\}$ NMR (202.4 MHz, 305 K, C_6D_6): δ = 69.7.

MS: calculated: $m/z = 519.38$; found (EI): $m/z = 519.20$ [M^+].

5.2.7.6 Phosphole 45d

The THF solution (6 mL) of dipotassium germolediide **K₂[31]**, synthesised by the reduction of dichlorogermole **31** (74 mg, 0.20 mmol) with potassium in THF (6 mL). Afterwards, the solvent was removed and the germolediide salt **K₂[31]** was dissolved in diethyl ether (4 mL). It was cooled to -50°C and dichloro(piperidino)phosphane **38d** (37 mg, 0.20 mmol), dissolved in THF (3 mL), was added. The reaction mixture was stirred for 30 minutes before the cold bath was

removed and the solution stirred at room temperature overnight. The solvent was removed under reduced pressure. The crude product was redissolved in pentane and filtered over a PTFE syringe filter. Removal of the solvent gave phosphole **45d** (66 mg, 0.19 mmol, 95%) as orange oil. Low temperature NMR measurements (-40°C) were performed to detect the signals of the piperidino substituent.



¹H NMR (499.9 MHz, 305 K, C₆D₆): δ = 0.39 (s, 18H, 2 x SiMe₃), 1.28-1.33 (m, 4H, NC₅H₁₀), 1.95 (d, ⁴J_{H,H} = 5.4 Hz, 6H, 2 x C^{2/3}-Me).

¹³C{¹H} NMR (125.7 MHz, 305 K, C₆D₆): δ = 0.9 (d, ³J_{C,P} = 3 Hz, SiMe₃), 18.0 (d, ³J_{C,P} = 6 Hz, C^{2/3}-Me), 27.4 (NC₅H₁₀), 142.9 (d, ¹J_{C,P} = 32 Hz, C^{1/4}), 154.3 (d, ²J_{C,P} = 16 Hz, C^{2/3}).

²⁹Si{¹H} INEPT NMR (99.3 MHz, 305 K, C₆D₆): δ = -11.0 (d, ²J_{Si,P} = 25 Hz).

³¹P{¹H} NMR (202.4 MHz, 305 K, C₆D₆): δ = 92.2.

MS: calculated: m/z = 339.20; found (EI): m/z = 338.98 [M⁺].

Spectra recorded at -40°C:

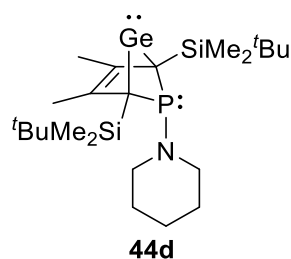
¹H NMR (499.9 MHz, 233 K, toluene-d₈): δ = 0.38 (s, 18H, SiMe₃), 1.41-1.47 (m, 4H, NC₅H₁₀), 1.87 (d, ⁴J_{H,P} = 5.4 Hz, 6H, C^{2/3}-Me), 2.22-2.28 (m, 3H, NC₅H₁₀), 3.06-3.14 (m, 3H, NC₅H₁₀).

¹³C{¹H} NMR (125.7 MHz, 233 K, toluene-d₈): δ = 0.6 (d, ³J_{C,P} = 3 Hz, SiMe₃), 17.8 (d, ³J_{C,P} = 6 Hz, C^{2/3}-Me), 27.4 (NC₅H₁₀, *meta*-CH₂, *para*-CH₂), 49.2 (d, ²J_{C,P} = 10 Hz, NC₅H₁₀, *ortho*-CH₂), 53.1 (d, ²J_{C,P} = 33 Hz, NC₅H₁₀, *ortho*-CH₂), 142.3 (d, ¹J_{C,P} = 30 Hz, C^{1/4}), 154.1 (d, ²J_{C,P} = 17 Hz, C^{2/3}).

³¹P{¹H} NMR (202.4 MHz, 233 K, toluene-d₈): δ = 91.5.

5.2.7.7 Germylene **44d** and Phosphole **46d**

Dipotassium germodiide **K₂[36]** was synthesised by the reduction of dichlorogermole **36** (90 mg, 0.20 mmol) with potassium in THF (6 mL). Afterwards, the solvent was removed and the germodiide salt **K₂[36]** was dissolved in diethyl ether (4 mL). It was cooled to -50°C and dichloro(piperidino)phosphane **38d** (37 mg, 0.20 mmol), dissolved in diethyl ether (3 mL), was added. The mixture was stirred for 30 minutes before the ice bath was removed and it was stirred for 30 minutes at room temperature. Pentane was added and the suspension filtered over a PTFE syringe filter. Removal of the solvent yielded a mixture that contained phosphole **46d** and germylene **44d** in a ratio of 7 : 93, in an overall yield of 71%.

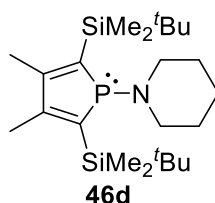


¹H NMR (500.1 MHz, 305 K, C₆D₆) δ = 0.23 (s, 6H, 2 x SiMe₂^tBu), 0.24–0.25 (m, 6H, 2 x SiMe₂^tBu), 1.12 (s, 18H, 2 x SiMe₂^tBu), 1.29–1.34 (m, 6H, NC₅H₁₀), 2.22 (s, 6H, 2 x CH₃), 2.69–2.74 (m, 4H, NC₅H₁₀).

¹³C{¹H} NMR (125.7 MHz, 305 K, C₆D₆) δ = -3.0 (d, ³J_{C,P} = 9 Hz, Si(Me₂)^tBu), -2.1 (d, ³J_{C,P} = 7 Hz, Si(Me₂)^tBu), 16.2 (d, ³J_{C,P} = 4 Hz, C^{2/3}-Me), 18.6–18.7 (m, Si(Me₂)^tBu), 25.5 (NC₅H₁₀), 28.0 (d, ³J_{C,P} = 3 Hz, Si(Me₂)^tBu), 49.3 (d, ²J_{C,P} = 11 Hz, NC₅H₁₀), 73.4 (d, ¹J_{C,P} = 37 Hz, C^{1/4}), 130.4 (d, ²J_{C,P} = 8 Hz, C^{2/3}).

²⁹Si{¹H} INEPT NMR (99.3 MHz, 305 K, C₆D₆) δ = 0.4 (d, ²J_{Si,P} = 17 Hz).

³¹P{¹H} NMR (202.4 MHz, 305 K, C₆D₆) δ = 59.8.



¹H NMR (499.9 MHz, 305 K, C₆D₆): δ = 0.39 (s, 12H, 2 x SiMe₂^tBu), 1.04 (s, 18H, SiMe₂^tBu), 2.06 (d, ⁴J_{H,P} = 5.3 Hz, C^{2/3}-Me). Signals of the piperidino substituent could not be assigned due to low concentration.

¹³C{¹H} NMR (125.7 MHz, 305 K, C₆D₆): δ = 140 (C^{1/4}), 155 (C^{2/3}). Data retrieved from the ¹H¹³C HMBC NMR spectrum. Assignment of the remaining signals was not possible due to low concentration of the phosphole.

²⁹Si{¹H} INEPT NMR (99.3 MHz, 305 K, C₆D₆): δ = -2.9 (d, ²J_{Si,P} = 22 Hz).

³¹P{¹H} NMR (202.4 MHz, 305 K, C₆D₆): δ = 95.9.

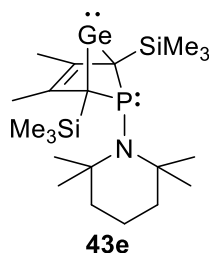
MS: calculated: m/z = 423.29; found (EI): m/z = 423.12 [M⁺].

5.2.7.8 Germylene 43e and Phosphole 45e

The THF solution (6 mL) of dipotassium germylene **K₂[31]**, synthesised by the reduction of dichlorogermole **31** (74 mg, 0.20 mmol) with potassium, was cooled to -50°C. Dichloro(tetramethylpiperidino)phosphane **38e** (48 mg, 0.20 mmol), dissolved in THF (3 mL), was added. The reaction mixture was stirred for 30 minutes whilst it was allowed to warm to

room temperature. After the solvent was removed, the crude product was redissolved in diethyl ether and filtered over a PTFE syringe filter. The solvent was removed and the residue dried in vacuo. NMR spectra were recorded in THF- d_8 immediately after drying. The product mixture contained phosphole **45e** and germylene **43e** in a mixture of 58 : 42.

To isolate the phosphole, the solution that had already changed colour from orange-brown to black, was diluted in pentane and filtered over silica gel. Removal of the solvent gave phosphole **45e** (15 mg, 0.04 mmol, 20%) as light orange solid. Keeping a pentane solution of the compound at -30°C overnight afforded colourless crystals suitable for XRD analysis.

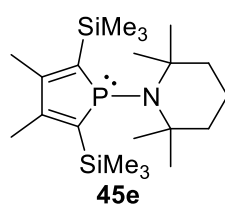


$^1\text{H NMR}$ (500.1 MHz, 305 K, C_6D_6): δ = 0.32 (s, 18H, 2 x SiMe_3), 1.04 (br s, 6H, 2 x TMP-Me), 1.34-1.39 (m, 6H, TMP), 1.73 (br s, 6H, 2 x TMP-Me), 2.19 (s, 6H, Me).

$^{13}\text{C}\{^1\text{H}\}$ NMR (125.7 MHz, 305 K, C_6D_6): δ = 2.2 (d, $^3J_{\text{C,P}} = 6$ Hz, 2 x SiMe_3), 16.4 (d, $^3J_{\text{C,P}} = 5$ Hz, $\text{C}^{2/3}\text{-Me}$), 18.1 (TMP , $\gamma\text{-C}$), 33.4 (2 x TMP-Me), 35.4 (d, $^3J_{\text{C,P}} = 27$ Hz, 2 x TMP-Me), 43.0 (TMP , $\beta\text{-C}$), 43.7 (TMP , $\beta\text{-C}$), 55.5 (d, $^2J_{\text{C,P}} = 12$ Hz, TMP , $\alpha\text{-C}$), 57.3 (d, $^2J_{\text{C,P}} = 25$ Hz, TMP , $\alpha\text{-C}$), 81.9 (d, $^1J_{\text{C,P}} = 48$ Hz, $\text{C}^{1/4}$), 134.1 (d, $^2J_{\text{C,P}} = 8$ Hz, $\text{C}^{2/3}$).

$^{29}\text{Si}\{^1\text{H}\}$ INEPT NMR (99.3 MHz, 305 K, C_6D_6): δ = -7.4 (d, $^2J_{\text{Si,P}} = 23$ Hz).

$^{31}\text{P}\{^1\text{H}\}$ NMR (202.4 MHz, 305 K, C_6D_6): δ = 30.5.



$^1\text{H NMR}$ (499.9 MHz, 305 K, C_6D_6): δ = 0.47 (s, 18H, 2 x SiMe_3), 1.33 (s, 12H, TMP , 4 x Me), 1.45-1.52 (m, 6H, TMP , 3 x CH_2), 2.06 (d, $^4J_{\text{H,P}} = 7.6$ Hz, 6H, 2 x $\text{C}^{2/3}\text{-Me}$).

$^{13}\text{C}\{^1\text{H}\}$ NMR (125.7 MHz, 305 K, C_6D_6): δ = 2.7 (d, $^3J_{\text{C,P}} = 2$ Hz, 2 x SiMe_3), 18.3 (TMP , *para*- C), 18.6 (d, $^3J_{\text{C,P}} = 7$ Hz, $\text{C}^{2/3}\text{-Me}$), 31.9 (d, $^3J_{\text{C,P}} = 8$ Hz, TMP , 4 x Me), 41.5 (d, $^4J_{\text{C,P}} = 2$ Hz, TMP , 2 x *meta*- C), 59.0 (d, $^2J_{\text{C,P}} = 6$ Hz, TMP , 2 x *ortho*- C), 142.7 (d, $^1J_{\text{C,P}} = 34$ Hz, $\text{C}^{1/4}$), 147.0 (d, $^2J_{\text{C,P}} = 26$ Hz, $\text{C}^{2/3}$).

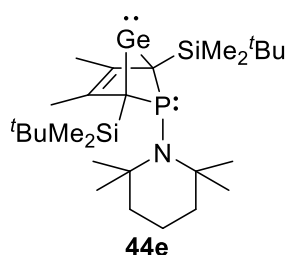
$^{29}\text{Si}\{^1\text{H}\}$ INEPT NMR (99.3 MHz, 305 K, C_6D_6): δ = -9.8 (d, $^2J_{\text{Si,P}} = 25$ Hz).

$^{31}\text{P}\{^1\text{H}\}$ NMR (202.4 MHz, 305 K, C_6D_6): δ = 54.2.

MS: calculated: $m/z = 395.26$; found (EI): $m/z = 395.09$ [M^+].

5.2.7.9 Germylene **44e** and Phosphole **46e**

The THF solution (6 mL) of dipotassium germylene **K₂[36]**, synthesised by the reduction of dichlorogermole **36** (90 mg, 0.20 mmol) with potassium, was cooled to -50°C. Dichlororo(tetramethylpiperidino)phosphane **38e** (48 mg, 0.20 mmol), dissolved in THF (3 mL), was added. The reaction mixture was stirred for 45 minutes whilst it was allowed to warm to room temperature. After the solvent was removed, the crude product was redissolved in pentane/diethyl ether (1:1) and filtered over a PTFE syringe filter. The solvent was removed and NMR spectra of the residue were recorded in benzene-*d*₆. The product mixture contained phosphole **46e** and germylene **44e** (alongside smaller impurities) in a mixture of 15 : 85, in an overall yield of 73%.

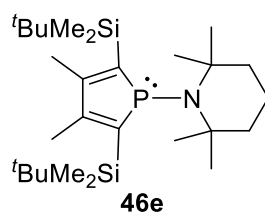


¹H NMR (499.9 MHz, 305 K, C₆D₆): δ = 0.26-0.27 (m, 6H, SiMe₂^tBu), 0.41 (s, 6H, SiMe₂^tBu), 1.01 (s, 3H, TMP-Me), 1.06 (s, 3H, TMP-Me), 1.10 (s, 18H, SiMe₂^tBu), 1.37-1.41 (m, 6H, TMP), 1.73 (s, 6H, 2 x TMP-Me), 2.24 (s, 6H, Me).

¹³C{¹H} NMR (125.7 MHz, 305 K, C₆D₆): δ = -1.9 (d, ³J_{C,P} = 10 Hz, SiMe₂^tBu), -0.5 (d, ³J_{C,P} = 5 Hz, SiMe₂^tBu), 18.0 (d, ³J_{C,P} = 5 Hz, C^{2/3}-Me), 18.2 (TMP, γ-C), 19.5 (d, ³J_{C,P} = 3 Hz, SiMe₂^tBu, ⁴C), 28.7 (SiMe₂^tBu), 33.9 (2 x TMP-Me), 35.1 (d, ³J_{C,P} = 26 Hz, 2 x TMP-Me), 42.3 (d, ³J_{C,P} = 1 Hz, TMP, β-C), 42.7 (d, ³J_{C,P} = 2 Hz, TMP, β-C), 55.6 (d, ²J_{C,P} = 12 Hz, TMP, α-C), 57.9 (d, ²J_{C,P} = 25 Hz, TMP, α-C), 81.6 (d, ¹J_{C,P} = 53 Hz, C^{1/4}), 135.1 (d, ²J_{C,P} = 8 Hz, C^{2/3}).

²⁹Si{¹H} INEPT NMR (99.3 MHz, 305 K, C₆D₆): δ = 0.2 (d, ²J_{Si,P} = 21 Hz).

³¹P{¹H} NMR (202.4 MHz, 305 K, C₆D₆): δ = 39.7.



¹H NMR (499.9 MHz, 305 K, C₆D₆): δ = 0.33 (s, 3H, SiMe₂^tBu), 0.53 (s, 9H, SiMe₂^tBu), 1.09 (s, 18H, SiMe₂^tBu), 2.13 (d, ⁴J_{H,P} = 7.5 Hz, 6H, C^{2/3}-Me).

¹³C{¹H} NMR (125.7 MHz, 305 K, C₆D₆): δ = 0.0 (d, ³J_{C,P} = 3 Hz, SiMe₂^tBu), 19.6 (SiMe₂^tBu, ⁴C), 20.1 (d, ³J_{C,P} = 7 Hz, C^{2/3}-Me), 28.7 (SiMe₂^tBu), 139.7 (d, ¹J_{C,P} = 39 Hz, C^{1/4}), 148.9 (d, ²J_{C,P} = 23 Hz, C^{2/3}). Assignment of the TMP signals was not done due to the low concentration of the phosphole.

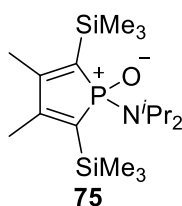
$^{29}\text{Si}\{^1\text{H}\}$ INEPT NMR (99.3 MHz, 305 K, C_6D_6): $\delta = -1.3$ (d, $^2J_{\text{Si,P}} = 22$ Hz).

$^{31}\text{P}\{^1\text{H}\}$ NMR (202.4 MHz, 305 K, C_6D_6): $\delta = 61.2$.

5.2.8 Group 16 Substituted Phospholes

5.2.8.1 Phosphole Oxide **75**

The THF solution (6 mL) of dipotassium germolediide **K₂[31]**, synthesised by the reduction of dichlorogermole **31** (74 mg, 0.20 mmol) with potassium, was cooled to -50°C . Dichloro(diisopropylamino)phosphane **38b** (40 mg, 0.20 mmol), dissolved in THF (3 mL), was added. The reaction mixture was stirred for 15 minutes. The cold bath was removed and the stopper of the Schlenk flask was exchanged for a tube filled with calciumdichloride as drying agent. The argon transfer was stopped and the solution was stirred overnight. A colourless precipitate was formed. The solvent was removed, the residue redissolved in pentane and filtered over a PTFE syringe filter. Removal of the solvent gave phosphole oxide **75** (60 mg, 0.16 mmol, 80%) as oily yellow residue.



^1H NMR (500.1 MHz, 305 K, $\text{C}_6\text{D}_5\text{Cl}$): $\delta = 0.36$ (s, 18H, 2 x SiMe_3), 1.23 (d, $^3J_{\text{H,H}} = 6.9$ Hz, 12H, $\text{N}(\text{CHMe}_2)_2$), 1.70 (d, $^4J_{\text{H,P}} = 2.4$ Hz, 6H, 2 x $\text{C}^{2/3}\text{-Me}$), 3.76 (sept, $^3J_{\text{H,H}} = 6.9$ Hz, 2H, $\text{N}(\text{CHMe}_2)_2$).

$^{13}\text{C}\{^1\text{H}\}$ NMR (125.7 MHz, 305 K, $\text{C}_6\text{D}_5\text{Cl}$): $\delta = 0.5$ (d, $^3J_{\text{C,P}} = 2$ Hz, SiMe_3), 17.6 (d, $^3J_{\text{C,P}} = 26$ Hz, $\text{C}^{2/3}\text{-Me}$), 24.7 ($\text{N}(\text{CHMe}_2)_2$), 45.8 (d, $^2J_{\text{C,P}} = 5$ Hz, $\text{N}(\text{CHMe}_2)_2$), 135.5 (d, $^1J_{\text{C,P}} = 71$ Hz, $\text{C}^{1/4}$), 160.0 (d, $^2J_{\text{C,P}} = 26$ Hz, $\text{C}^{2/3}$).

$^{29}\text{Si}\{^1\text{H}\}$ INEPT NMR (99.3 MHz, 305 K, $\text{C}_6\text{D}_5\text{Cl}$): $\delta = -9.9$ (d, $^2J_{\text{Si,P}} = 16$ Hz).

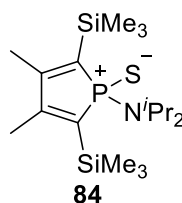
$^{31}\text{P}\{^1\text{H}\}$ NMR (202.4 MHz, 305 K, $\text{C}_6\text{D}_5\text{Cl}$): $\delta = 63.0$.

MS: calculated: $m/z = 371.22$; found (EI): $m/z = 371.05$ [M^+].

5.2.8.2 Phosphole Sulfide **84**

The THF solution (6 mL) of dipotassium germolediide **K₂[31]**, synthesised by the reduction of dichlorogermole **31** (74 mg, 0.20 mmol) with potassium, was cooled to -50°C . Dichloro(diisopropylamino)phosphane **38b** (40 mg, 0.20 mmol), dissolved in THF (3 mL), was added. The reaction mixture was stirred for 30 minutes before the solvent was removed. The residue was dissolved in toluene and filtered into a vial, equipped with cyclooctasulfur (13 mg,

0.05 mmol). Stirring overnight afforded a yellow solution with a colourless precipitate. Solid and solution were separated by centrifugation. The solvent was removed from the solution to give phosphole sulfide **84** (68 mg, 0.18 mmol, 90%) as yellow solid.



$^1\text{H NMR}$ (500.1 MHz, 305 K, $\text{C}_6\text{D}_5\text{Cl}$): δ = 0.43 (s, 18H, 2 x SiMe_3), 1.18 (d, $^3J_{\text{H,H}} = 7.0$ Hz, 12H, $\text{N}(\text{CHMe}_2)_2$), 1.69 (d, $^4J_{\text{H,P}} = 2.4$ Hz, 6H, 2 x $\text{C}^{2/3}\text{-Me}$), 4.19 (sept, $^3J_{\text{H,H}} = 7.0$ Hz, 2H, $\text{N}(\text{CHMe}_2)_2$).

$^{13}\text{C}\{^1\text{H}\}$ NMR (125.7 MHz, 305 K, $\text{C}_6\text{D}_5\text{Cl}$): δ = 0.9 (d, $^3J_{\text{C,P}} = 2$ Hz, SiMe_3), 17.4 (d, $^3J_{\text{C,P}} = 25$ Hz, $\text{C}^{2/3}\text{-Me}$), 25.1 (d, $^3J_{\text{C,P}} = 3$ Hz, $\text{N}(\text{CHMe}_2)_2$), 47.4 (d, $^2J_{\text{C,P}} = 7$ Hz, $\text{N}(\text{CHMe}_2)_2$), 138.9 (d, $^1J_{\text{C,P}} = 52$ Hz, $\text{C}^{1/4}$), 156.8 (d, $^2J_{\text{C,P}} = 22$ Hz, $\text{C}^{2/3}$).

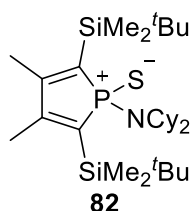
$^{29}\text{Si}\{^1\text{H}\}$ INEPT NMR (99.3 MHz, 305 K, $\text{C}_6\text{D}_5\text{Cl}$): δ = -9.3 (d, $^2J_{\text{Si,P}} = 18$ Hz).

$^{31}\text{P}\{^1\text{H}\}$ NMR (202.4 MHz, 305 K, $\text{C}_6\text{D}_5\text{Cl}$): δ = 92.0.

MS: calculated: $m/z = 387.20$; found (EI): $m/z = 387.01$ [M^+].

5.2.8.3 Phosphole Sulfide **82**

To a toluene/pentane solution of germylene **44c** (215 mg, 0.36 mmol), cyclooctasulfur (12 mg, 0.045 mmol) was added at room temperature. It was stirred for 20 minutes. After that time, a colourless precipitate was formed which was identified as germaniumsulfide after qualitative proof of sulfide ions. Monitoring the reaction revealed that it was not complete. An excess amount of cyclooctasulfur was added and the mixture was stirred overnight. The precipitates were filtered off and the solvent was removed. Phosphole sulfide **82** (145 mg, 0.26 mmol, 72%) was isolated as a yellow solid.



$^1\text{H NMR}$ (500.1 MHz, 305 K, C_6D_6): δ = 0.28 (s, 6H, SiMe_2^tBu), 0.60 (s, 6H, SiMe_2^tBu), 0.94-1.04 (m, 5H, Cy), 1.08 (s, 18H, SiMe_2^tBu), 1.17-1.27 (m, 5H, Cy), 1.50-1.60 (m, 6H, Cy), 1.68-1.74 (m, 4H, Cy), 1.88 (d, $^4J_{\text{H,H}} = 2.3$ Hz, 6H, 2 x CH_3), 1.91-1.96 (m, 4H, Cy), 3.73-3.85 (m, 2H, Cy, 2 x HC^{ipso}).

$^{13}\text{C}\{^1\text{H}\}$ NMR (125.7 MHz, 305 K, C_6D_6): $\delta = -3.0$ (SiMe_2^tBu), -1.7 (SiMe_2^tBu), 19.4 (SiMe_2^tBu , C^4), 19.6 ($\text{C}^{2/3}\text{-Me}$), 26.3 (Cy), 27.9 (Cy), 28.7 (SiMe_2^tBu), 36.7 (d, $^3J_{\text{C,P}} = 3$ Hz, Cy), 56.9 (d, $^2J_{\text{C,P}} = 5$ Hz, Cy, C^{ipso}), 137.4 (d, $^1J_{\text{C,P}} = 49$ Hz, $\text{C}^{1/4}$), 158.6 (d, $^2J_{\text{C,P}} = 21$ Hz, $\text{C}^{2/3}$).

$^{29}\text{Si}\{^1\text{H}\}$ INEPT NMR (99.3 MHz, 305 K, C_6D_6): $\delta = -2.1$ (d, $^2J_{\text{Si,P}} = 16$ Hz).

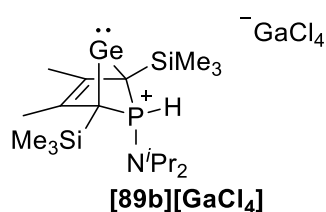
$^{31}\text{P}\{^1\text{H}\}$ NMR (202.4 MHz, 305 K, C_6D_6): $\delta = 95.8$ ($^2J_{\text{P,Si}} = 16$ Hz).

MS: calculated: $m/z = 551.36$; found (EI): $m/z = 551.16$ [M^+].

5.2.9 Phosphonium & Phospholium Salts

5.2.9.1 Phosphonium-BCH-Germylene Gallate [89b][GaCl₄]

The THF solution (6 mL) of dipotassium germolediide **K₂[31]**, synthesised by the reduction of dichlorogermole **31** (74 mg, 0.20 mmol) with potassium, was cooled to -50°C . Dichloro(diisopropylamino)phosphane **38b** (40 mg, 0.20 mmol), dissolved in THF (3 mL), was added. The solution was stirred for 5 minutes before a diethyl ether solution of $\text{H}^+ \text{GaCl}_4^-$, prepared from galliumtrichloride (35 mg, 0.20 mmol) and HCl (2M in Et_2O , 0.1 mL, 0.20 mmol), was added. The solution turned yellowish immediately. The cold bath was removed and the solution was stirred for 30 minutes at room temperature. Afterwards, the solvent was removed. The residue was dissolved in diethyl ether and filtered over a PTFE syringe filter. Recrystallisation from toluene yielded phosphonium gallate [89b][GaCl₄] (24 mg, 0.04 mmol, 20%) as colourless crystals, suitable for XRD analysis.



^1H NMR (500.1 MHz, 305 K, C_6D_6): $\delta = 0.35$ (s, 18H, 2 x SiMe_3), 0.80 (d, $^3J_{\text{H,H}} = 6.8$ Hz, 12 H, $\text{N}(\text{CHMe}_2)_2$), 1.91 (d, $^4J_{\text{H,P}} = 0.9$ Hz, 6H, $\text{C}^{2/3}\text{-Me}$), 2.99 (dsept, $^3J_{\text{H,P}} = 15.0$ Hz, $^3J_{\text{H,H}} = 6.8$ Hz, 2H, $\text{N}(\text{CHMe}_2)_2$), 7.97 (d, $^1J_{\text{H,P}} = 569.1$ Hz, 1H, P-H).

$^{13}\text{C}\{^1\text{H}\}$ NMR (125.7 MHz, 305 K, C_6D_6): $\delta = 1.0$ (d, $^3J_{\text{C,P}} = 4$ Hz, SiMe_3), 15.0 (d, $^3J_{\text{C,P}} = 6$ Hz, $\text{C}^{2/3}\text{-Me}$), 23.6 (d, $^3J_{\text{C,P}} = 2$ Hz, $\text{N}(\text{CHMe}_2)_2$), 48.4 (d, $^2J_{\text{C,P}} = 2$ Hz, $\text{N}(\text{CHMe}_2)_2$), 59.7 (d, $^1J_{\text{C,P}} = 48$ Hz, $\text{C}^{1/4}$), 124.5 (d, $^2J_{\text{C,P}} = 9$ Hz, $\text{C}^{2/3}$).

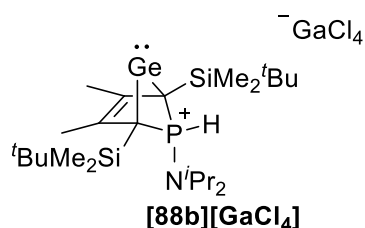
$^{29}\text{Si}\{^1\text{H}\}$ INEPT NMR (99.3 MHz, 305 K, C_6D_6): $\delta = -8.1$ (d, $^2J_{\text{Si,P}} = 3$ Hz).

^{31}P NMR (202.4 MHz, 305 K, C_6D_6): $\delta = 31.0$ (dt, $^1J_{\text{P,H}} = 569$ Hz (P-H), $^3J_{\text{P,H}} = 15$ Hz (P- $\text{N}(\text{CHMe}_2)_2$)).

$^{71}\text{Ga}\{^1\text{H}\}$ NMR (160.4 MHz, 305 K, C_6D_6): $\delta = 249.9$ (br).

5.2.9.2 Phosphonium-BCH-Germylene Gallate [88b][GaCl₄]

To a toluene/diethyl ether (4 mL) solution of germylene **44b** (0.20 mmol), a diethyl ether solution of H⁺ GaCl₄⁻, prepared from galliumtrichloride (35 mg, 0.20 mmol) and HCl (2M in Et₂O, 0.1 mL, 0.20 mmol), was added. The solution turned yellow immediately. It was stirred for 5 minutes at -30°C and afterwards 30 minutes at room temperature. A colourless precipitate had formed during that time. The solvent was removed and the residue was washed with pentane and toluene. Phosphonium-BCH-germylene gallate [88b][GaCl₄] was isolated as colourless solid. After a couple of hours in THF solution, the substance started to deprotonate and give the starting material, germylene **44b**, back.



¹H NMR (500.1 MHz, 305 K, THF-d₈): δ = 0.39 (s, 6H, SiMe₂tBu), 0.42 (s, 6H, SiMe₂tBu), 1.03 (s, 18H, SiMe₂tBu), 1.28 (d, ³J_{H,H} = 6.7 Hz, 12H, N(CHMe₂)₂), 2.53 (s, 6H, C^{2/3}-Me), 3.59-3.66 (m, 2H, N(CHMe₂)₂), 7.78 (d, ¹J_{H,P} = 580.3 Hz, 1H, P-H).

¹³C{¹H} NMR (125.7 MHz, 305 K, THF-d₈): δ = -2.9 (d, ³J_{C,P} = 1 Hz, SiMe₂tBu), -2.8 (d, ³J_{C,P} = 4 Hz, SiMe₂tBu), 16.8 (d, ³J_{C,P} = 5 Hz, C^{2/3}-Me), 19.4 (d, ³J_{C,P} = 6 Hz, SiMe₂tBu, C⁴), 24.4 (d, ³J_{C,P} = 3 Hz, N(CHMe₂)₂), 28.3 (SiMe₂tBu), 50.5 (m, N(CHMe₂)₂), 67.8 (C^{1/4}, hidden under solvent signal), 129.3 (d, ²J_{C,P} = 12 Hz, C^{2/3}).

²⁹Si{¹H} INEPT NMR (99.3 MHz, 305 K, THF-d₈): δ = 0.5 (d, ²J_{Si,P} = 2 Hz).

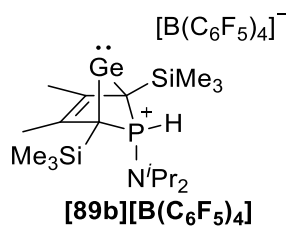
³¹P NMR (202.4 MHz, 305 K, THF-d₈): δ = 25.7 (dt, ¹J_{P,H} = 580 Hz (P-H), ³J_{P,H} = 15 Hz (P-N(CHMe₂)₂)).

⁷¹Ga{¹H} NMR (160.4 MHz, 305 K, THF-d₈): δ = 248.2.

5.2.9.3 Phosphonium-BCH-Germylene Borate [89b][B(C₆F₅)₄]

The THF solution (6 mL) of dipotassium germylene **K₂[31]**, synthesised by the reduction of dichlorogermole **31** (74 mg, 0.20 mmol) with potassium, was cooled to -50°C. Dichloro(diisopropylamino)phosphane **38b** (40 mg, 0.20 mmol), dissolved in THF (3 mL), was added. The solution was stirred for 5 minutes before hydrochloric acid (2M in Et₂O, 0.1 mL) was added. It was stirred for 10 minutes at that temperature. Afterwards, the solvent was removed. The residue was dissolved in chlorobenzene-d₅ (1.5 mL) and added to a Schlenk flask, equipped with potassium borate K[B(C₆F₅)₄] (144 mg, 0.20 mmol). The solution was stirred overnight at room temperature, before NMR spectra were recorded. Removal of the solvent gave

phosphonium-BCH-germylene borate **[89b][B(C₆F₅)₄]** (177 mg, 0.16 mmol, 80%) was received as slightly yellow solid.



¹H NMR (500.1 MHz, 305 K, C₆D₅Cl): δ = 0.04 (s, 18H, 2 x SiMe₃), 0.83 (d, ³J_{H,H} = 6.8 Hz, 12H, N(CHMe₂)₂), 2.03 (s, 6H, C^{2/3}-Me), 2.83-3.05 (m, 2H, N(CHMe₂)₂), 6.86 (d, ¹J_{H,P} = 568.8 Hz, 1H, P-H).

¹³C{¹H} NMR (125.7 MHz, 305 K, C₆D₅Cl): δ = 0.0 (d, ³J_{C,P} = 3 Hz, SiMe₃), 14.4 (d, ³J_{C,P} = 5 Hz, C^{2/3}-Me), 23.5 (N(CHMe₂)₂), 49.1-49.2 (m, N(CHMe₂)₂), 70.2 (d, ¹J_{C,P} = 52 Hz, C^{1/4}), 127.7 (d, ²J_{C,P} = 14 Hz, C^{2/3}).

²⁹Si{¹H} INEPT NMR (99.3 MHz, 305 K, C₆D₅Cl): δ = -6.4 (d, ²J_{Si,P} = 4 Hz).

³¹P{¹H} NMR (202.4 MHz, 305 K, C₆D₅Cl): δ = 14.5.

¹¹B{¹H} NMR (160.4 MHz, 305 K, C₆D₅Cl): δ = -16.0.

¹H NMR (500.1 MHz, 305 K, THF-d₈): δ = 0.30 (s, 18H, 2 x SiMe₃), 1.21 (d, ³J_{H,H} = 6.9 Hz, 12H, N(CHMe₂)₂), 2.17 (s, 6H, C^{2/3}-Me), 3.46-3.54 (m, 2H, N(CHMe₂)₂), 7.88 (d, ¹J_{H,P} = 579.7 Hz, 1H, P-H).

¹³C{¹H} NMR (125.7 MHz, 305 K, THF-d₈): δ = 1.0 (d, ³J_{C,P} = 4 Hz, SiMe₃), 15.1 (d, ³J_{C,P} = 6 Hz, C^{2/3}-Me), 24.2 (d, ³J_{C,P} = 2 Hz, N(CHMe₂)₂), 49.4 (d, ²J_{C,P} = 2 Hz, N(CHMe₂)₂), 60.6 (d, ¹J_{C,P} = 49 Hz, C^{1/4}), 125.6 (d, ²J_{C,P} =) Hz, C^{2/3}).

²⁹Si{¹H} INEPT NMR (99.3 MHz, 305 K, THF-d₈): δ = -7.6 (d, ²J_{Si,P} = 3 Hz).

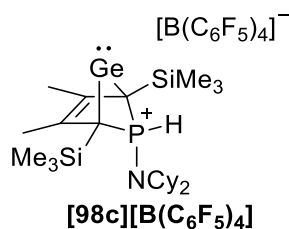
³¹P{¹H} NMR (202.4 MHz, 305 K, THF-d₈): δ = 28.4.

¹¹B{¹H} NMR (160.4 MHz, 305 K, THF-d₈): δ = -16.6.

5.2.9.4 Phosphonium-BCH-Germylene Borate **[89c][B(C₆F₅)₄]**

The THF solution (6 mL) of dipotassium germodiide **K₂[31]**, synthesised by the reduction of dichlorogermole **31** (148 mg, 0.40 mmol) with potassium, was cooled to -50°C. Dichloro(dicyclohexylamino)phosphane **38c** (112 mg, 0.20 mmol), dissolved in THF (5 mL), was added. The solution was stirred for 5 minutes before hydrochloric acid (2M in Et₂O, 0.1 mL) was added. It was stirred for 10 minutes at that temperature. Afterwards, the solvent was removed. The residue was dissolved in toluene (5 mL) and added to a Schlenk flask equipped with potassium borate (288 mg, 0.40 mmol). The solution was stirred overnight at room temperature.

The precipitates settled to the bottom and the solution was transferred into another flask. The solvent was removed and phosphonium-BCH-germylene borate **[89c][B(C₆F₅)₄]** (368 mg, 0.31 mmol, 78%) was received as slightly yellow solid.



¹H NMR (500.1 MHz, 305 K, C₆D₅Cl): δ = 0.06 (s, 18H, 2 x SiMe₃), 0.77-0.88 (m, 2H, NCy₂), 0.98-1.09 (m, 4H, NCy₂), 1.09-1.19 (m, 4H, NCy₂), 1.38-1.45 (m, 4H, NCy₂), 1.45-1.51 (m, 2H, NCy₂), 1.60-1.67 (m, 4H, NCy₂), 2.05 (s, 6H, C^{2/3}-Me), 2.53-2.67 (m, 2H, NCy₂), 6.96 (d, ¹J_{H,P} = 567.0 Hz, 1H, P-H).

¹³C{¹H} NMR (125.7 MHz, 305 K, C₆D₅Cl): δ = -0.1 (d, ³J_{C,P} = 3 Hz, SiMe₃), 14.4 (d, ³J_{C,P} = 5 Hz, C^{2/3}-Me), 25.1 (NCy₂), 26.2 (NCy₂), 35.0-35.1 (NCy₂), 58.5 (NCy₂), 69.9 (d, ¹J_{C,P} = 52 Hz, C^{1/4}), 127.6 (d, ²J_{C,P} = 13 Hz, C^{2/3}).

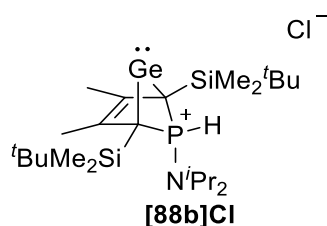
²⁹Si{¹H} INEPT NMR (99.3 MHz, 305 K, C₆D₅Cl): δ = -6.4 (d, ²J_{Si,P} = 4 Hz).

³¹P{¹H} NMR (202.4 MHz, 305 K, C₆D₅Cl): δ = 13.4.

¹¹B{¹H} NMR (160.4 MHz, 305 K, C₆D₅Cl): δ = -16.1.

5.2.9.5 Phosphonium-BCH-Germylene Chloride **[88b]Cl**

Phospha-BCH-germylene **44b** was freshly prepared from dipotassium germylene **K₂[36]** (0.20 mmol, 90 mg) and dichlorodiisopropylaminophosphane **38b** (0.20 mmol, 40 mg) according to the standard procedure. The solvent of the reaction mixture was removed. The residue was dissolved in pentane/Et₂O and filtered over a PTFE syringe filter. The filtrate was cooled to 0°C and HCl in Et₂O (2M, 0.1 mL) was added. The colour of the solution immediately changed from orange to yellow and a colourless precipitate was formed. After 15 minutes of stirring, the solution was restricted in volume and the precipitate was allowed to settle over night. The solution was removed via teflon tube. The colourless solid was dried *in vacuo*. Before NMR spectra were recorded in benzene-d₆. The phosphonium salt **[88b]Cl** decomposes over time to give the phosphole **46b**.



^1H NMR (500.1 MHz, 305 K, C_6D_6) δ = 0.24 (s, 6H, 2 x SiMe_2^tBu), 0.47 (s, 6H, 2 x SiMe_2^tBu), 0.93 (d, $^3J_{\text{H,H}} = 6.7$ Hz, 12H, $\text{N}(\text{CHMe}_2)_2$), 1.07 (s, 18H, 2 x SiMe_2^tBu), 2.01 (s, 6H, $\text{C}^{2/3}\text{-Me}$), 3.28 (sept, $^3J_{\text{H,H}} = 6.7$ Hz, 2H, $\text{N}(\text{CHMe}_2)_2$), 8.10 (d, $^1J_{\text{H,P}} = 577.8$ Hz, 1H, P-H).

$^{13}\text{C}\{^1\text{H}\}$ NMR (125.7 MHz, 305 K, C_6D_6) δ = -2.3 (d, $^3J_{\text{C,P}} = 4$ Hz, SiMe_2^tBu), 16.6 (d, $^3J_{\text{C,P}} = 6$ Hz, $\text{C}^{2/3}\text{-Me}$), 19.6 (d, $^3J_{\text{C,P}} = 7$ Hz, SiMe_2^tBu , C^4), 24.2 (d, $^3J_{\text{C,P}} = 2$ Hz, $\text{N}(\text{CHMe}_2)_2$), 29.0 (SiMe_2^tBu), 49.5 (d, $^2J_{\text{C,P}} = 3$ Hz, $\text{N}(\text{CHMe}_2)_2$), 62.5 (d, $^1J_{\text{C,P}} = 43$ Hz, $\text{C}^{1/4}$), 126.6 (d, $^2J_{\text{C,P}} = 9$ Hz, $\text{C}^{2/3}$).

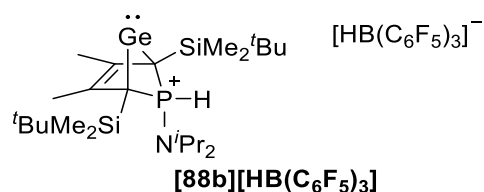
$^{29}\text{Si}\{^1\text{H}\}$ INEPT NMR (99.3 MHz, 305 K, C_6D_6): δ = -1.3.

^{31}P NMR (202.4 MHz, 305 K, C_6D_6): δ = 35.2 (d, $^1J_{\text{P,H}} = 577$ Hz).

5.2.9.6 Dihydrogen Activation with Germylene **44b** and BCF

To a mixture of germylene **44b** (36 mg, 0.07 mmol) and tris(pentafluorophenyl)borane (36 mg, 0.07 mmol) toluene- d_8 was added. The solution was stirred for one hour at room temperature before NMR spectra were recorded. No product formation occurred. The spectroscopic data matches the starting materials. The NMR sample was degassed via 2 cycles of the freeze-pump-thaw method and afterwards exposed to dihydrogen gas. After 10 minutes, the NMR tube was sealed and NMR spectra were recorded.

The reaction gave about 40% of the dihydrogen activation product, phosphonium-BCH-germylene borate **[88b][HB(C₆F₅)₃]**, alongside follow-up products due to integration in the NMR spectra. Spectroscopic data was collected out of the reaction mixture. $^{13}\text{C}\{^1\text{H}\}$ NMR data was extracted from the $^1\text{H}^{13}\text{C}$ HMBC NMR spectrum.



^1H NMR (500.1 MHz, 305 K, toluene- d_8): δ = -0.06 (s, 6H, SiMe_2^tBu), -0.04 (s, 6H, SiMe_2^tBu), 0.69 (s, 18H, SiMe_2^tBu), 0.74 (d, 12H, $^3J_{\text{H,H}} = 6.8$ Hz, $\text{N}(\text{CHMe}_2)_2$), 1.91 (s, 6H, $\text{C}^{2/3}\text{-Me}$), 2.82-2.94 (m, 2H, $\text{N}(\text{CHMe}_2)_2$), 3.74 (br, 1H, B-H), 6.74 (d, 1H, $^1J_{\text{H,P}} = 570.7$ Hz, P-H).

$^{13}\text{C}\{^1\text{H}\}$ NMR (125.7 MHz, 305 K, toluene- d_8): δ = -3.2 (SiMe_2^tBu), 16.4 ($\text{C}^{2/3}\text{-Me}$), 18.8 (SiMe_2^tBu), 23.9 ($\text{N}(\text{CHMe}_2)_2$), 27.8 (SiMe_2^tBu), 50.7 ($\text{N}(\text{CHMe}_2)_2$), 69.6 ($\text{C}^{1/4}$), 129.6 ($\text{C}^{2/3}$).

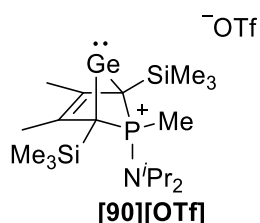
^{11}B NMR (160.4 MHz, 305 K, toluene- d_8): δ = -23.6 (d, $^1J_{\text{B,H}} = 82$ Hz).

$^{19}\text{F}\{^1\text{H}\}$ NMR (470.3 MHz, 305 K, toluene- d_8): $\delta = -159.5$ (t, 6F, $J = 21$ Hz), -132.6 (d, 3F, $J = 20$ Hz), -131.5 (d, 6F, $J = 22$ Hz).

$^{31}\text{P}\{^1\text{H}\}$ NMR (202.4 MHz, 305 K, toluene- d_8): $\delta = 22.7$.

5.2.9.7 Methylphosphonium-BCH-Germylene Triflate [90][OTf]

Germylene **43b** was prepared as described above. After addition of the dichlorophosphane, the mixture was only stirred for 5 minutes before the solvent was removed in the cold. The residue was dissolved in pentane (6 mL) and methyltriflate (33 mg, 0.20 mmol) was added immediately after. It was stirred for two hours whilst the reaction was allowed to warm to room temperature. The methylphosphonium salt precipitates upon formation. The solution was removed via syringe and the residue was washed with pentane (2 x 3 mL). It was dried *in vacuo* to give methylphosphonium triflate [90][OTf] as a colourless solid.



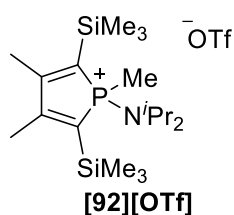
^1H NMR (500.1 MHz, 305 K, $\text{C}_6\text{D}_5\text{Cl}$): $\delta = 0.13$ (s, 18H, 2 x SiMe_3), 0.90 (d, $^3J_{\text{H,H}} = 7.1$ Hz, 12H, $\text{N}(\text{CHMe}_2)_2$), 2.07 (s, 6H, 2 x $\text{C}^{2/3}\text{-Me}$), 2.35 (d, $^2J_{\text{H,P}} = 12.6$ Hz, 2H, P-Me), 3.03 (sept, $^3J_{\text{H,H}} = 7.1$ Hz, 2H, $\text{N}(\text{CHMe}_2)_2$).

$^{13}\text{C}\{^1\text{H}\}$ NMR (125.7 MHz, 305 K, $\text{C}_6\text{D}_5\text{Cl}$): $\delta = 0.2$ (d, $^3J_{\text{C,P}} = 3$ Hz, SiMe_3), 12.6 (d, $^1J_{\text{C,P}} = 92$ Hz, P-Me), 14.3 (d, $^3J_{\text{C,P}} = 5$ Hz, $\text{C}^{2/3}\text{-Me}$), 22.6 ($\text{N}(\text{CHMe}_2)_2$), 47.5 ($\text{N}(\text{CHMe}_2)_2$), 67.2 (d, $^1J_{\text{C,P}} = 57$ Hz, $\text{C}^{1/4}$), 125.4 (d, $^2J_{\text{C,P}} = 11$ Hz, $\text{C}^{2/3}$).

$^{29}\text{Si}\{^1\text{H}\}$ INEPT NMR (99.3 MHz, 305 K, $\text{C}_6\text{D}_5\text{Cl}$): $\delta = -5.9$ (d, $^2J_{\text{Si,P}} = 5$ Hz).

$^{31}\text{P}\{^1\text{H}\}$ NMR (202.4 MHz, 305 K, $\text{C}_6\text{D}_5\text{Cl}$): $\delta = 54.5$.

The methylphosphonium triflate [92][OTf] was formed upon elimination of elemental germanium from the methylphosphonium triflate [90][OTf].



¹H NMR (500.1 MHz, 305 K, C₆D₅Cl): δ = 0.22 (s, 18H, 2 x SiMe₃), 1.05 (d, ³J_{H,H} = 6.8 Hz, 12H, N(CHMe₂)₂), 2.03 (d, ²J_{H,P} = 11.1 Hz, 3H, P-Me), 2.04 (d, ⁴J_{H,P} = 2.5 Hz, 6H, 2 x C^{2/3}-Me), 3.41 (sept, ³J_{H,H} = 6.8 Hz, 2H, N(CHMe₂)₂).

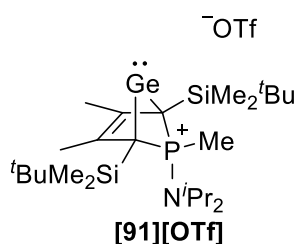
¹³C{¹H} NMR (125.7 MHz, 305 K, C₆D₅Cl): δ = 0.1 (d, ³J_{C,P} = 2 Hz, SiMe₃), 7.8 (d, ¹J_{C,P} = 63 Hz, P-Me), 18.8 (d, ³J_{C,P} = 25 Hz, C^{2/3}-Me), 23.9 (d, ³J_{C,P} = 3 Hz, N(CHMe₂)₂), 50.4 (d, ²J_{C,P} = 4 Hz, N(CHMe₂)₂), 128.0 (d, ¹J_{C,P} = 47 Hz, C^{1/4}), 169.7 (d, ²J_{C,P} = 22 Hz, C^{2/3}).

²⁹Si{¹H} INEPT NMR (99.3 MHz, 305 K, C₆D₅Cl): δ = -7.7 (d, ²J_{Si,P} = 16 Hz).

³¹P{¹H} NMR (202.4 MHz, 305 K, C₆D₅Cl): δ = 71.7.

5.2.9.8 Methylphosphonium-BCH-Germylene Triflate [91][OTf]

To a toluene solution of germylene **44b** (2 mL, 0.20 mmol), pentane (3 mL) was added. The solution was cooled to -30°C and methyltriflate (33 mg, 0.20 mmol) was added. The solution turned yellow immediately. Over the period of 30 minutes the solution was allowed to warm to room temperature. During that time a colourless precipitate had formed. The solvent was removed via teflon tube. The yellow residue was washed with pentane (2 x 2 mL) before it was dried under vacuum to give methylphosphonium-BCH-germylene triflate **[91][OTf]** (83 mg, 0.12 mmol, 60%) as a colourless solid. The recorded NMR spectra show that the product contained 2% of methylphosphonium triflate **[93][OTf]** which was presumably formed from the small amount of phosphole included in the starting material.



¹H NMR (500.1 MHz, 305 K, C₆D₅Cl): δ = 0.14 (s, 6H, SiMe₂^tBu), 0.15 (s, 6H, SiMe₂^tBu), 0.82 (s, 18H, SiMe₂^tBu), 1.03 (d, ³J_{H,H} = 6.9 Hz, 12H, N(CHMe₂)₂), 2.16 (s, 6H, 2 x C^{2/3}-Me), 2.30 (d, ²J_{H,P} = 11.6 Hz, 3H, P-Me), 3.32 (d, sept, ³J_{H,P} = 11.6 Hz, ³J_{H,H} = 6.9 Hz, 2H, N(CHMe₂)₂).

¹³C{¹H} NMR (125.7 MHz, 305 K, C₆D₅Cl): δ = -2.9 (d, ³J_{C,P} = 3 Hz, SiMe₂^tBu), -2.2 (SiMe₂^tBu), 13.3 (d, ¹J_{C,P} = 98 Hz, P-Me), 16.5 (d, ³J_{C,P} = 6 Hz, C^{2/3}-Me), 18.8 (d, ³J_{C,P} = 6 Hz, SiMe₂^tBu, C⁴), 23.9 (d,

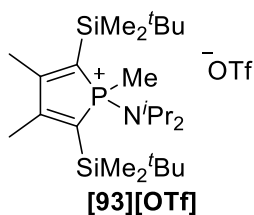
$^3J_{C,P} = 3$ Hz, $N(\underline{CHMe}_2)_2$, 27.5 ($SiMe_2^tBu$), 50.0 ($N(\underline{CHMe}_2)_2$), 68.4 (d, $^1J_{C,P} = 51$ Hz, $\underline{C}^{1/4}$), 128.0 (d, $^2J_{C,P} = 12$ Hz, $\underline{C}^{2/3}$).

$^{29}Si\{^1H\}$ INEPT NMR (99.3 MHz, 305 K, C_6D_5Cl): $\delta = 0.5$ (d, $^2J_{Si,P} = 2$ Hz).

^{31}P NMR (202.4 MHz, 305 K, C_6D_5Cl): $\delta = 57.5$ (sext, $^2J_{P,H} (P-\underline{CH}_3) = ^3J_{P,H} (N(\underline{CHMe}_2)_2) = 12$ Hz).

MS: calculated: $m/z = 528.27$; found (EI): $m/z = 528.12 [M^+]$.

The methylphospholium triflate **[93][OTf]** was additionally formed upon germanium elimination from the methylphosphonium-BCH-germylene triflate **[91][OTf]** after reaction with $(COD)Pd(CH_2SiMe_3)_2$.



1H NMR (500.1 MHz, 305 K, C_6D_5Cl): $\delta = 0.23$ (s, 6H, $SiMe_2^tBu$), 0.23 (s, 6H, $SiMe_2^tBu$), 0.82 (s, 18H, $SiMe_2^tBu$), 1.19 (d, $^3J_{H,H} = 6.8$ Hz, 12H, $N(\underline{CHMe}_2)_2$), 2.10 (d, $^2J_{P,H} = 11.5$ Hz, 3H, $P-\underline{Me}$), 2.15 (d, $^4J_{P,H} = 2.4$ Hz, 6H, $\underline{C}^{2/3}-\underline{Me}$), 3.57 (dsept, $^3J_{P,H} = 12$ Hz, $^3J_{H,H} = 6.8$ Hz, 2H, $N(\underline{CHMe}_2)_2$).

$^{13}C\{^1H\}$ NMR (125.7 MHz, 305 K, C_6D_5Cl): $\delta = -3.2$ ($SiMe_2^tBu$), -3.1 (d, $^3J_{C,P} = 4$ Hz, $SiMe_2^tBu$), 8.5 (d, $^1J_{C,P} = 62$ Hz, $P-\underline{Me}$), 21.0 (d, $^3J_{C,P} = 25$ Hz, $\underline{C}^{2/3}-\underline{Me}$), 24.5 (d, $^3J_{C,P} = 3$ Hz, $N(\underline{CHMe}_2)_2$), 27.7 ($SiMe_2^tBu$), 50.9 (d, $^2J_{C,P} = 4$ Hz, $N(\underline{CHMe}_2)_2$), 127.1 (d, $^1J_{C,P} = 44$ Hz, $\underline{C}^{1/4}$), 171.4 (d, $^2J_{C,P} = 21$ Hz, $\underline{C}^{2/3}$).

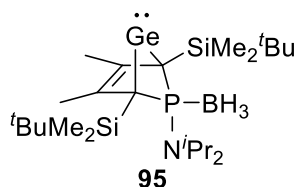
$^{29}Si\{^1H\}$ INEPT NMR (99.3 MHz, 305 K, C_6D_5Cl): $\delta = -0.7$ (d, $^2J_{Si,P} = 14$ Hz).

^{31}P NMR (202.4 MHz, 305 K, C_6D_5Cl): $\delta = 75.2$ (sextd, $^2J_{P,H} (P-\underline{CH}_3) = ^3J_{P,H} (N(\underline{CHMe}_2)_2) = 12$ Hz, $^4J_{P,H} (P-\underline{C}^{2/3}-\underline{Me}) = 2$ Hz).

MS: calculated: $m/z = 454.34$; found (EI): $m/z = 454.18 [M^+]$.

5.2.9.9 Germylene-Borane Adduct **95**

At $-20^\circ C$, borane-dimethylsulfide adduct (15 mg, 0.20 mmol) was added to a toluene solution of germylene **44b** (2 mL, 0.20 mmol). It was stirred 15 minutes at that temperature and another 15 minutes at room temperature. The solvent as well as residual borane adduct were removed under vacuum. Phospha-BCH-germylene-borane adduct **95** was obtained as pale yellow oil (79 mg, 0.15 mmol, 75%). According to integration in the $^{31}P\{^1H\}$ NMR spectrum, the product contained 5% of the phosphole-borane adduct **96**.



^1H NMR (500.1 MHz, 305 K, toluene- d_8): δ = 0.23 (s, 6H, SiMe_2^tBu), 0.62 (s, 6H, SiMe_2^tBu), 0.99 (s, 18H, SiMe_2^tBu), 0.8-1.4 (br, BH_3), 1.09 (d, $^3J_{\text{H,H}} = 7.0$ Hz, 12H, $\text{N}(\text{CHMe}_2)_2$), 2.08 (s, 6H, $\text{C}^{2/3}\text{-Me}$), 3.71-3.82 (m, 2H, $\text{N}(\text{CHMe}_2)_2$).

$^{13}\text{C}\{^1\text{H}\}$ NMR (125.7 MHz, 305 K, toluene- d_8): δ = -1.6 (d, $^3J_{\text{C,P}} = 2$ Hz, SiMe_2^tBu), -0.6 (SiMe_2^tBu), 16.9 ($\text{C}^{2/3}\text{-Me}$), 19.6 (d, $^3J_{\text{C,P}} = 6$ Hz, SiMe_2^tBu , C^4), 24.6 ($\text{N}(\text{CHMe}_2)_2$), 27.9 (SiMe_2^tBu), 49.7 ($\text{N}(\text{CHMe}_2)_2$), 71.0 (d, $^1J_{\text{C,P}} = 17$ Hz, $\text{C}^{1/4}$), 128.6 ($\text{C}^{2/3}$).

$^{29}\text{Si}\{^1\text{H}\}$ INEPT NMR (99.3 MHz, 305 K, toluene- d_8): δ = 0.8 (d, $^2J_{\text{Si,P}} = 7$ Hz).

^{31}P NMR (202.4 MHz, 305 K, toluene- d_8): δ = 79.6-83.0 (m).

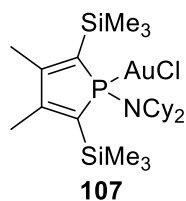
^{11}B NMR (160.4 MHz, 305 K, toluene- d_8): δ = (-35.1)-(-31.6) (m).

MS: calculated: $m/z = 527.28$; found (EI): $m/z = 527.10$ [M^+].

5.2.10 Transition Metal Complexes

5.2.10.1 Phosphole Gold Complex 107

Dicyclohexylaminophosphole **45c** (27 mg, 0.06 mmol) and dimethylsulfide gold(I)chloride (**106**) (18 mg, 0.06 mmol) were dissolved in THF (3 mL) and stirred for 2 hours at room temperature. Afterwards, the solvent was removed to give the phosphole gold complex as a dark solid.



^1H NMR (500.1 MHz, 305 K, C_6D_6): δ = 0.33 (s, 18H, 2 x SiMe_3), 1.71 (d, $^4J_{\text{H,P}} = 1.2$ Hz, 6H, 2 x $\text{C}^{2/3}\text{-Me}$).

$^{13}\text{C}\{^1\text{H}\}$ NMR (125.7 MHz, 305 K, C_6D_6): δ = 1.2 (SiMe_3), 18.1 (d, $^3J_{\text{C,P}} = 20$ Hz, $\text{C}^{2/3}\text{-Me}$), 136.9 (d, $^1J_{\text{C,P}} = 25$ Hz, $\text{C}^{1/4}$), 160.3 (d, $^2J_{\text{C,P}} = 18$ Hz, $\text{C}^{2/3}$).

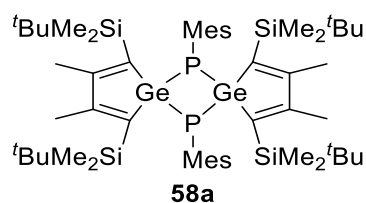
$^{29}\text{Si}\{^1\text{H}\}$ INEPT NMR (99.3 MHz, 305 K, C_6D_6): δ = -9.1 (d, $^2J_{\text{Si,P}} = 21$ Hz).

$^{31}\text{P}\{^1\text{H}\}$ NMR (202.4 MHz, 305 K, C_6D_6): δ = 78.1.

Dicyclohexylamino signals were not assigned due to poor spectral resolution.

5.2.11 Phosphagermapentafulvene Dimer

A THF solution of dipotassium germolediide **K₂[36]**, synthesised from dichlorogermole **36** (0.20 mmol, 90 mg), was cooled to -50°C. A THF solution of dichloromesitylphosphane **39a** (0.20 mmol, 44 mg) was added. The mixture was stirred for one hour whilst it was allowed to warm to room temperature. The solvent was removed. The residue was dissolved in pentane/Et₂O and filtered over a PTFE syringe filter. The solvent was removed and the residue was dried *in vacuo*. The crude product **58a** was obtained as a brown solid (100 mg, 0.19 mmol, 95%). It was analysed by NMR spectroscopy. HR-MS confirmed the presence of the dimeric compound.



¹H NMR (500.1 MHz, 305 K, C₆D₆): δ = -0.52 (s, 12H, SiMe₂tBu), 0.08 (s, 12H, SiMe₂tBu), 0.60 (s, 6H, para-Me), 1.00 (s, 36H, SiMe₂tBu), 2.11 (s, 12H, 2 x ortho-Me), 2.17 (s, 12H, C^{2/3}-Me), 6.74 (br s, 4H, meta-H).

¹³C{¹H} NMR (125.7 MHz, 305 K, C₆D₆): δ = -2.9 (SiMe₂tBu), -2.2 (SiMe₂tBu), 19.7 (SiMe₂tBu, ⁴C), 20.7 (ortho-Me), 23.6 (C^{2/3}-Me), 28.3 (para-Me), 28.5 (SiMe₂tBu), 129.8 (Mes), 136.9 (Mes), 137.7 (C^{1/4}), 163.7 (C^{2/3}).

²⁹Si{¹H} INEPT NMR (99.3 MHz, 305 K, C₆D₆): δ = -0.7.

³¹P{¹H} NMR (202.4 MHz, 305 K, C₆D₆): δ = -144.1.

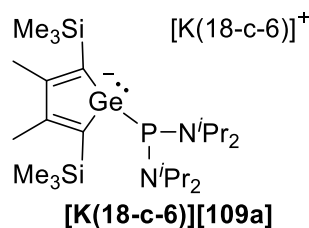
HR-MS calculated: m/z = 1064.4326; found: (EI) m/z = 1064.4311.

5.2.12 Diaminophosphanylgermolide Salts

5.2.12.1 Phosphanylgermolide Salt [K(18-c-6)][109a]

A freshly prepared solution of dipotassium germolediide **K₂[31]** (synthesised from dichlorogermole **31** (74 mg, 0.20 mmol) in THF (5 mL) was cooled to -50°C. A THF solution (3 mL) of chlorobis(diisopropylamino)phosphane (**108a**) (53 mg, 0.20 mmol) was added. The mixture turned red upon stirring for 15 minutes, which shows the formation of the potassium germolide **K[109a]** (δ ³¹P{¹H} = 97.3). To isolate the product, a THF solution (3 mL) of crownether (53 mg, 0.20 mmol) was added. The reaction mixture was stirred for one hour whilst being allowed to warm to room temperature. The solvent was removed under reduced pressure. The residue was redissolved in toluene and filtered over a PTFE syringe filter. Keeping the toluene solution

at -20°C afforded red crystals of bis(diisopropylaminophosphanyl)germolide salt **[K(18-c-6)][109a]** suitable for X-ray diffraction.



$^1\text{H NMR}$ (500.1 MHz, 305 K, THF- d_8): δ = 0.20 (s, 18H, SiMe₃), 0.97 (d, $^3J_{\text{C,P}}$ = 6.6 Hz, 12H, N(CHMe₂)₂), 1.11 (d, $^3J_{\text{C,P}}$ = 6.8 Hz, 12H, N(CHMe₂)₂), 2.10-2.14 (m, 6H, C^{2/3}-Me), 3.36-3.46 (m, 4H, N(CHMe₂)₂), 3.58 (s, 24(+8)H, 18-c-6).

$^{29}\text{Si}\{^1\text{H}\}$ INEPT NMR (99.3 MHz, 305 K, THF- d_8): δ = -14.0.

$^{31}\text{P}\{^1\text{H}\}$ NMR (202.4 MHz, 305 K, THF- d_8): δ = 101.9.

$^1\text{H NMR}$ (500.1 MHz, 193 K, THF- d_8): δ = 0.14 (s, 9H, SiMe₃), 0.20 (s, 9H, SiMe₃), 0.74-1.12 (m, 12H, N(CHMe₂)₂), 2.07 (d, $^4J_{\text{C,P}}$ = 5.5 Hz, 3H, C^{2/3}-Me), 2.12 (s, 3H, C^{2/3}-Me), 3.33 (br, 2H, N(CHMe₂)₂), 3.56 (s, 24(+7)H, 18-c-6).

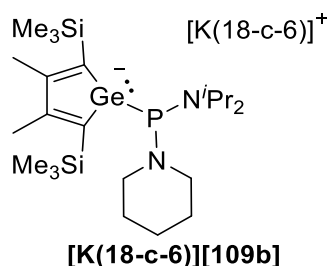
$^{13}\text{C}\{^1\text{H}\}$ NMR (125.7 MHz, 193 K, THF- d_8): δ = 3.4-3.6 (m, SiMe₃), 23.1-23.2 (m, C^{2/3}-Me), 24.1 (br, N(CHMe₂)₂), 51.8 (br, N(CHMe₂)₂), 70.8 (18-c-6), 146.0 (d, $^1J_{\text{C,P}}$ = 11 Hz, C^{2/3}), 148.4 (C^{2/3}), 160.7 (d, $^2J_{\text{C,P}}$ = 4 Hz, C^{1/4}), 164.1 (d, $^2J_{\text{C,P}}$ = 25 Hz, C^{1/4}).

$^{29}\text{Si}\{^1\text{H}\}$ INEPT NMR (99.3 MHz, 193 K, THF- d_8): δ = -14.2, -13.5.

$^{31}\text{P}\{^1\text{H}\}$ NMR (202.4 MHz, 193 K, THF- d_8): δ = 93.2.

5.2.12.2 Phosphanylgermolide Salt **[K(18-c-6)][109b]**

The THF solution of dipotassium germolediide **K₂[31]** (prepared from dichlorogermole **31** (74 mg, 0.20 mmol)) was cooled to -30°C . A vial was equipped with chloro(diisopropylamino)(piperidino)phosphane (**108b**) (50 mg, 0.20 mmol) and crown ether (53 mg, 0.20 mmol). THF was added and the solution was cooled to -30°C as well. It was then slowly added to the germolediide solution. Stirring was continued for 30 minutes. Afterwards, the solvent was removed. The residue was washed with pentane. It was then dissolved in diethyl ether and filtered over a PTFE syringe filter. The solvent was removed under vacuum to give potassium diaminophosphanylgermolide **[K(18-c-6)][109b]** (99 mg, 0.12 mmol, 60%) as dark red oil, containing the diphosphane **113b** as side product (about 35%, $\delta^{31\text{P}}$ = 81.7).



^1H NMR (500.1 MHz, 193 K, C_6D_6): δ = 0.68 (s, 18H, 2 x SiMe_3), 1.48 (d, $^3J_{\text{H,H}} = 6.5$ Hz, 6H, $\text{N}(\text{CHMe}_2)_2$), 1.39 (d, $^3J_{\text{H,H}} = 6.7$ Hz, 6H, $\text{N}(\text{CHMe}_2)_2$), 2.56 (d, $^5J_{\text{H,P}} = 5$ Hz, 6H, $\text{C}^{2/3}\text{-Me}$), 3.16 (2H, Pip), 3.20 (18-c-6), 3.24 (2H, Pip), 3.68–3.76 (m, 2H, $\text{N}(\text{CHMe}_2)_2$). Piperidino signals could partially not be assigned.

$^{13}\text{C}\{^1\text{H}\}$ NMR (125.7 MHz, 193 K, C_6D_6): δ = 3.9 (d, $^3J_{\text{C,P}} = 4$ Hz, SiMe_3), 70.0 (18-c-6), 151.5 (d, $^2J_{\text{C,P}} = 5$ Hz, $\text{C}^{2/3}$), 164.4 (d, $^1J_{\text{C,P}} = 9$ Hz, $\text{C}^{1/4}$). Remaining signals were not assigned due to the spectral resolution.

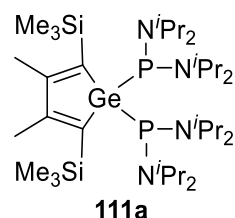
$^{29}\text{Si}\{^1\text{H}\}$ INEPT NMR (99.3 MHz, 193 K, C_6D_6): δ = -12.8.

$^{31}\text{P}\{^1\text{H}\}$ NMR (202.4 MHz, 193 K, C_6D_6): δ = 131.0.

5.2.13 Bis(diaminophosphanyl)germoles

5.2.13.1 Bi(*bis*(diisopropylamino)phosphanyl)germole 111a

Chlorobis(*diisopropylamino*)phosphane (**108a**) (106 mg, 0.40 mmol) was dissolved in THF (8 mL) and slowly added to a freshly prepared solution of dipotassium germolediide **K₂[31]** (prepared from dichlorogermole **31** (74 mg, 0.20 mmol)) at -45°C . The mixture was stirred for one hour at that temperature and was afterwards allowed to warm to room temperature overnight. The solvent was removed and the residue was dissolved in pentane. After filtration over a PTFE syringe filter, the yellow solution was restricted and kept at -20°C to afford yellow crystals of bi(*bis*(diisopropylamino)phosphanyl)germole **111a** (150 mg, 0.19 mmol, 48%) suitable for x-ray diffraction.



^1H NMR (500.1 MHz, 305 K, C_6D_6) δ = 0.53 (s, 18H, 2 x SiMe_3), 1.30–1.38 (m, 48H, 4 x $\text{N}(\text{CHMe}_2)_2$), 2.08 (s, 6H, 2 x $\text{C}^{2/3}\text{-Me}$), 3.60–3.72 (m, 8H, 4 x $\text{N}(\text{CHMe}_2)_2$).

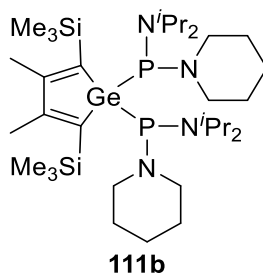
$^{13}\text{C}\{^1\text{H}\}$ NMR (125.7 MHz, 305 K, C_6D_6) δ = 3.9 (m, SiMe_3), 22.9 ($\text{C}^{2/3}\text{-Me}$), 26.0 ($\text{N}(\text{CHMe}_2)_2$), 50.6 (m, $\text{N}(\text{CHMe}_2)_2$), 146.2 (t, $^2J_{\text{C,P}} = 8$ Hz, $\text{C}^{1/4}$), 162.7 (t, $^3J_{\text{C,P}} = 2$ Hz, $\text{C}^{2/3}$).

$^{29}\text{Si}\{^1\text{H}\}$ INEPT NMR (99.3 MHz, 305 K, C_6D_6) $\delta = -10.0$.

$^{31}\text{P}\{^1\text{H}\}$ NMR (202.4 MHz, 305 K, C_6D_6) $\delta = 111.3$.

5.2.13.2 *Bis*((diisopropylamino)(piperidino)phosphanyl)germole **111b**

The THF solution of dipotassium germolediide **K₂[31]** (prepared from dichlorogermole **31** (184 mg, 0.50 mmol)) was cooled to -50°C . A THF solution of chloro(diisopropylamino)(piperidino)phosphane (**108b**) (251 mg, 1.00 mmol) was added and the mixture was stirred for 30 minutes. The cold bath was removed and the solvent was removed under vacuum. The residue was dissolved in pentane. The solvent was removed to give *bis*(diaminophosphanyl)germole **111b** (324 mg, 0.45 mmol, 90%) as an oily brown crude product. Storing a concentrated pentane solution at -20°C overnight afforded yellow crystals, suitable for XRD analysis.



Bis(diaminophosphanyl)germole **111b** has two diastereomers with the ratio 1 : 0.6, causing two sets of signals, that mostly overlay. Remark: For more detailed analysis and assignment, integrals of the signals in the $^{29}\text{Si}\{^1\text{H}\}$ INEPT NMR spectrum are given. This should usually not be done, however, here it was expected that due to the close similarity of the isomers, the polarisation transfer is equally efficient.

^1H NMR (499.9 MHz, 305 K, toluene- d_8): $\delta = 0.46\text{-}0.49$ (m, 18H, 2 x SiMe_3), 0.99 (d, $^4J_{\text{H,H}} = 6.5$ Hz, 7H, 2 x $\text{N}(\text{CHMe}_2)_2$), 1.13-1.19 (m, 17H, 2 x $\text{N}(\text{CHMe}_2)_2$), 1.39-1.46 (m, 7H, 2 x NC_5H_{10}), 1.50-1.64 (m, 5H, NC_5H_{10}), 2.05-2.12 (m, 6H, 2 x $\text{C}^{2/3}\text{-Me}$), 2.95-3.03 (m, 2H, $\text{N}(\text{CHMe}_2)_2$), 3.07-3.16 (m, 4H, NC_5H_{10}), 3.20-3.28 (m, 4H, NC_5H_{10}), 3.32-3.41 (m, 2H, $\text{N}(\text{CHMe}_2)_2$).

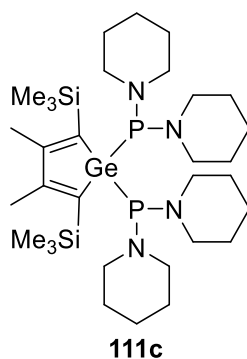
$^{13}\text{C}\{^1\text{H}\}$ NMR (125.7 MHz, 305 K, toluene- d_8): $\delta = 3.0\text{-}3.2$ (m, SiMe_3), 22.0-22.4 (m, $\text{C}^{2/3}\text{-Me}$), 24.5-25.3 (m, $\text{N}(\text{CHMe}_2)_2$, NC_5H_{10}), 27.7-28.1 (m, $\text{N}(\text{CHMe}_2)_2$, NC_5H_{10}), 52.5-53.1 (m, $\text{N}(\text{CHMe}_2)_2$), 55.1-55.4 (m, NC_5H_{10}), 144.7-146.3 (m, $\text{C}^{1/4}$), 161.0-162.3 (m, $\text{C}^{2/3}$).

$^{29}\text{Si}\{^1\text{H}\}$ INEPT NMR (99.3 MHz, 305 K, toluene- d_8) $\delta = -10.3, -9.8, -9.4$. (Ratio 0.3 : 1.0 : 0.3).

$^{31}\text{P}\{^1\text{H}\}$ NMR (202.4 MHz, 305 K, toluene- d_8): $\delta = 101.1, 102.2$. (Ratio 1.0 : 0.6).

5.2.13.3 Bis(dipiperidinophosphanyl)germole **111c**

The THF (6 mL) solution of the dipotassium germole diide **K₂[31]** (prepared from dichlorogermole **31** (74 mg, 0.20 mmol)) was cooled to -50°C. Chloro(dipiperidino)phosphane (**108c**) (47 mg, 0.20 mmol), dissolved in THF (3 mL), was added. The solution was allowed to warm to room temperature overnight. The solvent was removed and the residue redissolved in pentane. It was filtered over a PTFE syringe filter. Removal of the solvent yielded bis(dipiperidinophosphanyl)germole **111c** as a yellow oil, that solidified after some time. Keeping a pentane solution of the compound at -20°C afforded yellow crystals suitable for x-ray diffraction.



¹H NMR (500.1 MHz, 305 K, C₆D₆) δ = 0.54 (s, 18H, 2 x SiMe₃), 1.37–1.50 (m, 28H, 4 x NC₅H₁₀), 2.13 (s, 6H, 2 x C^{2/3}-Me), 3.14–3.21 (m, 16H, 4 x NC₅H₁₀).

¹³C{¹H} NMR (125.7 MHz, 305 K, C₆D₆) δ = 2.7 (m, SiMe₃), 22.0 (s, C^{2/3}-Me), 24.9 (s, NC₅H₁₀), 28.0 (m, NC₅H₁₀), 55.3 (m, NC₅H₁₀), 146.1 (t, ²J_{C,P} = 6 Hz, C^{1/4}), 160.7 (t, ³J_{C,P} = x Hz, C^{2/3}).

²⁹Si{¹H} INEPT NMR (99.3 MHz, 305 K, C₆D₆) δ = -9.6.

³¹P{¹H} NMR (202.4 MHz, 305 K, C₆D₆) δ = 125.0.

6 References

- [1] C. Weetman, R. A. Scott (Ed.), in *Encyclopedia of Inorganic and Bioinorganic Chemistry*, Wiley, **2021**, pp. 1-27.
- [2] W. B. Tolman, *Activation of Small Molecules: Organometallic and Bioinorganic Perspectives*, Wiley, **2006**.
- [3] G. H. Spikes, J. C. Fettinger, P. P. Power, *J. Am. Chem. Soc.* **2005**, *127*, 12232-12233.
- [4] P. P. Power, *Nature* **2010**, *463*, 171-177.
- [5] M. Ullrich, A. J. Lough, D. W. Stephan, *J. Am. Chem. Soc.* **2009**, *131*, 52-53.
- [6] Y. Apeloig, R. Pauncz, M. Karni, R. West, W. Steiner, D. Chapman, *Organometallics* **2003**, *22*, 3250-3256.
- [7] N. Nakata, V. Y. Lee (Ed.), in *Organogermanium Compounds, Volume 1*, Wiley, **2023**, pp. 387-433.
- [8] J. Baumgartner, C. Marschner, *Rev. Inorg. Chem.* **2014**, *34*, 119-152.
- [9] R. J. Somerville, J. Campos, *Eur. J. Inorg. Chem.* **2021**, *2021*, 3488-3498.
- [10] P. J. Davidson, D. H. Harris, M. F. Lappert, *J. Chem. Soc., Dalton Trans.* **1976**, 2268-2274.
- [11] N. Tokitoh, K. Manmaru, R. Okazaki, *Organometallics* **1994**, *13*, 167-171.
- [12] P. Jutzi, A. Becker, H. G. Stammer, B. Neumann, *Organometallics* **1991**, *10*, 1647-1648.
- [13] Y. Peng, J.-D. Guo, B. D. Ellis, Z. Zhu, J. C. Fettinger, S. Nagase, P. P. Power, *J. Am. Chem. Soc.* **2009**, *131*, 16272-16282.
- [14] M. Usher, A. V. Protchenko, A. Rit, J. Campos, E. L. Kolychev, R. Tirfoin, S. Aldridge, *Chem. Eur. J.* **2016**, *22*, 11685-11698.
- [15] A. Meller, C.-P. Gräbe, *Chem. Ber.* **1985**, *118*, 2020-2029.
- [16] O. Kühl, *Coord. Chem. Rev.* **2004**, *248*, 411-427.
- [17] C. Jones, R. P. Rose, A. Stasch, *Dalton Trans.* **2008**, 2871-2878.
- [18] G. C. Welch, R. R. S. Juan, J. D. Masuda, D. W. Stephan, *Science* **2006**, *314*, 1124-1126.
- [19] G. C. Welch, D. W. Stephan, *J. Am. Chem. Soc.* **2007**, *129*, 1880-1881.
- [20] L. Liu, L. L. Cao, Y. Shao, G. Ménard, D. W. Stephan, *Chem* **2017**, *3*, 259-267.
- [21] D. Schilter, *Nature Reviews Chemistry* **2018**, *2*, 255-255.
- [22] D. Holschumacher, T. Bannenberg, C. G. Hrib, P. G. Jones, M. Tamm, *Angew. Chem. Int. Ed.* **2008**, *47*, 7428-7432.
- [23] P. A. Chase, D. W. Stephan, *Angew. Chem. Int. Ed.* **2008**, *47*, 7433-7437.
- [24] A. Schäfer, M. Reißmann, A. Schäfer, W. Saak, D. Haase, T. Müller, *Angew. Chem. Int. Ed.* **2011**, *50*, 12636-12638.
- [25] M. Reißmann, A. Schäfer, S. Jung, T. Müller, *Organometallics* **2013**, *32*, 6736-6744.
- [26] A. Merk, H. Großekappenberg, M. Schmidtman, M.-P. Luecke, C. Lorent, M. Driess, M. Oestreich, H. F. T. Klare, T. Müller, *Angew. Chem. Int. Ed.* **2018**, *57*, 15267-15271.
- [27] A. Schäfer, M. Reißmann, A. Schäfer, M. Schmidtman, T. Müller, *Chem. Eur. J.* **2014**, *20*, 9381-9386.
- [28] M. Kira, S. Ishida, T. Iwamoto, C. Kabuto, *J. Am. Chem. Soc.* **1999**, *121*, 9722-9723.
- [29] Z. Dong, Z. Li, X. Liu, C. Yan, N. Wei, M. Kira, T. Müller, *Chem. Asian J.* **2017**, *12*, 1204-1207.
- [30] C. M. Mömning, E. Otten, G. Kehr, R. Fröhlich, S. Grimme, D. W. Stephan, G. Erker, *Angew. Chem. Int. Ed.* **2009**, *48*, 6643-6646.
- [31] D. W. Stephan, G. Erker, *Angew. Chem. Int. Ed.* **2010**, *49*, 46-76.
- [32] P. Spies, S. Schwendemann, S. Lange, G. Kehr, R. Fröhlich, G. Erker, *Angew. Chem. Int. Ed.* **2008**, *47*, 7543-7546.
- [33] P. A. Chase, G. C. Welch, T. Jurca, D. W. Stephan, *Angew. Chem. Int. Ed.* **2007**, *46*, 8050-8053.
- [34] P. J. Davidson, M. F. Lappert, *J. Chem. Soc., Chem. Commun.* **1973**, 317a-317a.

- [35] R. West, M. J. Fink, J. Michl, *Science* **1981**, *214*, 1343-1344.
- [36] A. G. Brook, F. Abdesaken, B. Gutekunst, G. Gutekunst, R. K. Kallury, *J. Chem. Soc., Chem. Commun.* **1981**, 191-192.
- [37] K. M. Baines, J. A. Cooke, *Organometallics* **1991**, *10*, 3419-3421.
- [38] K. M. Baines, J. A. Cooke, *Organometallics* **1992**, *11*, 3487-3488.
- [39] D. Wendel, T. Szilvási, C. Jandl, S. Inoue, B. Rieger, *J. Am. Chem. Soc.* **2017**, *139*, 9156-9159.
- [40] G. Becker, G. Gresser, W. Uhl, *Z. Naturforsch. B* **1981**, *36*, 16-19.
- [41] P. L. Floch, *Coord. Chem. Rev.* **2006**, *250*, 627-681.
- [42] C. Weetman, *Chem. Eur. J.* **2021**, *27*, 1941-1954.
- [43] V. Nesterov, N. C. Breit, S. Inoue, *Chem. Eur. J.* **2017**, *23*, 12014-12039.
- [44] J. Escudie, C. Couret, J. Satge, M. Andrianarison, J. D. Andriamizaka, *J. Am. Chem. Soc.* **1985**, *107*, 3378-3379.
- [45] M. Draeger, J. Escudie, C. Couret, H. Ranaivonjatovo, J. Satge, *Organometallics* **1988**, *7*, 1010-1013.
- [46] J. Escudie, C. Couret, M. Andrianarison, J. Satge, *J. Am. Chem. Soc.* **1987**, *109*, 386-390.
- [47] S. Yao, Y. Xiong, T. Szilvási, H. Grützmacher, M. Driess, *Angew. Chem. Int. Ed.* **2016**, *55*, 4781-4785.
- [48] Y. Wu, L. L. Liu, J. Su, J. Zhu, Z. Ji, Y. Zhao, *Organometallics* **2016**, *35*, 1593-1596.
- [49] Y. Xiong, S. Yao, T. Szilvási, E. Ballester-Martínez, H. Grützmacher, M. Driess, *Angew. Chem. Int. Ed.* **2017**, *56*, 4333-4336.
- [50] N. Del Rio, A. Baceiredo, N. Saffon-Merceron, D. Hashizume, D. Lutters, T. Müller, T. Kato, *Angew. Chem. Int. Ed.* **2016**, *55*, 4753-4758.
- [51] V. Nesterov, R. Baierl, F. Hanusch, A. E. Ferao, S. Inoue, *J. Am. Chem. Soc.* **2019**, *141*, 14576-14580.
- [52] D. Raiser, K. Eichele, H. Schubert, L. Wesemann, *Chem. Eur. J.* **2021**, *27*, 14073-14080.
- [53] V. Y. Lee, M. Kawai, A. Sekiguchi, H. Ranaivonjatovo, J. Escudié, *Organometallics* **2009**, *28*, 4262-4265.
- [54] Z. Dong, C. R. W. Reinhold, M. Schmidtman, T. Müller, *Angew. Chem. Int. Ed.* **2016**, *55*, 15899-15904.
- [55] Z. Dong, C. R. W. Reinhold, M. Schmidtman, T. Müller, *J. Am. Chem. Soc.* **2017**, *139*, 7117-7123.
- [56] Z. Dong, L. Albers, T. Müller, *Acc. Chem. Res.* **2020**, *53*, 532-543.
- [57] T. Kuwabara, M. Nakada, J. Hamada, J. D. Guo, S. Nagase, M. Saito, *J. Am. Chem. Soc.* **2016**, *138*, 11378-11382.
- [58] C. R. W. Reinhold, Z. Dong, J. M. Winkler, H. Steinert, M. Schmidtman, T. Müller, *Chem. Eur. J.* **2018**, *24*, 848-854.
- [59] Z. Dong, C. R. W. Reinhold, M. Schmidtman, T. Müller, *Organometallics* **2018**, *37*, 4736-4743.
- [60] Z. Dong, M. Schmidtman, T. Müller, *Chem. Eur. J.* **2019**, *25*, 10858-10865.
- [61] P. Tholen, Z. Dong, M. Schmidtman, L. Albers, T. Müller, *Angew. Chem. Int. Ed.* **2018**, *57*, 13319-13324.
- [62] L. Albers, P. Tholen, M. Schmidtman, T. Müller, *Chem. Sci.* **2020**, *11*, 2982-2986.
- [63] J. Liu, K. Singh, S. Dutta, Z. Feng, D. Koley, G. Tan, X. Wang, *Dalton Trans.* **2021**, *50*, 5552-5556.
- [64] X. Sun, L. Münzfeld, D. Jin, A. Hauser, P. W. Roesky, *Chem. Commun.* **2022**, *58*, 7976-7979.
- [65] Z. Dong, O. Janka, J. Kösters, M. Schmidtman, T. Müller, *Angew. Chem. Int. Ed.* **2018**, *57*, 8634-8638.
- [66] Z. Dong, J. M. Winkler, M. Schmidtman, T. Müller, *Chem. Sci.* **2021**, *12*, 6287-6292.
- [67] S. Kühn, *Bachelor Thesis, Carl von Ossietzky University* **2020**.
- [68] M. Asay, C. Jones, M. Driess, *Chem. Rev.* **2011**, *111*, 354-396.
- [69] C. Weetman, S. Inoue, *ChemCatChem* **2018**, *10*, 4213-4228.
- [70] M.-A. Légaré, C. Prankevicus, H. Braunschweig, *Chem. Rev.* **2019**, *119*, 8231-8261.

- [71] P. J. Fagan, W. A. Nugent, *J. Am. Chem. Soc.* **1988**, *110*, 2310-2312.
- [72] M. Saito, M. Yoshioka, *Coord. Chem. Rev.* **2005**, *249*, 765-780.
- [73] W. P. Freeman, T. D. Tilley, L. M. Liable-Sands, A. L. Rheingold, *J. Am. Chem. Soc.* **1996**, *118*, 10457-10468.
- [74] R. West, *Pure Appl. Chem.* **2008**, *80*, 563-569.
- [75] M. Westerhausen, B. Stein, M. W. Ossberger, H. Görls, J. C. G. Ruiz, H. Nöth, P. Mayer, *ARKIVOC* **2006**, *2007*, 46-59.
- [76] T. Müller, in *Science of Synthesis*, Thieme, **2020**.
- [77] W.-C. Joo, J.-H. Hong, S.-B. Choi, H.-E. Son, C. Hwan Kim, *J. Organomet. Chem.* **1990**, *391*, 27-36.
- [78] J.-H. Hong, P. Boudjouk, S. Castellino, *Organometallics* **1994**, *13*, 3387-3389.
- [79] U. Bankwitz, H. Sohn, D. R. Powell, R. West, *J. Organomet. Chem.* **1995**, *499*, C7-C9.
- [80] R. West, H. Sohn, U. Bankwitz, J. Calabrese, Y. Apeloig, T. Mueller, *J. Am. Chem. Soc.* **1995**, *117*, 11608-11609.
- [81] W. P. Freeman, T. D. Tilley, G. P. A. Yap, A. L. Rheingold, *Angew. Chem. Int. Ed.* **1996**, *35*, 882-884.
- [82] R. West, H. Sohn, D. R. Powell, T. Müller, Y. Apeloig, *Angew. Chem. Int. Ed.* **1996**, *35*, 1002-1004.
- [83] S.-B. Choi, P. Boudjouk, J.-H. Hong, *Organometallics* **1999**, *18*, 2919-2921.
- [84] B. Szathmári, C. Fekete, Z. Kelemen, T. Holczbauer, L. Nyulászi, I. Kovács, *Eur. J. Inorg. Chem.* **2023**, *26*, e202300316.
- [85] C. Reinhold, *Dissertation, Carl von Ossietzky University* **2017**.
- [86] L. Bührmann, *Ongoing Dissertation, Carl von Ossietzky University* **2020-2023**.
- [87] K. Tamao, S. Yamaguchi, M. Shiro, *J. Am. Chem. Soc.* **1994**, *116*, 11715-11722.
- [88] G. Märkl, B. Alig, *J. Organomet. Chem.* **1984**, *273*, 1-29.
- [89] R. B. King, N. D. Sadanani, *Synth. React. Inorg. Met.-Org. Chem.* **1985**, *15*, 149-153.
- [90] M. Alajarín, C. López-Leonardo, P. Llamas-Lorente, in *New Aspects in Phosphorus Chemistry V: -/-* (Ed.: J.-P. Majoral), Springer Berlin Heidelberg, Berlin, Heidelberg, **2005**, pp. 77-106.
- [91] R. Fu, B. Zhao, Y. Shi, *J. Org. Chem.* **2009**, *74*, 7577-7580.
- [92] L. Falivene, Z. Cao, A. Petta, L. Serra, A. Poater, R. Oliva, V. Scarano, L. Cavallo, *Nature Chemistry* **2019**, *11*, 872-879.
- [93] A. Poater, B. Cosenza, A. Correa, S. Giudice, F. Ragone, V. Scarano, L. Cavallo, *Eur. J. Inorg. Chem.* **2009**, *2009*, 1759-1766.
- [94] L. Falivene, R. Credendino, A. Poater, A. Petta, L. Serra, R. Oliva, V. Scarano, L. Cavallo, *Organometallics* **2016**, *35*, 2286-2293.
- [95] P. Ertl, *Chemistry-Methods* **2022**, *2*, e202200041.
- [96] C. Hansch, A. Leo, R. W. Taft, *Chem. Rev.* **1991**, *91*, 165-195.
- [97] W. C. Davies, *J. Chem. Soc.* **1935**, 462-464.
- [98] H. H. Karsch, W. A. Herrmann, *Synthetic Methods of Organometallic and Inorganic Chemistry, Vol. 3: Phosphorus, Arsenic, Antimony and Bismuth*, Georg Thieme Verlag Stuttgart, New York, **1996**.
- [99] C. Overländer, J. J. Tirrée, M. Nieger, E. Niecke, C. Moser, S. Spirk, R. Pietschnig, *Appl. Organomet. Chem.* **2007**, *21*, 46-48.
- [100] A. Orthaber, *Personal Communication, Uppsala University* **2022**.
- [101] L. Silaghi-dumitrescu, I. Haiduc, *Synth. React. Inorg. Met.-Org. Chem.* **1983**, *13*, 475-480.
- [102] V. Matuska, A. M. Z. Slawin, J. D. Woollins, *Inorg. Chem.* **2010**, *49*, 3064-3069.
- [103] E. Adams, D. Jeter, A. W. Cordes, J. W. Kolis, *Inorg. Chem.* **1990**, *29*, 1500-1503.
- [104] O. J. Scherer, H. Höntsch, *Chem. Ber.* **1979**, *112*, 1927-1933.
- [105] B. A. Chalmers, M. Bühl, K. S. Athukorala Arachchige, A. M. Z. Slawin, P. Kilian, *Chem. Eur. J.* **2015**, *21*, 7520-7531.
- [106] M. Ates, H. J. Breunig, A. Soltani-Neshan, M. Tegeler, *Z. Naturforsch. B* **1986**, *41*, 321-326.

- [107] P. Pyykkö, M. Atsumi, *Chem. Eur. J.* **2009**, *15*, 12770-12779.
- [108] P. Pyykkö, M. Atsumi, *Chem. Eur. J.* **2009**, *15*, 186-197.
- [109] L. Wang, Y. S. Lim, Y. Li, R. Ganguly, R. Kinjo, *Molecules* **2016**, *21*, 990.
- [110] K. Mitsuo, I. Shintaro, I. Takeaki, I. Masaaki, K. Chizuko, I. Lubov, S. Hideki, *Chem. Lett.* **1999**, *28*, 263-264.
- [111] A. V. Belyakov, A. Haaland, D. J. Shorokhov, V. I. Sokolov, O. Swang, *J. Mol. Struct.* **1998**, *445*, 303-309.
- [112] P. E. Baskakova, A. V. Belyakov, A. Haaland, H. V. Volden, *J. Mol. Struct.* **2001**, 567-568, 197-202.
- [113] J. Hydrio, M. Gouygou, F. Dallemer, Gilbert G. A. Balavoine, J.-C. Daran, *Eur. J. Org. Chem.* **2002**, 2002, 675-685.
- [114] M. Hesse, H. Meier, B. Zeeh, *Spektroskopische Methoden in der organischen Chemie, Vol. 7*, Thieme Verlag, **2005**.
- [115] O. Kühn, *Phosphorus-31 NMR Spectroscopy*, Springer Berlin, Heidelberg, **2008**.
- [116] R. Alfasser, C. Janiak, T. M. Klapötke, H.-J. Meyer, *Riedel Moderne Anorganische Chemie, 3. Auflage*, de Gruyter, Berlin, New York, **2007**.
- [117] A. Sidiropoulos, C. Jones, A. Stasch, S. Klein, G. Frenking, *Angew. Chem. Int. Ed.* **2009**, *48*, 9701-9704.
- [118] A. El-Hellani, J. Monot, S. Tang, R. Guillot, C. Bour, V. Gandon, *Inorg. Chem.* **2013**, *52*, 11493-11502.
- [119] D. G. Gusev, *Organometallics* **2009**, *28*, 6458-6461.
- [120] G. A. Ardizzoia, S. Brenna, *Phys. Chem. Chem. Phys.* **2017**, *19*, 5971-5978.
- [121] L. Zapf, M. Riethmann, S. A. Föhrenbacher, M. Finze, U. Radius, *Chem. Sci.* **2023**, *14*, 2275-2288.
- [122] M. Mantina, A. C. Chamberlin, R. Valero, C. J. Cramer, D. G. Truhlar, *J. Phys. Chem. A* **2009**, *113*, 5806-5812.
- [123] J. E. Kingcade, H. M. Nagarathna-Naik, I. Shim, K. A. Gingerich, *J. Phys. Chem.* **1986**, *90*, 2830-2834.
- [124] S. Berger, S. Braun, H.-O. Kalinowski, *NMR-Spektroskopie von Nichtmetallen, Band 3, ³¹P-NMR-Spektroskopie*, Georg Thieme Verlag, Stuttgart, New York, **1993**.
- [125] C. Couret, J. Escudie, J. Satge, J. D. Andriamizaka, B. Saint-Roch, *J. Organomet. Chem.* **1979**, *182*, 9-15.
- [126] J. Escudie, C. Couret, J. Satge, J. D. Andriamizaka, *Organometallics* **1982**, *1*, 1261-1265.
- [127] G. Fritz, R. Biastoch, *Z. anorg. allg. Chem.* **1986**, *535*, 95-105.
- [128] T. Heitkemper, J. Sarcevic, C. P. Sindlinger, *J. Am. Chem. Soc.* **2020**, *142*, 21304-21309.
- [129] T. Iwamoto, *Personal Communication, Carl von Ossietzky University* **2023**.
- [130] T. Müller, *Personal Communication, Carl von Ossietzky University* **2023**.
- [131] A. Maaninen, T. Chivers, M. Parvez, J. Pietikäinen, R. S. Laitinen, *Inorg. Chem.* **1999**, *38*, 4093-4097.
- [132] Z. Dong, M. Schmidtman, T. Müller, *Z. anorg. allg. Chem.* **2018**, *644*, 1041-1046.
- [133] E. H. Braye, W. Hübel, I. Caplier, *J. Am. Chem. Soc.* **1961**, *83*, 4406-4413.
- [134] D. Klintuch, K. Krekić, C. Bruhn, Z. Benkő, R. Pietschnig, *Eur. J. Inorg. Chem.* **2016**, 2016, 718-725.
- [135] I. G. M. Campbell, R. C. Cookson, M. B. Hocking, A. N. Hughes, *J. Chem. Soc.* **1965**, 2184-2193.
- [136] M. Hissler, C. Lescop, R. Réau, *Comptes Rendus Chimie* **2005**, *8*, 1186-1193.
- [137] F. Mathey, *Chem. Rev.* **1988**, *88*, 429-453.
- [138] M. Kumaravel, J. T. Mague, M. S. Balakrishna, *Tetrahedron Letters* **2014**, *55*, 2957-2961.
- [139] D. L. Quin, *Curr. Org. Chem.* **2006**, *10*, 43-78.
- [140] N. Wiberg, *Holleman-Wiberg: Lehrbuch der Anorganischen Chemie, 102. Auflage*, de Gruyter Berlin, New York, **2007**.
- [141] P. Coburger, F. Masero, J. Böskén, V. Mougél, H. Grützmacher, *Angew. Chem. Int. Ed.* **2022**, *61*, e202211749.
- [142] G. Harris, *J. Chem. Soc.* **1958**, 512-519.

- [143] R. J. H. Clark, B. Crociani, A. Wassermann, *J. Chem. Soc. A* **1970**, 2458-2460.
- [144] R. F. W. Bader, *Atoms in Molecules - A Quantum Theory*, Oxford University Press, New York, **1990**.
- [145] R. G. Pearson, *J. Am. Chem. Soc.* **1963**, *85*, 3533-3539.
- [146] P. Erdmann, J. Leitner, J. Schwarz, L. Greb, *ChemPhysChem* **2020**, *21*, 987-994.
- [147] K. Baba, M. Tobisu, N. Chatani, *Angew. Chem. Int. Ed.* **2013**, *52*, 11892-11895.
- [148] V. Diemer, A. Berthelot, J. Bayardon, S. Jugé, F. R. Leroux, F. Colobert, *J. Org. Chem.* **2012**, *77*, 6117-6127.
- [149] J. W. Akitt, K. R. Dixon, R. J. Goodfellow, O. W. Howarth, C. J. Jameson, J. D. Kennedy, B. E. Mann, J. Mason, H. C. E. McFarlane, W. McFarlane, H. W. E. Rattle, D. Rehder, *Multinuclear NMR*, Plenum Press, New York and London, **1987**.
- [150] F. M. Elms, G. A. Koutsantonis, C. L. Raston, *J. Chem. Soc., Chem. Commun.* **1995**, 1669-1670.
- [151] J. C. Carter, G. Jugie, R. Enjalbert, J. Galy, *Inorg. Chem.* **1978**, *17*, 1248-1254.
- [152] W. H. N. Vriezen, F. Jellinek, *Chemical Physics Letters* **1967**, *1*, 284.
- [153] C. Jiang, O. Blacque, H. Berke, *Organometallics* **2009**, *28*, 5233-5239.
- [154] F. Mathey, in *Modern Heterocyclic Chemistry*, pp. 2071-2116.
- [155] F. Mathey, A. Mitschler, R. Weiss, *J. Am. Chem. Soc.* **1977**, *99*, 3537-3538.
- [156] K. Okamoto, Y. Omoto, H. Sano, K. Ohe, *Dalton Trans.* **2012**, *41*, 10926-10929.
- [157] J. M. García, E. Ocando-Mavárez, T. Kato, D. S. Coll, A. Briceño, N. Saffon-Merceron, A. Baceiredo, *Inorg. Chem.* **2012**, *51*, 8187-8193.
- [158] M. T. Whited, A. M. Deetz, J. W. Boerma, D. E. DeRosh, D. E. Janzen, *Organometallics* **2014**, *33*, 5070-5073.
- [159] A. R. Naziruddin, A. Hepp, T. Pape, F. E. Hahn, *Organometallics* **2011**, *30*, 5859-5866.
- [160] Z. Dong, K. Bedbur, M. Schmidtman, T. Müller, *J. Am. Chem. Soc.* **2018**, *140*, 3052-3060.
- [161] S. Attar, W. H. Bearden, N. W. Alcock, E. C. Alyea, J. H. Nelson, *Inorg. Chem.* **1990**, *29*, 425-433.
- [162] K. Fourmy, S. Mallet-Ladeira, O. Dechy-Cabaret, M. Gouygou, *Organometallics* **2013**, *32*, 1571-1574.
- [163] M. Alcarazo, *Acc. Chem. Res.* **2016**, *49*, 1797-1805.
- [164] H. R. G. Bender, E. Niecke, M. Nieger, H. Westermann, *Z. anorg. allg. Chem.* **1994**, *620*, 1194-1202.
- [165] J. L. Bolliger, O. Blacque, C. M. Frech, *Angew. Chem. Int. Ed.* **2007**, *46*, 6514-6517.
- [166] W. Zeiß, C. Feldt, J. Weis, G. Dunkel, *Chem. Ber.* **1978**, *111*, 1180-1194.
- [167] H. Westerman, M. Nieger, E. Niecke, *Chem. Ber.* **1991**, *124*, 13-16.
- [168] H. Günther, *NMR-Spektroskopie, 2. verbesserte Auflage*, Georg Thieme Verlag, Stuttgart, New York, **1983**.
- [169] S. Stadlbauer, R. Frank, I. Maulana, P. Lönnecke, B. Kirchner, E. Hey-Hawkins, *Inorg. Chem.* **2009**, *48*, 6072-6082.
- [170] M. J. Frisch, G. W. Trucks, H. B. Schlegel, G. E. Scuseria, M. A. Robb, J. R. Cheeseman, G. Scalmani, V. Barone, G. A. Petersson, H. Nakatsuji, X. Li, M. Caricato, A. V. Marenich, J. Bloino, B. G. Janesko, R. Gomperts, B. Mennucci, H. P. Hratchian, J. V. Ortiz, A. F. Izmaylov, J. L. Sonnenberg, Williams, F. Ding, F. Lipparini, F. Egidi, J. Goings, B. Peng, A. Petrone, T. Henderson, D. Ranasinghe, V. G. Zakrzewski, J. Gao, N. Rega, G. Zheng, W. Liang, M. Hada, M. Ehara, K. Toyota, R. Fukuda, J. Hasegawa, M. Ishida, T. Nakajima, Y. Honda, O. Kitao, H. Nakai, T. Vreven, K. Throssell, J. A. Montgomery Jr., J. E. Peralta, F. Ogliaro, M. J. Bearpark, J. J. Heyd, E. N. Brothers, K. N. Kudin, V. N. Staroverov, T. A. Keith, R. Kobayashi, J. Normand, K. Raghavachari, A. P. Rendell, J. C. Burant, S. S. Iyengar, J. Tomasi, M. Cossi, J. M. Millam, M. Klene, C. Adamo, R. Cammi, J. W. Ochterski, R. L. Martin, K. Morokuma, O. Farkas, J. B. Foresman, D. J. Fox, Wallingford, CT, **2013**.

7 Appendix

7.1 Abbreviations and Symbols

BCF	tris(pentafluorophenyl)borane
BCH	bicyclohexene
DFT	density functional theory
Dipp	2,6- <i>bis</i> (diisopropyl)phenyl
DMAP	4-dimethylaminopyridine
e.g.	<i>exempli gratia</i> (for example)
et al.	<i>et alia</i> (and others)
equiv.	equivalents
FLP	frustrated Lewis pair
HMBC	heteronuclear multiple bond correlation
HMQC	heteronuclear multiple quantum correlation
INEPT	insensitive nuclei enhancement by polarisation transfer
n.a.	not available
NBO	natural bond orbital
n.d.	not determined
NHC	N-heterocyclic carbene
NMR	nuclear magnetic resonance
Pip	piperidino
QTAIM	quantum theory of atoms in molecules
SCF	self-consistent field
TMP	2,2,6,6-tetramethylpiperidino
vs.	versus
WBI	Wiberg bond index

7.2 Computational Details

DFT calculations were performed on the clusters CARL and ROSA, located at the Carl von Ossietzky Universität Oldenburg using the program package Gaussian09.^[170] Optimisations were performed using the M06-2X hybrid functional and the 6-311+G(d,p) basis set for the elements H, C, N, O, Si, P, S, Ge, As and the def2-tzvp basis set in combination with the corresponding pseudo potential for the elements Rh, Sb, Hf, Au. Subsequent frequency analysis allowed determination of the stationary points (number of imaginary frequencies (Nimag) = 0). The SCF energy (E(SCF)) and the Gibbs free energy (G(298 K); at 298.25 K and 0.101 MPa) for each optimised structure are given in Table 32. The corresponding xyz coordinates are provided on a compact disk. ³¹P NMR chemical shifts were calculated using the M06-L functional and the 6-311+G(2d,p) basis set. The calculated shifts were referenced against PH₃ (85% H₃PO₄ in H₂O): $\delta^{31\text{P}}(\text{PH}_3) = -239.1 \text{ (M06-L/6-311+G(2d,p))//M06-2X/6-311+G(d,p)}$.

Table 32 – Calculated energy (E(SCF)) and Gibbs free energy (G(298 K))
(M06-2X/6-311+G(d,p) (H, C, N, O, Si, P, S, Ge, As), def2-tzvp (Rh, Sb, Hf, Au)).

Compound	E(SCF) [a.u.]	G(298 K) [a.u.]
germolediide 31	-3127.55614	-3127.29139
germolediide 36	-3363.38575	-3362.95650
aminophosphane 38a	-1396.33296	-1396.27968
aminophosphane 38b	-1553.55935	-1553.39784
aminophosphane 38c	-1786.98846	-1786.69831
aminophosphane 38d	-1513.04217	-1512.92773
aminophosphane 38e	-1670.26488	-1670.03912
phospha-BCH-germylene 43b (E)	-3760.76027	-3760.30009
phospha-BCH-germylene 43b (Z)	-3760.71977	-3760.25399
phospha-BCH-germylene 43d	-3720.26093	-3719.84463
phospha-BCH-germylene 43e	-3877.46387	-3876.93696
phospha-BCH-germylene 44b-(A)	-3996.56981	-3995.94053
phospha-BCH-germylene 44b-(B)	-3996.57319	-3995.94454
phospha-BCH-germylene 44c	-4230.00910	-4229.25190
phospha-BCH-germylene 44d	-3956.07705	-3955.49538
germylene 43b-43b adduct 53	-7521.53409	-7520.59001
Ge-Ge bridged phospholes 45b	-7521.50302	-7520.55396

Appendix

digermanium ($^3\text{Ge}_2$)	-4153.88805	-4153.91217
DMAP (dimethylaminopyridine)	-382.18647	-382.05676
phosphagermafulvene isomer 43b	-3760.71440	-3760.25645
phosphagermafulvene isomer 43d	-3720.21495	-3719.79957
phosphagermafulvene isomer 43e	-3877.43097	-3876.90817
aminophosphole 45a	-1526.54959	-1526.19812
aminophosphole 45b	-1683.76499	-1683.29881
aminophosphole 45d	-1643.27125	-1642.85400
aminophosphole 45e	-1800.47812	-1799.94768
aminophosphole 46b	-1919.58035	-1918.95264
aminophosphole 46c	-2153.01485	-2152.25617
aminophosphole 46d	-1879.09013	-1878.50713
phosphonium-BCH-germylene [89b]	-3761.15799	-3760.68449
ammonium ion [89-N]	-3761.17013	-3760.69792
germylium ion [89-Ge]	-3761.10801	-3760.63962
carbenium ion [89-C]	-3761.12028	-3760.64639
methylphosphonium-BCH-germylene [90]	-3800.47470	-3799.97060
methylphospholium ion [92]	-1723.47182	-1722.96893
phospha-BCH-germylium (Ge-Me)	-3800.42843	-3799.93194
hafnocena-BCH-germylene 21	-3562.67923	-3562.24624
silab-BCH-germylene 47	-3496.96444	-3496.61982
model phospha-BCH-germylene 43'	-2707.63815	-2707.52288
model phospha-BCH-germylene H ₂	-2708.81591	-2708.67813
model phospha-BCH-germylene Ge-H ₂	-2710.02362	-2709.86845
model phosphonium-BCH-germylene [89]'	-2708.01459	-2707.88980
model phosphonium-BCH-germylene H ₂	-2709.19211	-2709.04403
model hafnocena-BCH-germylene 21'	-2666.77747	-2666.58706
model hafnocena-BCH-germylene H ₂	-2667.95182	-2667.73839
model silab-BCH-germylene 47'	-2601.06524	-2600.95910
model silab-BCH-germylene H ₂	-2602.24714	-2602.11854
model silab-BCH-germylene Ge-H ₂	-2603.45928	-2603.31307
reference germylene	-4309.90347	-4309.85266
reference germylene Ge-H ₂	-4311.08916	-4311.01632

mesitylphospha-BCH-germylene 54	-3818.50425	-3818.06801
mesitylphosphagermafulvene 56	-3818.48596	-3818.05147
mesitylphosphole	-1741.53448	-1741.09867
fulvene dimer 59a	-7637.06403	-7636.15905
fulvene dimer 58a (<i>incomplete optimisation</i>)*	-8108.67468	
terphenylphospha-BCH-germylene	-4398.45602	-4397.78549
terphenylphosphagermafulvene	-4398.43408	-4397.76862
terphenylphosphole	-2321.47670	-2320.80265
Fritz <i>et al.</i> dimer 60	-2711.44855	-2710.79612
phospha-BCH-germanone 78	-3835.94594	-3835.48406
phospha-BCH-germylene oxide 79	-3836.02168	-3835.55514
phosphole oxide 75	-1759.01838	-1758.55162
germaniumoxide (GeO)	-2152.18557	-2152.20532
dioxygen (³ O ₂)	-150.30858	-150.32450
phospha-BCH-germathione 80 (SiMe ₃)	-4158.960336	-4158.50009
phospha-BCH-germylene sulfide 81 (SiMe ₃)	-4158.981056	-4158.51622
germylene 43b Rh complex 100'	-4643.50920	-4642.86867
germylene 43b Rh complex 101'	-4643.50584	-4642.87728
germylene 43c Au complex (P-Au)	-4590.12648	-4589.53918
germylene 43c Au complex (Ge-Au)	-4590.09466	-4589.51006
phosphole 45c gold complex 107	-2513.11650	-2512.52580
germylene 43c GaCl ₃ adduct (P-Ga)	-7299.84112	-7299.24799
germylene 43c GaCl ₃ adduct (Ge-Ga)	-7299.81859	-7299.23347
phosphole 45c GaCl ₃ adduct	-5222.83546	-5222.24568
(amino)arsa-BCH-germylene	-5655.26160	-5654.80252
(amino)arsagermapentafulvene	-5655.23192	-5654.77355
(amino)arsole	-3578.26888	-3577.80856
(aryl)arsa-BCH-germylene	-6066.71887	-6066.03870
(aryl)arsagermapentafulvene	-6066.72252	-6066.04420
(aryl)arsole	-3989.74136	-3989.05781
(amino)stiba-BCH-germylene	-3659.57181	-3659.11643
(amino)stibagermapentafulvene	-3659.54869	-3659.09232
(amino)stibole	-1582.57726	-1582.11992
(aryl)stiba-BCH-germylene	-4071.03196	-4070.35413

Appendix

(aryl)stibagermapentafulvene	-4071.02948	-4070.35327
(aryl)stibole	-1994.04469	-1993.36602

* Due to very soft rotational modes, the PES of this molecule is very flat and complete optimisation fulfilling all presetted criteria was not achieved. The final structure has a predicted change in energy of less than 10^{-6} a.u..

7.3 Other Programs and Methods

SambVca 2.1 Web Program

The optimised structures must be saved as *.mol* file and can then be uploaded to the website. The coordinating atom and the axes can easily be defined on the interactive interface. Here, the sphere was set to a radius (R) of 350 pm. The ligand-metal distance (d) was determined to 210 pm. Mesh spacing for numerical integration was set to 0.05 and bond-radii were scaled to 1.17. Hydrogen atoms were included in the calculation.

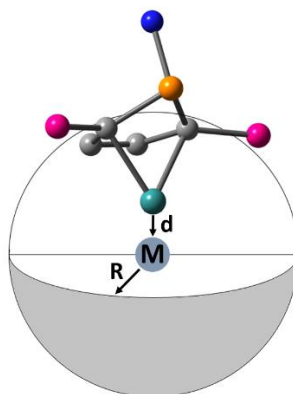


Figure 84 – Model for the calculation of the buried volume (% V_{bur}).

Yield Determination of Mixtures Based on ^{31}P NMR Spectroscopy:

The yield of mixtures of phospho-BCH-germylene and the respective phosphole was determined based on integration in the $^{31}\text{P}\{^1\text{H}\}$ NMR spectra. Therefore, the total mass was determined right before recording the NMR spectra. Via linear equation, the shares of phospho-BCH-germylene (*Ge*) and phosphole (*P*) were incorporated. The integral of the phosphole signal was scaled to 1. The integral of the phospho-BCH-germylene signal was expected to be *x*.

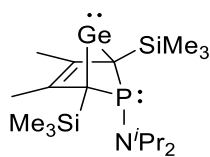
$$m_{total} = m_P + m_{Ge} = n_P M_P + n_{Ge} M_{Ge}$$

$$\text{With } n_P = \frac{1}{x} n_{Ge} \text{ counts:}$$

$$m_{total} = \frac{1}{x} n_{Ge} M_P + n_{Ge} M_{Ge}$$

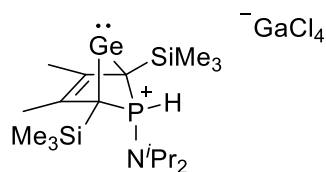
$$n_{Ge} = \frac{m_{total}}{\frac{1}{x} M_P + M_{Ge}} \Rightarrow n_{total}$$

7.4 Crystallographic Data

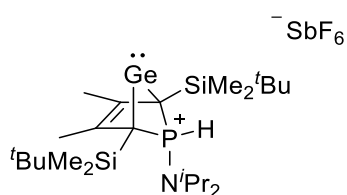


43b

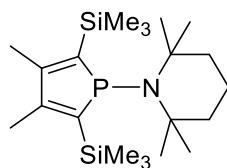
Identification code	msw141	
Empirical formula	C ₁₈ H ₃₈ Ge N P Si ₂	
Formula weight	428.23	
Temperature	100(2) K	
Wavelength	0.71073 Å	
Crystal system	Orthorhombic	
Space group	Pnma	
Unit cell dimensions	a = 12.4246(9) Å	α = 90°.
	b = 18.0809(13) Å	β = 90°.
	c = 10.2515(7) Å	γ = 90°.
Volume	2303.0(3) Å ³	
Z	4	
Density (calculated)	1.235 Mg/m ³	
Absorption coefficient	1.504 mm ⁻¹	
F(000)	912	
Crystal size	0.160 x 0.160 x 0.090 mm ³	
Theta range for data collection	2.253 to 40.249°	
Index ranges	-22 ≤ h ≤ 22, -32 ≤ k ≤ 32, -18 ≤ l ≤ 18	
Reflections collected	228190	
Independent reflections	7412 (R(int) = 0.0301)	
Observed reflections (I > 2(I))	6932	
Completeness to theta = 40.249°	100.0 %	
Absorption correction	Semi-empirical from equivalents	
Max. and min. transmission	1.0000 and 0.9007	
Refinement method	Full-matrix least-squares on F ²	
Data / restraints / parameters	7412 / 0 / 118	
Goodness-of-fit on F ²	1.076	
Final R indices (I > 2σ(I))	R1 = 0.0173, wR2 = 0.0498	
R indices (all data)	R1 = 0.0191, wR2 = 0.0505	
Extinction coefficient	n/a	
Largest diff. peak and hole	0.567 and -0.340 e.Å ⁻³	

**[89b][GaCl₄]**

Identification code	msw22_100k	
Empirical formula	C ₁₈ H ₃₉ Cl ₄ Ga Ge N P Si ₂	
Formula weight	640.76	
Temperature	100(2) K	
Wavelength	0.71073 Å	
Crystal system	Monoclinic	
Space group	P2 ₁ /n	
Unit cell dimensions	a = 15.9762(10) Å	α = 90°.
	b = 12.1459(8) Å	β = 111.3991(12)°.
	c = 16.1325(10) Å	γ = 90°.
Volume	2914.6(3) Å ³	
Z	4	
Density (calculated)	1.460 Mg/m ³	
Absorption coefficient	2.467 mm ⁻¹	
F(000)	1312	
Crystal size	0.360 x 0.260 x 0.220 mm ³	
Theta range for data collection	1.535 to 34.971°	
Index ranges	-25 ≤ h ≤ 25, -19 ≤ k ≤ 19, -25 ≤ l ≤ 26	
Reflections collected	145900	
Independent reflections	12810 (R(int) = 0.0358)	
Observed reflections (I > 2(I))	10999	
Completeness to theta = 34.971°	100.0 %	
Absorption correction	Numerical	
Max. and min. transmission	0.7002 and 0.4994	
Refinement method	Full-matrix least-squares on F ²	
Data / restraints / parameters	12810 / 0 / 269	
Goodness-of-fit on F ²	1.020	
Final R indices (I > 2σ(I))	R1 = 0.0221, wR2 = 0.0546	
R indices (all data)	R1 = 0.0298, wR2 = 0.0579	
Extinction coefficient	n/a	
Largest diff. peak and hole	1.035 and -0.645 e.Å ⁻³	

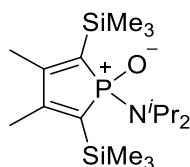
**[88b][SbF₆]**

Identification code	msw105	
Empirical formula	C ₂₄ H ₅₁ F ₆ Ge N P Sb Si ₂	
Formula weight	749.14	
Temperature	100(2) K	
Wavelength	0.71073 Å	
Crystal system	Monoclinic	
Space group	P2 ₁ /c	
Unit cell dimensions	a = 12.0024(9) Å	α = 90°.
	b = 11.8358(9) Å	β = 99.704(3)°.
	c = 23.4871(18) Å	γ = 90°.
Volume	3288.8(4) Å ³	
Z	4	
Density (calculated)	1.513 Mg/m ³	
Absorption coefficient	1.905 mm ⁻¹	
F(000)	1528	
Crystal size	0.120 x 0.120 x 0.090 mm ³	
Theta range for data collection	1.721 to 40.249°	
Index ranges	-21 ≤ h ≤ 21, -21 ≤ k ≤ 21, -42 ≤ l ≤ 42	
Reflections collected	217854	
Independent reflections	20716 (R(int) = 0.0509)	
Observed reflections (I > 2σ(I))	17712	
Completeness to theta = 40.249°	100.0 %	
Absorption correction	Semi-empirical from equivalents	
Max. and min. transmission	1.0000 and 0.9017	
Refinement method	Full-matrix least-squares on F ²	
Data / restraints / parameters	20716 / 0 / 409	
Goodness-of-fit on F ²	1.033	
Final R indices (I > 2σ(I))	R1 = 0.0328, wR2 = 0.0864	
R indices (all data)	R1 = 0.0404, wR2 = 0.0902	
Extinction coefficient	n/a	
Largest diff. peak and hole	2.893 and -1.525 e.Å ⁻³	

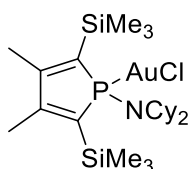


45e

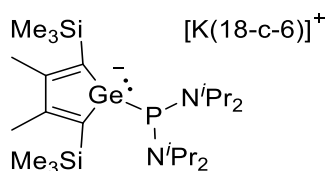
Identification code	tb13_4	
Empirical formula	C ₂₁ H ₄₂ N P Si ₂	
Formula weight	395.70	
Temperature	100(2) K	
Wavelength	0.71073 Å	
Crystal system	Monoclinic	
Space group	P2 ₁ /c	
Unit cell dimensions	a = 12.7167(3) Å	α = 90°.
	b = 30.5644(8) Å	β = 90.0130(13)°.
	c = 12.3609(3) Å	γ = 90°.
Volume	4804.4(2) Å ³	
Z	8	
Density (calculated)	1.094 Mg/m ³	
Absorption coefficient	0.219 mm ⁻¹	
F(000)	1744	
Crystal size	0.300 x 0.260 x 0.200 mm ³	
Theta range for data collection	1.601 to 34.971°	
Index ranges	-20 ≤ h ≤ 19, -48 ≤ k ≤ 49, -19 ≤ l ≤ 19	
Reflections collected	125982	
Independent reflections	20288 (R(int) = 0.0392)	
Observed reflections (I > 2(I))	17938	
Completeness to theta = 34.971°	96.1 %	
Absorption correction	Semi-empirical from equivalents	
Max. and min. transmission	1.0000 and 0.9623	
Refinement method	Full-matrix least-squares on F ²	
Data / restraints / parameters	20288 / 0 / 556	
Goodness-of-fit on F ²	1.040	
Final R indices (I > 2σ(I))	R1 = 0.0490, wR2 = 0.1227	
R indices (all data)	R1 = 0.0577, wR2 = 0.1277	
Extinction coefficient	n/a	
Largest diff. peak and hole	1.062 and -0.471 e.Å ⁻³	

**75**

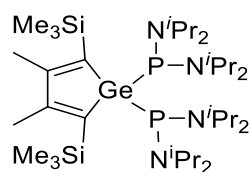
Identification code	msw60	
Empirical formula	C ₁₈ H ₃₈ N O P Si ₂	
Formula weight	371.64	
Temperature	100(2) K	
Wavelength	0.71073 Å	
Crystal system	Monoclinic	
Space group	P2 ₁ /n	
Unit cell dimensions	a = 10.2065(3) Å	α = 90°.
	b = 19.2905(5) Å	β = 96.0698(10)°.
	c = 11.5732(3) Å	γ = 90°.
Volume	2265.86(11) Å ³	
Z	4	
Density (calculated)	1.089 Mg/m ³	
Absorption coefficient	0.232 mm ⁻¹	
F(000)	816	
Crystal size	0.130 x 0.110 x 0.060 mm ³	
Theta range for data collection	2.061 to 36.317°	
Index ranges	-17 ≤ h ≤ 14, -32 ≤ k ≤ 32, -19 ≤ l ≤ 19	
Reflections collected	138771	
Independent reflections	10977 (R(int) = 0.0395)	
Observed reflections (I > 2(I))	9886	
Completeness to theta = 36.317°	100.0 %	
Absorption correction	Semi-empirical from equivalents	
Max. and min. transmission	1.0000 and 0.9489	
Refinement method	Full-matrix least-squares on F ²	
Data / restraints / parameters	10977 / 0 / 240	
Goodness-of-fit on F ²	1.082	
Final R indices (I > 2σ(I))	R1 = 0.0364, wR2 = 0.0901	
R indices (all data)	R1 = 0.0418, wR2 = 0.0933	
Extinction coefficient	n/a	
Largest diff. peak and hole	0.588 and -0.580 e.Å ⁻³	

**107**

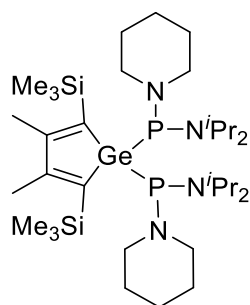
Identification code	msw19	
Empirical formula	C ₂₇ H ₄₆ Au Cl _{1.50} D _{2.50} N P Si ₂	
Formula weight	726.97	
Temperature	100(2) K	
Wavelength	0.71073 Å	
Crystal system	Monoclinic	
Space group	P ₂ ₁ /c	
Unit cell dimensions	a = 9.3602(4) Å	α = 90°.
	b = 15.8979(7) Å	β = 98.4396(18)°.
	c = 21.3569(10) Å	γ = 90°.
Volume	3143.7(2) Å ³	
Z	4	
Density (calculated)	1.536 Mg/m ³	
Absorption coefficient	4.951 mm ⁻¹	
F(000)	1460	
Crystal size	0.120 x 0.100 x 0.070 mm ³	
Theta range for data collection	1.603 to 40.249°	
Index ranges	-17 ≤ h ≤ 17, -28 ≤ k ≤ 28, -38 ≤ l ≤ 38	
Reflections collected	332522	
Independent reflections	19769 (R(int) = 0.0317)	
Observed reflections (I > 2(I))	18197	
Completeness to theta = 40.249°	100.0 %	
Absorption correction	Semi-empirical from equivalents	
Max. and min. transmission	0.6089 and 0.5110	
Refinement method	Full-matrix least-squares on F ²	
Data / restraints / parameters	19769 / 0 / 437	
Goodness-of-fit on F ²	1.157	
Final R indices (I > 2σ(I))	R1 = 0.0193, wR2 = 0.0384	
R indices (all data)	R1 = 0.0226, wR2 = 0.0391	
Extinction coefficient	n/a	
Largest diff. peak and hole	0.894 and -1.829 e.Å ⁻³	

**[K(18-c-6)][109a]**

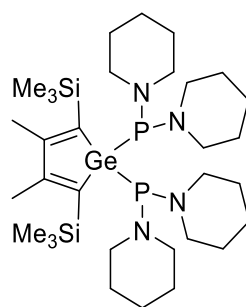
Identification code	msw59	
Empirical formula	C _{39.50} H ₈₀ Ge K N ₂ O ₆ P Si ₂	
Formula weight	877.89	
Temperature	100(2) K	
Wavelength	0.71073 Å	
Crystal system	Triclinic	
Space group	P-1	
Unit cell dimensions	a = 12.4354(7) Å	α = 107.723(2)°.
	b = 19.6392(10) Å	β = 92.763(2)°.
	c = 21.3774(11) Å	γ = 94.486(2)°.
Volume	4943.5(5) Å ³	
Z	4	
Density (calculated)	1.180 Mg/m ³	
Absorption coefficient	0.825 mm ⁻¹	
F(000)	1892	
Crystal size	0.120 x 0.120 x 0.050 mm ³	
Theta range for data collection	1.234 to 32.032°	
Index ranges	-18 ≤ h ≤ 17, -29 ≤ k ≤ 28, -31 ≤ l ≤ 31	
Reflections collected	284192	
Independent reflections	34430 (R(int) = 0.0538)	
Observed reflections (I > 2σ(I))	27995	
Completeness to theta = 32.032°	100.0 %	
Absorption correction	Semi-empirical from equivalents	
Max. and min. transmission	1.0000 and 0.9372	
Refinement method	Full-matrix least-squares on F ²	
Data / restraints / parameters	34430 / 20 / 1253	
Goodness-of-fit on F ²	1.014	
Final R indices (I > 2σ(I))	R1 = 0.0399, wR2 = 0.0931	
R indices (all data)	R1 = 0.0534, wR2 = 0.0993	
Extinction coefficient	n/a	
Largest diff. peak and hole	0.957 and -0.775 e.Å ⁻³	

**111a**

Identification code	msw592	
Empirical formula	C ₃₆ H ₈₀ Ge N ₄ P ₂ Si ₂	
Formula weight	759.75	
Temperature	100(2) K	
Wavelength	0.71073 Å	
Crystal system	Monoclinic	
Space group	C2/c	
Unit cell dimensions	a = 12.2385(10) Å	α = 90°.
	b = 20.3903(17) Å	β = 105.081(3)°.
	c = 18.1446(15) Å	γ = 90°.
Volume	4372.0(6) Å ³	
Z	4	
Density (calculated)	1.154 Mg/m ³	
Absorption coefficient	0.857 mm ⁻¹	
F(000)	1656	
Crystal size	0.200 x 0.150 x 0.080 mm ³	
Theta range for data collection	1.992 to 38.566°	
Index ranges	-21 ≤ h ≤ 21, -35 ≤ k ≤ 35, -31 ≤ l ≤ 31	
Reflections collected	142412	
Independent reflections	12365 (R(int) = 0.0539)	
Observed reflections (I > 2(I))	10937	
Completeness to theta = 38.566°	100.0 %	
Absorption correction	Semi-empirical from equivalents	
Max. and min. transmission	1.0000 and 0.8949	
Refinement method	Full-matrix least-squares on F ²	
Data / restraints / parameters	12365 / 33 / 271	
Goodness-of-fit on F ²	1.033	
Final R indices (I > 2σ(I))	R1 = 0.0461, wR2 = 0.1276	
R indices (all data)	R1 = 0.0525, wR2 = 0.1328	
Extinction coefficient	n/a	
Largest diff. peak and hole	2.398 and -1.455 e.Å ⁻³	

**111b**

Identification code	msf26	
Empirical formula	C ₃₄ H ₇₂ Ge N ₄ P ₂ Si ₂	
Formula weight	727.66	
Temperature	100(2) K	
Wavelength	0.71073 Å	
Crystal system	Monoclinic	
Space group	P2 ₁ /c	
Unit cell dimensions	a = 19.8737(9) Å	α = 90°.
	b = 11.2362(5) Å	β = 101.3720(18)°.
	c = 18.9475(9) Å	γ = 90°.
Volume	4148.0(3) Å ³	
Z	4	
Density (calculated)	1.165 Mg/m ³	
Absorption coefficient	0.900 mm ⁻¹	
F(000)	1576	
Crystal size	0.130 x 0.110 x 0.110 mm ³	
Theta range for data collection	2.091 to 36.319°	
Index ranges	-33 ≤ h ≤ 33, -18 ≤ k ≤ 18, -31 ≤ l ≤ 31	
Reflections collected	307594	
Independent reflections	20090 (R(int) = 0.0406)	
Observed reflections (I > 2(I))	17873	
Completeness to theta = 36.319°	100.0 %	
Absorption correction	Semi-empirical from equivalents	
Max. and min. transmission	1.0000 and 0.9321	
Refinement method	Full-matrix least-squares on F ²	
Data / restraints / parameters	20090 / 0 / 404	
Goodness-of-fit on F ²	1.062	
Final R indices (I > 2σ(I))	R1 = 0.0254, wR2 = 0.0650	
R indices (all data)	R1 = 0.0309, wR2 = 0.0680	
Extinction coefficient	n/a	
Largest diff. peak and hole	1.829 and -0.581 e.Å ⁻³	

**111c**

Identification code	msw76	
Empirical formula	C ₃₂ H ₆₄ Ge N ₄ P ₂ Si ₂	
Formula weight	695.58	
Temperature	100(2) K	
Wavelength	0.71073 Å	
Crystal system	Monoclinic	
Space group	P2 ₁ /n	
Unit cell dimensions	a = 10.7866(4) Å	α = 90°.
	b = 33.0047(12) Å	β = 115.2103(12)°.
	c = 11.9122(4) Å	γ = 90°.
Volume	3836.9(2) Å ³	
Z	4	
Density (calculated)	1.204 Mg/m ³	
Absorption coefficient	0.970 mm ⁻¹	
F(000)	1496	
Crystal size	0.140 x 0.110 x 0.110 mm ³	
Theta range for data collection	1.234 to 40.249°	
Index ranges	-19 ≤ h ≤ 19, -60 ≤ k ≤ 60, -21 ≤ l ≤ 21	
Reflections collected	245252	
Independent reflections	24151 (R(int) = 0.0337)	
Observed reflections (I > 2(I))	21623	
Completeness to theta = 40.249°	100.0 %	
Absorption correction	Semi-empirical from equivalents	
Max. and min. transmission	1.0000 and 0.9566	
Refinement method	Full-matrix least-squares on F ²	
Data / restraints / parameters	24151 / 0 / 378	
Goodness-of-fit on F ²	1.068	
Final R indices (I > 2σ(I))	R1 = 0.0253, wR2 = 0.0604	
R indices (all data)	R1 = 0.0304, wR2 = 0.0621	
Extinction coefficient	n/a	
Largest diff. peak and hole	0.655 and -0.418 e.Å ⁻³	

I hereby declare that I wrote this thesis independently and that I used only the indicated sources. I did not submit this thesis as a whole or in parts to any other university for evaluation for a conferral of a doctorate.

I confirm that I followed the general principals of good scientific practice, as they are specified in the guidelines of the Carl von Ossietzky Universität Oldenburg. In connection with this dissertation project, I did not claim any commercial mentoring services.

Oldenburg, 22.02.2024